Utrecht University

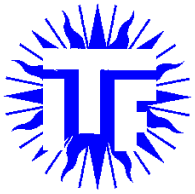

Graduate School of Natural Sciences

Institute for Theoretical Physics

Centre for Complex Systems

A functional approach to stochastic Lotka-Volterra equations

Master's thesis

Maarten Droste

Supervisors:

Prof. Dr. Cristiane Morais Smith
Utrecht University, ITP

Dr. Paul Zegeling
Utrecht University, Mathematics Dep.

MSc. Rodrigo Arouca de Albuquerque
Utrecht University, ITP

August, 2021

Abstract

In this work, a stochastic two species Lotka-Volterra model with additive noise is studied, using a field-theoretical formalism. This nonlinear model describes the evolution of predator and prey populations, which are affected by stochastic external environmental effects described by the noise. The functional approach applied to this model is the Martin-Siggia-Rose (MSR) formalism. This method describes the evolution of observables of a stochastic system as a stochastic field theory. This allows an analytical description of noise effects. First, stochastic systems and methods are studied in general, before turning to functional descriptions of these systems. After a derivation of the MSR formalism and an analytical and numerical study of the deterministic Lotka-Volterra model, the stochastic case is investigated. Simulations of this model for different noise realizations are performed, for which an ensemble average is computed. For large simulation time, the average stochastic trajectory shows an inward spiraling motion towards the fixed point, starting from the periodic solution of the deterministic system. This inward motion increases for larger noise amplitudes or larger simulation time, which is caused by the diffusion of the individual simulations due to noise effects. Using the MSR formalism, the general behavior of the populations under the influence of noise is studied. This is done by deriving expressions for the one- and two-point correlation functions of the fluctuations in terms of Feynman diagrams. These are calculated and compared with the simulated results. For small simulation time, the one-point functions and the resulting total average populations show similar behavior. For larger simulation time, the analytical results obtained with the MSR formalism grow exponentially compared to the simulated results, which causes large deviations in all correlation functions.

Acknowledgements

First of all, I would like to thank my supervisors Prof. Dr. Cristiane Morais Smith and Dr. Paul Zegeling for giving me the opportunity to work on this project. Even though real life meetings were hard to organize, they kept me motivated with inspiring thoughts and challenging questions. Their support stimulated me, even while writing this at home or in the library. Thanks to their scientific view and experience, this research got the form as it appears in this thesis. I would like to thank Cristiane for all her support and time during the project. Whenever I got stuck, she knew how to continue or how to adapt to the issue. This year has not been easy for her, but she made every effort to help me during this project. She and her group made me feel welcome and inspired me to look further than I could have imagined. I would like to thank Paul for the fruitful discussions we had in the Freudenthal building. His direct and mathematical approach helped me in understanding what we were actually studying and how to interprete what we observed. These few real life meetings gave me an exciting glimpse of what doing research together on a blackboard can feel like.

Also, I would like to thank my daily supervisor Rodrigo Arouca de Albuquerque, for always being there when I had any questions. Our long lasting discussions helped me a lot and improved my research. Even online and at long distance, it was always possible to reach you. Collaborating with you was the best thing that could have happened to me for this project.

At last, I would like to thank my fellow master students, friends and family. The interesting discussions, study and non-study related, and breaks together is what kept me going. Thank you for enjoying the 'eureka' moments with me, but also for listening to my complaints whenever things were not working out. Without you joining me in the library, this year would have been very hard. I would like to thank my parents for their limitless support and interest in my research. Thanks to you I started this adventure and I got where I am today.

Contents

Glossary

N: Number of particles in a system.
$\boldsymbol{r}(t)$: Position of a particle at time t.
$\boldsymbol{p}(t)$: Momentum of a particle at time t.
$X(t)$: A random variable with parameter t, taking values in a state space S.
$\{X(t)\}$: A stochastic process, which is a set of random variables $X(t)$.
$P_X(x,t)$: Probability distribution (density function) of a random variable $X(t)$, which gives the probability that $X = x$ at time t, for some $x \in S$.
$\{x(t)\}$: A realization/trajectory of a stochastic process, which is a fixed configuration.
$\langle O(X(t))\rangle$: Expectation value of a function $O(X)$ with respect to the probability density function $P_X(x,t)$.
$\langle X(t)^n\rangle$: n^{th} moment of $X(t)$.
$Y(t)$: Observable of a physical system, that evolves in time t.
$\eta(t)$: A random function or noise in a physical system, that can be described by a stochastic process, with realization $\{h(t)\}$.
$C(Y,t)$: Function that describes the deterministic evolution of an observable $Y(t)$.
$D(Y,t)$: Function that describes the coupling of an observable $Y(t)$ to the noise $\eta(t)$ in the system.
Ξ: Amplitude of the autocorrelation function of white noise.
$\xi(t-t')$: Autocorrelation function for colored noise.
τ_c: Autocorrelation time of a physical process.
$P(A|\,B)$: Conditional probability that an event A occurs, given that B occurs.
$P(x_n,t_n|\,x_{n-1},t_{n-1})$: Transition probability for a stochastic process $X(t)$ from state x_{n-1} at time t_{n-1} to state x_n at time t_n.
$P_{\text{eq}}(y)$: Equilibrium distribution of an observable $Y(t)$ that takes values y.
$\langle O(Y)\rangle$: Ensemble average of a function $O(Y)$ with respect to $P_{\text{eq}}(y)$.
$\overline{O(Y)}$: Time average of a function $O(Y)$.
$W(x_f|\,x_k)$: Transition probability rate (time independent), i.e. the probability per unit time that during an infinitesimal time interval the system changes from state x_k to x_f.
$F_n(x)$: The n^{th} Fokker-Planck moment. Usually one writes $F_1(x) = A(x)$ and $F_2(x) = B(x)$.
$\boldsymbol{v}(t)$: Velocity of a particle at time t.
k_B: Boltzmann constant.
T: Temperature.
$P_{\text{MB}}(v)$: The Maxwell-Boltzmann distribution, which is the equilibrium velocity distribution of a one dimensional gas.
D: Diffusion coefficient, equal to $k_BT/\gamma m$.
Γ: Phase space of a dynamical system, containing all its possible states.
$\rho(y,t)$: Phase space distribution function.
y^*: Fixed point of a dynamical system $\dot{y} = g(y)$, for which $g(y^*) = 0$.
$\mathcal{J}(y)$: Jacobian matrix at point y of a dynamical system $\dot{y} = g(y)$.
λ: Lyapunov exponent.
$\mathcal{C}[r_b, 0, \mathcal{B}, t]$: All trajectories $r(t')$ that start in $r(0) = r_b$ and end up in a domain $\mathcal{B} \subseteq \mathbb{R}^n$ at time t.
$\mathrm{d}_W r(t')$: Wiener measure for a path integral over paths $r(t')$.
$W(t)$: A Wiener process.
$Y(y_0, t, [\eta])$: An observable Y with initial value y_0, that is a functional of the noise $\eta(t)$.
$\mathcal{D}y(t)$: The functional measure for a function $y(t)$.
$\mathcal{P}[\eta]$: Probability density functional of a random function $\eta(t)$.
$Z[J]$: (Moment) Generating functional.

$J(t)$: Source function.
$K[J]$: Cumulant generating functional.
$\left\langle \prod_{i=1}^{2m} X(t_i) \right\rangle_{(c)}$: (Connected) Correlation function.
$G(t,s)$: Two-point correlation function, which is usually also a Green's function.
$S[r]$: Action of a dynamical system with variable r.
$q(t)$: Auxiliary field, also called response field.
$R(t,t')$: Response function.
$\Theta(t-t')$: Heaviside step function.
$Z_0[J]$: Free generating functional.
$S_0[y(t)]$: Free action, without interactions.
$S_I[y(t)]$: Interacting part of the action.
$y_s(t)$: Solution to the saddle point equation(s) of the action.
$u(t)$: Prey population in the two species predator-prey Lotka-Volterra model.
$v(t)$: Predator population in the two species predator-prey Lotka-Volterra model.
r_u: Growth rate of prey in the absence of predators.
r_v: Loss rate of predators in the absence of prey.
α: Predation/consumption rate of prey.
β: Growth rate of predators by consumption of prey.
(u_0, v_0): Initial prey and predator population at time $t = 0$.
K_i: Carrying capacity of species i.
T_{lin}: Period of the linearized Lotka-Volterra model.
M: Constant of motion for the predator-prey Lotka-Volterra model.
T_{sim}: Simulation time used for the simulations and calculations.
m: The number of linear cycles that are simulated.
Δt: Time step size.
$(u_d(t), v_d(t))$: Periodic solution of the deterministic Lotka-Volterra model.
$w(t)$: Fluctuations in the prey species with respect to the deterministic evolution $u_d(t)$.
$z(t)$: Fluctuations in the predator species with respect to the deterministic evolution $v_d(t)$.
$(\langle u_n(t)\rangle, \langle v_n(t)\rangle)$: Average of simulations of multiple different noise realizations of a stochastic Lotka-Volterra model with additive noise.
$(q_u(t), q_v(t))$: Auxiliary fields for the MSR formalism corresponding to the prey and predator species.
$G^B(t,t')$: Bare Green's function.
$G^M(t,t')$: Mean-field Green's function.
$Z_{\text{cl}}[\boldsymbol{J_y}]$: Deterministic contribution to the generating functional.
$Z_\psi[\boldsymbol{J_y}, \boldsymbol{J_\varphi}]$: Contribution of the fluctuations to the generating functional.
$B(t,t')$: Mean-field Green's matrix.

Abbreviations

MSR: Martin-Siggia-Rose.
EoM: Equations of motion.
SDE: Stochastic differential equation.
PDF: Probability density function.
QFT: Quantum field theory.
PD$\mathcal{F}$: Probability density functional.
ODE: Ordinary differential equation.
SQUID: Superconducting quantum interference device.
PLR: Pupil light reflex.

1 Introduction

To describe the evolution of equilibrium systems, standard approaches in physics include Hamilton's equations [1] or methods from statistical physics [2]. Whenever the system is out of equilibrium, the macroscopic and deterministic equations of motion (EoM) are perturbed by fluctuations at the microscopic level. To investigate these deviations from the deterministic behavior, the system can be studied at the intermediate mesoscopic level, where the fluctuations can be described as random effects [3]. Such a stochastic approach yields stochastic differential equations (SDEs) as EoM, which contain noise perturbations next to the deterministic evolution [4]. Often, these stochastic effects are assumed to be caused by Gaussian white noise [3]. The stochastic system can be investigated further by means of a master equation [5] or a Fokker-Planck equation [3], which describe the evolution of the probability density function (PDF) of the observables in the system.

A more physical approach, which is based on the corresponding SDE, was constructed by Langevin in 1908 to describe the velocity of a Brownian particle [6]. This method was extended by Wiener in 1921 [7]. He was the first to use path integrals, even before Feynman [8] and Dirac [9] introduced them for quantum field theory (QFT), to find an expression for the probability density functional (PD$\mathcal{F}$) for the position of a Brownian particle. Chandrasekhar [10] used the same approach in 1943 to describe the velocity of the particle, for which he obtained the same results earlier found by Langevin. These findings opened the way for describing stochastic systems by means of a functional formalism, comparable to the field-theoretical approach to quantum systems. Using the operator formalism, this eventually led to a method to study classical stochastic systems, developed by Martin, Siggia and Rose in 1973 [11]. Near a phase transition, the order parameter satisfies a Langevin-like equation. To investigate classical fluctuations, they developed a method which would later be called the MSR formalism. The approach was extended to the equivalent path integral interpretation in 1976 by Janssen [12] and de Dominicis [13]. This method transforms the SDE, describing the evolution of the system's observables, to a stochastic field theory, which allows an analytical description of the noise effects. In the years after, the formalism was applied to a wide variety of systems, ranging from quantum systems [14, 15] to stochastic models in neurodynamics [16–19].

Another recent application of the MSR formalism can be found in the field of population ecology. The evolution of interacting species can be described by a (generalized) Lotka-Volterra model [20, 21]. To account for external environmental effects that influence the populations, a noise contribution can be included in the model. When the number of species is large, this allows for a field-theoretical or statistical description of the system [22, 23]. The MSR formalism was shown to describe well the general behavior of such a stochastic system [24, 25]. A functional approach can also be applied to the model for a small number of species. The simplest and original form of the Lotka-Volterra equations is a two species model, describing the time evolution of interacting predators and prey [26]. In the deterministic case, this model has periodic solutions, for which no explicit analytical expression exists [27]. Stochastic versions of this two species system have been studied widely, mostly through simulations [28–30] or mathematical analysis [31–33].

In this work, a stochastic version of the two species predator-prey Lotka-Volterra model with additive Gaussian white noise is studied, by means of the MSR formalism. Since this formalism has never before been applied to this stochastic model, the results are compared with numerical simulations. First, a general overview of stochastic methods in physics and complex systems is discussed. These methods are generalized to a functional approach and compared with their quantum mechanical analogs. Then, the MSR formalism is derived and applied to a linear and nonlinear SDE. Before studying a stochastic case, the deterministic two species Lotka-Volterra model is studied carefully.

This is done through an analytical investigation of the corresponding phase space and a numerical study, as the model does not have an analytical solution.

The stochastic Lotka-Volterra model with additive noise is first analyzed through simulations. Because this model has not been studied previously for a large enough simulation time, this already yields interesting new results. We found that after performing an ensemble average over a large amount of simulations, the averaged simulated trajectory in phase space shows an inward spiraling motion towards the fixed point of the deterministic model. After carefully analyzing this and other results, the MSR formalism is used to derive analytical expressions for the correlation functions of the fluctuations and the total populations, which are compared with the results obtained from the simulations. Our main result is that for small enough simulation time, the average fluctuations in both species obtained with the MSR formalism show behavior that is comparable with the (ensemble) averaged fluctuations obtained from the simulations. This also results in total populations that show the same general evolution for both methods. For larger simulation time, the analytical correlation functions show exponentially deviating behavior compared to the simulated ones. From our findings, we can conclude that the MSR formalism yields reliable results for this stochastic Lotka-Volterra model, for small enough simulation times. For larger simulation times, improvements are necessary to obtain comparable results.

2 Stochastic methods in physics and complex systems

To incorporate external environmental effects in the Lotka-Volterra model, a noise contribution has to be included. This noise is random, resulting in a stochastic instead of a deterministic system. Therefore, it is useful to study stochastic systems in general first. This section starts with an introduction to stochastic processes and stochastic differential equations (SDEs), together with their origin in physics and complex systems. Then, methods to describe stochastic systems, such as a master equation, Fokker-Planck equation and the Langevin approach, are discussed. This last method was used by Paul Langevin to understand Brownian motion [6], which is a very important physical stochastic problem that will be treated elaborately. Langevin's approach can be used to solve several SDEs and it is also important for the connection to field-theoretical methods. The Langevin equation for Brownian motion was one of the first SDEs to be solved by means of a functional approach, from which later the MSR formalism followed, as will be discussed in Section 3. This section ends with a generalization of the theory of stochastic systems and methods to complex systems. First, the necessary tools to analyze dynamical systems are discussed briefly. These are combined with stochastic methods to describe some examples of stochastic complex systems.

2.1 Stochastic processes in physics

Consider a system consisting of N classical particles with positions $\boldsymbol{r}_i(t)$ and momenta $\boldsymbol{p}_i(t)$, $i = 1, ..., N$. Furthermore, assume that this system is closed and that its Hamiltonian $\mathcal{H}(\boldsymbol{r}^N, \boldsymbol{p}^N, t)$ is known, where the positions $\boldsymbol{r}^N = \{\boldsymbol{r}_1(t), ..., \boldsymbol{r}_N(t)\}$ and momenta $\boldsymbol{p}^N = \{\boldsymbol{p}_1(t), ..., \boldsymbol{p}_N(t)\}$ together describe a microstate of the system. The time evolution of the system is now completely and uniquely determined by Hamilton's equations [1]. So, the entire future behavior of this system can be deduced from this microscopic description.

In principle, N is very large[1], so it becomes intractable to determine the behavior of many-particle systems from the dynamics of every individual particle by using Hamilton's equations. Therefore, one turns to a statistical mechanical description of the system, which relates macroscopic thermodynamical observables, such as the temperature and pressure, to the microscopic single-particle level. Suppose that the energy and number of particles of an isolated many-particle system is known and fixed. The fundamental assumption of statistical mechanics tells that, in thermodynamic equilibrium, the system can be found in every microstate (corresponding to a macrostate) with equal probability [35]. Here, the condition of thermodynamic equilibrium is necessary, and using this assumption the branch of equilibrium statistical mechanics can be explored.

2.1.1 A stochastic approach

The method described above works well for phenomena in equilibrium systems, but not for the out of equilibrium case, as the fundamental assumption does not hold. As emphasized above, one cannot hope to use a full microscopic description of the system. Therefore, an intermediate approach can be used, which is at the *mesoscopic* level. To obtain a macroscopic description, an elimination of microscopic variables is required, which results in a small set of variables obeying some deterministic EoM [3]. These equations are only an approximation, so fluctuations around their (average) solutions should be taken into account. These fluctuations define the crossover between the macroscopic and microscopic level, and are therefore called mesoscopic. Figure 2.1 shows an intuitive picture of these different levels of description. The problem is that these fluctuations still

[1] A typical amount of matter that one encounters in every day life has a mass in the order of grams. For carbon, 1 mol ^{12}C = 12 g, which already contains $6.02 \cdot 10^{23}$ particles [34].

depend on the behavior of the system at the microscopic level. To solve this, one can describe them in a stochastic way, by assigning a certain randomness. In this way, the complete microscopic picture does not need to be described, as the fluctuations due to phenomena at the microscale can be treated as random effects on the average macroscopic behavior.

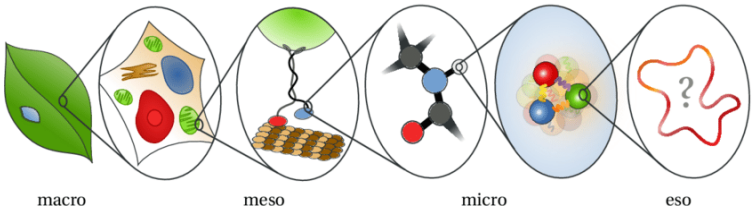

Figure 2.1: An intuitive view on the different levels of description. At the macroscopic level, one can describe the leaf that obeys a deterministic EoM by approximation. Zooming in, the mesoscopic level is reached, where the cells and its constituents are studied. For this description, fluctuations play an important role. Zooming in further, one arrives at the microscopic level of atoms and the elementary particles, which obey their own deterministic laws. The last level is the esoteric level, at which fundamental theories are presumed to hold. This figure has been extracted from Ref. [36].

All microscopic details of the system are thus contained in this stochastic description, which functions as a coarse-graining method. Since all these details are usually very complicated to compute and in the non-equilibrium case not even known completely, they can only be treated in this stochastic sense. In addition, real physical systems are never perfectly isolated. It is a useful assumption to investigate the intrinsic properties of a system, but a realistic model takes into account effects of the surrounding environment. Since most of the time interactions with the environment are either of minor influence or partially unknown, they can also be described stochastically [3].

The discussion above motivates the definition of a stochastic process. This is a set of random variables $\{X(t)\}$, where the parameter t usually represents time. Since every $X(t)$ is a random variable, its value for fixed t is not uniquely determined, but subject to a probability distribution $P_X(x,t)$ for some $x \in S$, the state space of $X(t)$. This probability distribution is either a probability mass function for a discrete random variable or a probability density function (PDF) for a continuous random variable. For the latter case, the *expectation value* or average of a function $O(X)$ is defined as

$$\langle O(X(t))\rangle = \int O(x) P_X(x,t)\,\mathrm{d}x, \tag{2.1}$$

for a normalized PDF $P_X(x,t)$. From this general expression, the n^{th} moment of X can be defined as $\langle X^n(t)\rangle$. A fixed configuration $\{x(t)\}$ of the stochastic process is called a *realization* or a trajectory.

The time evolution of a physical system subject to noise can be described by a stochastic process, due to the stochastic nature of the fluctuations. Hence, every system whose dynamics is influenced by some random effect can be represented by a stochastic process, and can therefore be called a *stochastic system*. Usually, the evolution of an observable of a deterministic system can be described by some (partial) differential equation [37]. Similarly, observables $Y(t)$ in stochastic systems obey a stochastic differential equation (SDE). A SDE is a differential equation of which at least one of the terms is a stochastic process. For the systems discussed here, a general SDE can be written as

$$\frac{\mathrm{d}Y(t)}{\mathrm{d}t} = C(Y,t) + D(Y,t)\eta(t). \tag{2.2}$$

The function $C(Y,t)$ represents the deterministic evolution of $Y(t)$ and $D(Y,t)$ represents the coupling of $Y(t)$ to a random function $\eta(t)$, which is a stochastic process often called noise [4]. The deterministic behavior of the 'slow' variable $Y(t)$ is thus perturbed by the second term, which includes all other degrees of freedom that in comparison fluctuate rapidly. For constant $D(Y,t)$, the noise is called[2] additive, while for any other form of $D(Y,t)$ it is called multiplicative. The main difference with ordinary differential equations (ODEs) is that SDEs do not have a unique solution. Let $Y(t_0) = y_0$ be the initial condition for Eq. (2.2). Since for every t the stochastic process $\eta(t)$ takes a random value in its state space S, the solution $Y(y_0, t, [\eta])$ of Eq. (2.2) is a functional of $\eta(t)$ and is therefore also a stochastic process [3]. Only when a noise trajectory $\{h(t)\}$ is fixed, the SDE reduces to an ODE and its solution $y(t, h(t))$ is unique for the initial condition $y(t_0) = y_0$.

The noise $\eta(t)$ thus completely determines the fluctuating behavior of a stochastic system and its observables $Y(t)$. As mentioned above, the noise in a SDE can be additive or multiplicative. Next to this, the noise itself can also have certain properties, which distincts different kinds of noise. A general property is that the expectation value $\langle \eta(t) \rangle = 0$ for all kinds of noise, to enable the system to reach equilibrium[3]. This also makes sense intuitively, since the noise term in Eq. (2.2) describes the deviation of $Y(t)$ from its deterministic evolution. If the average fluctuations would be nonzero, their average effect could be included in $C(Y,t)$ as a part of the deterministic evolution.

The most common kind of noise is called *white noise*. Next to a vanishing expectation value, this noise is characterized by its *autocorrelation function*[4]

$$\langle \eta(t)\eta(t') \rangle = \Xi\, \delta(t - t'), \tag{2.3}$$

where Ξ is a constant autocorrelation amplitude and $\delta(t - t')$ is the Dirac delta function. This means that fluctuations at different times are uncorrelated. The fluctuations are also independent of all other quantities in the system. The reason that this noise is called white is because its spectral density[5] is equal to the constant Ξ. Hence, this is independent of the frequency, so every frequency contributes equally to the spectral density, making it a white spectrum, analogous to white light.

This immediately leads to the definition of colored noise. Its expectation value is also zero, but its autocorrelation function is given by

$$\langle \eta(t)\eta(t') \rangle = \xi(t - t'). \tag{2.4}$$

The autocorrelation function $\xi(t - t')$ is usually peaked around zero, but it has a finite width and is therefore not a Dirac delta function. Consequently, its spectral density is not constant, so some frequencies contribute more than others. This explains the name 'colored' noise, in contrast to white noise. Since $\xi(t - t')$ is peaked, it may be negligible or zero for $|t - t'| > \tau_c$, where τ_c is the *autocorrelation time*. Obviously, $\tau_c = 0$ for white noise, but this is not the case for colored noise. This makes it much more difficult to solve SDEs with colored noise analytically. Therefore, one usually assumes the autocorrelation time to be small [3], allowing for an expansion in powers of τ_c, of which the zeroth order is the white noise result.

Both types of noise discussed above only specify the first moment and the autocorrelation. To further characterize $\eta(t)$, one has to investigate its PDF. If $\eta(t)$ has a Gaussian distribution, it is

[2] In the literature, the noise is usually called additive or multiplicative, but mathematically this is wrong, as instead the complete SDE should be called additive or multiplicative [3].

[3] If an equilibrium exists for the EoM without noise.

[4] This is the second moment of $\eta(t)$, but for different times t, t', so it is called a correlation function.

[5] This is just the Fourier transform of the autocorrelation function of $\eta(t)$, in frequency space.

called Gaussian noise. This also specifies all higher moments of $\eta(t)$. If the Gaussian noise is also white, it is completely determined by its autocorrelation amplitude Ξ. If the noise has some other distribution, it is generally called non-Gaussian. Non-Gaussian white noise cannot be described by the single parameter Ξ, but requires all parameters Ξ_n, which are related to the n^{th} correlation function [3].

In most stochastic systems, the fluctuations are assumed to be Gaussian white noise, since this often holds approximately and it is much easier to handle in calculations. For example, thermal or Johnson-Nyquist noise [38], occurring in electrical conductors and resistors due to random thermal motion of electrons and ions, is approximately white. A well-known example of colored noise is pink noise[6], which often occurs in biological systems [39].

Now that the concept of noise has been understood, we can again turn to the physical processes influenced by it. Let us illustrate the importance of stochastic processes in physics by mentioning a few examples. The best known physical stochastic process is Brownian motion [40], where a mesoscopic particle immersed in a fluid shows random displacements due to collisions with the surrounding fluid particles. The velocity of a Brownian particle can be described by a SDE called the Langevin equation. This problem and Langevin's approach will be discussed extensively in Section 2.3, for its major importance and wide applicability to stochastic systems.

Another well-known example is the decay process of a radioactive material [3]. The number of nuclei $N(t)$ after time t that did not decay yet can be modeled by a stochastic process. The SDE of this process can be obtained by taking $C(N,t) = -\kappa N(t)$, where κ is the decay rate, and $D(N,t)\eta(t)$ as some Gaussian white noise. This last term represents fluctuations in the decay rate due to the unpredictable nature of radioactive decay. Hence, the expected number of nuclei $\langle N(t)\rangle$ follows a differential equation without noise, that has the well-known solution $N(t) = N(0)\exp(-\kappa t)$ for exponential decay. This SDE can be used to model any decay process with random fluctuations, such as emission of light by atoms or even the killing of enemy troops by random shooting [3].

2.1.2 Markov processes

Before introducing another important stochastic process, a subclass of stochastic processes, called Markov processes, has to be discussed first. Let $\{t_0, t_1, ..., t_{n-1}, t_n\}$ be a set of successive times, and write $P(A|\,B)$ as the conditional probability that an event A occurs, given that B occurs. A stochastic process $\{X(t)\}$ is a Markov process if it satisfies

$$P(x_n, t_n|\,x_{n-1}, t_{n-1}; ...; x_0, t_0) = P(x_n, t_n|\,x_{n-1}, t_{n-1}), \tag{2.5}$$

with x_n a realization of $X(t)$ at time t_n. This is called the Markov property, which basically states that the process is memoryless, in the sense that its future state only depends on its present state and is not affected by the earlier states. The quantity $P(x_n, t_n|\,x_{n-1}, t_{n-1})$, which is intuitively called the transition probability, is the probability that $X(t_n) = x_n$, given that $X(t_{n-1}) = x_{n-1}$. The Markov property simplifies calculations considering transition rates and probabilities drastically, since only the present state of the system has to be taken into account, instead of its whole history.

The examples above of Brownian motion and decay processes are Markov processes [3]. Another important stochastic process that is Markovian is the Poisson process, which occurs in counting experiments [41]. A lot of physical stochastic processes are in fact (approximately) Markovian.

[6] It is also called $1/f$ noise due to the spectral density being inversely proportional to the frequency f.

If successive observations $i, i+1$ of a physical stochastic process are such that $|t_{i+1} - t_i| > \tau_c$, with τ_c the autocorrelation time of the (noise in the) process, then the autocorrelation function $\xi(t_{i+1} - t_i)$ is negligible or zero. This implies that the successive observations are uncorrelated, so the process satisfies the Markov property [3]. Consequently, a system with white noise can always be described by a (multicomponent) Markov process. So, if $\eta(t)$ is white, a solution $\{Y(t)\}$ of Eq. (2.2) is a Markov process. On the other hand, sytems with colored noise are only Markovian on timescales larger than their autocorrelation time. Hence, analyzing systems with colored noise in their Markovian limit is directly related to the expansion in powers of τ_c.

The (approximate) Markovian character of physical processes results from the repeated randomness assumption or *Stosszahlansatz*, as it was called by Ehrenfest [42], which also accounts for irreversibility in dynamical systems. By including all microscopic variables, the evolution of any isolated physical system could be described by a multicomponent Markov process, and in fact its evolution would be deterministic [3]. As this is intractable for most systems, physicists want to find a small set of (macroscopic) variables that by approximation still evolve as a multicomponent Markov process. This is the case for both the equilibrium and stochastic approach.

A very useful property of Markov processes is that their transition probabilities obey the Chapman-Kolmogorov equation [3], given by

$$P(x_f, t_f | x_i, t_i) = \int P(x_f, t_f | x_k, t_k) P(x_k, t_k | x_i, t_i) \, \mathrm{d}x_k, \tag{2.6}$$

for $t_i < t_k < t_f$. For an observable $Y(t)$ that evolves according to a continuous stochastic process, the transition probabilities are related to its PDF $P_Y(y,t)$. In the next section, an equation for the time evolution of $P_Y(y,t)$ will be introduced, that can be derived from the Chapman-Kolmogorov equation.

Markov processes are also useful to describe equilibrium systems and their fluctuations. Suppose an isolated system has quantities $Y(t)$ that can be treated like a multicomponent Markov process. After reaching equilibrium, $P_Y(y,t)$ reduces to the time-independent equilibrium distribution $P_{\mathrm{eq}}(y)$. This implies time-invariance for the transition probabilities, so $P_Y(y_2, t_2 | y_1, t_1) = P_Y(y_2 | y_1; \tau)$ with $\tau = t_2 - t_1$ the length of the time interval. This automatically results in a time-invariant evolution of the system. The Markov process $Y(t)$ with this property is called *stationary*. Using the equilibrium distribution $P_{\mathrm{eq}}(y)$, the average behavior and the fluctuations around it can be studied. A very important stationary Markov process is the Ornstein-Uhlenbeck process [43], which describes the behavior of the velocity of a Brownian particle. Its equilibrium distribution is a Gaussian distribution. The (normalized) equilibrium probability density also allows the definition of a so-called *ensemble average*

$$\langle O(Y) \rangle = \int O(y) P_{\mathrm{eq}}(y) \, \mathrm{d}y, \tag{2.7}$$

of any function $O(Y)$ of the observables $Y(t)$. Note the resemblance to the expectation value $\langle O(Y(t)) \rangle$ in Eq. (2.1), only now with respect to the equilibrium distribution $P_{\mathrm{eq}}(y)$, resulting in a time independent average $\langle O(Y) \rangle$. On the other hand, one could measure $O(y(t))$ for a time τ and divide by the length of the time interval. This gives rise to the definition of a *time average*

$$\overline{O(Y)} = \lim_{\tau \to \infty} \frac{1}{\tau} \int_{t_0}^{t_0 + \tau} O(y(t)) \, \mathrm{d}t. \tag{2.8}$$

Systems that have $\langle O(Y)\rangle = \overline{O(Y)}$ for all functions $O(y)$ are called *ergodic* [5]. This property is only proven for a few systems, but often it is assumed to be true. However, when the system is not in equilibrium, the PDF $P_Y(y,t)$ is time dependent. In that case, the expectation value $\langle O(Y(t))\rangle$ also changes in time. This destroys ergodicity, since the time average can obviously not be time dependent.

Another important subclass of Markov processes are *homogeneous* processes. These are non-stationary, but their transition probabilities only depend on the time difference τ. Often, homogeneity is assumed for Markov processes that are related to physical systems. Since systems out of equilibrium are non-stationary, this property can therefore also be used to study these.

Despite the usefulness of the Markov property and its (approximate) legitimacy in many processes, there also exist processes in physical systems that are non-Markovian. The best known example is magnetization of a ferromagnet [45]. This process is schematically shown in Figure 2.2. If an external magnetic field with strength H is applied to a ferromagnetic material with zero magnetization, it gets magnetized. When H varies monotonically, the magnetization B follows a loop that does not overlap with the initial magnetization curve. Hence, the magnetization B depends on the history of the material[7] and consequently this process is non-Markovian.

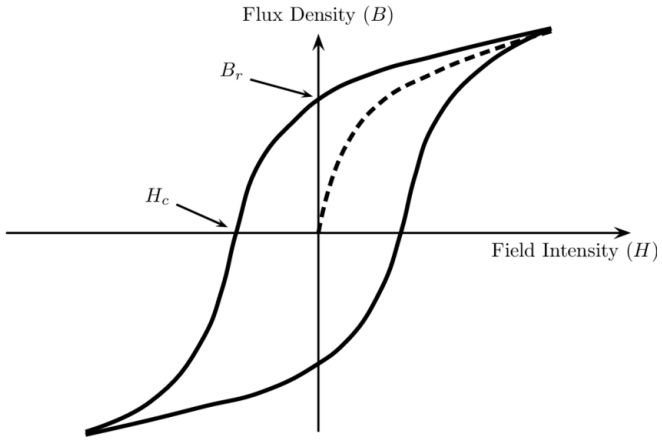

Figure 2.2: A schematic illustration of the magnetization process. Starting from the origin and applying a magnetic field with strength H, the magnetization B of the ferromagnetic material follows the dashed curve. After decreasing H monotonically to zero, the magnetization follows the solid line till B_r, called the *remanence*. If a magnetic field is applied in the opposite direction, the magnetization keeps decreasing along the same line and vanishes at the *coercivity* H_c of the material. The relation between H and B is now given by the depicted loop, which does not overlap with the dashed curve showing the initial magnetization. This figure has been extracted from Ref. [44].

A lot of (non-equilibrium) systems require a stochastic description of their behavior. The examples above are just a few, which already have many applications. Therefore, studying stochastic systems is of major importance for understanding dynamical systems.

2.2 Master equation & Fokker-Planck equation

In this section, some methods to study stochastic systems will be developed. Since the evolution of the state of such a system is subject to a random effect, the most insightful quantity to investigate is the PDF of the observables in the system. This density is directly related to the transition probabilities and it will be shown to obey similar relations.

[7] This dependency is called *hysteresis*.

2.2.1 Master equation

Consider a stochastic system, of which the evolution of one or more variables can be described by a homogeneous Markov process $\{X(t)\}$. This Markov process takes values in its state space S, and has (an unknown) PDF[8] $P(x,t)$. Starting from the Chapman-Kolmogorov equation (2.6), one can derive an expression for the time evolution of $P(x_f,t_k)$ through its transition probabilities $P(x_f,t_f|\,x_i,t_i)$. Such an expression is called a *master equation*, which is given by

$$\frac{\partial P(x_f,t_k)}{\partial t_k} = \int \left[P(x_k,t_k)W(x_f|\,x_k) - P(x_f,t_k)W(x_k|\,x_f)\right]\,\mathrm{d}x_k. \tag{2.9}$$

A derivation of this equation is performed in Ref. [5]. The transition probability rates[9] $W(x_f|\,x_k)$ are defined as the probability per unit time that, during an infinitesimal time interval, the system changes its state from x_k to x_f. The master equation is just the differential form of the Chapman-Kolmogorov equation (2.6), but it is more convenient to use due to its linearity. Furthermore, it also provides a more direct physical interpretation for the time evolution of the PDF $P(x_f,t_k)$ in terms of a 'gain' and 'loss'. The first term increases the probability due to transitions from states x_k to state x_f, while the second term reduces it via transitions from state x_f to (all) other states x_k. The rate of probability change is thus very intuitively given by these gain and loss processes. Also, the transition probability rates $W\left(x_f|\,x_k\right)$ are the infinitesimal analogues of transition probabilities. Therefore, they are an inherent property of the examined physical system. Hence, the master equation contains specific information on the transition probabilities that determine the mesoscopic state of the system, in contrast to the nonlinear Chapman-Kolmogorov equation that only arises from the Markov property.

For the decay process discussed in Section 2.1.1, one can write down the master equation for the probability $P(N,t)$ that there are N radioactive nuclei at time t. In this case, the states N are discrete, since they describe the number of nuclei, the decay rate κ is independent of time, and the only possible transition is from N to $N-1$ nuclei. Thus, we can write $W(M|\,N) = \kappa N \delta_{M,N-1}$ for the transition probability rates and the master equation of the decay process reduces to

$$\frac{\partial P(N,t)}{\partial t} = \kappa(N+1)P(N+1,t) - \kappa N P(N,t). \tag{2.10}$$

In general, calculating the transition probability rates $W(y|\,x)$, with x, y states of the system, directly requires a complete microscopic description of the system and is therefore usually intractable. However, a lot of approximation methods exist to calculate these probabilities. The best known one is time-dependent perturbation theory, which results in Fermi's Golden Rule for quantum systems [46]

$$W(f|\,i) = \frac{2\pi}{\hbar}|\langle f|H'|i\rangle|^2 \rho(E_f). \tag{2.11}$$

Here $|i\rangle$ and $|f\rangle$ are, respectively, the initial and final state, $\langle f|H'|i\rangle$ is the matrix element of the perturbed Hamiltonian and $\rho(E_f)$ is the density of states at the energy E_f of the final state. Fermi's Golden Rule gives the transition probability rate of a quantum system in an energy eigenstate to other eigenstates, due to a perturbation.

Another method to find the transition probability rates is by imposing conditions on them. If a system is in a steady state, $P(x,t)$ is not an explicit function of time and therefore $\partial P(x,t)/\partial t = 0$.

[8] From now on, the subscript X is omitted.

[9] These are time-independent due to the assumed homogeneity of the Markov process.

Looking at Eq. (2.9), a steady state thus implies a total balance of probability flow. Here, total balance means that the rate of transitions into a state x is equal to the rate of transitions out of state x. An even stronger and also sufficient condition for reaching a stationary probability distribution is *detailed balance*, which, as the name hints, is given by

$$P(x,t)W(y|\,x) = P(y,t)W(x|\,y). \tag{2.12}$$

So, for each pair of states x, y the rate of transitions is balanced. The transition probability rates $W(y|\,x)$ can now be chosen such that they obey

$$P(x,t\to\infty)W(y|\,x) = P(y,t\to\infty)W(x|\,y), \tag{2.13}$$

where $P(x,t\to\infty)$ is the equilibrium distribution $P_{\text{eq}}(x)$, which is also stationary. Detailed balance implies that such an equilibrium distribution exists, and thus guarantees that the system reaches an equilibrium state after waiting for a sufficient amount of time. It turns out that a thermal equilibrium state necessarily satisfies detailed balance, while other steady states only satisfy total balance [47]. It can be proven that closed, isolated and finite physical systems satisfy detailed balance under certain restrictions [3]. This also explains their tendency towards (an) equilibrium (distribution). A well-known explicit application of the principle of detailed balance comes from Einstein. He used this in his quantum theory of emission and absorption of radiation [48].

2.2.2 Fokker-Planck equation

The master equation (2.9) is already easier to handle than the Chapman-Kolmogorov equation (2.6), but it is still an integro-differential equation. Therefore, we derive[10] a more tractable equation from the master equation.

Let x_i be the initial state of the system and s the size of the 'jump' that the process makes in an infinitesimal time interval. Then, the transition probability rates can be written in terms of x and s as $W(x|\,x_i) = W(x-s,s)$ where $s = x - x_i$. Note that s is well-defined if a state x is given by the value of some observable of the system. The master equation for the probability distribution $P(x,t)$ is then given by

$$\frac{\partial P(x,t)}{\partial t} = \int P(x-s,t)W(x-s,s)\,\mathrm{d}s - P(x,t)\int W(x,-s)\,\mathrm{d}s. \tag{2.14}$$

We now make two assumptions. First, it is assumed that only small jumps occur, so $W(x-s,s)$ is peaked around $s=0$. As a second assumption, we take $P(x,t)$ and $W(x-s,s)$ to be varying slowly with x. Now, the expression in the first integral in Eq. (2.14) can be expanded as a Taylor series around x up to second order, yielding

$$\begin{aligned}\frac{\partial P(x,t)}{\partial t} \simeq &\int P(x,t)W(x,s)\,\mathrm{d}s - \int s\frac{\partial}{\partial x}\left[P(x,t)W(x,s)\right]\,\mathrm{d}s \\ &+ \frac{1}{2}\int s^2\frac{\partial^2}{\partial x^2}\left[P(x,t)W(x,s)\right]\,\mathrm{d}s - P(x,t)\int W(x,-s)\,\mathrm{d}s.\end{aligned} \tag{2.15}$$

In fact, one can include all terms of the expansion, which is then called the Kramers-Moyal expansion [49, 50]. Since $W(x,s)$ is assumed to be symmetric in the jump size s, the first and fourth term cancel. For notational convenience, it is useful to define the Fokker-Planck moments as

$$F_n(x) = \int s^n W(x,s)\,\mathrm{d}s. \tag{2.16}$$

[10] The derivation in Section 8 of Ref. [3] is followed closely.

In terms of these Fokker-Planck moments, Eq. (2.15) now simplifies to the Fokker-Planck equation

$$\frac{\partial P(x,t)}{\partial t} = -\frac{\partial}{\partial x}\left[F_1(x)P(x,t)\right] + \frac{1}{2}\frac{\partial^2}{\partial x^2}\left[F_2(x)P(x,t)\right]. \tag{2.17}$$

Note that the Fokker-Planck equation is an approximate substitute for the master equation, to describe the evolution of the PDF for Markov processes with small jumps. The first term on the right-hand side is called the drift term, and the second one is called the diffusion term. These names should not necessarily be interpreted in a physical way, but they will make sense in the treatment of Brownian motion in Section 2.3. In the literature, the Fokker-Planck moments are usually written as $F_1(x) = A(x)$ and $F_2(x) = B(x)$. This notation will be used from now on. A restriction is that $B(x) > 0\ \forall x$, which is easily verified from the definition of $F_2(x)$ in Eq. (2.16).

Since the Fokker-Planck equation is by definition linear in $P(x,t)$, the adjective 'linear' can be used to indicate a special kind of Fokker-Planck equations. These are called linear if $A(x) = A_0 + A_1 x$ and $B(x) = B_0$, for some $A_0, A_1, B_0 \in \mathbb{R}$. If $A_1 < 0$ the linear Fokker-Plank equation describes a stationary Markov process which has a Gaussian stationary distribution. This is exactly the earlier mentioned Ornstein-Uhlenbeck process [43], which corresponds to a diffusion process for the velocity of a Brownian particle.

The Fokker-Planck equation is easier to use than the master equation since it is a differential instead of integro-differential equation. A more important advantage is that not all transition probability rates $W(x,s)$ for every pair of states x, y need to be known, but only the first and second Fokker-Planck moments $A(x)$ and $B(x)$. One could argue that this still requires knowledge of $W(x,s)$ through Eq. (2.16), but in fact this equation can be used to express $A(x)$ and $B(x)$ in terms of the average fluctuations. Eq. (2.16) is exactly the time derivative of the n^{th} moment of the fluctuation $s = x - x_i$, because $W(x,s)$ is a transition probability rate. So, we obtain

$$\frac{\partial}{\partial t}\langle s\rangle = A(x), \quad \frac{\partial}{\partial t}\langle s^2\rangle = B(x). \tag{2.18}$$

Hence, by determining these average fluctuations for a short time interval, the Fokker-Planck moments can be obtained and the resulting Fokker-Planck equation can be used to find the long time behavior of the system. After some manipulations, as performed in Ref. [3], we can write Eq. (2.18) in terms of the moments of x itself as

$$\frac{\partial}{\partial t}\langle x\rangle = \langle A(x)\rangle, \quad \frac{\partial}{\partial t}\langle x^2\rangle = \langle B(x)\rangle + 2\langle xA(x)\rangle. \tag{2.19}$$

The Fokker-Planck equation can also be generalized to a N-dimensional case, where the state x of the system is a random vector containing random variables x_m. The evolution of the PDF of the corresponding multivariate (Markov) process can be shown to obey

$$\frac{\partial P(x,t)}{\partial t} = -\sum_{m=1}^{N}\frac{\partial}{\partial x_m}\left[A_m(x)P(x,t)\right] + \frac{1}{2}\sum_{m,n=1}^{N}\frac{\partial^2}{\partial x_m \partial x_n}\left[B_{mn}(x)P(x,t)\right], \tag{2.20}$$

which is the multivariate Fokker-Planck equation.

2.3 Brownian motion & the Langevin equation

Brownian motion was already discussed briefly in Section 2.1.1 as an example of a physical process that can be described by a SDE. In this section, the problem is discussed more elaborately because of its historic value and the wide applicability of Langevin's approach.

Brownian motion is named after Robert Brown, who did an extensive study of the irregular motion of pollen immersed in a fluid in 1827 [51]. The motion he observed can be generalized to any heavy[11] mesoscopic particle immersed in a fluid. The lighter fluid particles collide with the mesoscopic particle in a random way, resulting in a randomly fluctuating velocity $v(t)$ for the mesoscopic particle. One can assume that the velocity change $\mathrm{d}v$ depends on the current velocity $v(t)$, since on average there will be more collisions in front than at the back of the particle. However, $\mathrm{d}v$ is not affected by earlier velocities, so the velocity evolution can be modeled as a Markov process.

The collisions and velocity changes occur so rapidly that displacements between successive collisions were not visible under a microscope when Brown studied the phenomenon, but the resulting position after many collisions could be observed. This is shown in Figure 2.3. This was also understood by Einstein [40] and Smoluchowski [53] in their independent explanation of Brownian motion in the early twentieth century. In their description they used the atomistic ideas from the kinetic theory of gases, which therefore supported the existence of the particle structure of matter. If one considers successive measurements $r_1, r_2, ...$ of the position of a Brownian particle, the displacements are random due to the random nature of the collisions. So, the next position r_n only depends on the current position r_{n-1}, which yields a Markov process. Note however that this process occurs on a coarse-grained time scale with respect to the process describing the velocity evolution. Hence, Brownian motion can be described by different Markov processes, depending on the scale at which it is studied. This is a feature of many physical stochastic processes and in solving the problem of Brownian motion this will be exploited. An important remark is that both these processes are Markovian only by approximation. Collisions between particles are not instantaneous and therefore the velocity change can depend on earlier collisions, i.e. on earlier velocities. Therefore, the autocorrelation time τ_c of the velocity is nonzero, which gives rise to (weakly) correlated successive displacements [3].

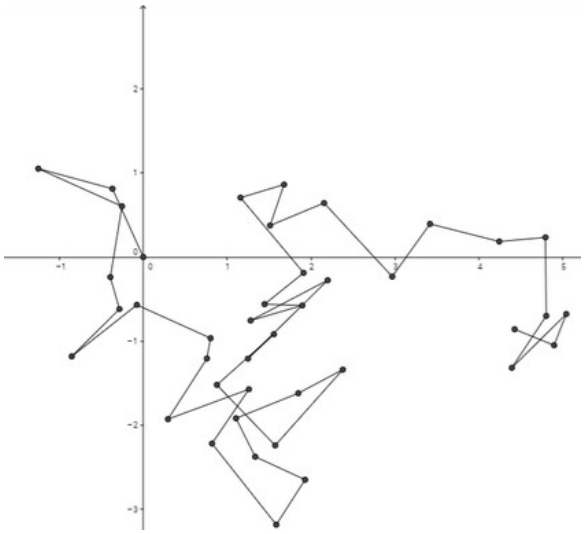

Figure 2.3: A possible two dimensional trajectory of a heavy mesoscopic particle, showing random net displacements after many collisions with its surrounding fluid particles. This figure has been extracted from Ref. [52].

2.3.1 Langevin's approach

Since the velocity $v(t)$ of a Brownian particle with mass m is subject to random fluctuations, one can write down a SDE to model its evolution. This is the Langevin equation, proposed by Paul

[11] Heavy with respect to the fluid particles.

Langevin in 1908 [6], which in one dimension is given by

$$m\frac{\mathrm{d}v(t)}{\mathrm{d}t} = -\alpha v(t) + F(t). \tag{2.21}$$

This is just Newton's second law for the evolution of the particles velocity. The right-hand side represents the forces exerted on the particle, which are given by a linear friction force with coefficient α and a random force $F(t)$ exerted by the random collisions. If no external force is applied, this yields, after dividing by the mass m of the particle,

$$\dot{v}(t) = -\gamma v(t) + f(t), \tag{2.22}$$

where $\gamma = \alpha/m$ is the damping coefficient and $f(t) = F(t)/m$ is the random force per unit mass m. This SDE has a general solution for an initial condition $v(0) = v_0$ given by

$$v(t) = v_0\mathrm{e}^{-\gamma t} + \mathrm{e}^{-\gamma t}\int_0^t \mathrm{e}^{\gamma t'} f(t')\mathrm{d}t'. \tag{2.23}$$

To solve this, the random force or noise $f(t)$ needs to be investigated further. The collisions with the molecules of the fluid occur approximately instantaneously, such that the noise fluctuates rapidly and is not correlated with any quantity at different times. Furthermore, one can assume $f(t)$ to be zero on average, as is usual for noise. Hence, the properties of the random force can be summarized as

$$\langle f(t)\rangle = 0, \quad \langle f(t)v(t')\rangle = 0, \quad \langle f(t)f(t')\rangle = G\delta(t-t'), \tag{2.24}$$

where G is a constant autocorrelation amplitude. Hence, the random force $f(t)$ is assumed to be white noise[12], with a Gaussian distribution.

The stochastic character of $f(t)$ makes that the velocity $v(t)$ is also a stochastic process. Since $\langle f(t)\rangle$ vanishes, the initial velocity decays exponentially on average: $\langle v(t)\rangle = v_0\exp(-\gamma t)$. For the second moment of $v(t)$, the autocorrelation function of $f(t)$ yields

$$\begin{aligned}\left\langle v^2(t)\right\rangle &= v_0^2\mathrm{e}^{-2\gamma t} + G\mathrm{e}^{-2\gamma t}\int_0^t\int_0^t \mathrm{e}^{\gamma(t'+t'')}\langle f(t')f(t'')\rangle\,\mathrm{d}t'\,\mathrm{d}t'',\\ &= \langle v(t)\rangle^2 + \frac{G}{2\gamma}\left(1-\mathrm{e}^{-2\gamma t}\right).\end{aligned} \tag{2.25}$$

To find an expression for the unknown constant G, we can take the limit of $t\to\infty$. In this limit, it can be expected that the system has reached thermal equilibrium, where the equipartition theorem from statistical mechanics can be applied [2]. In one dimension, this gives

$$\lim_{t\to\infty}\left\langle v^2(t)\right\rangle = \frac{G}{2\gamma} = \frac{k_BT}{m}, \tag{2.26}$$

where k_B is the Boltzmann constant and T is the temperature. This relates the amplitude of the autocorrelation function G and therefore the fluctuations to the damping coefficient γ. Hence, the noise can be expressed completely in terms of the damping and the temperature. Such a relation

[12] In reality, the collisions are not instantaneous. The autocorrelation function $\langle f(t)f(t')\rangle$ should therefore be a function of $|t-t'|$, sharply peaked, with a width equal to the time a collision takes (which is related to the autocorrelation time τ_c). This results in colored noise. Hence, assuming the noise to be white is equivalent to treating Brownian motion as a Markov process. This turns out to be a good approximation for $|t-t'| \gg \tau_c$.

turns out to exist for many systems and Eq. (2.26) is a simple version of the more general *fluctuation-dissipation theorem*, that holds for any system obeying detailed balance [54]. This theorem states that, for every process dissipating energy, there must occur a reverse process causing fluctuations. In the case of Brownian motion, the damping term $-\gamma v(t)$ tries to reduce the particles velocity, while the random force $f(t)$ causes it to remain nonzero. The resulting balance between these two processes is exactly the equilibrium Maxwell-Boltzmann distribution $P_{\mathrm{MB}}(v)$ [2]. Another very important example of the fluctuation-dissipation theorem is the earlier mentioned Johnson-Nyquist noise in resistors [38]. This originates from thermal fluctuations of electrons and ions, arising from dissipating electrical energy due to resistance.

Since the velocity $v(t)$ is stochastic, it is insightful to study its probability distribution $P(v,t|\,v_0)$. The fact that the noise $f(t)$ is Gaussian implies that $v(t)$ is Gaussian too [3], so it is completely determined by its first two moments that were calculated above. The quadratic deviation or *variance* is given by

$$\left\langle (\Delta v(t))^2 \right\rangle = \left\langle v^2(t) \right\rangle - \langle v(t) \rangle^2 = \frac{k_B T}{m} \left(1 - \mathrm{e}^{-2\gamma t}\right), \tag{2.27}$$

where Eq. (2.25) is used for $\langle v^2(t) \rangle$ and Eq. (2.26) for G. Plugging in this expression and the expectation value $\langle v(t) \rangle$ in a general Gaussian form yields

$$P\left(v,t|\,v_0\right) = \left\{ \frac{m}{2\pi k_B T \left[1 - \exp(-2\gamma t)\right]} \right\}^{1/2} \exp\left\{ -\frac{m\left[v - v_0 \exp(-\gamma t)\right]^2}{2k_B T \left[1 - \exp(-2\gamma t)\right]} \right\}. \tag{2.28}$$

Taking again the limit of $t \to \infty$, the Maxwell-Boltzmann distribution $P_{\mathrm{MB}}(v)$ is obtained. This distribution is known to be the equilibrium velocity distribution of a (one-dimensional) gas, so this is a useful validation of this method.

For the position $r(t)$ of the particle, a similar calculation can be performed by integrating all expressions for the velocity in time. The details will not be shown, but there is one important result that should be mentioned. For sufficiently long times ($t \gg 1/\gamma$), the mean square displacement is given by

$$\left\langle (\Delta r(t))^2 \right\rangle = \frac{2k_B T}{\gamma m} t = 2Dt, \tag{2.29}$$

where D is the diffusion coefficient. This result was derived by Einstein in 1905 [40]. In the same long time limit, one can obtain an expression for the probability distribution $P(r,t|\,v_0,r_0)$ of the particle's position, if it is also assumed to be Gaussian, as

$$P(r,t|\,v_0,r_0) = (4\pi D t)^{-1/2} \exp\left[-\frac{(r - r_0 - v_0/\gamma)^2}{4Dt} \right]. \tag{2.30}$$

This is exactly the solution of a one-dimensional diffusion equation

$$\frac{\partial P(r,t)}{\partial t} = D \frac{\partial^2 P(r,t)}{\partial r^2}, \tag{2.31}$$

with diffusion coefficient D, which clarifies the name for the constant D.

2.3.2 Fokker-Planck equations for Brownian motion

In Langevin's treatment of Brownian motion, the earlier discussed methods for stochastic systems, like the master equation or the Fokker-Planck equation, were not applied at all. The reason for this is that Langevin's approach is physically very insightful and also gives a more concrete view on the problem. Here, Brownian motion will be investigated briefly using Fokker-Planck equations, to compare both methods. First, the process is studied at the (finer) time scale on which the velocity of the particle can be described by a Markov process. Consider the Langevin equation without a random force $f(t)$, so there is only a linear damping given by $-\gamma v$. Through Eq. (2.18), the first Fokker-Planck moment is obtained as

$$A(v) = \frac{\partial}{\partial t}\langle \Delta v \rangle = -\gamma v. \tag{2.32}$$

This clarifies the name of this first moment, as it corresponds to a drift or damping in this physical process. For the second Fokker-Planck moment, it is known that $B(v) > 0$, hence it is taken to be a constant B_0, which is reasonable for small velocities. Filling in these moments in Eq. (2.17) gives the Fokker-Planck equation for the evolution of the probability distribution for the velocity of a Brownian particle

$$\frac{\partial P(v,t)}{\partial t} = \gamma \frac{\partial}{\partial v}[vP(v,t)] + \frac{B_0}{2}\frac{\partial^2 P(v,t)}{\partial v^2}. \tag{2.33}$$

To find an expression for the constant B_0, recall that the equilibrium distribution $P_{\text{eq}}(v)$ for the velocity v of a particle (in an ideal gas) is given by the Maxwell-Boltzmann distribution $P_{\text{MB}}(v)$. Substituting this distribution in Eq. (2.33) yields $B_0 = 2\gamma k_B T/m$, which is the same expression as (2.26) that was found for the autocorrelation amplitude G via the Langevin approach. Eq. (2.33) now reduces to

$$\frac{\partial P(v,t)}{\partial t} = \gamma \left\{ \frac{\partial}{\partial v}\left[vP(v,t)\right] + \frac{k_B T}{m}\frac{\partial^2 P(v,t)}{\partial v^2} \right\}, \tag{2.34}$$

which is a linear Fokker-Planck equation corresponding to the Ornstein-Uhlenbeck process, that has a Gaussian stationary distribution. From Eq. (2.34), one can directly derive that the moments of $v(t)$ correspond to the expressions found by Langevin's method. Also, the probability distribution $P(v,t|\, v_0)$ in Eq. (2.28) is the solution to this Fokker-Planck equation.

Looking at the coarser description, in which the position of the Brownian particle constitutes a Markov process, one can also write down a Fokker-Planck equation. For convenience, the initial position and velocity of the particle are taken to be zero, hence this is the no-drift case. Since the problem is now symmetric and independent of the starting point, one can take $A(r) = 0$, $B(r) = \text{const.} = B_1$ [3], yielding

$$\frac{\partial P(r,t)}{\partial t} = \frac{B_1}{2}\frac{\partial^2 P(r,t)}{\partial r^2}, \tag{2.35}$$

as the Fokker-Planck equation for the probability distribution of the particle's position. This is similar to the diffusion equation (2.31) with diffusion coefficient $D = B_1/2$. So, for $r_0 = v_0 = 0$, it also has the same solution as found by Langevin's method, given by Eq. (2.30) .

From the analysis above, it seems that Langevin's approach is equivalent to the Fokker-Planck equation. However, this is not entirely the case. To calculate the moments of $v(t)$ from the Langevin equation, $f(t)$ was assumed to be Gaussian white noise in Eq. (2.24). This allowed us to calculate only up to the second moment of $v(t)$, while the Fokker-Planck equation determines the whole stochastic process $v(t)$. It can be shown that, see Ref. [3], the Langevin equation with Gaussian

white noise with an amplitude G represents the same Markov process $v(t)$ as the Fokker-Planck equation in Eq. (2.33), if $B_0 = G$. Hence, under these conditions for the noise, both descriptions are equivalent.

2.3.3 General Langevin approach

The reason that Langevin's treatment of Brownian motion is so succesful is that it is physically very intuitive for describing the fluctuations that lead to the particle's displacement. In fact, this method is used to model the effect of fluctuations in many physical systems. It can be used for almost any dynamical system described by a SDE of the form (2.2). To see how this can be done, it is useful to write down a general formulation of the Langevin approach. Consider a physical system with known macroscopic behavior, that exhibits fluctuations. To find the effect of these fluctuations, one should

1. Find the macroscopic EoM of the system, which are deterministic.
2. Add a random force (or noise) $\eta(t)$ to the EoM, which is assumed to be white, with autocorrelation amplitude Ξ.
3. Find an expression for the autocorrelation amplitude Ξ in terms of observables in the system. This can be done by obtaining the stationary solution and fitting it to results known from equilibrium statistical mechanics, or via other methods.

The Langevin equation (2.22) can be generalized by also including external forces $F_{\text{ext}}(t)$ like gravity, which usually appear in the equation as the derivative $V'(r)$ of some external potential. Another generalization can be obtained by using colored noise, resulting in a non-Markovian process and a much more involved analysis [55]. Brownian motion and the Langevin equation turn out to appear in a lot of systems, see Ref. [56]. A few of these applications will be discussed in Section 2.4.2.

Although Langevin's method is more concrete and intuitive than the Fokker-Planck equation, it faces some difficulties in the nonlinear case. By assuming that $\langle \eta(t) \rangle = 0$, a linear Langevin equation reduces to the deterministic macroscopic EoM after averaging. Now, consider a system with an observable $Y(t)$ obeying a deterministic EoM $\dot{Y} = C(Y,t)$ for some nonlinear function $C(Y,t)$, to which a noise term $\eta(t)$ is added to account for fluctuations,

$$\dot{Y} = C(Y,t) + \eta(t). \tag{2.36}$$

Even if one assumes the noise $\eta(t)$ to have a vanishing expectation value, the macroscopic EoM is not recovered after averaging this equation, since $\langle C(Y,t) \rangle \neq C(\langle Y \rangle, t)$ in general. This also means that in determining $\langle Y \rangle$, the higher moments of $\eta(t)$ are required, which are usually unknown or fixed by making assumptions for its PDF. Eq. (2.36) is a *quasilinear* Langevin equation, since the noise $\eta(t)$ is still additive. Taking $\eta(t)$ to be Gaussian white noise with autocorrelation amplitude Ξ, this equation can be shown, see Ref. [3], to be equivalent to a quasilinear Fokker-Planck equation

$$\frac{\partial P(y,t)}{\partial t} = -\frac{\partial}{\partial y}\left[C(y,t)P(y,t)\right] + \frac{\Xi}{2}\frac{\partial^2 P(y,t)}{\partial y^2}, \tag{2.37}$$

for a realization $y(t)$ of $Y(t)$. The Fokker-Planck moments can usually be determined from fluctuation data and using Eq. (2.18). Hence, we can now pose a similar conclusion for the general Langevin approach as for the specific Brownian case. If the noise $\eta(t)$ is Gaussian and white, the

solution of the SDE (2.36) is a Markov process $\{Y(t)\}$, for which the PDF $P(y,t)$ satisfies the associated Fokker-Planck equation (2.37). Therefore, both descriptions are equivalent in this case.

The completely nonlinear Langevin equation is given by

$$\dot{Y} = C(Y,t) + D(Y,t)\eta(t), \tag{2.38}$$

for some nonlinear functions $C(Y,t)$ and $D(Y,t)$. Here, the noise term is multiplicative, which leads to much more difficulties. Luckily, this can be reduced to the quasilinear case via some transformations [3]. The corresponding Fokker-Planck equation is then given by

$$\frac{\partial P(y,t)}{\partial t} = -\frac{\partial}{\partial y}\left[C(y,t)P(y,t)\right] + \frac{\Xi}{2}\frac{\partial}{\partial y}\left\{D(y,t)\frac{\partial}{\partial y}\left[D(y,t)P(y,t)\right]\right\}. \tag{2.39}$$

There is however a problem of interpretation for Eq. (2.38). The noise $\eta(t)$ takes a random value at an instantaneous time t, causing a sudden jump in $\dot{Y}$, that affects the observable $Y(t)$. Hence, at time t, the value of $Y(t)$ and consequently $D(Y(t),t)$ are not determined yet. Eq. (2.38) does not specify if one should take for $Y(t)$ in $D(Y(t),t)$ its value before or after the jump, or the mean of these. This results in multiple Fokker-Planck equations, which have different solutions. This interpretation issue was studied by both Stratonovich [57] and Itô [58], who each opted for a different choice. Stratonovich proposed to take the mean value of $Y(t)$ before and after the jump. This allows for the usual transformation of variables, resulting in a Fokker-Planck equation of the form (2.39). It is proven that this choice is appropriate in the limit of $\tau_c \to 0$, which is the white noise limit [59]. However, the autocorrelation time cannot be exactly equal to zero, to prevent an infinitely sharp $\delta-$peak for the correlations. The Itô interpretation, on the other hand, which takes the value of $Y(t)$ before the jump, is only valid for white noise with $\tau_c = 0$. This interpretation is preferred by mathematicians, but it does not allow for a simple transformation to a quasilinear equation. The corresponding Fokker-Planck equation is not given by Eq. (2.39), but takes the form

$$\frac{\partial P(y,t)}{\partial t} = -\frac{\partial}{\partial y}\left[C(y,t)P(y,t)\right] + \frac{\Xi}{2}\frac{\partial^2}{\partial y^2}\left[D^2(y,t)P(y,t)\right]. \tag{2.40}$$

For constant $D(y,t)$, i.e. additive noise, both interpretations result in the same Fokker-Planck equation (2.37) after rescaling Ξ. An example of where Itô's choice is appropriate is for decay processes. The master equation for such a stochastic process is given by Eq. (2.10), which describes the evolution of the probability $P(N,t)$ that there are N radioactive nuclei at time t. This probability is proportional to the number of nuclei N before the jump, which is exactly what Itô proposed.

In the treatment of Langevin's approach, the source of the fluctuations was never considered. In dynamical systems, noise can be separated in two general types[13]. There exist fluctuations that are added to the system by applying some external random force, which is called *external* noise. When this noise is turned off, the system is governed by a deterministic equation $\dot{Y} = C(Y,t)$. External noise often occurs in engineering problems and electrical circuits, but also in external effects on population growth, like the weather. The other type of fluctuations is *internal* noise. As the name suggests, this is a property of (parts of) the system, which cannot be turned off. Therefore, it is not possible to find a deterministic equation that governs the system without noise. As the general Langevin approach starts from a deterministic EoM, it does not work for (nonlinear) systems with

[13]Note that this distinction is completely separate from the additive or multiplicative character of the noise. This is determined by the form of the noise coupling $D(Y,t)$, which relates the noise to other observables. The source of the noise determines if it is external or internal.

internal noise. Nevertheless, it is possible to write down a SDE for such a system in the Langevin form (2.2), only without a clear distinction between a deterministic and noise contribution. For example, $C(Y,t)$ could already include internal noise effects, which in the small noise limit reduces to the deterministic evolution. It is not decided if the Itô and Stratonovich interpretation each correspond to a kind of noise, which would only matter if the noise is multiplicative, as stated earlier. Usually, external noise is approximately white, allowing for both interpretations, depending on the assumptions for the autocorrelation time τ_c. Also, there are examples of processes with internal noise, like the decay process, chemical reactions, emission processes and diseases in population growth, where Itô's choice seems more appropriate.

2.4 Stochastic approach for complex systems

Brownian motion and other examples like radioactive decay and magnetization already showed that a stochastic approach to physical systems can be very useful. However, the techniques described above are not restricted to physical applications. The N-particle system that was introduced at the beginning of this section can be generalized to any dynamical system consisting of many interacting agents, which is generally called a *complex system*. The microscopic description of such a system suffers from the same difficulties as the N-particle system. The amount and interaction of the agents give rise to a large number of unknown and uncontrollable variables, that can be reduced by using the same stochastic approach [60]. This results in the familiar noise effects in the system on a mesoscopic level, which also restrict the predictability due to their random nature. Hence, the ideas described in Section 2.1.1 can be used in many complex dynamical systems to study their (nonlinear) behavior in terms of stochastic processes. It is therefore not surprising that the Langevin approach and other stochastic methods like the Fokker-Planck equation are, next to previous examples, also useful for other (non)physical complex systems. Here, some of their applications are studied in short, but first a few useful tools for analyzing the behavior of dynamical systems are discussed.

2.4.1 Dynamical systems analysis

The *phase space* Γ of a (stochastic) dynamical system consists of all possible microscopic states that the system can occupy [61]. It corresponds[14] to the state space S of a stochastic process $\{Y(t)\}$, if $\{Y(t)\}$ is the process that describes the evolution of all canonical variables in the complex system. Every possible state is represented by a *phase point*. For the N-particle system, a phase point is given by $(\boldsymbol{r}^N, \boldsymbol{p}^N)$, where $\boldsymbol{r}^N = \{\boldsymbol{r}_1(t), ..., \boldsymbol{r}_N(t)\}$ and $\boldsymbol{p}^N = \{\boldsymbol{p}_1(t), ..., \boldsymbol{p}_N(t)\}$ represent, respectively, the coordinates and momenta of the N particles. Its phase space is therefore $6N$-dimensional, but in general Γ contains all degrees of freedom of the system. The time evolution of the variables $Y(t)$ can now be seen as a motion of the phase point along a *(phase) trajectory* $\{y(t)\}$. A trajectory $\{y(t)\}$ is a solution of the EoM of the system, for an initial condition $y(t_0) = y_0$. In the deterministic case, the EoM are given by ODEs that usually have a unique solution for any initial condition y_0 [37]. This implies that different trajectories cannot intersect, since otherwise their uniqueness would be violated. Due to the random fluctuations in stochastic systems, their EoM are given by SDEs [4]. As explained in Section 2.1.1, a solution $\{Y(t)\}$ is a stochastic process since it is a functional of the noise $\eta(t)$. Therefore, the solution is not a uniquely determined trajectory in phase space, but it is subject to randomness, which allows trajectories to intersect. Only for a noise realization $\{h(t)\}$, the EoM reduce to ODEs, and the process follows a unique trajectory $\{y(t)\}$. This is an important difference between deterministic and stochastic systems, that will also appear in the path integral

[14] The state space can also correspond to a part of the phase space, if not all degrees of freedom are included in the stochastic process $\{Y(t)\}$.

approach in Section 3. This distinction is illustrated in Figure 2.4, in which the black line is the trajectory of a two-dimensional deterministic system, governed by some ODEs. The red and blue trajectories, fluctuating around the black line, are solutions of SDEs given by the same ODEs with some external noise. These trajectories are not the same and can even intersect, since they are solutions of different SDEs due to a different realization of the noise $\eta(t)$.

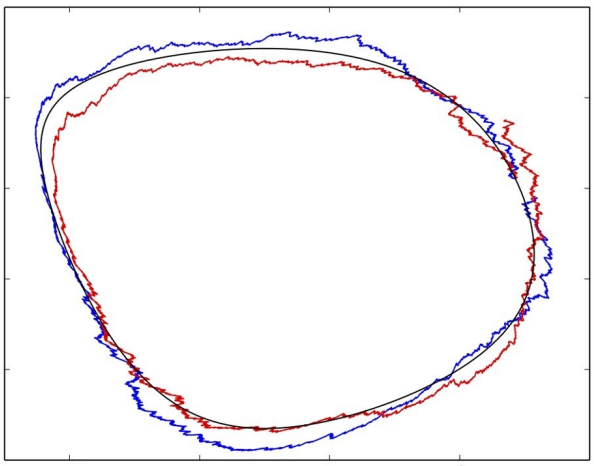

Figure 2.4: A phase portrait of a two-dimensional nonlinear system. The black trajectory represents a solution of the corresponding ODEs. The red and blue lines are solutions of SDEs, that are obtained from the ODEs by adding noise, which results in trajectories fluctuating around the solution of the ODEs. These trajectories are distinct, since the noise has a different realization for each solution of the SDEs. This figure has been extracted from Ref. [62].

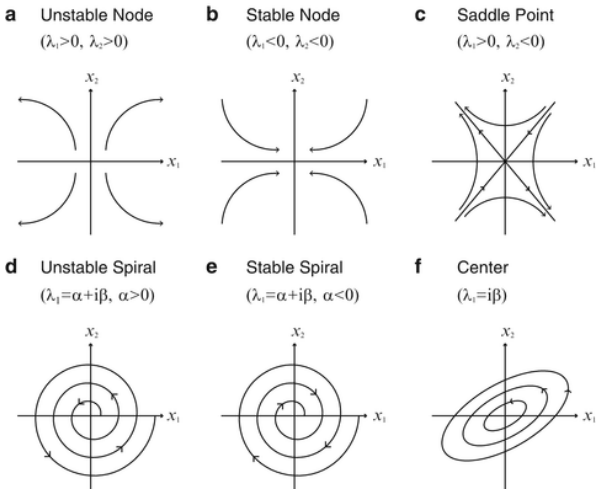

Figure 2.5: Classification of fixed points x^* in a two-dimensional dynamical system with variables x_1, x_2. Note that this figure does not contain all possible fixed points. The eigenvalues of the Jacobian $\mathcal{J}(x^*)$, λ_1 and λ_2, completely determine the character of the fixed point. For all upper cases, the eigenvalues are real, while for the lower cases they are complex. The real part determines the stability. This figure has been extracted from Ref. [63].

If all n canonical variables of a stochastic complex system are contained in $Y(t)$, then the phase space distribution function $\rho(y,t)$ determines the probability of the system to be in an infinitesimal part $\mathrm{d}^n y = \mathrm{d}\Gamma$ of its phase space. This $\rho(y,t)$ is exactly equivalent to the PDF $P(y,t)$ of the stochastic process $\{Y(t)\}$, so it will be written as $P(y,t)$ from now on. If the system is in equilibrium, the partial time derivative of $P(y,t)$ vanishes, resulting in a stationary phase space distribution that is equivalent to the equilibrium distribution $P_{\mathrm{eq}}(y)$ of the stochastic process [5].

Now that the concept of phase space is understood, one can look at interesting features of the evolution of the system. In general, the EoM of a dynamical system can be written as $\dot{y} = g(y)$, for some function $g(y)$. Note that $y \in \mathbb{R}^n$, since it contains all n variables of the system, and that $g(y) : \mathbb{R}^n \to \mathbb{R}^n$ also contains the noise if the system is stochastic. If $g(y^*) = 0$ for a point y^* in the phase space, then the system has a vanishing time evolution at that point. Therefore, y^* is called a *fixed point*. A fixed point y^* is attracting if all trajectories starting in its neighborhood approach y^* for $t \to \infty$. If the neighborhood condition is dropped, y^* is globally attracting. If all trajectories starting in the neighborhood of y^* also remain close to it for all time, y^* is called Lyapunov stable. If it is both attracting and Lyapunov stable, it is called a stable fixed point. If it is neither attracting nor Lyapunov stable, y^* is called unstable. A further classification of the system can be done by

qualitatively analyzing its *phase portrait*, which is a plot of trajectories in the corresponding phase space like in Figure 2.4, that can be found directly from properties of $g(y)$. This analysis is done extensively in Ref. [61], so only the most important features are mentioned here.

It is insightful to study the trajectories of a (nonlinear) system near a fixed point y^*. To do this, one can linearize $\dot{y} = g(y)$ around y^*, yielding

$$\dot{y} = \mathcal{J}(y^*)(y - y^*), \text{ where } \mathcal{J}(y^*) = \left.\frac{\partial g_i}{\partial y_j}\right|_{y=y^*} \tag{2.41}$$

is the Jacobian matrix evaluated at the fixed point, with $i, j = 1, ..., n$. This linearized system can be studied by performing a linear stability analysis. This is done by determining the eigenvalues of $\mathcal{J}(y^*)$. Depending on the nature[15] of these eigenvalues, the behavior of the system around y^* is different. For real eigenvalues, the fixed points are nodes or saddle points, while for complex eigenvalues, they are spirals or centers. For a two-dimensional system, these different cases are shown in Figure 2.5. The Hartman-Grobman theorem [64] states that if no eigenvalue is purely imaginary, the system's behavior is topologically equivalent to the behavior of its linearization, near the fixed point. Fixed points for which the eigenvalues of the Jacobian have nonzero real part are called *hyperbolic*. Hence, in these cases, the linearization procedure does not qualitatively change the system and its trajectories near the fixed point, which is very useful for a stability analysis.

Other interesting features of a phase portrait are closed trajectories, which are periodic solutions to the EoM. An example of a closed trajectory is the black trajectory shown in Figure 2.4. Isolated and closed trajectories are called *limit cycles*, isolated meaning that trajectories in its neighborhood are not closed[16]. Hence, they spiral either towards or away from the limit cycle, giving rise to stable, unstable and half-stable limit cycles. If a stable limit cycle exists, then the system can show self-sustained oscillations [61].

Until now the function $g(y)$ was taken to be fixed, and only the evolution of the variable(s) y was considered. When parameters in a complex dynamical system are varied, i.e. $g(y)$ is altered, the topological structure of the phase portrait can change. Such a change is called a *bifurcation* Examples of a bifurcation are a change in the number or stability of fixed points or closed orbits. Bifurcations can be divided into two categories. Local bifurcations happen in the neighborhood of fixed points or closed orbits. Examples of these include the creation or destruction of fixed points in saddle-node, transcritical or pitchfork bifurcations, which all have in common that one eigenvalue of $\mathcal{J}(y^*)$ is zero [61]. Hopf bifurcations, which occur when a stable spiral becomes unstable and surrounded by a limit cycle, are also local. There are also global bifurcations, which are not confined to a small neighborhood around a fixed point. Examples of these are saddle-node bifurcations of cycles, and homoclinic bifurcations where a saddle point collides with a limit cycle.

All tools and concepts discussed above are useful for any kind of dynamical system, either deterministic or stochastic, governed by an EoM of the form $\dot{y} = g(y)$. Especially bifurcations are insightful, since they describe the effect of a change in parameters on the behavior of the system, in terms of the phase portrait. These parameters can however be varied in a controlled way. The noise in a stochastic system changes in a random way and consequently $g(y)$ also varies randomly. Hence, next to (deterministic) bifurcations, it is also interesting to study how (much) a stochastic system

[15] The eigenvalues can be real (positive or negative), complex or purely imaginary.

[16] This implies that limit cycles do not exist in linear systems, since then any multiple of a periodic solution is also periodic.

is affected by noise. This can even give rise to the same kind of qualitative changes in the phase portrait as happens for bifurcations. Since these changes are caused by random noise instead of varying parameters, they are called *noise-induced transitions* [65].

Sometimes it is difficult to tell whether a system is stochastic and shows random behavior due to fluctuations, or whether it is just deterministic but shows chaotic behavior. Chaos can be loosely defined as an extreme dependence on initial conditions [61]. Suppose that two trajectories in phase space start at phase points x_0 and $x_0 + \delta(0)$. If their separation at time t is given by $|\delta(t)| = \mathrm{e}^{\lambda t}|\delta(0)|$, then the trajectories separate exponentially fast with Lyapunov exponent λ [61]. This is schematically shown in Figure 2.6. If the phase space is n-dimensional, λ is an n-dimensional vector. The largest entry of this Lyapunov exponent vector is defined by

$$\lambda_{\max} = \lim_{t\to\infty} \lim_{|\delta(0)|\to 0} \frac{1}{t} \log \frac{|\delta(t)|}{|\delta(0)|}. \tag{2.42}$$

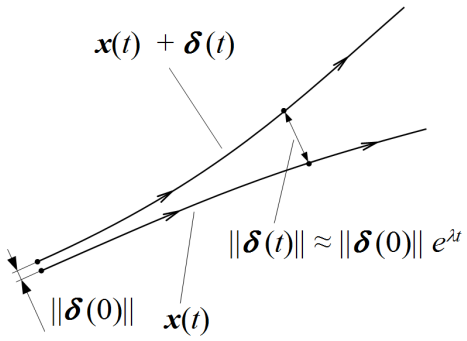

Figure 2.6: Two trajectories in a two-dimensional phase space, separated by a distance $|\delta(0)|$ at $t = 0$. If at time t their separation is given by $|\delta(t)| = \mathrm{e}^{\lambda t}|\delta(0)|$, then λ is the Lyapunov exponent. Its maximal component $\lambda_{\max}$ can indicate chaotic behavior in the system. This figure has been extracted from Ref. [66].

If $\lambda_{\max} > 0$, there is a direction in which the separation $\delta(t)$ grows exponentially. So, the trajectories starting with separation $\delta(0)$ at $t = 0$, separate exponentially fast in this direction, indicating an extreme dependence of the behavior on initial conditions. Usually, this implies chaotic behavior. If $\lambda_{\max} \leq 0$, none of the components of the Lyapunov exponent are positive. Hence, there is no direction in which the trajectories separate exponentially fast, i.e. they stay relatively close together. In this case the systems behavior is therefore not chaotic.

Now the theory for analyzing dynamical systems is set up properly, it can be applied to study complex systems. In the next section, some of the tools discussed above, together with the stochastic methods from Section 2.1 and 2.2, are used to describe the behavior of some stochastic complex systems. To get an idea of the wide range of applicability of these methods, both physical and nonphysical examples will be discussed.

2.4.2 Applications of stochastic methods in complex systems

From the general Langevin approach, as discussed in Section 2.3.3, it is clear that it can model several stochastic processes in physics, as long as the macroscopic EoM can be written as SDEs in the form of Eq. (2.2) and the noise is external. Again, this can be generalized to any complex system with this kind of EoM. A first physical application of Langevin's method is the $RLC-$circuit. The dynamics of the magnetic flux ϕ through the interior of such a circuit are governed by

$$C\ddot{\phi} + \frac{RC}{L}\dot{\phi} + \frac{\phi}{L} = I_f(t), \text{ where } \langle I_f(t)\rangle = 0, \ \langle I_f(t)I_f(t')\rangle = \frac{2RCk_BT}{L}\delta(t-t'). \tag{2.43}$$

Clearly, this is a Langevin equation for a potential $U(\phi) = \phi^2/2L$ [67], where the fluctuating current $I_f(t)$ arises from the thermal or Johnson-Nyquist noise [38]. Note that in this case the fluctuations

are fully determined by the temperature T, the resistance R, the capacitance C and the inductance L. A similar Langevin equation appears in so-called superconducting quantum interference devices (SQUIDs) [68]. In a superconducting material, the bosonic Cooper pairs are condensed into the same quantum state, resulting in a wavefunction that extends beyond the material. When bringing two superconductors close together, the tails of their wavefunctions can spatially overlap in the vacuum between them. This overlap gives rise to a current without any applied voltage, which is called the *Josephson effect* [69]. This effect also appears when two superconductors are connected by a weak link, called a *Josephson junction*, which is a non-superconducting material. It can be represented by a RLC-circuit, since the weak link acts like a resistor, a capacitor and a nonlinear element in parallel. It is worth knowing that both saddle-node and homoclinic bifurcations occur in Josephson junctions [61].

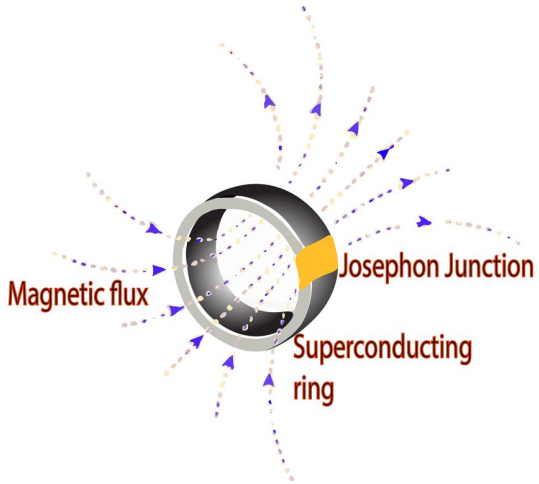

Figure 2.7: An illustration of a superconducting ring connected by a non-superconducting weak link, which is a Josephson junction, in a magnetic field. If the temperature $T < T_c$, the magnetic flux is trapped inside the ring and quantized in units of $\phi_0 = hc/e$. The flux can escape through the weak link, which is measured by a SQUID through a voltage difference. This figure has been extracted from Ref. [70].

Now consider a ring of superconducting material with a weak link built in, yielding a Josephson junction, like in Figure 2.7. If a magnetic field is applied perpendicular to the ring and the temperature T is brought below the critical temperature T_c of the material, the magnetic flux is trapped in the interior of the ring. Furthermore, the amount of flux in the interior is quantized in units of the flux quantum $\phi_0 = hc/e$. However, the flux can escape in multiples of ϕ_0 through the weak link. This principle is used in SQUIDs to measure very small amounts of flux up to the flux quantum, via a resulting voltage difference. The escaping flux results in a fluctuating current $I_f(t)$. Therefore, the dynamics of the magnetic flux inside a SQUID obey a Langevin equation similar to Eq. (2.43), for a different potential $U(\phi)$ [71].

As a first well-known example of a complex system, the climate system is considered. Our climate is affected by many processes on several different spatio-temporal scales. Therefore, to describe its behavior, stochastic methods are required to model the influence of processes at small scales, such as weather fluctuations. There exist, for example, stochastic models of turbulence, where an external random force is added to the Navier-Stokes equations [72]. Another interesting phenomenon in the climate system is the observed transition between warm and cold phases, with a regularity of approximately 100,000 years. This is in phase with Milankovitch cycles, which are changes in radiation resulting from the varying orbital parameters of the Earth. In 1982, Benzi et al. [73] tried to relate these cycles by adding fluctuations to a climate model. If X is a change in temperature near an equilibrium point T_0, then one can write down the following Langevin equation

$$\frac{\mathrm{d}X}{\mathrm{d}t} = X - X^3 + B(t)\sin(\omega t) + \eta(t), \tag{2.44}$$

where $B(t)$ is the forcing amplitude, ω is the frequency of the Milankovitch cycle and $\eta(t)$ is some Gaussian white noise with autocorrelation amplitude σ. The first two terms in the SDE arise from

a simple climate model including only feedback due to radiation. For a small and slowly varying force $B(t) = B\cos(\omega t)$, there is a resonant range for σ, in which the small periodic perturbation $B(t)$ synchronizes with the random behavior caused by the noise $\eta(t)$. This yields an amplified periodic output, as can be seen in Figure 2.8. This mechanism is called *stochastic resonance*. It is counterintuitive, since the fluctuations cooperate with the system to enhance its periodic behavior.

Unfortunately, the simulated results of Eq. (2.44) showing stochastic resonance did not agree with observed temperature changes. This can however also be due to the simplistic climate model that was used. Nevertheless, the concept of stochastic resonance has become important in all kinds of complex systems. It can occur in any system containing a signal and white noise, in which the frequencies of the signal resonate with the corresponding noise frequencies, thereby increasing the signal-to-noise ratio. This can be technologically useful and stochastic resonance has found its applications in biology and in the earlier mentioned SQUIDs [75].

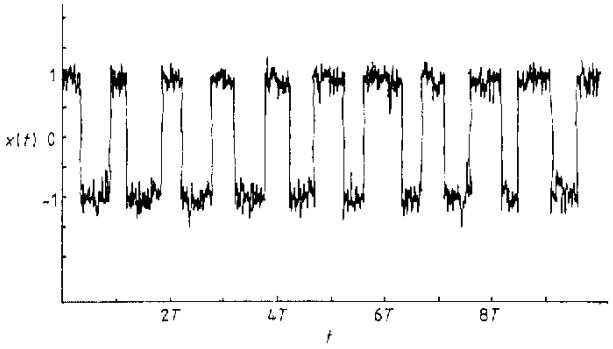

Figure 2.8: Numerical solution of a Langevin equation similar to Eq. (2.44), for small and slowly varying $B(t)$ and σ in the resonant range. This yields a large periodic output for $X(t)$. This figure has been extracted from Ref. [74].

It turns out that stochastic methods also appear in the nonphysical context of finance. In 1900, before Einstein, Smoluchowski and Langevin, Louis Bachelier was the first to give a mathematical description of Brownian motion [76]. He used this for modelling the stock market, which marked the birth of mathematical finance. More recently, it has been shown that the probability distribution of price changes on the foreign exchange market obeys a Fokker-Planck equation, which can be transformed to a Langevin equation with multiplicative noise in the Itô interpretation [77].

Most of the examples discussed above are Markovian by the assumption of the noise being white. As stated in Section 2.1.1, this usually holds only as an approximation. A class of non-Markovian stochastic processes that occur frequently in the study of populations are *branching processes* [78]. Consider an organism that multiplies by division. If a is the age of the organism, its probability to divide into two organisms during the next time interval $\mathrm{d}t$ is given by $\kappa(a)\mathrm{d}t$. This process continues and the main question is to determine the probability $P(n, t|\, q, 0)$ of having n organisms after a time t, given that there are q organisms at time $t = 0$. In general, this process is non-Markovian, since κ depends on the age a of the organism, so on its entire life or history. This is a simple model that does not include a probability of dying, but it already has a lot of applications. For example, the number of freely moving neutrons in a nuclear reactor can be modeled by a branching process. However, in this case, the process is Markovian, since κ is independent of the 'age' of the neutrons.

Another non-Markovian process occurs in the human body. In nerve circuits, neurons usually form a feedback loop, which is a path in a neural system from the input to its output, and back to its input. Since the propagation of neurons along the loop takes a finite amount of time, the evolution of neural activity depends on its present state, as well as on earlier states. This creates a neural delayed feedback system [60]. It is interesting to study the origin of fluctuations in these systems, and whether or not they suppress oscillatory behavior. A neural system that is relatively easy to

study experimentally is the pupil light reflex (PLR). This system contains a negative[17] feedback loop, from which a deterministic equation for the time evolution of the pupil area A can be derived [60]. The equation predicts a stable fixed point A^* that changes into an oscillation if the delay in the PLR is increased. This indicates a stable limit cycle, and therefore a Hopf bifurcation has occurred. Nevertheless, the predictions of the deterministic equation and this Hopf bifurcation do not agree with observations, which asks for the inclusion of a noise contribution. In the PLR, noise originates from *hippus*, which is a fluctuation of the pupil area occurring for a constant light flux. Hippus is colored noise, which seems to arise from neural noise, with an autocorrelation time of approximately one second. Adding this effect yields a better agreement with data, and also shows a noise-induced transition. The noise stabilizes the fixed point A^*, before it becomes unstable with a surrounding stable limit cycle for a larger delay. Hence, the noise postpones the initiation of oscillations in the pupil area.

As a last application of stochastic methods in complex systems, the Verhulst model is considered [79]. This already gives a glimpse towards the Lotka-Volterra equations, since it is a different model for studying population dynamics, but for only one species. For the population of a single species $N(t) \geq 0$, the Verhulst equation is given by

$$\dot{N} = \mu N - N^2. \tag{2.45}$$

This is essentially the logistic equation[18] [61], but with rescaled variables such that the quadratic term has unit coefficient. This nonlinear term models overcrowding due to limited resources. The coefficient μ is the growth rate, which is given by the difference between birth and death rates. For $\mu < 0$, the population obviously gets extinct, and so $N = 0$ is a stable fixed point. If $\mu > 0$, $N = 0$ becomes an unstable fixed point and a new stable fixed point is given by $N = \mu$. Therefore, μ can also be called the *carrying capacity*, which is the stable population size (in these units). This model thus shows a very simple bifurcation due to a change in μ.

In real populations, the growth rate is of course not a constant, but depends on environmental effects like the weather and diseases, which cause it to fluctuate. To incorporate this, the constant μ can be replaced by $\mu(t) = \langle\mu\rangle + \eta(t)$, which is a stochastic process with expectation value $\langle\mu\rangle$ and a Gaussian white noise $\eta(t)$ that has autocorrelation amplitude σ. Taking these fluctuations into account transforms Eq. (2.45) to the SDE

$$\dot{N} = \langle\mu\rangle N - N^2 + N\eta(t), \tag{2.46}$$

which is a nonlinear Langevin equation with multiplicative noise. This modification has profound effects. It turns out that the average population is not equal to $\langle\mu\rangle$, as one might expect, but slightly smaller. This effect becomes larger for increasing noise amplitude σ, until eventually the population faces extinction in its steady state for very large fluctuations.

To quantitatively analyze this behavior, it is useful to consider the Fokker-Planck equation for the probability distribution $P(N, t)$ corresponding to Eq. (2.46). Since this Langevin equation is nonlinear and has multiplicative noise, different Fokker-Planck equations can be derived, in either the Itô or the Stratonovich interpretation. First, the Itô interpretation will be considered. Then,

[17] An increase in light flux decreases the pupil area, and vice versa.

[18] Its discrete-time version, called the *logistic map*, actually shows exponentially diverging trajectories (i.e. a positive Lyapunov exponent) for certain values of μ, and therefore chaotic behavior [61].

the Fokker-Planck equation has the form of Eq. (2.40) and yields

$$\begin{aligned}\frac{\partial P(N,t)}{\partial t} &= -\frac{\partial}{\partial N}\left[\left(\langle\mu\rangle N - N^2\right)P(N,t)\right] + \frac{\sigma}{2}\frac{\partial^2}{\partial N^2}\left[N^2 P(N,t)\right], \\ &= \frac{\partial}{\partial N}\left\{\left[N^2 - \langle\mu\rangle N\right]P(N,t) + \frac{\sigma}{2}\frac{\partial}{\partial N}\left[N^2 P(N,t)\right]\right\},\end{aligned} \tag{2.47}$$

for the stochastic Verhulst model. By putting the left-hand side to zero, one finds that the stationary probability distribution is given by

$$P_{\text{eq}}(N) = cN^{2(\langle\mu\rangle/\sigma - 1)}e^{-2N/\sigma}, \quad \text{for } \frac{2\langle\mu\rangle}{\sigma} > 1. \tag{2.48}$$

The condition follows from the restriction of $P_{\text{eq}}(N)$ being normalizable, with finite normalization constant c [60]. The form of $P_{\text{eq}}(N)$ changes when $\sigma = \langle\mu\rangle$, at which $N = 0$ becomes the most probable population[19]. This is shown in Figure 2.9. The behavior of the population changes qualitatively due to the noise, which indicates a noise-induced transition. If the fluctuations become so large that $\sigma \geq 2\langle\mu\rangle$, the condition in Eq. (2.48) is violated and therefore $P_{\text{eq}}(N)$ does not have the given form. Instead, the population gets extinct and $P_{\text{eq}}(N) = \delta(N)$ is the stationary probability distribution, even though the growth rate is still positive. This is another transition due to the fluctuations, which can be called a noise-induced extinction.

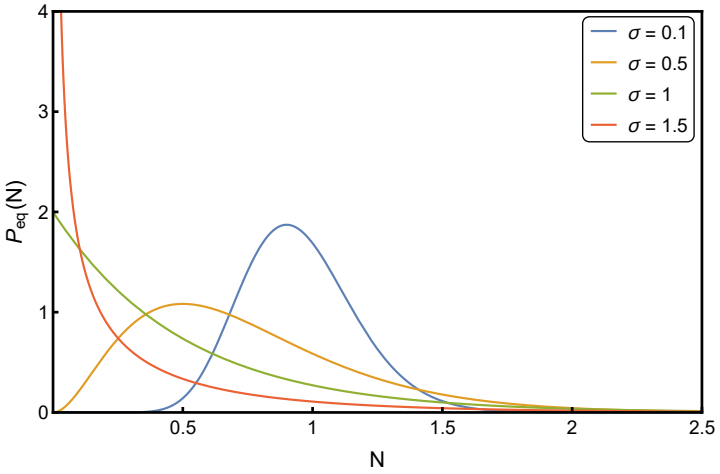

Figure 2.9: Plot of the stationary probability distribution $P_{\text{eq}}(N)$ of a stochastic Verhulst model, obtained from the Fokker-Planck equation in the Itô interpretation. The results are calculated for an average growth rate $\langle\mu\rangle = 1$ and multiple values of the noise autocorrelation amplitude σ. Even for small σ, $P_{\text{eq}}(N)$ already shows a right skewness, indicating an average population below $\langle\mu\rangle$. For $\sigma = \langle\mu\rangle$, where $N = 0$ becomes the most probable population, the form of $P_{\text{eq}}(N)$ suddenly changes, showing the noise-induced transition.

In the Stratonovich interpretation, the Fokker-Planck equation has the form of Eq. (2.39), which results in

$$\begin{aligned}\frac{\partial P(N,t)}{\partial t} &= -\frac{\partial}{\partial N}\left[\left(\langle\mu\rangle N - N^2\right)P(N,t)\right] + \frac{\sigma}{2}\frac{\partial}{\partial N}\left\{N\left[\frac{\partial}{\partial N}NP(N,t)\right]\right\}, \\ &= \frac{\partial}{\partial N}\left\{\left[N^2 - \langle\mu\rangle N\right]P(N,t) + \frac{\sigma}{2}N\frac{\partial}{\partial N}\left[NP(N,t)\right]\right\}, \\ &= \frac{\partial}{\partial N}\left\{\left[N^2 - \langle\mu\rangle N - \frac{\sigma}{2}N\right]P(N,t) + \frac{\sigma}{2}\frac{\partial}{\partial N}\left[N^2 P(N,t)\right]\right\}.\end{aligned} \tag{2.49}$$

[19] For $\sigma = \langle\mu\rangle$, $P_{\text{eq}}(N)$ is just exponential decay which takes its highest value for $N = 0$. For $2\langle\mu\rangle > \sigma > \langle\mu\rangle$, $P_{\text{eq}}(N)$ decays even faster, with an asymptote at $N = 0$.

Luckily, this equation has a stationary solution of the same form as Eq. (2.48) for the Itô case, after a transformation $\langle\mu\rangle \to \langle\mu\rangle + \sigma/2$. The normalizability condition is now given by $\langle\mu\rangle/\sigma > 0$, which is always satisfied for a positive average growth rate. The other stationary solution $P_{\text{eq}}(N) = \delta(N)$ holds only for $\langle\mu\rangle < 0$, i.e. on average there are more deaths than births. Hence, in the Stratonovich interpretation, the system does not show the noise-induced extinction for a positive growth rate, as in the Itô case. This demonstrates the difference between both interpretations and the important distinctions it can make in the qualitative behavior of dynamical systems. The other noise-induced transition, where $N = 0$ becomes the most probable population, does still occur in the Stratonovich case, but now at a noise amplitude $\sigma = 2\langle\mu\rangle$.

3 Functional approach to stochastic systems

To describe the evolution of an observable $Y(t)$ in a stochastic system, a general SDE (2.2) was introduced in Section 2.1. For an initial condition $Y(t_0) = y_0$, its solution is given by $Y(y_0, t, [\eta])$, which is a functional of the noise $\eta(t)$. So, due to its random nature, the SDE has a unique solution only for a noise realization $\{h(t)\}$. Analogously, random effects also appear in quantum phenomena, although here the fluctuations arise from the inherent unpredictability in quantum mechanics. To deal with this, a functional formalism called the *Feynman path integral* was developed in 1948 [8]. Later, it was realized that this formalism indeed relates quantum and stochastic processes [80]. This allowed functional methods to describe stochastic systems, which is especially useful for coupled nonlinear systems where a Fokker-Planck or Langevin's approach can break down. In fact, the first notion of a path integral appeared in 1921 in the work of Norbert Wiener, in his solution to Brownian motion [7]. This section will start with this intuitive introduction to path integrals. This idea is then generalized from a stochastic point of view and the relation with quantum mechanics is discussed. The connection between the functional formalism and SDEs will be used to derive the MSR formalism, which is the most important technique used in this work. This method is then applied to solve both a linear and nonlinear Langevin equation.

3.1 Path integrals for Brownian motion

In the (coarser) position description, the PDF $P(r,t)$ of a Brownian particle in one dimension at position r at time t is governed by a diffusion equation (2.31) with diffusion coefficient $D = k_B T/\gamma m$, as was noted in Section 2.3. This result was already derived by Einstein in his theory of Brownian motion [40], before Langevin proposed its solution. For an initial condition $r(0) = r_0$, or formally $\lim_{t\to 0} P(r,t) \to \delta(r - r_0)$, the diffusion equation is solved by

$$P(r,t|\, r_0) = \frac{1}{\sqrt{4\pi D t}} \exp\left[-\frac{(r-r_0)^2}{4Dt}\right]. \tag{3.1}$$

3.1.1 Wiener's approach

Inspired by the description of Brownian motion in terms of randomness, Norbert Wiener tried to give a mathematically rigorous description of the problem [7]. Instead of discussing Wiener's complete treatment, only his main results will be presented here, following the line of thought of Ref. [81].

For a one-dimensional Brownian particle, starting in $r(0) = 0$, the probability to find it in an interval $[A, B]$ at time t is given by

$$P\{r(t) \in [A,B]\} = \int_A^B P(r,t)\, \mathrm{d}r. \tag{3.2}$$

Wiener derived another expression for this probability. Before arriving in $[A, B]$, the particle

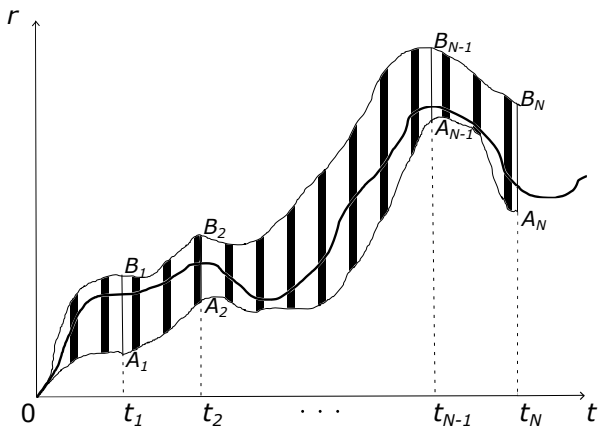

Figure 3.1: A possible trajectory of a Brownian particle, starting at $r(0) = 0$. At each time t_i, the particle traverses an interval $[A_i, B_i]$. The 'propagating' interval is depicted by the striped area.

traverses N intervals $[A_i, B_i]$ at times $t_i = i\Delta t$, where $\Delta t = t/N$. This time-slicing procedure is shown in Figure 3.1. In Section 2.3, we explained that successive observations $r(t_i) = r_i$ of the position of a Brownian particle can constitute a Markov process. Hence, by the Markov property (2.5), successive displacements are independent and $P\{r_i \in [A_i, B_i]\}$ only depends on the current position r_{i-1} through $\lim_{t\to t_{i-1}} P(r_i, t) \to \delta(r - r_{i-1})$. So, it is possible to write

$$\begin{aligned}
&P\{r(t_1) \in [A_1, B_1], r(t_2) \in [A_2, B_2], ..., r(t_N) \in [A_N, B_N]\} \\
&= P\{r(t_1) \in [A_1, B_1]\}\, P\{r(t_2) \in [A_2, B_2] \big| r_1\} ... P\{r(t_N) \in [A_N, B_N] \big| r_{N-1}\}, \\
&= \prod_{i=1}^{N} \int_{A_i}^{B_i} P(r_i, t_i |\, r_{i-1})\, \mathrm{d}r_i, \qquad (3.3) \\
&= \prod_{i=1}^{N} \int_{A_i}^{B_i} \frac{1}{\sqrt{4\pi D(t_i - t_{i-1})}} \exp\left[-\frac{(r_i - r_{i-1})^2}{4D(t_i - t_{i-1})}\right] \mathrm{d}r_i,
\end{aligned}$$

by inserting the Chapman-Kolmogorov equation (2.6) N times in the third line. Using this expression in the continuous time limit $N \to \infty$ (i.e. $\Delta t \to 0$), the probability that the particle passes through an infinite number of infinitesimal intervals $\mathrm{d}r_i$ is given by

$$\begin{aligned}
&\lim_{N\to\infty} \prod_{i=1}^{N} \exp\left[-\frac{(r_i - r_{i-1})^2}{4D(t_i - t_{i-1})}\right] \frac{\mathrm{d}r_i}{\sqrt{4\pi D(t_i - t_{i-1})}} \\
&= \lim_{N\to\infty} \exp\left[-\frac{1}{4D} \sum_{i=1}^{N} \left(\frac{r_i - r_{i-1}}{\Delta t}\right)^2 \Delta t\right] \prod_{i=1}^{N} \frac{\mathrm{d}r_i}{\sqrt{4\pi D\, \Delta t}}, \qquad (3.4) \\
&= \exp\left[-\frac{1}{4D} \int_0^t \dot{r}^2(t')\, \mathrm{d}t'\right] \prod_{t'=0}^{t} \frac{\mathrm{d}r(t')}{\sqrt{4\pi D\, \mathrm{d}t'}}.
\end{aligned}$$

This is essentially the probability of a particle following the trajectory $r(t')$. All trajectories $r(t')$ that start in $r(0) = 0$ and end up in $[A, B]$ at $t' = t$ are denoted by the set $\mathcal{C}[0, 0, [A, B], t]$. To calculate $P\{r(t) \in [A, B]\}$, one needs to sum the probabilities (3.4) of all trajectories in this set $\mathcal{C}[0, 0, [A, B], t]$. Since the trajectories are continuous, this yields an integral

$$P\{r(t) \in [A, B]\} = \int_{\mathcal{C}[0,0,[A,B],t]} \exp\left[-\frac{1}{4D} \int_0^t \dot{r}^2(t')\, \mathrm{d}t'\right] \prod_{t'=0}^{t} \frac{\mathrm{d}r(t')}{\sqrt{4\pi D\, \mathrm{d}t'}}. \qquad (3.5)$$

This expression should now be equivalent to Eq. (3.2). But here, instead of integrating the PDF of the final position $r(t)$ over the interval $[A, B]$, one integrates over all paths $r(t')$ that end up in $[A, B]$ at $t' = t$. Therefore, the integration over the set $\mathcal{C}[0, 0, [A, B], t]$ is called the *Wiener path integral* [81]. The exponential integrand together with the product measure is called the *Wiener measure*, which is usually denoted by $\mathrm{d}_W r(t')$. Hence, this approach makes use of a measure and integral over the *functional* space of all trajectories $r(t')$, which has infinite dimension by construction.

If the final position $r(t)$ is also fixed by setting $A = B = r_t$, all trajectories in the set $\mathcal{C}[0, 0, r_t, t]$ end up in r_t, as is shown in Figure. 3.2. Equating Eq. (3.2) and Eq. (3.5) for this case gives

$$\int_{\mathcal{C}[0,0,r_t,t]} \mathrm{d}_W r(t') = \frac{1}{\sqrt{4\pi D\, t}} \exp\left[-\frac{r_t^2}{4D\, t}\right], \qquad (3.6)$$

which is exactly the (conditional) PDF of a one-dimensional Brownian particle starting at $r(0) = 0$ and arriving at r_t at time t. This naturally shows the equivalence of both approaches.

Wieners solution makes use of the description of Brownian motion in terms of a stochastic process. Next to the Markov property, this particular process satisfies other conditions, which allows for the definition of a *Wiener process* [7]. The Wiener process is a continuous-time stochastic process, denoted by $W(t)$, that has the following properties [72]:

1) $W(0) = 0$, or $\lim_{t\to 0} P(w,t) \to \delta(w)$ for every realization $w(t)$.

2) It has independent increments: Future increments $W(s+t) - W(s)$ are independent of $W(u)$ for every $t, s \geq 0$, $u \leq s$.

3) The increments $W(s+t) - W(s)$ have a Gaussian distribution with average 0 and variance t.

4) $W(t)$ is almost surely continuous in t.

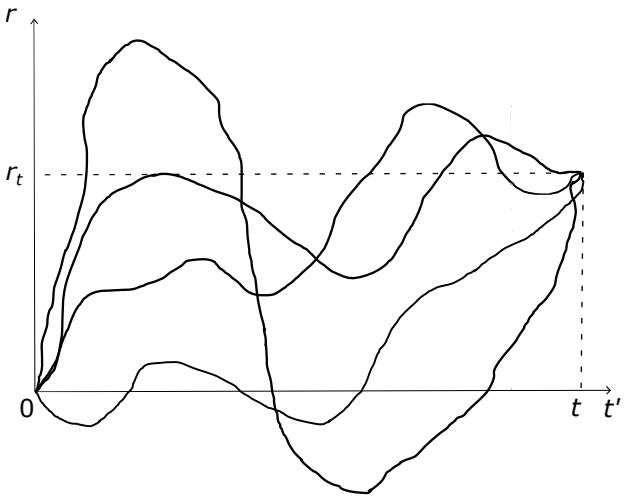

Figure 3.2: Different trajectories $r(t')$ of a one-dimensional Brownian particle, with fixed initial position $r(0) = 0$ and final position $r(t) = r_t$.

Taking $s = 0$ in property 3) directly results in a Gaussian PDF for $W(t)$ with average zero and variance t, as in the right-hand side of Eq. (3.6) for a one-dimensional Brownian particle with $D = 1$. The Wiener process is usually treated as a synonym for Brownian motion, while it actually is its mathematical generalization. For example, the independent increments in property 2) reduce to independent (successive) displacements in Brownian motion. Although defining the Wiener process seems more of a formality, it has an interesting connection to white noise. The time derivative of a Wiener process $\mathrm{d}W(t)/\mathrm{d}t$ is exactly equal to a Gaussian white noise process $\eta(t)$ that is delta correlated, as in Eq. (2.3). Integrating Gaussian white noise from time 0 to t results again in the Wiener process at time t. Due to this connection and its useful properties, the Wiener process has a lot of applications, both in fundamental and applied mathematics [82].

3.1.2 A functional approach to the Langevin equation

Wiener was the first to use path integrals to solve Brownian motion. Note however that he studied the problem in the position representation, which does not contain any noise $\eta(t)$, due to the coarser level of description. The diffusion equation (2.31) is therefore just a partial differential equation. Chandrasekhar [10] also applied functional methods to the problem of Brownian motion. He used them to solve the Langevin equation for the velocity of a Brownian particle. Just as for Wiener's approach, only the main results will be presented, following the line of thought of Ref. [83].

The Langevin equation (2.22) for Brownian motion has a general solution (2.23) given by

$$v(t) = v_0 \mathrm{e}^{-\gamma t} + \mathrm{e}^{-\gamma t} \int_0^t \mathrm{e}^{\gamma t'} f\left(t'\right) \mathrm{d}t', \tag{3.7}$$

for initial velocity $v(0) = v_0$ and damping coefficient γ. Instead of immediately specifying properties of the random force $f(t')$ to calculate moments of the velocity $v(t)$, as was done in Section 2.3, one can take a careful look at this general solution. Due to the integration over time, a solution $v(t)$ depends on the values of the noise $f(t')$ over the whole time interval $[0, t]$. Hence, $v(t)$ is a functional of $f(t')$ and can be denoted by $v(v_0, t, [f])$, just as was done for a general observable $Y(y_0, t, [\eta])$ governed by a SDE with noise $\eta(t')$. To relate this to Wiener's approach, one can think of a function $Y(y_0, t, \eta_0, \eta_1, ..., \eta_N)$ of $N + 3$ variables, with $\eta_i = \eta(t_i)$ and $t_i = i\Delta t = it/N$. From this time-slicing procedure, the functional $Y(y_0, t, [\eta])$ is then defined by the continuous time limit of this discretization, yielding

$$Y(y_0, t, [\eta]) = \lim_{N\to\infty} Y(y_0, t, \eta_0, \eta_1, ..., \eta_N). \tag{3.8}$$

Functional integration can be understood in a similar way, by taking the limit of $N \to \infty$ in the multidimensional integral of $Y(y_0, t, \eta_0, \eta_1, ..., \eta_N)$ over the $N+1$ variables η_i. However, this can lead to divergences. In the cases that are considered here, this is dealt with by introducing a *weighting functional* $\Phi[\eta]$ for the integration variables. Now, the functional integral $I[\eta]$ of a functional[20] $Y[\eta]$ over the function $\eta(t')$ can be written as

$$\begin{aligned} I[\eta] &= \lim_{N\to\infty} I(\eta_0, \eta_1, ..., \eta_N), \\ &= \lim_{N\to\infty} \int ... \int Y(\eta_0, \eta_1, ..., \eta_N)\Phi(\eta_0, \eta_1, ..., \eta_N) \prod_{i=0}^{N} \mathrm{d}\eta_i, \\ &= \int Y[\eta]\Phi[\eta]\, \mathcal{D}\eta(t'). \end{aligned} \tag{3.9}$$

Here, the functional measure $\mathcal{D}\eta(t')$ is defined as

$$\mathcal{D}\eta(t') = \lim_{N\to\infty} \prod_{i=0}^{N} \mathrm{d}\eta_i, \tag{3.10}$$

which accounts for all trajectories of the noise $\eta(t')$, for $t' \in [0, t]$. The functional integral $I[\eta]$ is again a functional, but now of $\eta(t)$. If the function $\eta(t')$ describes the possible trajectories $r(t')$ of a Brownian particle, the complete integration measure $\Phi[r]\,\mathcal{D}r(t')$ is exactly the Wiener measure $\mathrm{d}_W r(t')$. The Wiener path integral is therefore also a kind of functional integral. By the definition of $\mathrm{d}_W r(t')$ through Eq. (3.5), the weighting functional is then given by

$$\Phi[r] = \exp\left[-\frac{1}{4D}\int_0^t \dot{r}^2(t')\,\mathrm{d}t'\right], \tag{3.11}$$

where the normalization constant $\mathcal{N} = \left(\sqrt{4\pi D\,\mathrm{d}t'}\right)^{-1}$ is absorbed in $\mathcal{D}r(t')$. This is the *probability density functional* (PD$\mathcal{F}$) $\mathcal{P}[r]$ for the position of a Brownian particle. For a general random function $\eta(t)$, this can be understood as the continuum limit of a multivariate PDF[21]

$$\mathcal{P}[\eta] = \lim_{N\to\infty} P(\eta_0, \eta_1, ..., \eta_N), \tag{3.12}$$

[20] The dependence on initial condition y_0 and time t are disregarded from now on, for notational convenience.

[21] A PDF describes the probability distribution of one or more random variables, while the PD$\mathcal{F}$ describes the probability distribution of a random function. A PD$\mathcal{F}$ is therefore a functional generalization of a PDF.

as performed in Eq. (3.4) for a Brownian particle. The PD$\mathcal{F}$ $\mathcal{P}[\eta]$ is related to the PDF $P(\eta, t)$ via the transition probability $P(\eta, t|\, \eta_0, t_0)$. $P(\eta, t)$ is equal to $P(\eta, t|\, \eta_0, t_0)$, for an initial condition $P(\eta, t_0) = \delta(\eta(t_0) - \eta_0)$. Also, the transition probability can be written in terms of the PD$\mathcal{F}$ as a functional integral

$$P(\eta, t|\, \eta_0, t_0) = \int_{\eta(t_0)=\eta_0}^{\eta(t)=\eta} \mathcal{P}[\eta]\, \mathcal{D}\eta(t'). \tag{3.13}$$

In most cases, the weighting functional $\Phi[\eta]$ for a random function $\eta(t')$ is indeed given by its PD$\mathcal{F}$ $\mathcal{P}[\eta]$. Then, the functional integral in Eq. (3.9) reduces to a *functional average*, i.e. $I[\eta] = \langle Y[\eta] \rangle$, if $\mathcal{P}[\eta]$ is properly normalized[22]. This is the functional generalization of the expectation value in Eq. (2.1). It can be interpreted as the expected trajectory $\{y(y_0, t, [\eta])\}$ of a stochastic process $Y(y_0, t, [\eta])$, averaged over the random function $\eta(t)$. Although the normalization constant, given by the product over t' in Eq. (3.4) for $\mathcal{P}[r]$, is infinite in the continuum limit $\mathrm{d}t' \to 0$, moments with respect to the PD$\mathcal{F}$ are still well-defined [84]. Therefore, the normalization constant of a PD$\mathcal{F}$ is just denoted by $\mathcal{N}$, since it drops out when calculating moments and other correlation functions.

It might seem artificial to just plug a weighting functional in a functional integral to deal with divergences, but in fact this cannot be omitted. Going back to the Langevin equation, only integrating the random force $f(t')$ over time would imply that every noise value has an equal probability. In Section 2.3.1, the random force was assumed to be Gaussian white noise. Therefore, the Gaussian PDF should also be taken into account when integrating $f(t')$. To perform a functional integral over all trajectories $f(t')$, the PD$\mathcal{F}$ $\mathcal{P}[f]$, that specifies the probability distribution of the function $f(t')$, should be included instead of the PDF, that specifies the probability distribution of the random force $f(t_i)$ at a single time instance t_i. $\mathcal{P}[f]$ is given by the continuum limit of the multivariate Gaussian PDF [83] that depends on random forces $f_i = f(t_i)$. Since the random force is uncorrelated at different times, the random variables f_i are independent, hence the multivariate Gaussian PDF reduces to a product of single-variable Gaussian PDFs[23]. Hence, this yields for the PD$\mathcal{F}$

$$\begin{aligned} \mathcal{N}\, \mathcal{P}[f]\, \mathcal{D}f(t') &= \lim_{N\to\infty} \exp\left[-\frac{1}{2G}\sum_{i=1}^{N} f_i^2\, \Delta t\right] \prod_{i=1}^{N} \frac{\Delta t\, \mathrm{d}f_i}{\sqrt{2\pi G}}, \\ &= \mathcal{N} \exp\left[-\frac{1}{2G}\int_0^t f^2(t')\, \mathrm{d}t'\right] \mathcal{D}f(t'), \end{aligned} \tag{3.14}$$

with G the autocorrelation amplitude of $f(t')$, $\mathcal{D}f(t')$ the functional measure and $\mathcal{N}$ the constant that normalizes $\mathcal{P}[f]$. This is the exact same procedure as carried out in Eq. (3.4), so in fact Wiener also made use of functional integration. Consequently, in general functional integrals over random functions $\eta(t')$, the weighting functional $\Phi[\eta] = \mathcal{P}[\eta]$ emerges naturally to account for the probability of each trajectory or path to be taken.

Now, the theory above can be applied to the velocity functional $v(v_0, t, [f])$ for a Brownian particle, defined by Eq. (3.7), as was done by Chandrasekhar [10]. For comparison with the results obtained by Langevin, which are stated in Section 2.3.1, it is interesting to calculate the first and second moments of the velocity, but now with respect to $\mathcal{P}[f]$, which could be called *functional moments*. This requires knowledge of the functional moments of $f(t')$. Using that $\mathcal{P}[f]$ is just the continuum

[22] Normalization in terms of functional integration means that $\mathcal{N}\int \mathcal{P}[\eta]\mathcal{D}\eta(t') = 1$

[23] This is shown explicitly in Eq. (3.3) for the displacements $r_i - r_{i-1}$ of a Brownian particle, which are independent due to the Markov property.

limit of a product of independent normally distributed random forces f_i with zero average and variance G, it is clear that

$$\langle f(\tau)\rangle = \mathcal{N}\int f(\tau)\mathcal{P}[f]\,\mathcal{D}f(t') = 0, \tag{3.15}$$

$$\langle f(\tau)f(\tau')\rangle = \mathcal{N}\int f(\tau)f(\tau')\mathcal{P}[f]\,\mathcal{D}f(t') = G\,\delta(\tau-\tau') \tag{3.16}$$

for $0 \leq \tau, \tau' \leq t$ [83]. Note that these are functional averages. The resulting average and autocorrelation function are exactly the properties of the random force specified in Eq. (2.24). This should not be surprising, since these properties were implicitly used for each f_i in deriving $\mathcal{P}[f]$. Nevertheless, it is reassuring that this also holds in the functional formalism. Starting from Eq. (3.7), the first velocity moment is now given by

$$\begin{aligned}
\langle v(v_0,t,[f])\rangle &= \mathcal{N}\int v(v_0,t,[f])\mathcal{P}[f]\,\mathcal{D}f(t'),\\
&= \mathcal{N}\int\left\{v_0\mathrm{e}^{-\gamma t} + \mathrm{e}^{-\gamma t}\int_0^t \mathrm{e}^{\gamma t'} f\left(t'\right)\mathrm{d}t'\right\}\mathcal{P}[f]\,\mathcal{D}f(t'),\\
&= v_0\mathrm{e}^{-\gamma t}\mathcal{N}\int\mathcal{P}[f]\,\mathcal{D}f(t') + \mathrm{e}^{-\gamma t}\int_0^t \mathrm{e}^{\gamma t'}\left\{\mathcal{N}\int f\left(t'\right)\mathcal{P}[f]\,\mathcal{D}f(t')\right\}\mathrm{d}t',\\
&= v_0\mathrm{e}^{-\gamma t},
\end{aligned} \tag{3.17}$$

where Eq. (3.15) and the normalization of $\mathcal{P}[f]$ were used in the last line. This is equivalent to the result found by Langevin. The second velocity moment $\langle v(v_0,t,[f])^2\rangle$ follows easily by the functional analogue of the calculation in Eq. (2.25), which also yields the same result.

It seems unnecessarily cumbersome to solve the Langevin equation by functional integration, especially since it yields the same results as Langevin's approach. However, translating this problem to a functional language allows for the application of other useful methods, that will be treated in the next section, to calculate interesting quantities. In particular, the functional approach can be used for nonlinear SDEs by means of perturbation theory.

3.2 Functional methods for stochastic and quantum systems

A few years after Chandrasekhar's solution to the Langevin equation, Richard Feynman developed a functional formalism to describe quantum mechanics, which is the Feynman path integral[24] [8]. Feynman's approach was revolutionary and it led to interesting new insights [85]. Later, the methods developed in this formalism were again used to study the statistical mechanics and fluctuations of systems near a phase transition [80]. The critical dynamics of such a system are actually governed by an order parameter that obeys a Langevin equation [86]. The correlation length diverges when the system approaches the critical point, allowing for a continuous description in terms of functionals and fields. This led to the application of all functional methods to stochastic systems and later to the development of the MSR formalism. Here, a general functional approach to stochastic systems will be developed, by introducing important concepts and quantities from a stochastic point of view. Afterwards, the connection to quantum mechanics will be explained briefly.

[24] In fact, Paul Dirac already developed the ideas for a path integral formulation of quantum mechanics in 1932 [9].

3.2.1 Generating functionals

In Section 2.1.1, the expectation value of a random variable[25] X was defined in Eq. (2.1), from which the n^{th} moment of X could be defined as

$$\langle X^n \rangle = \int x^n P(x,t)\,\mathrm{d}x. \tag{3.18}$$

The moments are insightful quantities to characterize the behavior of a stochastic system. For example, the first moment is equal to the expectation value $\langle X \rangle$, and the second moment is related to the variance σ^2 of the corresponding PDF, which is a measure for the average deviation from the mean. Therefore, it is useful to define a *(moment) generating function*

$$Z(J) = \langle \mathrm{e}^{Jx} \rangle = \int \mathrm{e}^{Jx} P(x,t)\,\mathrm{d}x, \tag{3.19}$$

which is the Laplace transform of the PDF. Now, the moments can be obtained by taking derivatives of $Z(J)$ as

$$\langle X^n \rangle = \frac{1}{Z(0)} \frac{\mathrm{d}^n}{\mathrm{d}J^n} Z(J) \bigg|_{J=0}, \tag{3.20}$$

with respect to an auxiliary (complex) variable J, usually called a *source*. Note that if $P(x,t)$ would be normalized, $Z(0) = 1$. As will turn out later, it is useful to not require this normalization condition, hence the normalization constant $\mathcal{N}$ is neglected. It is also interesting to look at the *cumulants* of a PDF, which are defined by

$$\langle X^n \rangle_c \equiv \frac{\mathrm{d}^n}{\mathrm{d}J^n} K(J) \bigg|_{J=0}, \tag{3.21}$$

where the *cumulant generating function* is given by

$$K(J) = \log Z(J). \tag{3.22}$$

It can easily be seen that $\langle X \rangle_c = \langle X \rangle$ and $\langle X^2 \rangle_c = \langle X^2 \rangle - \langle X \rangle^2 \equiv \sigma^2$. To get an idea of the usefulness of generating functions, take for example a (time-independent) Gaussian PDF with mean μ and variance G. Its generating function is

$$\begin{aligned} Z(J) &= \int_{-\infty}^{\infty} \mathrm{e}^{-(x-\mu)^2/2G + Jx} \mathrm{d}x, \\ &= \int_{-\infty}^{\infty} \mathrm{e}^{-\frac{1}{2}G^{-1}(x - JG - \mu)^2 + J\mu + \frac{1}{2}JG^2} \mathrm{d}x, \\ &= \sqrt{2\pi\, G}\, \mathrm{e}^{J\mu + \frac{1}{2}JG^2}, \\ &= Z(0)\, \mathrm{e}^{J\mu + \frac{1}{2}JG^2}, \end{aligned} \tag{3.23}$$

where completing the square was used for the second line and a shifted Gaussian integral was recognized and performed for the third line. The resulting normalization constant is given by $Z(0)$ in the fourth line. The cumulant generating function is obtained by taking the logarithm of Eq. (3.23), yielding

$$K(J) = J\mu + \frac{1}{2}JG^2 + \log Z(0). \tag{3.24}$$

[25] This can be the value of a stochastic process $\{X(t)\}$ at a fixed time t. To avoid confusion with a random function $X(t)$, the dependence on t is suppressed in the expectation values.

Using these generating functions, the moments and cumulants are given by $\langle X\rangle_c = \langle X\rangle = \mu$ and $\langle X^2\rangle_c = G$, as could have been expected.

The concepts above can be generalized to a n-dimensional random vector $X = (X_1, X_2, ..., X_n)$ and source vector $J = (J_1, J_2, ..., J_n)$. For a multivariate Gaussian PDF with zero mean, the generating function can be written as

$$\begin{aligned} Z(J) &= \int \mathrm{e}^{-\sum_{k,l}\frac{1}{2}x_k G^{-1}_{kl} x_l + \sum_k J_k x_k} \prod_{i=1}^{n} \mathrm{d}x_i, \\ &= Z(0)\,\mathrm{e}^{\sum_{k,l}\frac{1}{2}J_k G_{kl} J_l}. \end{aligned} \tag{3.25}$$

The variance is now generalized to a *covariance matrix* $(G_{kl})_{k,l=1,..,n} = G$, with inverse G^{-1}, which can be assumed to be symmetric. For symmetric G^{-1}, one can always find an orthonormal basis B, such that $B \cdot G^{-1} \cdot B^{-1}$ is diagonal [87]. By completing the square, one arrives at the second line in Eq. (3.25), where $Z(0) = (2\pi)^{n/2}(\det G)^{1/2}$. The m^{th} moment, now consisting of combinations of X_i, is given by

$$\left\langle \prod_{i=1}^{m} X_i \right\rangle = \frac{1}{Z(0)} \prod_{i=1}^{m} \frac{\partial}{\partial J_i} Z(J)\bigg|_{J_i=0}. \tag{3.26}$$

The continuum limit can be applied to this multivariate Gaussian case. By using the same time-slicing procedure as before, one arrives at the *generating functional* of a random function $X(t)$

$$\begin{aligned} Z[J] &= \int \mathrm{e}^{-\frac{1}{2}\int x(t)G^{-1}(t,s)x(s)\,\mathrm{d}s\,\mathrm{d}t + \int J(t)x(t)\,\mathrm{d}t}\,\mathcal{D}x(t), \\ &= Z[0]\,\mathrm{e}^{\frac{1}{2}\int J(t)G(t,s)J(s)\,\mathrm{d}s\,\mathrm{d}t}, \end{aligned} \tag{3.27}$$

where $J(t)$ is a source function and $G(t,s)$ is a function that will be specified later. In this continuum limit, the functional integration is over all trajectories or paths $\{x(t)\}$ that the random function $X(t)$ can take. Furthermore, the normalization constant $Z[0] = \lim\limits_{n\to\infty}(2\pi)^{n/2}(\det G)^{1/2}$ of this functional integral is infinite, as was warned for in Section 3.1.2. Nevertheless, a proper definition of the moments still exists in terms of functional derivatives with respect to the source function

$$\left\langle \prod_{i=1}^{2m} X(t_i) \right\rangle = \frac{1}{Z[0]} \prod_{i=1}^{2m} \frac{\delta}{\delta J(t_i)} Z[J]\bigg|_{J(t)=0} = \sum_{\text{pairings}} G(t_{i_1}, t_{i_2}) \cdots G(t_{i_{2m-1}}, t_{i_{2m}}). \tag{3.28}$$

Since the moments now consist of combinations $X(t_i)$, which are values of a random function, they will be called *correlation functions*. This is to distinguish the functional case from the rest, since moments are calculated for random variables at the same point in time, while correlation functions are (in general) calculated at different times. In the same sense, the cumulants are defined by the functional generalization of Eq. (3.21), through a cumulant generating functional $K[J]$. The cumulants are now called *connected* correlation functions, which will make sense later in Section 3.2.2. The last equality in Eq. (3.28) follows from the fact that the generating functional is quadratic in the source function $J(t)$. Hence, the only nonzero correlation functions are the ones with an even number of terms $X(t_i)$. Then, the functional derivatives should be paired up in an appropriate way to get a nonzero result. This is called *Wick's theorem* [88].

The correlation function for $X(t)$ at two different times is called the two-point correlation function. This is exactly equivalent to an autocorrelation function, which was used to define white and colored

noise, respectively, in Eq. (2.3) and (2.4). Obtaining the autocorrelation of a quantity $X(t)$, like for example Eq. (2.25) for the velocity $v(t)$ of a Brownian particle, can be very useful for understanding the behavior of a system. Using Wick's theorem, one obtains

$$\langle X(t_1)X(t_2)\rangle = \frac{1}{Z[0]}\frac{\delta}{\delta J(t_1)}\frac{\delta}{\delta J(t_2)}Z[J]\bigg|_{J=0} = G(t_1,t_2). \tag{3.29}$$

Hence, the function $G(t,s)$ is the two-point correlation function, with inverse $G^{-1}(t,s)$. Just as the mean, the two-point function is an interesting quantity to calculate analytically, since it can also be measured experimentally. Hence, this yields an experimental test to see if the proposed theory for a system, from which the correlation functions arise, is reliable. Correlation functions also characterize the PDF of the system under consideration. As the PDF describes the complete (evolution of) a stochastic system, it is therefore important to find expressions for these correlation functions.

3.2.2 Connection to quantum mechanics

Stochastic effects also arise in quantum mechanics, as was already mentioned in the introduction of this section, due to its inherent unpredictability. Richard Feynman independently developed a functional formalism, called the Feynman path integral [8], without using the path integral introduced by Wiener. This approach to quantum mechanics is equivalent to the Schrödinger and Heisenberg pictures [87]. However, it turns out that the path integral description is easier to generalize to relativistic quantum mechanics and quantum field theory (QFT) [88], which will be discussed later. The concepts introduced in the last section all originate from the Feynman's functional formalism, or at least have a quantum mechanical counterpart.

The goal of the Feynman path integral is to calculate the quantum mechanical transition amplitude $Q(r_f,t_f|\,r_b,t_b)$ of a particle to go from position $r(t_b)=r_b$ to $r(t_f)=r_f$. This is the quantum mechanical equivalent of the transition probability $P(r_f,t_f|\,r_b,t_b)$. The Feynman path integral is actually a generalization of the classical Lagrange formalism to quantum mechanics. Therefore, it is useful to first define an *action* S, which governs the dynamics of the system of interest. The action is a functional of the degrees of freedom of the system, in this case the position, defined by

$$S[r] = \int_{t_b}^{t_f} L(r(t),\dot{r}(t),t)\,\mathrm{d}t, \tag{3.30}$$

where $L(r(t),\dot{r}(t),t)$ is the Lagrangian. In classical mechanics, the classical path $r_{\mathrm{cl}}(t)$ from r_b to r_f is determined by minimizing the action along that path, i.e. by putting the functional derivative of $S[r]$ with respect to $r(t)$ to zero along $r(t)=r_{\mathrm{cl}}(t)$. This is called the principle of least action [1], that results in the Euler-Lagrange equations, which are the (classical) EoM of the system. These equations are deterministic, hence classically only the path $r_{\mathrm{cl}}(t)$ contributes to the transition probability. In the quantum mechanical case, all other paths also contribute to $Q(r_f,t_f|\,r_i,t_i)$, according to some weighting that determines their probability. Therefore, in calculating the transition amplitude, one has to sum over all possible paths. By applying the meanwhile familiar time-slicing procedure[26], this becomes a path integral in the continuum limit

$$Q(r_f,t_f|\,r_b,t_b) = \mathcal{N}\int_{r(t_b)=r_b}^{r(t_f)=r_f} \exp\left\{\frac{i}{\hbar}S[r]\right\}\mathcal{D}r(t), \tag{3.31}$$

[26] This can be interpreted as the quantum mechanical equivalent of the Chapman-Kolmogorov equation.

where $\mathcal{N}$ is a normalization constant, $i = \sqrt{-1}$ and $\hbar$ is Planck's constant divided by 2π [87]. Hence, the weighting functional is given by an exponent of the action $S[r]$. In the classical limit $\hbar \to 0$, the only nonzero contribution is indeed given by the classical path $r_{\mathrm{cl}}(t)$, as this minimizes the action. This is a useful reality check.

To give a first illustration of the connection between quantum and stochastic systems, the Schrödinger picture for quantum mechanics can be considered. In this approach, the wave function $\psi(r,t)$ of a one-dimensional non-relativistic free particle with mass m in the position representation, evolves according to the Schrödinger equation, yielding

$$\frac{-\hbar^2}{2m}\frac{\partial^2}{\partial r^2}\psi(r,t) = i\hbar\frac{\partial}{\partial t}\psi(r,t). \tag{3.32}$$

This has the same form as the diffusion equation (2.31) for the PDF $P(r,t)$. In fact, by setting the diffusion constant equal to $D = -\hbar/2m$ and performing a *Wick rotation* $t \to -it$ [87], the diffusion equation transforms into the Schrödinger equation. This procedure can be extended to the Fokker-Planck equation (2.17), which contains also a first-order derivative. This results in a Schrödinger equation with a non-Hermitian Hamiltonian [83].

With Eq. (3.31), the connection of quantum systems with stochastic systems can be generalized. Since the stochastic systems that are considered here are classical, their fluctuations are of a non-quantum nature. Therefore, one has to perform a (backward) Wick rotation $-it \to t$. This is done to describe the evolution of a classical stochastic system instead of the evolution of a quantum system. Then, the transition amplitude in Eq. (3.31) is directly related to the classical transition probability in Eq. (3.13), so the PD$\mathcal{F}$ $\mathcal{P}[r]$ can be read of as

$$\mathcal{P}[r] = \mathrm{e}^{-S_{\mathrm{eff}}[r]}, \tag{3.33}$$

where $S_{\mathrm{eff}}[r]$ is an effective classical action of the stochastic system. From this expression, the generating functional follows by using the functional generalization of Eq. (3.19), as was done in Eq. (3.27), to obtain

$$\begin{aligned} Z[J] &= \int \mathrm{e}^{\int J(t)r(t)\,\mathrm{d}t}\mathcal{P}[r]\,\mathcal{D}r(t), \\ &= \int \mathrm{e}^{-S_{\mathrm{eff}}[r]+\int J(t)r(t)\,\mathrm{d}t}\,\mathcal{D}r(t). \end{aligned} \tag{3.34}$$

It can now be seen that all expressions inside the exponents in Eqs. (3.11), (3.14) and (3.27) are in fact actions depending on the random function over which the functional integration is performed.

3.2.3 Extension to quantum field theory

The functional formalism can also be applied to quantum field theory (QFT), where the quantities of interest are quantum *fields*, which are usually functions of both space and time. This framework is an alternative for the operator formulation of quantum mechanics, which is especially convenient for describing quantum many-body systems [87]. It allows for important techniques, which can also be applied to classical stochastic systems. By denoting the classical fields of a stochastic system as $\varphi(r,t)$, the generating functional in Eq. (3.34) can easily be generalized to field theory as

$$\begin{aligned} Z[J] &= \int \mathrm{e}^{-S_{\mathrm{eff}}[\varphi(r,t)]+\int J(r,t)\varphi(r,t)\,\mathrm{d}^n r\,\mathrm{d}t}\,\mathcal{D}\varphi, \\ &= \int \mathrm{e}^{\int J(r,t)\varphi(r,t)\,\mathrm{d}^n r\,\mathrm{d}t}\mathcal{P}[\varphi]\,\mathcal{D}\varphi, \end{aligned} \tag{3.35}$$

where n is the spatial dimension. Again, this seems like an extra complication, but next to the tools already discussed in the last section, this allows for other helpful methods.

For a vanishing source field $J(r,t) = 0$, the generating functional $Z[J=0]$ in Eq. (3.35) is just the integrated PD$\mathcal{F}$. However, after a Wick rotation, $Z[0]$ becomes an important quantity in (quantum) statistical mechanics, called the *partition function*. This contains all equilibrium properties of a many-body system [87].

It is interesting to compare Eq. (3.34) with the expression in Eq. (3.27) for a generating functional of a Gaussian PD$\mathcal{F}$. This shows that there should be some kind of relation between the action S_{eff} and the two-point correlation function $G(t,s)$. By the principle of least action, the EoM can be derived from the action. The function $G(t,s)$ is exactly the fundamental solution of these EoM, in the sense that

$$\mathcal{L}G(t,s) = \delta(t-s) \tag{3.36}$$

for some differential operator $\mathcal{L}$ that represents the EoM. $G(t,s)$ is now called a *Green's function*. This can be generalized to field theory by adding a n-dimensional Dirac delta function $\delta(r_1 - r_2)$ in Eq. (3.36). Note that the generating functional (3.27) itself contains the inverse $G^{-1}(t,s)$ of the Green's function, before completing the square. The notion of a Green's function becomes particularly useful when the random function $Y(t)$ or field $\varphi(r,t)$ obeys some SDE, as will be the case in Section 3.3. It can even be shown that the Green's function satisfies a convolution product, which is similar to the Chapman-Kolmogorov equation for transition probabilities [83]. As an example of a Green's function, consider the diffusion equation (2.31). The solution found by Wiener in Eq. (3.5), that determines the probability to move from $r(0) = 0$ to $r(t) \in [A,B]$, is in fact a Green's function of the differential operator that corresponds to the diffusion equation.

Related to this is the transition amplitude $Q(r_f, t_f | r_b, t_b)$ in Eq. (3.31), that determines the quantum mechanical probability for a particle to propagate from $r(t_b) = r_b$ to $r(t_f) = r_f$. Therefore, $Q(r_f, t_f | r_b, t_b)$ is usually also called the (one-particle) *propagator*. The propagator can be defined as the Green's function for the EoM of the 'free' fields, so without interactions, but it can also be generalized to interacting field theories. Assuming no interactions implies that the effective action $S_{\text{eff}}[\varphi(r,t)]$ is at most quadratic in the fields $\varphi(r,t)$. Then, the encountered integrals are of a Gaussian form, and therefore much easier to solve. In that case, the two-point correlation function $G(t,s)$ is proportional to the propagator, and can be obtained by taking functional derivatives of the *free generating functional* $Z_0[J]$ as in Eq. (3.29), where the subscript 0 indicates a free field theory.

Suppose that the action is not quadratic, i.e. it can be written as $S_{\text{eff}}[\varphi] = S_0[\varphi] + S_I[\varphi] = \int \{L_0[\varphi] + L_I[\varphi]\} \,\mathrm{d}^n r \,\mathrm{d}t$. Here, S_0 is the free action and S_I is the interacting action, containing higher powers of $\varphi(r,t)$. Then, one can write the complete generating functional $Z[J]$ in terms of $Z_0[J]$ as

$$\begin{aligned} Z[J] &= \int \mathrm{e}^{-S_0[\varphi(r,t)] - S_I[\varphi(r,t)] + \int J(r,t)\varphi(r,t)\,\mathrm{d}^n r\,\mathrm{d}t}\,\mathcal{D}\varphi, \\ &= \int \mathrm{e}^{-\int L_I\left[\frac{\delta}{\delta J(r,t)}\right]\mathrm{d}^n r\,\mathrm{d}t} \mathrm{e}^{\int \{-L_0[\varphi(r,t)] + J(r,t)\varphi(r,t)\}\,\mathrm{d}^n r\,\mathrm{d}t}\,\mathcal{D}\varphi, \\ &= \mathrm{e}^{-\int L_I\left[\frac{\delta}{\delta J(r,t)}\right]\mathrm{d}^n r\,\mathrm{d}t} Z_0[J]. \end{aligned} \tag{3.37}$$

By expanding the exponent in the last line, a perturbation theory around $Z_0[J]$ is obtained. Note that the free generating functional $Z_0[J]$ contains the two-point correlation functions $G(r_1,t,r_2,s)$

in $L_0[\varphi(r,t)]$, as in Eq. (3.27), and the other exponent contains the interactions. To conveniently organize the perturbative terms, it is useful to draw them as *Feynman diagrams* [88], in which the correlation functions and interactions are represented by lines and vertices according to Feynman rules. This can be done for any field theory that contains interactions. In the next section, an example will be presented for a nonlinear Langevin equation.

The expansion above is useful when interaction terms are small. In the case of SDEs, one could also expand in orders of the autocorrelation amplitude of the noise, if the noise effects are small compared to the deterministic evolution. This weak noise expansion is also called a *semiclassical* or *loop expansion*, for reasons that will become clear in the next section. Furthermore, it is insightful to also expand the cumulant generating functional $K[J]$. It can be shown that this expansion only contains *connected* diagrams [88]. This explains why the corresponding cumulants are called connected correlation functions.

3.3 Martin-Siggia-Rose (MSR) formalism

For a random variable X or a random function $Y(t)$, it is now clear how to calculate a generating functional and derive the corresponding correlation functions. However, what if an observable $Y(t)$ of a stochastic system is governed by a SDE? As mentioned earlier, functional methods were used to study stochastic systems near a phase transition. Around that point, the order parameter satisfies a (nonlinear) Langevin equation, so it can be interpreted as a random variable. This was realized in 1973 by Martin, Siggia, and Rose, who were the first to use techniques of QFT to describe classical stochastic systems [11]. They developed a method in the operator formalism, which would later be called the Martin-Siggia-Rose formalism, to study classical fluctuations. It was extended to functional integrals by Janssen [12] and de Dominicis [13] in 1976, which is why in some literature it is called the MSRJD formalism. In this work, it will be referred to as the MSR formalism.

3.3.1 Derivation of the general formalism

The goal of the MSR formalism is to write the dynamics of the observable $Y(t)$ as a stochastic field[27] theory by means of path integrals. This is done by finding a generating functional for $Y(t)$, which obeys a SDE. Consider a general Langevin equation

$$\dot{Y} = C(Y,t) + D(Y,t)\eta(t), \tag{3.38}$$

as in Eq. (2.2), with initial condition $Y(t_0) = y_0$. For simplicity, only one observable $Y(t)$ is considered, resulting in a one-dimensional Langevin equation. This expression can be nonlinear through the functions $C(Y,t)$ and $D(Y,t)$, which respectively[28] govern the deterministic evolution and noise coupling. The noise $\eta(t)$ is assumed to be Gaussian white noise with autocorrelation amplitude Ξ. Later, the formalism will be generalized to Gaussian colored noise. Depending on the form of $D(Y,t)$, $\eta(t)$ can be either additive or multiplicative noise. In the latter case, the interpretation of Eq. (3.38) depends in general on the chosen prescription, as explained in Section 2.3.3. Since $\eta(t)$ is assumed to be white noise, it is appropriate to use the Itô prescription. So, the general Langevin equation can be written as an Itô SDE [4]

$$\mathrm{d}Y = C(Y,t)\mathrm{d}t + D(Y,t)\mathrm{d}W(t) + y_0\mathbf{1}_{t_0}(t), \tag{3.39}$$

[27] Although the random function $Y(t)$ does not necessarily depend on the position r, it can still be interpreted as a field, as the MSR formalism requires path integrals.

[28] This is valid for external noise. For internal noise, these functions can have another interpretation, see Section 2.3.3.

where $W(t)$ is a Wiener process, which arises from integrating the Gaussian white noise $\eta(t)$. By adding an indicator function[29] $\mathbf{1}_{t_0}(t)$, the initial condition $Y(t_0) = y_0$ is fixed in the SDE. This turns out to be useful in the functional formalism.

To find a generating functional for $Y(t)$, it is first convenient to derive its PD$\mathcal{F}$. This can be done properly by applying a time-slicing procedure, to obtain a discretization of Eq. (3.39). In the Itô prescription, the N-step discretization on the interval $t \in [t_0, t_f]$ is given by

$$y_{j+1} - y_j = C(y_j, t_j)\Delta t + D(y_j, t_j) w_j \sqrt{\Delta t} + y_0\, \delta_{0,j}, \tag{3.40}$$

where $t_j = t_0 + j\Delta t$, $\Delta t = t_f/N$ and $y_j = Y(t_j)$. w_j is a Gaussian distributed random variable with zero mean and variance Ξ, since $\eta(t)$ has autocorrelation amplitude Ξ. This follows from the third property of a Wiener process. The multiplication factor $\sqrt{\Delta t}$ arises from the same property. Note that, by using the Itô prescription, y_{j+1} only depends on quantities at time t_j. It is now possible to write down the PDF of the vector $y = (y_1, ..., y_N)$, conditioned on $w = (w_0, ..., w_{N-1})$ and y_0, as

$$P(y|\, w, y_0) = \prod_{j=0}^{N} \delta(y_{j+1} - y_j - C(y_j, t_j)\Delta t - D(y_j, t_j) w_j \sqrt{\Delta t} - y_0\, \delta_{0,j}). \tag{3.41}$$

Hence, the PDF is obtained by multiplying N Dirac delta functions, each enforcing the discretized SDE (3.40) as a constraint on y_{j+1}. This is an example of the Faddeev-Popov trick [89], that implements constraints, such as gauge invariance, in path integrals. In this case, it ensures that every y_{j+1} that has a nonzero contribution to the PDF obeys the discretized SDE. A Fourier transformation of the Dirac delta functions yields

$$P(y|\, w, y_0) = \int \prod_{j=0}^{N} \mathrm{e}^{-i \sum_j q_j [y_{j+1} - y_j - C(y_j,t_j)\Delta t - D(y_j,t_j) w_j \sqrt{\Delta t} - y_0\, \delta_{0,j}]} \frac{\mathrm{d}q_j}{2\pi}, \tag{3.42}$$

for some auxiliary variable q_j. To obtain the conditional PDF $P(y|\, y_0)$, the random variables w_j need to be integrated over. Since w_j is a Gaussian distributed random variable with mean zero and variance Ξ, this gives

$$\begin{aligned}
P(y|\, y_0) &= \int P(y|\, w, y_0) \prod_{j=0}^{N} P(w_j)\, \mathrm{d}w_j, \\
&= \int \int \prod_{j=0}^{N} \mathrm{e}^{-i \sum_j q_j [y_{j+1} - y_j - C(y_j,t_j)\Delta t - D(y_j,t_j) w_j \sqrt{\Delta t} - y_0\, \delta_{0,j}]} \frac{\mathrm{d}q_j}{2\pi} \prod_{j=0}^{N} \mathrm{e}^{-\frac{1}{2\Xi} w_j^2} \frac{\mathrm{d}w_j}{\sqrt{2\pi\Xi}}, \\
&= \int \prod_{j=0}^{N} \mathrm{e}^{-i \sum_j q_j [y_{j+1} - y_j - C(y_j,t_j)\Delta t - y_0\, \delta_{0,j}]} \frac{\mathrm{d}q_j}{2\pi} \int \prod_{j=0}^{N} \mathrm{e}^{i q_j D(y_j,t_j) w_j \sqrt{\Delta t} - \frac{1}{2\Xi} w_j^2} \frac{\mathrm{d}w_j}{\sqrt{2\pi\Xi}}, \\
&= \int \prod_{j=0}^{N} \mathrm{e}^{-i \sum_j q_j [(y_{j+1} - y_j)/\Delta t - C(y_j,t_j) - y_0\, \delta_{0,j}/\Delta t]\Delta t - \sum_j \frac{1}{2}\Xi q_j^2 D^2(y_j,t_j)\Delta t} \frac{\mathrm{d}q_j}{2\pi},
\end{aligned} \tag{3.43}$$

where the last line followed from completing the square and performing the Gaussian integrals for all w_j. It is important to note that the resulting PDF is independent of the random variables w_j.

[29] The indicator function $\mathbf{1}_{t_0}(t)$ satisfies $\mathbf{1}_{t_0}(t_0) = 1$ and $\mathbf{1}_{t_0}(t) = 0$, $\forall t \neq t_0$.

As before, the continuum limit $\Delta t \to 0$ and $N \to \infty$ can be taken such that $t_f = N\Delta t$, to arrive at a functional description for the PD$\mathcal{F}$

$$\mathcal{P}[y(t)|\, y_0, t_0] = \mathcal{N}_q \int \mathrm{e}^{-\int q(t)[\dot{y}(t) - C(y(t),t) - y_0\,\delta(t-t_0)]\,\mathrm{d}t + \int \frac{1}{2}\Xi\, q^2(t) D^2(y(t),t)\,\mathrm{d}t}\, \mathcal{D}q(t). \tag{3.44}$$

This requires a transformation of the discrete variables y_j to a continuous function or field $y(t)$, which is a realization of $Y(t)$. The auxiliary variables iq_j transform to an *auxiliary field* $q(t)$, which has normalization $\mathcal{N}_q$. By using Eqs. (3.33) and (3.34), it is now possible to write down the *MSR action* [12, 13] as

$$S[y,q] = \int \left\{ q(t)\,[\dot{y}(t) - C(y(t),t) - y_0\,\delta(t-t_0)] - \frac{1}{2}\Xi\, D^2(y(t),t) q^2(t) \right\} \mathrm{d}t. \tag{3.45}$$

This does not contain a factor i due to the definition of the imaginary auxiliary field $q(t)$. As this is independent of the noise $\eta(t)$, by performing the Gaussian integrals, this can be interpreted as an effective action. Therefore, the MSR formalism can be seen as a method for deriving an effective field theory. The corresponding generating functional is given by

$$Z[J_y, J_q] = \int \mathrm{e}^{-S[y,q] + \int J_y(t) y(t)\,\mathrm{d}t + \int J_q(t) q(t)\,\mathrm{d}t}\, \mathcal{D}q(t)\, \mathcal{D}y(t), \tag{3.46}$$

where the normalization $\mathcal{N}_q$ is neglected for later convenience. Note that, in this case, two source functions $J_y(t)$ and $J_q(t)$ have to be introduced, since the functional integral is over two fields $y(t)$ and $q(t)$. Since all correlation functions of $Y(t)$ can be derived from the generating functional, it can be seen as the solution of the SDE (3.38). This is the MSR formalism for writing a Langevin equation in terms of functional integrals [11–13]. From here on, all kinds of field-theoretical methods, like perturbation theory and renormalization group treatments [90], can be used to further investigate the dynamics and correlation functions.

The formalism can be summarized in a continuous description for averages of functionals $O[y(t)]$. If, for a noise realization $\eta(t)$, the unique solution of the SDE (3.38) is written by y_η, the functional average is given by

$$\begin{aligned}
\langle O[y|\, y(t_0) = y_0] \rangle &= \int O[y] \mathcal{P}[y|\, y_0, t_0]\, \mathcal{D}y, \\
&= \int O[y] \delta[y - y_\eta] \mathcal{P}[\eta(t)]\, \mathcal{D}y\, \mathcal{D}\eta(t), \\
&= \mathcal{N}_\eta \int O[y] \delta[\dot{y} - C(y,t) - D(y,t)\eta(t) - y_0\,\delta(t-t_0)]\, \mathrm{e}^{-\int \frac{1}{2\Xi}\eta^2(t)\mathrm{d}t}\, \mathcal{J}\, \mathcal{D}y\, \mathcal{D}\eta(t), \\
&= \mathcal{N}_\eta \mathcal{N}_q \int O[y] \mathrm{e}^{-\int [q(\dot{y} - C(y,t) - D(y,t)\eta(t) - y_0\,\delta(t-t_0)) + \frac{1}{2\Xi}\eta^2(t)]\,\mathrm{d}t}\, \mathcal{J}\, \mathcal{D}q\, \mathcal{D}y\, \mathcal{D}\eta(t), \\
&= \mathcal{N}_q \int O[y] \mathrm{e}^{-S[y,q]}\, \mathcal{J}\, \mathcal{D}q\, \mathcal{D}y,
\end{aligned} \tag{3.47}$$

where the time dependence of the fields $y(t)$ and $q(t)$ is suppressed for notational convenience. The Dirac delta functional in the second line illustrates again that the functional integral is restricted to paths allowed by the dynamics, such that only solutions $y(t)$ of the Langevin equation contribute to the expectation value. In the third line, a change of variables $y(t) \to \dot{y}(t)$ is performed in the argument of the Dirac delta functional, to substitute the SDE for $\dot{y}_\eta(t)$. This gives rise to a Jacobian $\mathcal{J} \propto (\det D(y,t))^{-1}$ in the Itô prescription, for which an exact expression is derived in Appendix A.

In the Stratonovich interpretation, the expression for the Jacobian also contains other contributions. For additive noise, this Jacobian does not depend on y, but for multiplicative noise it can give rise to extra (nonlinear) contributions to the effective action as $S_{\text{eff}} = S[y,q] + \text{Tr}[\log D]$. The Gaussian PD$\mathcal{F}$ $\mathcal{P}[\eta]$ with normalization constant $\mathcal{N}_\eta$ is also inserted in the third line. In the last lines, the MSR action $S[y,q]$ is derived by Fourier transforming the Dirac delta functional, completing the square in the exponent and performing the functional integration over $\eta(t)$. For $O[y] = y$, this expression reduces to the first moment $\langle y(t)\rangle$, which can also be obtained by taking the familiar functional derivative of $Z[J_y, J_q]$ with respect to $J_y(t)$.

Once again, the different prescriptions result in minor but important changes, since it affects the measure of the path integrals and consequently the Jacobian. The Stratonovich convention seems to be more physical, since the autocorrelation time τ_c is small but nonzero and it allows for the usual transformation of variables. However, due to its discretized SDE (A.2), which differs slightly from the Itô case (3.40), this prescription gives rise to difficulties in calculations. From this perspective, the Itô prescription is more convenient, since it allows for intuitive simulations and easier calculations due to the simpler Jacobian. Therefore, Itô's convention will be used throughout the rest of this work. In Section 3.3.3, it will be seen that both prescriptions result in a different condition on the Green's function, where Itô's choice is again more intuitive.

The derivation of the MSR formalism above is only valid for Gaussian white noise. Nevertheless, it is also possible to generalize this to Gaussian colored noise that has autocorrelation function $\langle \eta(t)\eta(t')\rangle = \xi(t-t')$. Then, the PD$\mathcal{F}$ $\mathcal{P}[\eta]$ is given by

$$\mathcal{P}[\eta] = \mathcal{N} \mathrm{e}^{-\frac{1}{2}\int \eta(t)\xi^{-1}(t-t')\eta(t')\,\mathrm{d}t\,\mathrm{d}t'}, \tag{3.48}$$

where $\xi^{-1}(t-t')$ can be interpreted as a generalization of $1/\Xi$. Indeed, for $\xi(t-t') = \Xi\delta(t-t')$, Eq. (3.48) reduces to the regular Gaussian PD$\mathcal{F}$. Following the same procedure as for white noise, the resulting MSR action can be obtained [72] as

$$S[y,q] = \int q(t)[\dot{y}(t) - C(y(t),t) - y_0\,\delta(t-t_0)]\,\mathrm{d}t - \frac{1}{2}\int q(t)D(y(t),t)\xi(t-t')q(t')D(y(t'),t')\,\mathrm{d}t\,\mathrm{d}t'. \tag{3.49}$$

Expectation values $\langle O[y]\rangle$ and the generating functional $Z[J_y, J_q]$ follow from this action through similar calculations as above.

Now that the formalism is set up properly, it is useful to see what interesting quantities can be obtained. Just as before, all correlation functions $\langle \prod_i y(t_i)\rangle$ can be calculated directly from the generating functional $Z[J_y, J_q]$ by taking functional derivatives with respect to $J_y(t_i)$, as in Eq. (3.28). However, the MSR action $S[y,q]$ also contains the auxiliary field $q(t)$, for which the source function $J_q(t)$ arises in the generating functional. Therefore, it is possible to construct coupled correlation functions, that contain combinations of $y(t)$ and $q(t)$, such that

$$\left\langle \prod_{i=1}^{m}\prod_{k=1}^{n} y(t_i)q(t_k) \right\rangle = \frac{1}{Z[0,0]} \prod_{i=1}^{m}\prod_{k=1}^{n} \frac{\delta}{\delta J_y(t_i)} \frac{\delta}{\delta J_q(t_k)} Z[J_y, J_q]\bigg|_{J_y, J_q = 0}. \tag{3.50}$$

For both cases, it is also possible to calculate the cumulants or connected correlation functions, by taking functional derivatives of the cumulant generating functional $K[J_y, J_q]$.

Another important quantity is the *response function* $R(t,t')$, defined by

$$R(t,t') = \frac{\delta\langle y(t)\rangle}{\delta f(t')}\bigg|_{f(t')=0}, \tag{3.51}$$

where $t > t'$ by causality. The response function determines the response of the average $\langle y(t)\rangle$ to an external force $f(t')$, which is applied to the SDE governing $y(t)$. Hence, the Langevin equation (3.38) becomes

$$\dot{y} = C(y,t) + f(t) + D(y,t)\eta(t). \tag{3.52}$$

This gives rise to a new action $S_f[y,q] = S[y,q] - \int q(t)f(t)\,\mathrm{d}t$ and generating functional $Z_f[0,0] = \int \mathrm{e}^{-S_f}\mathcal{D}q\mathcal{D}y$, where the source functions are put to zero for convenience. Calculating the expectation value $\langle y(t)\rangle$ with respect to this generating functional Z_f and taking the functional derivative with respect to $f(t')$ then yields for the response function

$$\begin{aligned} R(t,t') &= \frac{\delta}{\delta f(t')}\left[\frac{1}{Z_f}\int y(t)\mathrm{e}^{-S_f}\,\mathcal{D}q\,\mathcal{D}y\right]\Big|_{f(t')=0}, \\ &= \Theta(t-t')\left[\langle y(t)q(t')\rangle - \langle y(t)\rangle\langle q(t')\rangle\right], \\ &= \Theta(t-t')\,\left\langle y(t)q(t')\right\rangle_c, \end{aligned} \tag{3.53}$$

where $\Theta(t-t')$ is a Heaviside step function that arises from the causality condition. The correlation functions in the second and third line are determined with respect to the non-perturbed generating functional $Z[J_y, J_q]$, since the external force $f(t')$ is put to zero. Since the correlation function in the last line is connected, the response function is directly related to the cumulant generating functional $K[J_y, J_q]$ via functional differentiation. This also shows that the auxiliary field $q(t)$ is not just added for convenience, but it actually determines the response function. Due to this connection, $q(t')$ is often also called the *response field*. Hence, when computing a (connected) correlation function of some observable $O[y]$ multiplied by $q(t')$, one actually calculates the response of $O[y]$ to a small and instantaneous external force at time t'. For Gaussian white noise, it can be shown [14] that the response function can be written in terms of a noise average as

$$R(t,t') = \left\langle \frac{\delta y(t)}{\delta \eta(t')} \right\rangle_\eta. \tag{3.54}$$

This is a case of the fluctuation-dissipation theorem, since it relates the dissipating energy, due to the external force $f(t')$, directly to the fluctuations $\eta(t')$.

3.3.2 Applications of the MSR formalism

The MSR formalism yields an analytical description in terms of fields for dynamics governed by SDEs. As this allows field-theoretical tools such as perturbation theory and renormalization group theory, this can be applied to a wide variety of systems. Originally, the formalism was used in the operator language by Martin, Siggia and Rose to study classical fluctuations near phase transitions [11]. Later, it was translated to path integrals by Janssen [12] and de Dominicis [13] to study Langevin dynamics for disordered systems. They applied it to the Random Field Ising model and the Ising spin glass. They also realized the physical importance of the auxiliary field $q(t)$ as more than just a useful tool. This description was used by Hertz et al. [14] to investigate systems with quenched interactions, such as soft and hard spin models. They also derived a supersymmetric form for the MSR formalism.

Next to these theoretical models, there are also other complex systems for which the MSR formalism turns out to be useful. Via the RFD model, which describes the dynamics of Lagrangian velocity gradients, the functional integral approach can be used to obtain a stochastic model of turbulence [72]. The instanton method applied here is equivalent to the semiclassical approach

that will be discussed in Section 3.4.1. Stochastic neurodynamics and neural network activity were studied by Bressloff [16] and Buice & Chow [17, 18]. In Ref. [19], they looked at a stochastic neuron model, called the Fitzhugh-Nagumo model, using path integrals. The analytical results for the correlation functions obtained from the MSR generating functional were compared with numerical simulations of the model, which fit well for small noise amplitudes. Buice & Chow also used the MSR approach for a network of coupled oscillators described by the Kuramoto model [91].

Section 3.2.2 already showed the analogy between quantum mechanics and stochastic systems. Here, the relation between the Schrödinger equation and the Fokker-Planck equation was discussed briefly. This relation can also be extended to the MSR formalism. The Schrödinger equation can be seen as the differential equation corresponding to the quantum mechanical Feynman path integral. It can be shown [15] that, in the same sense, the Fokker-Planck equation is the dynamical equation corresponding to the MSR path integral. This follows directly from the derivation procedure of the MSR path integral from the general Feynman path integral. In fact, the MSR formalism can be interpreted as the classical limit of the Keldysh formalism, which can be used to describe nonequilibrium quantum systems.

A last interesting application of the MSR formalism is in the description of population dynamics subject to random effects. This is studied by Sidhom & Galla in Ref. [24, 92], where they look at an N species Lotka-Volterra model with random interactions. This N-dimensional system of coupled differential equations describes the evolution of the population of each species. In their work, Sidhom & Galla study the ecological communities and stability in this model, under the influence of random effects. They take the limit of the number of species $N \to \infty$ to arrive at a continuous description for the populations in terms of a stochastic process. The MSR approach is also applied by Täuber [25] to a spatial version of the Lotka-Volterra model for only two species, which are a predator and a prey species. These examples will be discussed more elaborately in Section 5.1, as they form the inspiration for the application of the MSR formalism to the two species Lotka-Volterra model in this work.

To put the MSR formalism to work and observe its usefulness directly and easily, two examples are considered here. First, a linear Langevin equation is studied in the following section. Later, in Section 3.4, a nonlinear Langevin equation is investigated, which requires perturbation theory due to the higher-order interactions.

3.3.3 MSR approach to a linear Langevin equation

One of the simplest SDEs that can be considered is a linear Langevin equation, with $C(y,t) = -\gamma y(t)$ and $D(y,t) = 1$, yielding

$$\dot{y}(t) = -\gamma y(t) + \eta(t), \tag{3.55}$$

with initial condition $y(t_0) = y_0$ and noise amplitude Ξ. This corresponds to the Langevin equation (2.22) for Brownian motion, or an equivalent Ornstein-Uhlenbeck process. Although this equation has been solved twice already, it is still an insightful example and validity check for the MSR formalism. Here, the derivation follows the one in Ref. [19]. The MSR action can be obtained directly from Eq. 3.45 as

$$\begin{aligned} S[y,q] &= \int \left\{ q(t)[\dot{y}(t) + \gamma y(t) - y_0\,\delta(t-t_0)] - \frac{\Xi}{2} q^2(t) \right\} \mathrm{d}t, \\ &= \int q(t) G^{-1}(t-t') y(t') \,\mathrm{d}t\,\mathrm{d}t' - y_0 \int q(t)\delta(t-t_0)\,\mathrm{d}t - \frac{\Xi}{2}\int q^2(t)\,\mathrm{d}t, \end{aligned} \tag{3.56}$$

where $G^{-1}(t-t')$ is an inverse Green's function in the sense of Eq. (3.36), defined by

$$G^{-1}(t-t') = \left(\frac{\mathrm{d}}{\mathrm{d}t} + \gamma\right)\delta(t-t'). \tag{3.57}$$

Before this equation is solved to find an explicit form for the Green's function $G(t-t')$, it is useful to exploit this general form of the action. The generating functional $Z[J_y, J_q]$ follows directly from Eq. (3.46), which consequently also contains $G^{-1}(t-t')$. Since $S[y,q]$ is quadratic in the fields, the Green's function is non-interacting, so the functional integrals in $Z[J_y, J_q]$ could be evaluated exactly as Gaussian integrals, just as before. However, to already connect to the perturbation theory, which will be discussed in the next section, it is more convenient to first define the *free* part of the action as

$$S_0[y,q] = \int q(t)G^{-1}(t-t')y(t')\,\mathrm{d}t\,\mathrm{d}t'. \tag{3.58}$$

It is now possible to expand $Z[J_y, J_q]$ around the free generating functional

$$\begin{aligned} Z_0[J_y, J_q] &= \int \mathrm{e}^{-S_0[y,q]+\int J_y(t)y(t)\,\mathrm{d}t+\int J_q(t)q(t)\,\mathrm{d}t}\,\mathcal{D}q(t)\,\mathcal{D}y(t), \\ &= \mathrm{e}^{\int J_y(t)G(t,t')J_q(t')\,\mathrm{d}t\,\mathrm{d}t'}. \end{aligned} \tag{3.59}$$

The second line follows from completing the square, like for Eq. (3.27), which can be used since the free action is quadratic. By using Eq. (3.37), the expansion around Z_0 yields for the complete generating functional

$$\begin{aligned} Z[J_y, J_q] &= \exp\left\{y_0 \int q(t_1)\delta(t_1-t_0)\,\mathrm{d}t_1 + \frac{\Xi}{2}\int q(t_2)^2\,\mathrm{d}t_2\right\} Z_0[J_y, J_q], \\ &= \exp\left\{-\int L_I\left[\frac{\delta}{\delta J_q(t_{1(2)})}, \frac{\delta}{\delta J_y(t_{1(2)})}\right]\mathrm{d}t_{1(2)}\right\} Z_0[J_y, J_q], \\ &= \exp\left\{y_0 \int \delta(t_1-t_0)\frac{\delta}{\delta J_q(t_1)}\,\mathrm{d}t_1 + \frac{\Xi}{2}\int\left(\frac{\delta}{\delta J_q(t_2)}\right)^2\mathrm{d}t_2\right\} Z_0[J_y, J_q], \\ &= \exp\Bigg\{y_0 \int J_y(t)G(t,t_0)\,\mathrm{d}t + \frac{\Xi}{2}\int J_y(t)G(t,t_2)J_y(t')G(t',t_2)\,\mathrm{d}t\,\mathrm{d}t'\,\mathrm{d}t_2 \\ &\quad + \int J_y(t)G(t,t')J_q(t')\,\mathrm{d}t\,\mathrm{d}t'\Bigg\}, \end{aligned} \tag{3.60}$$

where the expression for the interacting Lagrangian L_I, which is also quadratic in this case, follows from taking functional derivatives of $Z_0[J_y, J_q]$ with respect to the source fields, to obtain the right terms. For the last step, the first exponent in the third line should be written as a Taylor expansion, to properly apply the functional derivatives to $Z_0[J_y, J_q]$. This can result in a lot of extra contributions. However, due to Wick's theorem and L_I being only quadratic in the fields $y(t)$ and $q(t)$, the nonzero contributions are summable, yielding again an expansion that can be written as an exponent [19]. So, effectively, the functional derivatives are applied directly to expression (3.59) for Z_0, to obtain the last line. In Section 3.4, an example with a higher-order interaction will be studied, for which this last step is generally not possible. Instead, this requires a perturbative expansion in terms of Feynman diagrams.

Now that an expression for the generating functional is derived, an explicit form for $G(t,t')$ is required to calculate correlation functions. From Eq. (3.57), it is clear that the Green's function is

the solution of

$$\left(\frac{\mathrm{d}}{\mathrm{d}t}+\gamma\right)G(t,t')=\delta(t-t'), \tag{3.61}$$

which is given by

$$G(t,t')=\Theta(t-t')\mathrm{e}^{-\gamma(t-t')}. \tag{3.62}$$

The exact form of this function depends on the chosen prescription. The Heaviside step function $\Theta(t-t')$ has the property that $\lim_{t\to t'}\Theta(t-t')=1$, for $t>t'$. For Itô's, choice $\Theta_I(0)=0$, while for the Stratonovich case, $\Theta_S(0)=1/2$ [80]. This corresponds to the physical interpretation of both prescriptions. Again, Itô's choice guarantees that $y(t)$ is not correlated with $\eta(t')$ for $t>t'$. Since it is also more convenient in calculations, this is another argument to use the Itô prescription. So, as stated earlier, this interpretation is used and the index I on the Heaviside step function is discarded. This distinction is directly related to the retarded and advanced Green's functions [88], of which the difference is the full Green's function. The causal retarded part gives the important contributions to physical quantities, while the anti-causal advanced part is usually ignored.

With the expression for $G(t,t')$, it is straightforward to calculate (connected) correlation functions from the generating functional via Eq. (3.50). By taking the logarithm of Eq. (3.60), the cumulant generating functional is given by

$$\begin{aligned}K[J_y,J_q]=&y_0\int J_y(t)G(t,t_0)\,\mathrm{d}t+\frac{\Xi}{2}\int J_y(t)G(t,t_2)J_y(t')G(t',t_2)\,\mathrm{d}t\,\mathrm{d}t'\,\mathrm{d}t_2\\&+\int J_y(t)G(t,t')J_q(t')\,\mathrm{d}t\,\mathrm{d}t'.\end{aligned} \tag{3.63}$$

From the form of $K[J_y,J_q]$, it can already be observed that the only nonzero connected correlation functions contain either one or two fields. The average of $y(t)$ is

$$\langle y(t)\rangle=y_0G(t,t_0)=y_0\Theta(t-t_0)\mathrm{e}^{-\gamma(t-t_0)}. \tag{3.64}$$

The response function $R(t,t')$ from Eq. (3.53), which is equivalent to the connected correlation function $\langle y(t)q(t')\rangle_c$ for $t>t'$, directly follows as

$$\begin{aligned}R(t,t')&=\langle y(t)q(t')\rangle_c,\\&=\frac{\delta}{\delta J_y(t)}\frac{\delta}{\delta J_q(t')}K[J_y,J_q]\bigg|_{J_y=J_q=0},\\&=G(t,t'),\\&=\Theta(t-t')\mathrm{e}^{-\gamma(t-t')}.\end{aligned} \tag{3.65}$$

The second cumulant or the *covariance* of $y(t)$ is obtained by

$$\begin{aligned}\langle y(t)y(t')\rangle_c&=\frac{\delta}{\delta J_y(t)}\frac{\delta}{\delta J_y(t')}K[J_y,J_q]\bigg|_{J_y=J_q=0},\\&=\Xi\int G(t,t_2)G(t',t_2)\,\mathrm{d}t_2,\\&=\Xi\int_{t_0}^{t'}\Theta(t-t_2)\Theta(t'-t_2)\mathrm{e}^{-\gamma(t-t_2)}\mathrm{e}^{-\gamma(t'-t_2)}\,\mathrm{d}t_2,\\&=\Xi\frac{\mathrm{e}^{\gamma(t-t')}-\mathrm{e}^{-\gamma(t+t'-2t_0)}}{2\gamma},\end{aligned} \tag{3.66}$$

for $t' \geq t \geq t_0$. For $t' = t$, this reduces to the connected equal-time correlation function

$$\langle y^2(t)\rangle_c = \Xi \frac{1 - \mathrm{e}^{-2\gamma(t-t_0)}}{2\gamma}, \tag{3.67}$$

which is in fact the connected part of the second moment of $y(t)$.

These results give important insights. Both the average and the response function are exponentially decaying with a decay constant γ, which is exactly the damping coefficient for Brownian motion. This indicates a dissipative system, which is intuitive for Brownian motion. For $t_0 = 0$, the average $\langle y(t)\rangle$ is equal to the expression derived in Eq. (3.17) by using Chandrasekhar's functional approach to Brownian motion. Furthermore, this is also equivalent to Langevin's result derived in Section 2.3.1. The same holds for the covariance $\langle y(t)y(t')\rangle_c$, which is contained in Langevin's expression (2.27) for the second moment of the velocity of a Browian particle. Therefore, this can be seen as a validation of the MSR formalism for SDEs that have analytic solutions. However, as mentioned before in Section 2.3.3, problems arise in the Langevin approach to nonlinear SDEs, which are usually not exactly solvable. Here, the fruitfulness of the MSR formalism becomes clear, since it can be applied to SDEs without analytical solution, by means of perturbation theory. This will be discussed in the next section.

3.4 Perturbative methods for nonlinear Langevin equations

As was already demonstrated in Eq. (3.37) for a generic action $S_{\text{eff}} = S_0 + S_I$, it is possible to express the generating functional $Z[J]$ in terms of functional derivatives with respect to the source field $J(t)$ acting on the free generating functional $Z_0[J]$. For the linear Langevin equation, this resulted in exactly solvable integrals and consequently in Eq. (3.60) for $Z[J_y, J_q]$, since the MSR action $S[y, q]$ is quadratic in the fields $y(t)$ and $q(t)$. This is not possible in general when the action contains higher-order interactions, i.e., the interacting part of the action S_I contains cubic or higher-order contributions. Luckily, if the higher-order interactions are small with respect to the linear and quadratic terms, it is possible to perform a perturbative expansion around $Z_0[J_y, J_q]$. Usually, this is done by assigning a (small) coupling constant to the interactions. The exponent, containing the functional derivatives acting on Z_0, can then be written as a Taylor expansion in orders of this coupling constant.

To see how this general perturbative approach works in the MSR formalism, a nonlinear Langevin equation with a quadratic contribution is taken as an example. This is given by

$$\dot{y}(t) = -\gamma y(t) + \frac{\beta}{2} y^2(t) + \eta(t), \tag{3.68}$$

for some constant β. Just as for the linear case, the initial condition is $y(t_0) = y_0$ and the noise $\eta(t)$ is additive, with noise amplitude Ξ. As the nonlinear contribution is simple, this equation is still tractable even though perturbation theory is required. This nonlinear equation is also studied in Ref. [19], but here it is formulated in a more structured way by using different Feynman rules. The corresponding MSR action can again be obtained from Eq. (3.45), yielding

$$\begin{aligned} S[y, q] &= \int \left\{ q(t)[\dot{y}(t) + \gamma y(t) - \frac{\beta}{2} y^2(t) - y_0\, \delta(t - t_0)] - \frac{\Xi}{2} q^2(t) \right\} \mathrm{d}t, \\ &= S_0[y, q] - \frac{\beta}{2} \int q(t) y^2(t)\, \mathrm{d}t - y_0 \int q(t)\delta(t - t_0)\, \mathrm{d}t - \frac{\Xi}{2} \int q^2(t)\, \mathrm{d}t. \end{aligned} \tag{3.69}$$

Again, the free action S_0 only contains the contribution from the Green's function, which results in Eq. (3.59) for the free generating functional Z_0, just as in the linear case. All other contributions are considered as a part of the interacting action S_I. Below it will be clear that this choice is more convenient for drawing the Feynman diagrams corresponding to the terms in the perturbative expansion. Eq. (3.69) shows that the quadratic term in the nonlinear Langevin equation (3.68) gives rise to a cubic contribution to the MSR action, i.e., S_I contains a cubic interaction. In general, nonlinear terms in the SDE translate to cubic or higher-order interactions in the corresponding effective field theory that is derived via the MSR formalism.

The perturbative expansion of $Z[J_y, J_q]$ around the free generating functional (3.59) is now obtained by writing the interacting contributions in terms of functional derivatives with respect to the sources $J_y(t)$ and $J_q(t)$, acting on $Z_0[J_y, J_q]$. This yields

$$\begin{aligned}
Z[J_y, J_q] &= \exp\left\{\frac{\beta}{2}\int q(t_1)y^2(t_1)\,\mathrm{d}t_1 + y_0\int q(t_2)\delta(t_2-t_0)\,\mathrm{d}t_2 + \frac{\Xi}{2}\int q^2(t_3)\,\mathrm{d}t_3\right\} Z_0[J_y, J_q], \\
&= \exp\Bigg\{\frac{\beta}{2}\int \frac{\delta}{\delta J_q(t_1)}\left(\frac{\delta}{\delta J_y(t_1)}\right)^2 \mathrm{d}t_1 + y_0\int \delta(t_2-t_0)\frac{\delta}{\delta J_q(t_2)}\,\mathrm{d}t_2 \\
&\quad + \frac{\Xi}{2}\int\left(\frac{\delta}{\delta J_q(t_3)}\right)^2 \mathrm{d}t_3\Bigg\} \exp\left\{\int J_y(t)G(t,t')J_q(t')\,\mathrm{d}t\,\mathrm{d}t'\right\}, \qquad (3.70) \\
&= \sum_{V=0}^{\infty}\frac{1}{V!}\Bigg[\frac{\beta}{2}\int \frac{\delta}{\delta J_q(t_1)}\left(\frac{\delta}{\delta J_y(t_1)}\right)^2 \mathrm{d}t_1 + y_0\int \delta(t_2-t_0)\frac{\delta}{\delta J_q(t_2)}\,\mathrm{d}t_2 \\
&\quad + \frac{\Xi}{2}\int\left(\frac{\delta}{\delta J_q(t_3)}\right)^2 \mathrm{d}t_3\Bigg]^V \sum_{P=0}^{\infty}\frac{1}{P!}\left[\int J_y(t)G(t,t')J_q(t')\,\mathrm{d}t\,\mathrm{d}t'\right]^P,
\end{aligned}$$

where in the last step both exponents are written as a Taylor expansion. Note that there is a clear distinction between the time points at which the functional derivatives act on Z_0, as this is important for the proper calculation of correlation functions and corresponding Feynman diagrams. In the expansions, V represents the number of *vertices* and P the number of *propagators*. The terms or vertices in the V-expansion act on the sources $J_y(t)$ and $J_q(t)$ in the P-expansion through functional differentiation, annihilating some of them. Since the vertices are different, it is convenient to assign each a separate value. This can be done by splitting the V-expansion in three separate expansions, yielding a total number of vertices given by $V_\beta + V_{y_0} + V_\Xi$. The remaining sources, after taking all functional derivatives, are called *external legs*. Their numbers E_y and E_q are, for fixed V and P, given by

$$E_y = P - 2V_\beta, \qquad (3.71)$$

$$E_q = P - V_{y_0} - V_\beta - 2V_\Xi. \qquad (3.72)$$

These expressions can be combined into

$$E_q - E_y = V_\beta - V_{y_0} - 2V_\Xi. \qquad (3.73)$$

To find extra conditions for the number of vertices and external legs, next to this consistency relation, the expansion in orders of β and other interaction terms in Eq. (3.70) should be considered. Taking the coupling constant β to be small[30] is equivalent to assuming a small nonlinear disturbance

[30] Small with respect to the other parameters γ and Ξ that determine the evolution of $y(t)$.

to the linear dynamics (3.55) of $y(t)$. By using this assumption, the expansion up to first order in β can be considered as a justified approximation to the exact generating functional. Hence, in this approximation, $V_\beta \leq 1$. Furthermore, the same correlation functions as for the linear case will be calculated. To have a non-vanishing contribution to one of these quantities, the functional derivatives acting on $Z[J_y, J_q]$ should exactly annihilate the remaining sources. All other contributions vanish, either by setting $J_y = J_q = 0$ for the remaining external legs, or by a vanishing functional derivative. So, the only nonzero contributions to the correlation functions of interest have one or two external J_y legs, and zero or one external J_q leg. This sets $E_y = 1, 2$ and $E_q = 0, 1$. By using these conditions for E_y, E_q, V_β and the consistency relation (3.73), all possible other values for V_{y_0}, V_Ξ and P can be calculated.

Writing down the expansion of the generating functional $Z[J_y, J_q]$ up to first order in β explicitly will result in a lengthy expression, even up to two external sources. Therefore, this is done in an organized way in terms of Feynman diagrams, which are graphical representations of the lengthy integral expressions. The Feynman rules for the Green's function and external sources of this interacting field theory are given by

$G(t, t') =$, $\int J_q(t)\mathrm{d}t =$, $\int J_y(t)\mathrm{d}t =$. (3.74)

The three different terms in the V-expansion give rise to three kinds of vertices in the diagrammatic expansion[31]. These vertices are represented by

$\frac{\beta}{2}\int \mathrm{d}t =$ 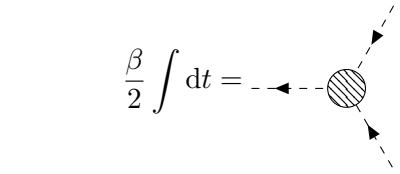 , $\Xi \int \mathrm{d}t =$ 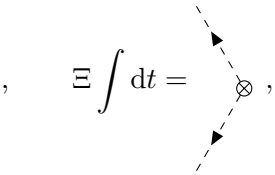 , (3.75)

$y_0 \int \delta(t - t_0)\mathrm{d}t =$ 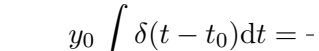 , (3.76)

where the dotted lines represent incoming and outgoing sources and propagators, that should be attached to the vertices.

The conditions derived above for E_y, E_q, V_β and the consistency relation (3.73) now determine all possible Feynman diagrams, up to first order in β, that have a non-vanishing contribution to the correlation functions. Using the Feynman rules above, the expansion of the generating functional $Z[J_y, J_q]$, up to first order in β and up to two external source fields, is given by

$Z[J_y, J_q] = \exp[$ 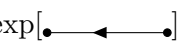 $]\Big[1 +$ 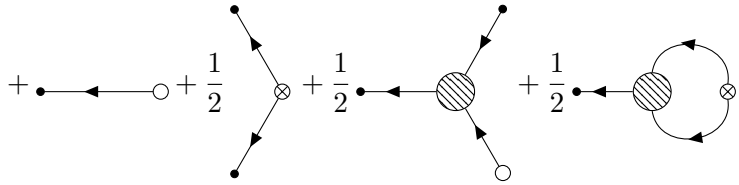

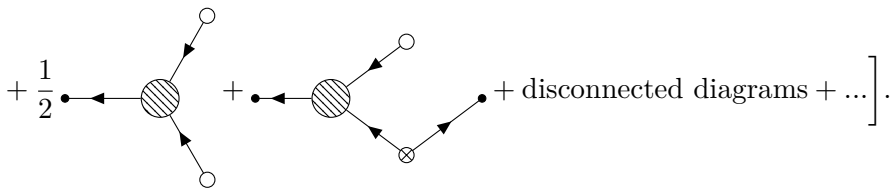 $+ \mathrm{disconnected\ diagrams} + \ldots\Big]$. (3.77)

[31] For this reason, it was convenient to assign each vertex a separate value, that counts the number of appearances of that kind of vertex.

The first exponent corresponds to $Z_0[J_y, J_q]$, with the rest of the expansion written in orders of β and terms of the V-expansion. The prefactors of some diagrams arises from their symmetry factor. Note that only the *connected* diagrams are shown explicitly. All other *disconnected* diagrams are combinations of the connected ones, since a general diagram consists of products of connected diagrams [88]. Usually, these disconnected diagrams drop out when physically interesting quantities are calculated, so only the connected ones are relevant. For example, a connected correlation function consists only of the connected contributions to the correlation function, hence the name.

To obtain the same quantities as for the linear case, one should take the appropriate functional derivatives with respect to the source fields $J_y(t)$ and $J_q(t)$. In terms of the Feynman rules (3.74) defined above, this corresponds to taking away a filled dot. As usual, any remaining source fields are put to zero after the differentiation. This translates nonzero contributions to diagrams with zero filled dots. The resulting correlation functions up to first order in β become

$\langle y(t)\rangle =$ 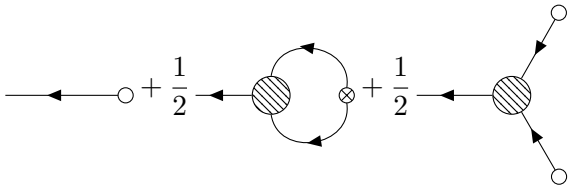 $+ \ldots,$ (3.78)

$\langle y(t)y(t')\rangle_c =$ 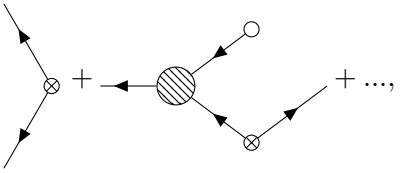 $+ \ldots,$ (3.79)

$R(t,t') = \langle y(t)q(t')\rangle_c =$ 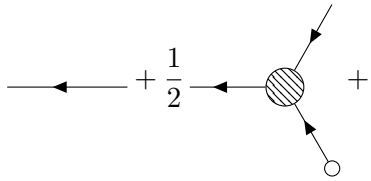 $+ \ldots$ (3.80)

For the average of $y(t)$, only the connected contributions are shown. The other quantities contain only connected diagrams by definition. These diagrammatic expressions can be compared directly to the results (3.64)-(3.66) obtained for the linear Langevin equation, by writing the diagrams back into integral expressions using the Feynman rules (3.74)-(3.76). This shows that the first contribution to these correlation functions, which is of zeroth order in β, is the exact result for the linear case. The other contributions contain the corrections up to first order in β, due to the small nonlinear disturbance of the dynamics. Hence, in the limit of $\beta \to 0$, the results for the linear case are retrieved, which confirms the validity of this perturbative approximation.

The results above show that the MSR formalism can also be applied to SDEs without analytical solution, via perturbation theory. Therefore, this approach is very useful for nonlinear differential equations, such as the Lotka-Volterra model, to which a noise term is added.

3.4.1 The semiclassical approach

Instead of expanding around the coupling constant β of the nonlinearity, it is also possible to perform an expansion around the noise amplitude Ξ. This is equivalent to assuming a weak noise effect on

the dynamics. The general MSR action (3.45) can be rescaled by transforming the auxiliary field $q(t) \to \Xi q(t) = \tilde{q}(t)$, yielding

$$S[y,\tilde{q}] = \frac{1}{\Xi}\int \left\{ \tilde{q}(t)\left[\dot{y}(t) - C(y(t),t) - y_0\,\delta(t-t_0)\right] - \frac{1}{2}\tilde{q}^2(t)D^2(y(t),t)\right\} \mathrm{d}t. \tag{3.81}$$

In the weak noise limit $\Xi \to 0$, the generating functional $Z[J_y, J_q] \propto \mathrm{e}^{-S[y,q]} = \mathrm{e}^{-\frac{1}{\Xi}S[y,\tilde{q}]}$ is dominated by the saddle points of the exponent. These saddle points can be obtained by solving

$$\left.\frac{\delta S[y,\tilde{q}]}{\delta y(t)}\right|_{y=y_s} = J_y(t), \quad \left.\frac{\delta S[y,\tilde{q}]}{\delta \tilde{q}(t)}\right|_{\tilde{q}=\tilde{q}_s} = J_{\tilde{q}}(t), \tag{3.82}$$

which are called the saddle-point equations [80]. In general, these equations can have multiple solutions. The field configurations $y_s(t)$ and $\tilde{q}_s(t)$, which are the solutions of Eq. (3.82), exactly correspond to the trajectory of a (stochastic) system that has the largest probability. In QFT, these fields correspond to the classical path, which are the solutions to the Euler-Lagrange equations[32] [87]. For this reason, this method is called the *semiclassical* approach. It will not be performed explicitly for the nonlinear Langevin equation, but only discussed briefly in general.

The saddle-point expansion of the action is given by

$$S[y,\tilde{q}] = S[y_s,\tilde{q}_s] + \frac{1}{2}\int \begin{pmatrix}\delta y(t) & \delta\tilde{q}(t)\end{pmatrix} \left.\begin{pmatrix} \frac{\delta^2 S}{\delta y^2} & \frac{\delta^2 S}{\delta y \delta \tilde{q}} \\ \frac{\delta^2 S}{\delta \tilde{q}\delta y} & \frac{\delta^2 S}{\delta \tilde{q}^2}\end{pmatrix}\right|_{\substack{y=y_s \\ \tilde{q}=\tilde{q}_s}} \begin{pmatrix}\delta y(t') \\ \delta\tilde{q}(t')\end{pmatrix} \mathrm{d}t\,\mathrm{d}t' + ..., \tag{3.83}$$

where it is assumed that there is only one saddle point. This is just a Taylor expansion around the saddle point solutions $y_s(t)$ and $\tilde{q}_s(t)$, with fluctuations $\delta y = y - y_s$ and $\delta\tilde{q} = \tilde{q} - \tilde{q}_s$. The first-order term is not included, since this cancels the source fields $J_y(t)$ and $J_q(t)$ by definition (3.82) of the fields $y_s(t)$ and $\tilde{q}_s(t)$. The generating functional $Z[J_y, J_q]$ can now be approximated by using the expansion above, via the method of steepest descents [93]. In the literature, this is usually called a WKB approximation [94].

In general however, it is difficult to solve the saddle-point equations analytically. As an example, consider the nonlinear Langevin equation with action (3.69). The saddle-point equations reduce to coupled ODEs for $y_s(t)$ and $\tilde{q}_s(t)$, given by

$$\dot{y}_s(t) = \tilde{q}_s(t) - \gamma y_s(t) + \frac{\beta}{2}y_s^2(t) + y_0\delta(t-t_0) + J_{\tilde{q}}(t), \tag{3.84}$$

$$\dot{\tilde{q}}_s(t) = \tilde{q}_s(t)[\gamma - \beta y_s(t)] - J_y(t). \tag{3.85}$$

These are nonlinear differential equations which do not have an analytic solution. There exist methods, like the cumulant expansion from statistical field theory [95], to approximate the resulting action.

Since this method is only valid in the weak noise limit, it is necessary to compute for each contribution its order in Ξ. Just as for the earlier perturbative expansion, this can be done conveniently in terms of Feynman diagrams. By rescaling the action, also the Feynman rules change. Each edge now contributes a factor Ξ, while every vertex has a factor $1/\Xi$ [19]. If the number of external edges is E, internal edges I and vertices V, then a connected diagram is of order Ξ^{E+I-V}. The number of

[32] These are the classical EoM that follow from the principle of least action [1].

loops L in a connected diagram is given by $L = I - V + 1$ [80], which can be proven by induction. Hence, the order[33] of a connected diagram is Ξ^{E+L-1}. For a connected correlation function, E is fixed, so the expansion in Ξ scales with L. Therefore, this semiclassical approach is often called the *loop expansion*. As can be seen from the Feynman rules (3.74)-(3.76), the loops arise from the possible connection between the β- and Ξ-vertices, i.e. the coupling between the nonlinearity and the noise. Note that the semiclassical approach is a perturbation theory up to all orders in β, so all contributions of the nonlinear interaction are taken into account.

The generating functional and correlation functions can now be calculated up to some order in Ξ, by taking into account all diagrams with the same number of loops L. Consider for example the mean $\langle y(t)\rangle$, which is given by Eq. (3.78) for the nonlinear Langevin equation. The second term in this expansion contains one loop, which has indeed a factor $\beta\Xi/2$. Taking into account only contributions without loops, which are called *tree* diagrams, is equivalent to an approximation of $\langle y(t)\rangle$ up to zeroth order in Ξ. This corresponds to a perturbative expansion of the solution to the nonlinear equation (3.68) without noise. Similarly, consider Eq. (3.84) up to zeroth order in Ξ. This results in disgarding $\tilde{q}_s(t)$, which is first order in Ξ due to the transformation rule. Setting the source fields to zero, as is necessary to calculate correlation functions, the nonlinear Langevin equation is retrieved for the saddle point field $y_s(t)$. This shows that, up to zeroth order in the noise, the solution $y_s(t)$ of the saddle-point equation is indeed the average solution $\langle y(t)\rangle$. As the saddle-point equations can have multiple solutions, this procedure corresponds to picking a saddle point with $q_s(t) = 0$, which results in $S[y_s, q_s] = 0$. It can be shown [15] that such a choice generally yields a solution to the classical[34] EoM, and thus recovers the average solution $\langle y(t)\rangle$.

The examples for the (non)linear Langevin equation are insightful, but remain simple as they are one-dimensional. As mentioned earlier, the MSR formalism was applied to a Lotka-Volterra model consisting of N species with random interactions [92]. However, this approach has never been used to describe a two species Lotka-Volterra system with fixed interactions and a direct stochastic effect. In Section 5, the MSR formalism will be applied explicitly to a stochastic version of the two species predator-prey Lotka-Volterra equations, which describe the dynamics of interacting predator and prey populations. The stochastic perturbation added to this two-dimensional system models random environmental effects that influence these populations. In a similar way as for the examples above, analytical expressions for the correlation functions will be derived, which give a clear view on general stochastic effects in this system. Also, as the noise perturbation is small with respect to the deterministic evolution of the populations, a semiclassical approach will be used.

[33] In QFT, this leads to an expansion in $\hbar$, which again clarifies why this is called the semiclassical approach.

[34] In the quantum mechanical interpretation of the semiclassical approach. From a probabilistic point of view, this would be the noise-averaged EoM.

4 Deterministic Lotka-Volterra model

In Section 2.4.2, we studied the Verhulst model, which describes the dynamics of a single species population $N(t)$ with logistic growth. It turned out that including stochastic effects in terms of multiplicative noise still allowed for a quantitative description of the model, as it was possible to derive an expression for the stationary probability distribution $P_{\mathrm{eq}}(N)$ via a Fokker-Planck equation. In the following sections, we consider the Lotka-Volterra equations, which is another population model describing multiple interacting species. First, the deterministic version of the model is studied in this section, before turning to a stochastic case in Section 5. To become familiar with the model, an introduction to and an interpretation of these equations are discussed. Then, the two species case with one predator and one prey is analyzed by means of the dynamical systems methods from Section 2.4.1.

4.1 Introduction to the Lotka-Volterra equations

The original model was proposed by Lotka [26] in 1910 for studying periodic chemical reactions, which he later extended to predator-prey systems [20]. The same equations were published independently by Volterra in 1926, to explain fluctuating fish catches in the Adriatic Sea [21]. The original Lotka-Volterra equations describe the evolution of an ecological system, consisting of two interacting species. These are one prey and one predator species, like for example rabbits and foxes. This is modeled by a coupled two-dimensional system of nonlinear differential equations, given by

$$\begin{aligned} \dot{u}(t) &= r_u u(t) - \alpha u(t) v(t) \\ \dot{v}(t) &= -r_v v(t) + \beta u(t) v(t). \end{aligned} \tag{4.1}$$

Here, $u(t) \geq 0$ represents the number of prey and $v(t) \geq 0$ represents the number of predators at time t. These equations describe the change of these populations $\dot{u}$ and $\dot{v}$ in time. In this model, it is assumed that the prey population grows exponentially with growth rate r_u without the presence of predators. The predators on the other hand, are assumed to die or emigrate exponentially fast with a loss rate r_v in the absence of prey, i.e. food. The coupling $-\alpha uv$ describes the predation on the prey, which is assumed to be proportional to the meeting rate of both species. The other coupled contribution βuv represents the growth of the predator population due to the consumption of prey. Note that the predation rate α is not necessarily equal to the growth rate β, as eating one rabbit does not necessarily result in the birth of one fox. As the model parameters r_u, r_v, α and β are all rates, they are related to the time t as $1/t$. As the Lotka-Volterra model is analyzed in a general way without considering any ecological application, the choice of the unit of time is arbitrary and will therefore not be specified.

As will turn out in the next section, the solution to Eq. (4.1) is periodic for all initial populations $u_0 = u(0) > 0$ and $v_0 = v(0) > 0$. An example solution for $u_0 = 80$ and $v_0 = 40$ is shown in Figure 4.1. Figure 4.2 shows the corresponding phase space for the same solution. This parametric plot clearly illustrates how the same periodic cycle is traversed multiple times in counterclockwise direction by the blue trajectory. Also, it contains the fixed points of the dynamical system. At $(0, 0)$, there is a saddle point that represents extinction of both species. The fixed point $(20, 40)$ is a center, at which the species coexist. The stability of these fixed points and the periodicity of the solutions will be discussed quantitatively in the next section. The periodic behavior of the populations, represented by the blue trajectory in Figure 4.2, can already be understood intuitively from an ecological point of view. Starting with a population of 80 prey and 40 predators, the

predators have enough food, as the prey population is at its maximum[35]. This allows the predator population to grow, at the expense of the prey. This continues until there are approximately 115 predators and 20 prey, at which point the prey population has reduced so much that the predators grow hungry. As there are still a lot of predators, the prey population keeps decreasing almost up to extinction, resulting in an even faster decay of the predators. Only when there are approximately 5 prey and 10 predators left, the prey population is able to grow again due to rare encounters with predators. Both populations now keep growing, with a delay for the predators, until the system arrives again at the maximum prey population of 80. Then, the periodic cycle starts over again.

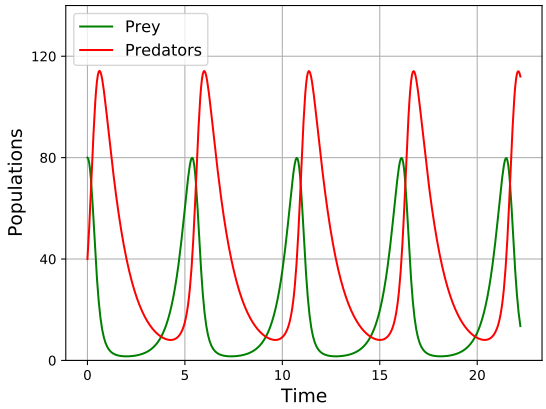

Figure 4.1: A periodic solution of the two species predator-prey Lotka-Volterra model, with parameters $r_u = 2$, $r_v = 1$, $\alpha = \beta = 0.05$ and initial conditions $u_0 = 80$, $v_0 = 40$. The green line represents the prey population, while the red line represents the predator population. The time t is in units of $1/r_v$.

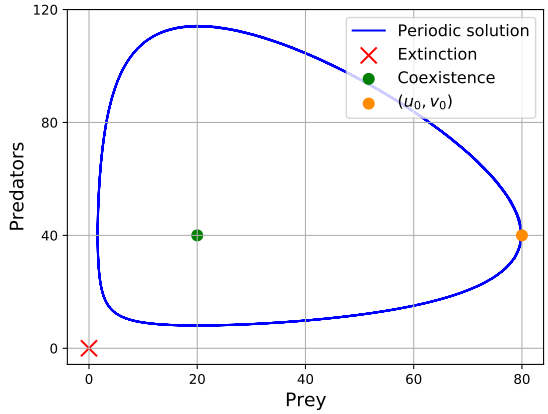

Figure 4.2: The corresponding phase space of the Lotka-Volterra model, with the blue trajectory as the periodic solution. The trajectory traverses the cycle multiple times, in counter clockwise direction. The green dot at $(20, 40)$ represents the center, while the red cross is extinction. The orange dot are the initial populations (u_0, v_0).

From an ecological perspective, the predator-prey Lotka-Volterra model has a couple of unrealistic assumptions. The prey species grows exponentially in the absence of predators, which means that they have limitless food. Even if the prey species are herbivores, this is not the case for large enough populations. To take finite resources into account, it is possible to include a quadratic contribution $-r_u u^2/K_u$ in Eq. (4.1). Similarly as for the Verhulst model in Section 2.4.2, this gives rise to a carrying capacity K_u for the prey. Furthermore, the populations $u(t)$ and $v(t)$ only depend on time and not on the position of the animals. This automatically yields unrealistic predation, as predators should meet the prey somewhere in their environment. There are spatial extensions that apply lattice Lotka-Volterra models to reaction-diffusion systems with chemical reactions [22]. This spatial independence requires assumptions for the food supply of the predators. It is assumed that predators are always hungry, and that their food depends only on the size of the prey population. To model the predation realistically, the consumption rate should be a function of the prey density. For ecological systems, this is called the *functional response* [96], which resulted in the Rozenzweig-MacArthur model [97]. Both this model and the Lotka-Volterra model have been used to analyze the dynamics of predator-prey populations in nature, despite the unrealistic

[35] This statement depends heavily on the model parameters. Only in this specific case, the maximum prey population is 80.

features. Two cases are a wolf and moose system in the Isle Royale National Park [98] and lynx and snowshoe hare populations [99]. Lotka-Volterra-like equations also appear in economic theories, such as the Goodwin model [100].

Another inherent feature of the model that is not very likely to occur in real-life ecosystems, is the behavior at small prey population. For initial conditions far away from the fixed point, e.g. like in Figure. 4.2, the prey population can become very small, while the predator population remains much larger, before decreasing rapidly. Yet, the prey species still recovers. In realistic populations, the prey species would get extinct, due to predation or external environmental effects. In fact, environmental effects are not taken into account at all, since all model parameters do not depend on time. This also implies that the (interaction of) the species themselves do(es) not change. Including time-dependent parameters increases the complexity of the model rapidly. Also, a lot of different external effects play a role in real-life ecological systems. Therefore, it would be easier to include (partially) unknown environmental factors through a stochastic approach, by introducing stochastic contributions as small perturbations to the deterministic model (4.1). Depending on the type of fluctuations, the effects can be modeled by additive or multiplicative noise, yielding an SDE of the form (2.2). This stochastic Lotka-Volterra model, which gives rise to interesting new behavior, will be the topic of Section 5. The question remains if such a stochastic model is ecologically more realistic. In this work, the general (stochastic) features of this model are studied by using the MSR formalism, for which the results are compared with simulations. Therefore, the ecological interpretation and applications are of less importance.

So far, only species with predator-prey interaction have been considered. There are however other types of interactions between species in nature, such as competitive and mutualistic interactions. Variations of the Lotka-Volterra equations (4.1) exist, with different types of interactions. A generalized model for the dynamics of N interacting species can be written as

$$\frac{dx_i(t)}{dt} = r_i x_i(t) \left(K_i + \sum_{j=1}^{N} a_{ij} x_j(t) \right), \quad (4.2)$$

for each species x_i. The type of interaction is captured by the interaction matrix A, which has entries a_{ij}. When species i and j show competitive interactions, the coefficients are $a_{ij}, a_{ji} < 0$. If species i hunts species j, this predator-prey relation corresponds to $a_{ij} > 0$ and $a_{ji} < 0$. When the relation is mutualistic, i.e. both species benefit from the interaction, $a_{ij}, a_{ji} > 0$. This model also includes a carrying capacity, which is given by K_i if $a_{ii} = -1$, to account for limited resources for each species. This generalized Lotka-Volterra model is discussed extensively in Ref. [27].

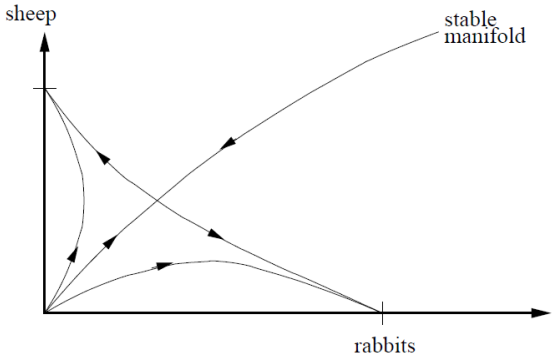

Figure 4.3: Phase space of a two species competitive Lotka-Volterra system, consisting of rabbits and sheep. As the species are competing for the same resources, only one can survive in the end. This is also reflected by the instability of the saddle point at coexistence. At $(0, 0)$ there is now an unstable node. The other two fixed points, where one of the species is extinct, are stable. The stable manifold is the part of phase space that leads to a fixed point, the saddle point in this case. This figure has been extracted from Ref. [101].

As an example, consider a system with two competitive species, as in Figure 4.3. It is clear that in the long term, only one of these species can survive. Indeed, when carrying capacities are included, the coexisting fixed point[36] is a saddle point, which is unstable. The extinction point $(0, 0)$ is an unstable node in this case. There also appear two other fixed points for this system, at which one of the species is extinct. These points are stable, and are exactly equal to the carrying capacity of the surviving species. A complete phase diagram of this system can be found in Ref. [61]. A complete classification of Lotka-Volterra models for $N = 2$ species is performed by Bomze in Ref. [102], with every possible combination of growth rates and interactions. Another interesting case is one with two predators and one prey [27, 103]. This results in the famous Lotka-Volterra principle. This ecological exclusion principle states that the more succesful predator will win from the other, yielding an effective two species system. In this case, more 'succesful' means that the species requires less food to reproduce itself. Interestingly, when stochastic effects are included, Zhang et al. [104] found that coexistence of two predators and a single prey is possible.

4.2 Analysis of the two species Lotka-Volterra model

Now, we focus again on the original Lotka-Volterra model. The deterministic predator-prey Lotka-Volterra equations for two species are given by

$$\dot{u} = r_u u - \alpha uv \tag{4.3}$$

$$\dot{v} = -r_v v + \beta uv. \tag{4.4}$$

It is not possible to write down an analytical solution in terms of known functions for this coupled system of nonlinear equations. Nevertheless, one can analyze the phase diagram of this system by using the dynamical systems methods described in Section 2.4.1. In addition, by recombining the differential equations, a solution of the system can be found in terms of a constant of motion that only depends on the initial populations at $t = 0$. These solutions are also found numerically.

From a mathematical perspective, it would be convenient to rescale these equations by setting $u \to \beta u/r_v$ and $v \to \alpha v/r_u$, which is similar to a *gauge transformation*. As a consequence, the only free parameters will be the growth rates r_v and r_u. All other parameters are absorbed in the normalization of $t, u(t)$ and $v(t)$. However, this transformation is not applied here because of the noise that will be introduced later. To determine the direct effect of this noise, the noise amplitude has to be compared with the other parameters in this model. Therefore, it is more useful to keep all original parameters, which also allows for a more intuitive interpretation of the results.

4.2.1 Solution & Dynamics

To characterize this model, the first thing to do is to calculate the fixed points, where $\dot{u} = 0 = \dot{v}$. These are easily found to be

$$(u^*, v^*) = \begin{cases} (0, 0) \\ \left(\frac{r_v}{\beta}, \frac{r_u}{\alpha}\right). \end{cases} \tag{4.5}$$

The first fixed point represents extinction for both species, while the second represents coexistence[37]. These fixed points are also depicted in Figure 4.2. As was explained in Section 2.4.1, the Jacobian

[36] Note that this is the same point as for the predator-prey case.

[37] In a periodic solution, the species also coexist, but this case is special as the populations remain constant while coexisting.

$\mathcal{J}(u,v)$ of the model should be evaluated at the fixed points (u^*, v^*), to determine their stability. This is given by

$$\mathcal{J}(u,v) = \begin{pmatrix} r_u - \alpha v & -\alpha u \\ \beta v & \beta u - r_v \end{pmatrix}. \tag{4.6}$$

The Jacobian for the (two species) Lotka-Volterra model evaluated at a fixed point is called the *community matrix* [105]. For the fixed point $(u_e^*, v_e^*) \equiv (0,0)$, where both species are extinct, the community matrix is given by

$$\mathcal{J}(0,0) = \begin{pmatrix} r_u & 0 \\ 0 & -r_v \end{pmatrix}. \tag{4.7}$$

Hence, its eigenvalues are $\lambda_1 = r_u$ and $\lambda_2 = -r_v < 0$. According to the classification of fixed points in Figure 2.5, $(0,0)$ is a saddle point, hence it is unstable. So, extinction is not an attractive fixed point in this model. As a consequence, the system will still recover even if populations are very close to zero. As mentioned above, this is not a realistic assumption. For the coexisting fixed point $(u^*, v^*) = (r_v/\beta, r_u/\alpha)$, the community matrix yields

$$\mathcal{J}\left(\frac{r_v}{\beta}, \frac{r_u}{\alpha}\right) = \begin{pmatrix} 0 & -\frac{\alpha r_v}{\beta} \\ \frac{\beta r_u}{\alpha} & 0 \end{pmatrix}. \tag{4.8}$$

This community matrix has eigenvalues $\lambda_{1,2} = \pm i\sqrt{r_v r_u}$. Inspecting Figure 2.5 again, it is observed that $(r_v/\beta, r_u/\alpha)$ is a center or an elliptic fixed point. Such a point is neutrally stable, so it is neither attracting nor repelling.

To study the behavior of the model close to the fixed points, we may linearize the system around these points. For the Lotka-Volterra model, this linearization is given by

$$\begin{pmatrix} \dot{u} \\ \dot{v} \end{pmatrix} = \mathcal{J}(u^*, v^*) \begin{pmatrix} u - u^* \\ v - v^* \end{pmatrix}, \tag{4.9}$$

as in Eq. (2.41). Around the fixed point $(u_e^*, v_e^*) = (0,0)$, this yields a simple uncoupled set of equations $\{\dot{u} = r_u u, \dot{v} = -r_v v\}$, which are respectively solved by exponential growth and decay. This makes sense intuitively, since for $u, v \simeq 0$, the species rarely meet. Hence, this results in the Lotka-Volterra model without interactions. Close to $(u^*, v^*) = (r_v/\beta, r_u/\alpha)$, the linearized model is given by

$$\dot{u} = \frac{\alpha r_v}{\beta}\left(\frac{r_u}{\alpha} - v\right), \tag{4.10}$$

$$\dot{v} = \frac{\beta r_u}{\alpha}\left(u - \frac{r_v}{\beta}\right). \tag{4.11}$$

These coupled equations describe a simple harmonic motion around the fixed point $(r_v/\beta, r_u/\alpha)$, where the prey and predator populations have a phase difference of $\pi/2$. This linearization can be interpreted as neglecting the self-interaction of the species, i.e., neglecting the contributions from their own respective exponential growth and death. The only contribution taken into account here is the (linearized) interaction, so how one species affects the other. As the linearized equations describe simple harmonic motion, their solutions are periodic and perfectly circular. These solutions have a frequency $\omega = \sqrt{\lambda_1 \lambda_2} = \sqrt{r_v r_u}$ [61]. Hence, the populations oscillate with a period

$$T_{\text{lin}} = \frac{2\pi}{\omega} = \frac{2\pi}{\sqrt{r_u r_v}}. \tag{4.12}$$

To investigate solutions of the two species Lotka-Volterra model, the nonlinearized behavior should also be analyzed. If one assumes that $u > 0$ and $v \neq r_u/\alpha$, the coupled equations (4.3) can be combined as

$$\frac{\mathrm{d}v}{\mathrm{d}u} = \frac{v}{u}\frac{\beta u - r_v}{r_u - \alpha v}. \tag{4.13}$$

By performing a separation of variables and integrating, we obtain

$$\begin{aligned} \beta u(t) + \alpha v(t) - r_v \log u(t) - r_u \log v(t) &= \beta u_0 + \alpha v_0 - r_v \log u_0 - r_u \log v_0, \\ F(u, v) &= M, \end{aligned} \tag{4.14}$$

where $u_0 = u(0)$ and $v_0 = v(0)$ are the initial prey and predator populations, and M is a *constant of motion*. It is clear that $F(u, v)$ is a conserved quantity for each solution $\{(u(t), v(t)) \,|\, u(0) = u_0, v(0) = v_0\}$ of the model, that is equal to the value of the constant of motion

$$M = F(u_0, v_0) = \beta u_0 + \alpha v_0 - r_v \log u_0 - r_u \log v_0. \tag{4.15}$$

The function $F(u, v)$ diverges both for $u, v \to 0$ and for $u, v \to \infty$. It attains its minimum in the center $(r_v/\beta, r_u/\alpha)$, given by $F(r_v/\beta, r_u/\alpha) = r_v + r_u - r_v \log r_v/\beta - r_u \log r_u/\alpha \equiv M^*$. As the model is conservative, it can be translated to a Hamiltonian system with Hamiltonian $H(u, v) = F(u, v) - M^*$ and energy $E = M - M^* \geq 0$. This is done by performing a coordinate transformation $p = \log(u)$, $q = \log(v)$. This translates the Lotka-Volterra equations (4.3) to Hamilton's equations $\dot{q} = \partial H/\partial p$, $\dot{p} = -\partial H/\partial q$, for generalized position q and conjugate momentum p. From the structure of the nondiagonal interaction matrix A, it can even be proven that there should be a conserved quantity [101], which results in a conservative system. According to the theory of conservative systems [61], every energy $E > 0$ defines a periodic solution around the fixed point $(r_v/\beta, r_u/\alpha)$, where $E = 0$. As the energy E depends on the initial populations u_0 and v_0 through M^*, every set of initial populations yields a periodic solution. This can also be observed in Figure 4.4, which shows the phase space of the system with numerically obtained periodic solutions, for different initial populations. A geometric proof for the periodicity of solutions of the two species Lotka-Volterra model is given in Ref. [27].

So, as expected from the linearization, the solutions close to the center are periodic[38]. In general, solutions of conservative systems close to a center are closed curves around it, which have a period close to the period $T_{\text{lin}} = 2\pi/\sqrt{r_u r_v}$ of the linearized case. However, this only holds close to the center. Further away from the fixed point, the linearization breaks down, and the period increases. Integral expressions for the period $T(E)$ of solutions of the Lotka-Volterra model with energy E are derived in Ref. [106].

Exponential growth of the prey species in the absence of predators is one of the unrealistic features of the two species Lotka-Volterra model. When limited resources are taken into account, by introducing a carrying capacity for the prey species, its growth becomes logistic instead of exponential, due to the negative quadratic contribution. Adding such a self-interaction to the system transforms the neutrally stable center to a stable spiral, resulting in spiraling solutions towards the fixed point [103]. This can be observed in Figure. 4.5, where the prey are rabbits and the predators are foxes. From the perspective of conservative systems, the interpretation is that the carrying capacity breaks the symmetry of the interaction matrix. Hence, there is no conserved quantity, and the system becomes dissipative. However, if the parameters of the model are time dependent and other conditions are obeyed, the system can still have a unique, globally attracting periodic orbit [101].

[38] In fact, this expectation is tricky, as centers are not hyperbolic, hence the Hartman-Grobman theorem [64] does not apply. However, for conservative systems it can be proven that nonlinear centers also have periodic solutions around it [61].

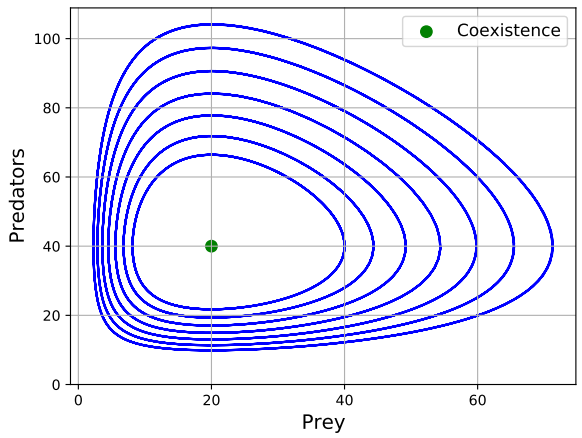

Figure 4.4: Phase space of the Lotka-Volterra model, with seven numerically calculated periodic solutions (blue) for different initial populations $u_0 = 40, ..., 64$. Model parameters are $r_u = 2$, $\alpha = \beta = 0.05$ and $r_v = 1$. At the fixed point (green) there is a center where the species coexist in equilibrium.

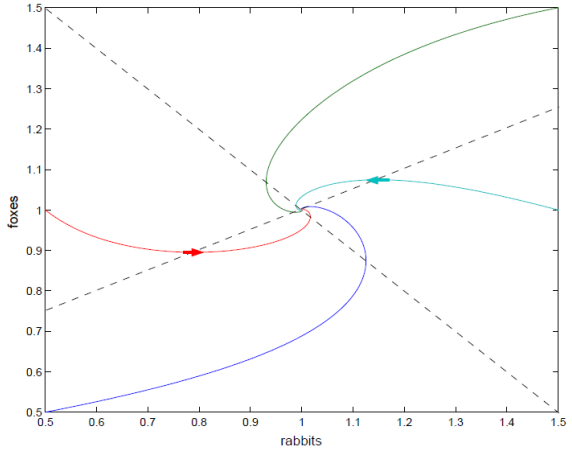

Figure 4.5: Phase space of a Lotka-Volterra model with carrying capacities. Parameters are $r_u = 4$, $\alpha = 2$, $\beta = 1$, $r_v = 1$ and $K_u = 2$, $K_v = 2$. Solutions are shown for two different initial populations. Including K_i transforms the fixed point from a center to a stable spiral. This figure has been extracted from Ref. [101].

4.2.2 Numerical implementation

As the solutions of the two species predator-prey Lotka-Volterra equations can not be expressed in terms of known functions, the equations have to be solved numerically. A naive way of doing this would be by using the explicit or implicit Euler method. For this model, this will respectively result in outward or inward spiraling solutions [107], instead of the periodic solutions that should be obtained. Hence, by using these methods, the populations either explode or collapse in the fixed point. As a solution to this problem, symplectic Euler methods can be applied, for which one variable is treated as explicit and the other as implicit. This still leaves us with two possible numerical schemes, which both give periodic solutions that move around the actual periodic solutions [107]. Taking the average of these two symplectic Euler methods yields a good approximation of the solutions of the system. This procedure already points out that this system is difficult to solve numerically without a significant error.

For the reasons above, it is better to make use of a standard solver of differential equations that is already optimized. In Python, this could be `ode` or `odeint`, which again use different methods, depending on the type of ODE. As the Lotka-Volterra model will be extended to a stochastic version later, it is better to use the package `sdeint`, which is already optimized for SDEs [108]. This solver has two algorithms for Itô SDEs, `itoint` and `itoEuler`. Just as for the definition of a general SDE (2.2), the algorithms require a separate deterministic and stochastic part of the evolution. Hence, to study the deterministic Lotka-Volterra equations numerically using these algorithms, the stochastic part can simply be put to zero. Other specifications of this integrator will be discussed later in Section 5.2. Our Python code for the numerical solutions and calculations for the deterministic Lotka-Volterra model can be found in Ref. [109].

To explore the solutions of the model in a structured way, it is convenient to choose a fixed set

of parameters, which in our case will be the same as used earlier for Figures 4.1-4.4: $r_u = 2$, $\alpha = \beta = 0.05$ and $r_v = 1$. A first reason for this choice is that it yields reasonable population sizes of 10-100 predators and prey. Although we do not give priority to the ecological interpretation of the model, it is useful to have realistic population sizes, such that a proportional noise amplitude can be chosen in the stochastic case later. Furthermore, these parameters are used by Vadillo [29] to study different stochastic Lotka-Volterra models. Therefore, to compare with his results, the same model parameters must be used. The standard initial populations are chosen as $u_0 = v_0 = 40$, which is relatively close to the fixed point $(r_v/\beta, r_u/\alpha) = (20, 40)$.

To determine an appropriate simulation time, the period $T(E)$ of one cycle should be obtained, which depends on the energy E of the periodic trajectory. Formulas for this period are provided in Ref. [106]. However, as the goal is to simulate only a few cycles, the period can be approximated by the period of the linearized solution around the fixed point (4.12), which is given by $T_{\text{lin}} = \pi\sqrt{2}$ for the standard parameters. This is slightly smaller than one complete period $T(E)$ for $E > 0$, but it is not necessary to calculate an exact integer number of cycles. The total simulation time is then given by $T_{\text{sim}} = mT_{\text{lin}}$, for some integer $m \simeq 5$ that represents the number of linear cycles.

As the numerical solutions of the Lotka-Volterra equations show an inaccuracy, it is useful to perform an error estimation of the different possible algorithms. This can be done by using the energy E or constant of motion M. Because it only depends on the choice of parameters and initial populations through Eq. (4.15), the constant of motion can be determined for every numerical solution. Since this should be conserved along any solution of the deterministic Lotka-Volterra model, a deviation from this constant implies an error in the numerical solution. To give a quantitative measure to this error, it can be defined as

$$\Delta M = \left| \frac{M(T_{\text{sim}}) - M_0}{M_0} \right| \cdot 100\,\%, \tag{4.16}$$

where $M(T_{\text{sim}}) = F(u(T_{\text{sim}}), v(T_{\text{sim}}))$ is the constant of motion at the end of the numerical calculation, following from Eq. (4.14), and $M_0 = F(u_0, v_0)$ is its initial value. The value of M at the end of the numerical trajectory is chosen, as the error grows with the total simulation time T_{sim}. The main cause of this error, however, is the size of the time step Δt that is used for the numerical solution of a differential equation. For the standard integrators `ode` and `odeint`, this time step is determined by the algorithm itself, which yields errors around 0.0001%. These cases are useful for comparison, as the time step for the `sdeint` package has to be determined manually. Because the total runtime of the code scales linearly with the number of time steps, Δt has to be as large as possible, while still providing accurate solutions. For a time step $\Delta t = 0.002$, the error in the `itoEuler` algorithm is already around 0.4 %, while the error in the `itoint` algorithm is only $2 \cdot 10^{-6}$ %. Hence, it makes sense to use the `itoint` algorithm. Even for $\Delta t = 0.2$, the error in the `itoint` algorithm is only 0.2 %. In the code [109], the time step size is determined as $\Delta t = T_{\text{sim}}/N$, where $N = nm$ is the total number of time steps, yielding $\Delta t = T_{\text{lin}}/n = \pi\sqrt{2}/n$. Setting the number of time steps per linear cycle as $n = 100$, yields $\Delta t \simeq 0.04$ and an error of $7 \cdot 10^{-3}$ % for $m = 5$. This is considered to be an accurate numerical solution.

Using this error measure, it can be explained why it is important to have initial populations relatively close to the fixed point. The inaccuracy of the numerical solution becomes larger when the nonlinear effects are more prominent, which occurs for solutions far away from the fixed point, as the linearization breaks down there. This inaccuracy causes the numerical solution to spiral inward for the `sdeint` algorithm, which is the same effect occurring for several explicit numerical methods.

An example of a numerical solution with a small error (blue), starting close to the fixed point, and a solution with a large error (red), starting far away from the fixed point, are depicted in Figure 4.6. The respective errors are 0.033% and 58.5%, after a total simulation time of $T_{\text{sim}} = 25T_{\text{lin}}$ and $n = 100$. This also justifies the choice of $m \simeq 5$, as the error also scales with the total simulation time. Furthermore, the red trajectory allows for the extreme case with almost extinct prey population and still significant predator population. As discussed in the introduction of this section, this is ecologically unrealistic. So, there is both a numerical and ecological argument to study solutions with initial populations close to the fixed point. For the chosen parameters, the fixed point is $(20, 40)$, justifying the standard initial populations to be $(u_0, v_0) = (40, 40)$.

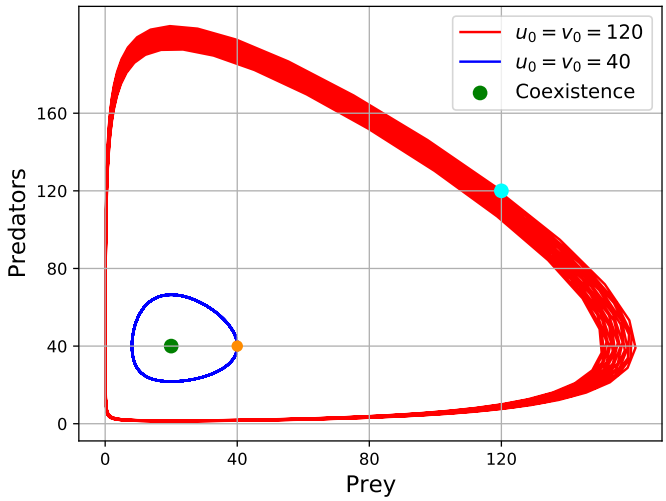

Figure 4.6: An illustration of the numerical error for a solution far away from the fixed point $(20, 40)$, after a total simulation time of $25T_{\text{lin}}$. The blue solution starts in the orange dot at $(40, 40)$, showing periodic motion as the error is only 0.033%. The red solution starts in the cyan dot at $(120, 120)$, showing inward spiraling motion with an error of 58.5%.

5 Stochastic Lotka-Volterra equations

The previous section considered the deterministic Lotka-Volterra model. External effects in this predator-prey system can be investigated through the addition of noise to the deterministic equations. Stochastic versions of this model were studied by Vadillo [29], Liu & Fan [31] and Arnold et al. [32]. Noise effects were also investigated for extensions of the two species Lotka-Volterra model by Zhang et al. [104], Sidhom & Galla [24] and Mobilia et al. [22]. In this work, the stochastic two species Lotka-Volterra model with additive noise is studied, which is given by

$$\begin{aligned} \dot{u}(t) &= r_u u(t) - \alpha u(t)v(t) + \sqrt{\Xi_u}\,\eta_u(t), \\ \dot{v}(t) &= -r_v v(t) + \beta u(t)v(t) + \sqrt{\Xi_v}\,\eta_v(t). \end{aligned} \tag{5.1}$$

The parameters r_u, r_v, α and β represent the same quantities as in the deterministic case (4.3). $\eta_u(t)$ and $\eta_v(t)$ are independent Gaussian white noise processes with respective amplitudes Ξ_u and Ξ_v. Independent in this case means that all combined correlation functions, like $\langle \eta_u(t)\eta_v(t')\rangle$, vanish. Note that the noise amplitudes are written explicitly in the noise coupling matrix in these SDEs, instead of contained in the autocorrelation functions of the noises. From a simulation perspective, this is convenient. The noise coupling matrix is given by the function $D(y,t)$ in Eq. (2.2). As the noise contribution in the MSR action scales with $D^2(y,t)$, the square roots are canceled.

Comparing these equations with earlier obtained SDEs, they can be interpreted as a coupled two-dimensional system of nonlinear Langevin equations. As this model contains multiple interacting species, it is not possible to derive a closed-form expression for the stationary probability distribution. Therefore, this requires methods for nonlinear systems like the MSR formalism. Using this field-theoretical approach, expressions for correlation functions will be determined analytically, and compared with results of simulations of Eq. (5.1). As this model is nonlinear, the analytical calculations will make use of the semiclassical approach and perturbation theory. Before diving into these calculations, it is insightful to give an interpretation to this model and to see what results have already been investigated in the literature.

5.1 Interpretation and literature

The deterministic Lotka-Volterra is a very simple model in population ecology. However, despite some unrealistic biological features that were discussed in Section 4.1, it already includes the most important features like the growth, decay, and interactions of an isolated two species predator-prey system. Because it can also be easily extended by incorporating carrying capacities or functional responses, it is an interesting starting point for modeling the evolution of predator and prey populations.

In real life, ecosystems are never completely isolated. External factors due to environmental variability always influence the populations and their interactions. As there are usually a lot of external effects of which the exact influence on the populations is unclear or unknown, it makes sense to model these as a stochastic term in the system. Because the environment varies on a time scale much shorter than the macroscopic evolution of the populations, this stochastic contribution can be assumed to be Gaussian white noise. Furthermore, the habitat is global and interacts with both species in a way that does not depend on the state of the system. Usually, such a stochastic effect is modeled by additive noise. The effect of the environment can be different for both species, which justifies the choice of two independent Gaussian white noises $\eta_u(t)$ and $\eta_v(t)$. In real ecosystems, these stochastic fluctuations can arise from changes in the weather or climate in the habitat of the

species, or even more drastic events like natural disasters. The random effects can also describe immigration to somewhere outside the habitat.

From a mathematical point of view, additive noise is one of the simplest random influences that can be studied. Incorporating this in the simple ecological Lotka-Volterra model allows for a general study of noise effects in the evolution of populations, which can easily be extended to more difficult systems. External noise effects are particularly interesting for this model. As the system of SDEs is nonlinear, it yields a nontrivial phase portrait that can be influenced by the noise. When applying the MSR formalism to this model, this nonlinearity requires the use of perturbation theory in terms of Feynman diagrams. The Feynman rules for the additive noise case are not so intricate and yield tractable calculations that can be extended to other kinds of noise. This could, for example, be multiplicative noise, which can arise from a varying birth rate r_u and dying rate r_v in the model, or from stochastic interactions due to seasonal changes. Multiplicative noise can model a larger variety of realistic ecological factors in the populations, but as the main interest is to study general noise effects in this model that are state-independent, this work will focus on additive noise. A more elaborated interpretation of noise in ecosystems is given in Ref. [33].

The two species Lotka-Volterra model with stochastic effects has been studied widely, especially for multiplicative noise. One of the first analyses was done by Arnold et al. [32]. They found that for multiplicative white noise, there exists no stationary solution of the model, although the explosion to infinite population has zero probability. For multiplicative colored noise, stationary solutions can exist, depending on the spectral density of the noise. In more recent mathematical studies, Liu & Fan [31] proposed a new definition for permanence in stochastic Lotka-Volterra models with multiplicative white noise and carrying capacities. Tian et al. [30] were one of the few that studied additive noise in Lotka-Volterra equations with a carrying capacity. Next to the evolution in time, they also included spatial diffusion of both species. By looking at phase transitions in the spatial domain, they found that the noise has a destabilising effect on the dynamics through a Hopf bifurcation. The resulting phase space for a fixed spatial location is shown in Figure 5.1. At this point, the system shows an outward spiraling motion, until it reaches a limit cycle.

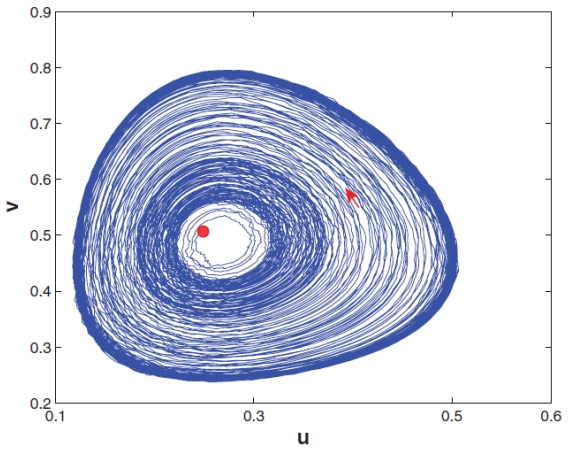

Figure 5.1: The phase space of a spatio-temporal Lotka-Volterra model with carrying capacities and additive noise, at fixed coordinates. The arrow indicates the direction of the trajectory and the dot represents the initial populations. This figure has been extracted from Ref. [30].

A paper by Vadillo [29] is one of the few that considers Lotka-Volterra models without carrying capacities. Although he considers multiplicative noise, this makes it easier to compare his results with the simulations performed for this work. Therefore, as mentioned earlier in Section 4.2.2, the parameters chosen by Vadillo will also be used in the analytical calculations and simulations in Section 5.4. In Ref. [29], these are given by a prey growth rate $r_u = 2$ and a predator decay rate $r_v = 1$. The predation rate α and predator growth rate β are given by the same value $\alpha = \beta = 0.05$. These parameters result in reasonable population numbers of several tens for each species. Vadillo

considers three different stochastic Lotka-Volterra models, each with a different multiplicative noise coupling function $D(y,t)$, for which the mean extinction time is calculated. The phase space of the averaged simulations for 10^3 noise realizations for these three models is shown in Figure 5.2. The red and blue lines depict trajectories of models that are not suited to compare with model (5.1). The green line shows the trajectory of a Lotka-Volterra model given by

$$\begin{aligned} \dot{r} &= r(2-\alpha f) - \sigma_1 r\,\eta_1(t), \\ \dot{f} &= f(\alpha r - 1) - \sigma_2 f\,\eta_2(t). \end{aligned} \tag{5.2}$$

Here, r represents the number of prey (rabbits) and f represents the number of predators (foxes). $\eta_1(t)$ and $\eta_2(t)$ are independent Gaussian white noises with respective amplitudes σ_1 and σ_2. These equations are similar to Eq. (5.1), except for the multiplicative noise. Because the three models are only simulated for $0 \leq t \leq 12$, the trajectories remain close to each other and the red and green ones even overlap, despite the different kinds of noise used in the models.

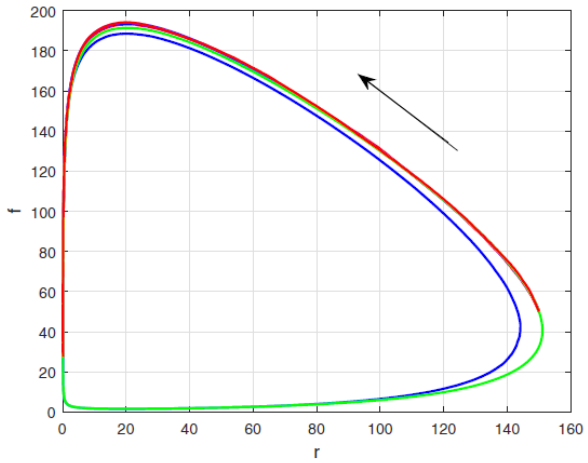

Figure 5.2: Phase space for averaged numerical simulations for 10^3 noise realizations for $0 \leq t \leq 12$, for three stochastic Lotka-Volterra models with multiplicative noise. Each color represents a different model. Initial populations are $r(0) = 150$ prey and $f(0) = 50$ predators. For the green line, the noise amplitudes are $\sigma_1 = \sigma_2 = 0.001$ and $\alpha = 0.05$. This figure has been extracted from Ref. [29].

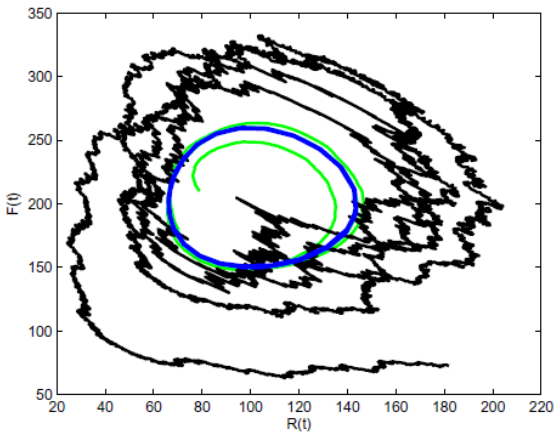

Figure 5.3: Phase space of a stochastic Lotka-Volterra model with multiplicative noise. The blue line corresponds to the deterministic model, while the black line is a simulation of the stochastic model for one noise realization for $0 \leq t \leq 20$. The green line is the average of 100 noise realizations for $0 \leq t \leq 12$. Initial populations are $R(0) = 100$ and $F(0) = 150$, and $\alpha = 0.01$. This figure has been extracted from Ref. [28].

A different stochastic model is considered by de la Hoz & Vadillo [28], for R rabbits and F foxes, where the noise coupling functions are given by $D(R,t) = \sqrt{R(2+\alpha F)}$ and $D(F,t) = \sqrt{F(\alpha R + 1)}$. This is a slightly more difficult multiplicative noise, which also has no explicit amplitude σ. The parameters are the same as in Ref. [29], except for $\alpha = \beta = 0.01$. The phase space of this model in Figure 5.3 shows an interesting feature. Although the average green trajectory is only simulated for $0 \leq t \leq 12$, it seems to show an inward spiraling motion towards the fixed point $(100, 200)$ of the model. This behavior will be investigated further in Section 5.2.1.

When generalizations of the two species Lotka-Volterra model are considered, the theory of statistical physics and disordered systems becomes useful. This is, for example, used in Altieri et al. [23],

where a disordered multiple species Lotka-Volterra model similar to Eq. (4.2) with multiplicative noise and carrying capacities is studied. The disorder in the system arises from a random interaction matrix A, which has independent and identically distributed elements a_{ij}. This model is studied using ensemble methods from statistical physics and the replica formalism. They show that for sufficiently heterogeneous interactions measured by σ and small noise amplitude proportional to an effective temperature T, the system has multiple equilibria (see Figure 5.4). The number of stable equilibria is exponential in the number of species. For even smaller noise amplitudes, there is a *Gardner transition* to a marginally stable state. Such a transition is also observed in jamming of amorphous materials [110].

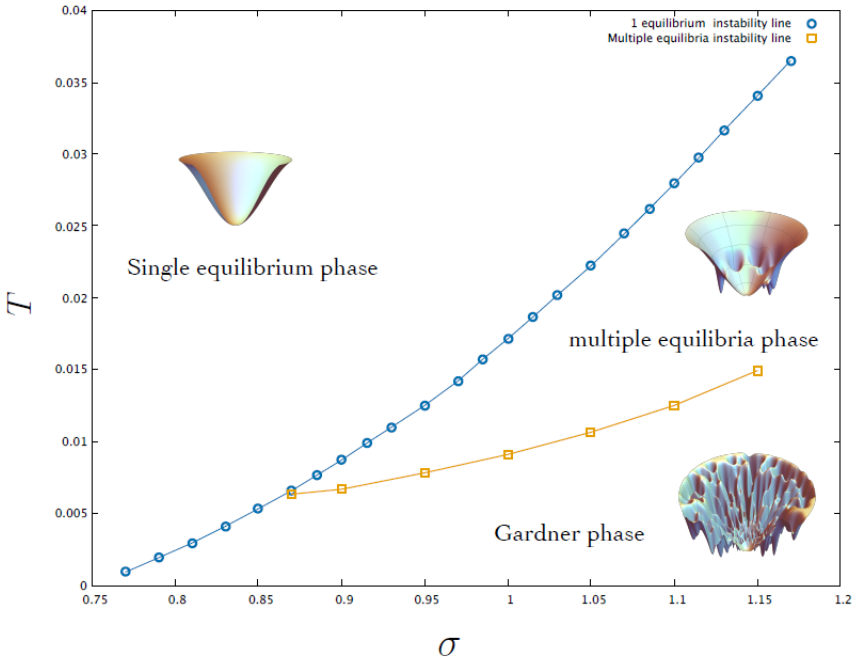

Figure 5.4: A phase diagram of the temperature T, representing the noise amplitude, versus the degree of heterogeneity σ. The three possible phases are a single equilibrium, multiple equilibria and a Gardner phase. This figure has been extracted from Ref. [23].

Sidhom & Galla also investigate a multispecies disordered Lotka-Volterra model in Ref. [24], which contains a random interaction matrix, to which they later add additive Gaussian colored noise. To derive expressions for correlation functions for this N species system, they use field-theoretical methods, one of which is the MSR formalism. First, they perform a disorder average over all possible realizations of the random interaction matrix entries a_{ij} in the limit $N \to \infty$. This yields an effective SDE, to which the MSR formalism is applied. This is later used to study the dynamics of ecological communities and stability in this model. The approach that they adopt is somewhat different from a direct use of the MSR formalism to an SDE. Nevertheless, this was the inspiration for this work, to study stochastic Lotka-Volterra models by using the MSR formalism.

Functional methods are not restricted to multispecies Lotka-Volterra models and can be applied to other generalizations. In Ref. [25], which is a continuation of Ref. [22], Täuber uses a field-theoretical approach to study a spatio-temporal stochastic Lotka-Volterra model for two species. This model includes carrying capacities and multiplicative noise. As this is an extension in space, it

also contains spatial diffusion of both species. He also makes use of the MSR formalism[39] to derive the action of the model. It is shown that population oscillations result in spatio-temporal structures in this model. The analytical results are compared with Monte Carlo lattice simulations.

One thing that all Lotka-Volterra models have in common is that the species interact. This yields nonlinear differential equations for the evolution of the populations. It is usually difficult, or even impossible, to find a stationary PDF for such a system. Therefore, the intuitive Langevin and Fokker-Planck approach are not applicable to study general noise effects in these systems. As the work by Sidhom & Galla [24] and Täuber [25] shows, field-theoretical methods are well suited to analyze these kind of models. One of those methods is the MSR formalism. It has, however, never been applied to the simple two species predator-prey case (5.1) with additive noise. As extra effects like carrying capacities are not included, the deterministic version of this model results in the periodic solutions found in Section 4.2. Using the MSR formalism, a description of the noise effects on these periodic solutions can be derived in terms of correlation functions for the fluctuations around these solutions. Furthermore, it is interesting to see if this field-theoretical approach is also useful in the case of a more difficult model than the nonlinear Langevin equation.

Because the MSR formalism has never been applied to this simple model, our results must be verified via other methods. This is done by comparing the analytical findings with results from simulations. These latter are already interesting by themselves, as simulations of this specific stochastic model have never been done in the limit of long time. In the next section, it is explained how these simulations are performed.

5.2 Simulations

The stochastic Lotka-Volterra model with additive noise in Eq. (5.1) can be solved numerically in Python, in a similar way as the deterministic case. There is, however, a fundamental difference between both models. The deterministic one is a system of ODEs, which has a unique solution for every initial population (u_0, v_0). Hence, its numerically calculated solution is unique, despite the small numerical inaccuracy. The stochastic case consists of coupled SDEs, which by definition do no have a unique solution, as the solution is a functional of the noises $\eta_u(t)$ and $\eta_v(t)$. Only for a fixed noise realization $(h_u(t), h_v(t))$, the system reduces to ODEs. Hence, every numerical solution of this stochastic system will be different. This is why several simulations of this model are performed, each using a different noise realization. To obtain reliable results for the general behavior of this stochastic system, ensemble averages have to be calculated over a large number of simulations. Our code for the simulations is given in Ref. [109]. Below, we discuss the important features of these simulations and show some preliminary results, before comparing with the analytical calculations.

The stochastic simulations make use of the same Python package `sdeint` as the deterministic case, as this is already optimized for the solution of SDEs [108]. The `itoint` algorithm from the `sdeint` package is used to perform the numerical integration for each noise realization, using Itô's principle. This choice is based on the error considerations calculated in Section 4.2.2. In this algorithm, SDEs are separated in a deterministic function $C(\boldsymbol{y}(t), t)$ and a noise coupling function $D(\boldsymbol{y}(t), t)$. For the Lotka-Volterra model, $\boldsymbol{y}(t) = (u(t), v(t))$ and $C(\boldsymbol{y}(t), t)$ contains the deterministic Lotka-Volterra equations (4.1). The noise coupling matrix only contains the noise amplitudes. As both species are perturbed by independent Gaussian white noises, this is given by a diagonal matrix

$$D(\boldsymbol{y}(t), t) = \begin{pmatrix} \sqrt{\Xi_u} & 0 \\ 0 & \sqrt{\Xi_v} \end{pmatrix}. \tag{5.3}$$

[39] Rather, he makes use of the extension of the formalism by Janssen [12] and de Dominicis [13].

In the algorithm, this two-dimensional function automatically couples to the noises, which are Gaussian and white by default. To generate the noise as a stochastic process, the package makes use of `random.normal`, which is a pseudo-random number generator[40] that draws independent random variables from a Gaussian distribution. At each point in time that the integrator is called, the function `random.normal` draws a random number that represents the value of the noise realization at that moment. Next to independent noise values at each point in time in one simulation, this method also ensures that the noise realization is different for another simulation. Hence, the system of SDEs is solved by numerically calculating the combined evolution resulting from the deterministic function $C(\boldsymbol{y}(t), t)$ and the stochastic contribution, at every point in time for a fixed number of time points with separation Δt. The deterministic solution is also calculated, in the same way as explained in Section 4.2.2. For both models, the solution is then given by a discrete array in time.

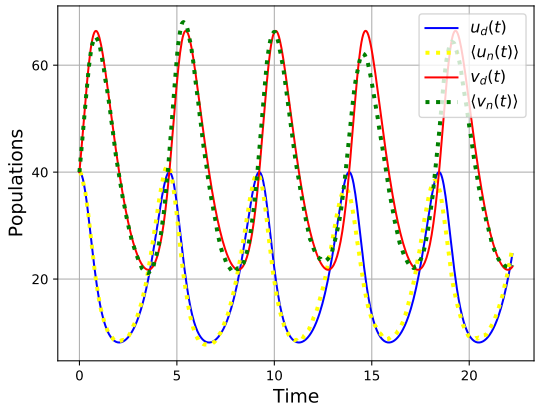

Figure 5.5: Periodic solution (u_d, v_d) of the deterministic model represented by the solid lines and a simulation for one noise realization (u_n, v_n) represented by the dotted lines. The simulations are performed with the standard parameters and noise amplitudes $\Xi_u = 0.2, \Xi_v = 0.4$, for $5T_{\text{lin}}$.

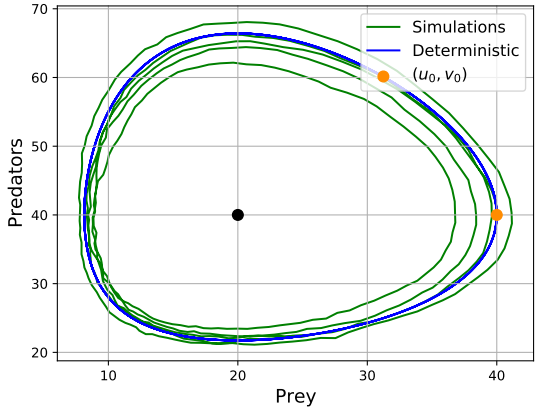

Figure 5.6: Corresponding phase space for deterministic solution (blue) and simulation of one noise realization (green) of the stochastic Lotka-Volterra model. The orange dot represents the initial populations $(u_0, v_0) = (40, 40)$. The black dot is the fixed point $(20, 40)$ of the model.

Figure 5.5 shows the simulated result for the evolution of both populations in time, $(u_d(t), v_d(t))$ for the deterministic case and $(u_n(t), v_n(t))$ for one noise realization. It can be observed that the populations for the stochastic model deviate only slightly from the deterministic solutions. The simulations are performed for a time $T_{\text{sim}} = 5T_{\text{lin}}$ with noise amplitudes $\Xi_u = 0.2$ and $\Xi_v = 0.4$. The model parameters are the standard parameters, given by $r_u = 2$, $\alpha = \beta = 0.05$ and $r_v = 1$. These will also be used for all other simulations, unless stated otherwise. The fluctuating behavior around the deterministic solution is better visible in the phase space in Figure 5.6, corresponding to the same solutions. Both the deterministic and stochastic solution have the same (standard) initial populations $(u_0, v_0) = (40, 40)$, which are also fixed for most simulations. The green trajectory, representing the stochastic simulation for one noise realization, fluctuates around the deterministic solution given in blue. This visual argument strengthens the interpretation of the noise perturbing the deterministic solution at every point in time. As the noise amplitudes are small compared to

[40] Pseudo-random number generators appear to generate random numbers, but are inherently deterministic. Yet, the deterministic behavior can only be observed for extremely large amounts of random numbers. For most problems that make use of random numbers, like the stochastic Lotka-Volterra model, this method is well-suited.

the actual populations and thus small compared to the deterministic contributions to the evolution, the stochastic trajectory remains close to the deterministic one.

Just as for the numerical solutions of the deterministic model, the simulation time is chosen to be $T_{\text{sim}} = mT_{\text{lin}}$, where m is the number of linear cycles with period $T_{\text{lin}} = 2\pi/\sqrt{r_u r_v} = \pi\sqrt{2}$. Since a solution of the stochastic model is not periodic due to the fluctuations, this justifies using T_{lin} as the characteristic time scale of the system. For most simulations, the number of linear cycles is taken to be $m \leq 10$, such that the system completes a few cycles. The total number of time steps in each simulation is given by $N = nm$. As $n = 100$ yielded an accurate numerical solution in the deterministic case, this is also used for the stochastic case. This gives a time step size of $\Delta t = \pi\sqrt{2}/n \simeq 0.04$. The total runtime of the simulation depends on the choice for m and n. Both are sufficiently small, such that a large amount of noise realizations (10^4) can be performed in a reasonable amount of time, which is a few hours.

The most important parameters in the stochastic model are the noise amplitudes Ξ_u for the prey and Ξ_v for the predators. For most simulations, these are fixed as $\Xi_u = 0.2$ and $\Xi_v = 0.4$. The noise amplitude for the predators is twice as large as for the prey, as the fixed point of the system is $(20, 40)$ for the standard parameters. Hence, the ratio between the noise amplitudes is the same as the ratio between the stationary populations. This is to ensure that the effect of the noise on both species is of a comparable size. Also, similar values for the noise amplitude are used in other studies of stochastic Lotka-Volterra models. Vadillo [29], who uses the same standard model parameters, uses multiplicative noise with an amplitude of $\sigma = 0.001$. However, as this noise is multiplicative, this leads to a total amplitude of $0.01 - 0.1$ for the same population sizes. Tian et al. [30] set the noise amplitude to $\sigma = 0.01$, but also their model parameters yield population sizes around $0.1 - 1$. Liu & Fan [31] use $\sigma \simeq 0.3$ for multiplicative noise, but as their population sizes are also of order 1, this barely changes the total noise amplitude. Hence, the noise amplitudes used in this work are comparable to the ones used in other studies. Another important consideration to take into account when determining an appropriate noise amplitude, are the field-theoretical methods used for the analytical calculations. Perturbation theory is only applicable if the coupling constants, in this case the interaction coefficients α and β and the noise amplitudes Ξ_u and Ξ_v, are small compared to the coefficients of the linear contributions. For the standard parameters and the noise amplitudes used here, this condition is satisfied.

The solutions of the deterministic Lotka-Volterra model are periodic and positive for all initial populations $(u_0, v_0) > 0$. Hence, both species never go extinct in this ecological system in equilibrium. However, when noise is added, fluctuations can give rise to a sudden extinction of one or both of the species. For the standard noise amplitudes and initial populations, extinction almost never happens, as the noise effect is only small and the populations do not get close to zero. Nevertheless, this should be taken into account in the simulations. The original Lotka-Volterra model is only defined for nonnegative populations, as a negative number of prey of predators does not have any biological meaning. Also mathematically, negative $u(t)$ or $v(t)$ would yield a completely different evolution, which would not be periodic. Therefore, the simulations should also be defined for nonnegative populations only. If one of the species goes extinct, a simple solution is to just keep this population at zero in the simulation, while the evolution of the other species can continue indefinitely. If the prey goes extinct, the predator growth represented by βuv vanishes, as there is no food. Hence, the predator population decays exponentially with rate r_v. However, when the predator goes extinct, this allows for exponential growth of the prey with rate r_u. Next to the fact that this is biologically unrealistic, this also results in an exploding number of prey, which will have a large influence on

the average result after many simulations. Therefore, the prey is set to remain constant when the predator goes extinct. In this way, extinction for both species is accounted for in the simulations.

To describe the noise effects, the main goal is to analyze the corresponding phase space and calculate correlation functions for both populations. These quantities are interesting as they show properties of the PDF and the structure of the time evolution in the system. This is especially useful if the PDF can not be computed or analyzed explicitly, which is the case for this Lotka-Volterra model. To obtain reliable results for the correlation functions through simulations, a large amount of simulations has to be performed, each with a different noise realization[41]. For each simulation, the trajectories $u(t)$ and $v(t)$ are determined at each point in time, as well as products like $u(t)v(t)$ by multiplying the states of the populations at each point in time. Summing the results of all simulations at every time point and dividing by the number of simulations then yields ensemble averages of the correlation functions, like $\langle u(t)\rangle$, $\langle v(t)\rangle$ and $\langle u(t)v(t)\rangle$. Note that these are indeed ensemble averages in the sense of Eq. (2.7) instead of time averages, as the results are still time dependent and the (unknown) PDF is taken into account through the Gaussian PDF of the noise. Usually, the number of simulations is taken to be 10^3 or 10^4. These numbers are based on the observation that in this case, the average results for the correlation functions only show small deviations when the code runs a second time. Hence, these can be considered accurate ensemble averages.

As is shown in Figure 5.5, a stochastic trajectory fluctuates around the deterministic one for small noise amplitudes. Hence, it is interesting to study the fluctuations $w(t) \equiv u(t) - u_d(t)$ in the prey and $z(t) \equiv v(t) - v_d(t)$ in the predators. The average total prey population is then given by $\langle u(t)\rangle = u_d(t) + \langle w(t)\rangle$, as the deterministic trajectory $u_d(t)$ remains the same for every noise realization. So, the average fluctuations in the prey $\langle w(t)\rangle$ can easily be obtained from the average total prey population $\langle u(t)\rangle$. The two-point correlation function is given by $\langle u(t)u(t')\rangle = u_d^2(t) + u_d(t)\langle w(t')\rangle + u_d(t')\langle w(t)\rangle + \langle w(t)w(t')\rangle$, so this can also be calculated directly. With these expressions, the following interesting relation for the connected contributions can be derived

$$\langle u(t)u(t')\rangle_c \equiv \langle u(t)u(t')\rangle - \langle u(t)\rangle\langle u(t')\rangle = \langle w(t)w(t')\rangle - \langle w(t)\rangle\langle w(t')\rangle \equiv \langle w(t)w(t')\rangle_c. \tag{5.4}$$

Hence, the covariance in the total prey population is equivalent to the covariance in its fluctuations. Similar relations can be derived for the total predator population $v(t)$ and its fluctuations $z(t)$.

The analytical expressions for the two-point correlation functions $\langle i(t)j(t')\rangle$ for $i, j \in \{u, v\}$ will be calculated at different points t, t' in time. For both the simulations and the analytical calculations, the two-point correlation functions will be determined at different points in time and at equal times $t = t'$. The response functions can also be calculated analytically via the MSR formalism and Eq. (3.53). However, this expression is not useful for the simulations, as the auxiliary fields do not arise here. It could be possible to obtain these from the simulations via their definition Eq. (3.51), but this is outside the scope of this work. Therefore, only analytical results for the response functions are obtained.

5.2.1 Simulation results

To see if the simulations give reliable results and all effects are implemented correctly, it is useful to reproduce results that were found in other studies. Unfortunately, a stochastic Lotka-Volterra model with additive noise and without carrying capacities is barely considered in earlier research.

[41] This condition is taken care of by the `random.normal` function.

The ones that get closest to the model (5.1) studied in this work are the models used by de la Hoz & Vadillo in Refs. [28] and [29]. Their models, like Eq. (5.2), include multiplicative noise, but this can easily be implemented by changing the structure of the noise coupling matrix $D(\boldsymbol{y}, t)$ (5.3) in the `itoint` algorithm. Simulating these models with the same parameters[42] as were used by de la Hoz & Vadillo yields Figures 5.7-5.8. Only the simulation time is $T_{\text{sim}} = mT_{\text{lin}} \simeq 13.3$ instead of 12, used by them. This is due to a restriction in the code that only allows integer values for the number of linear cycles m.

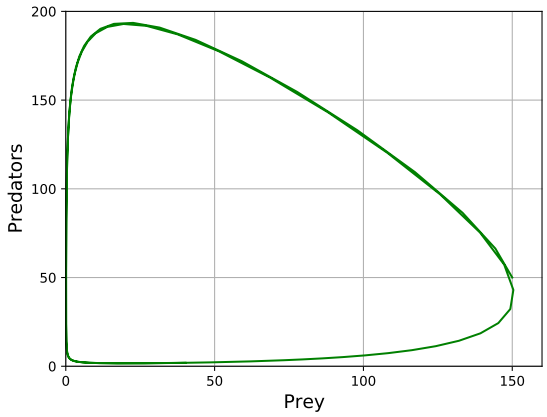

Figure 5.7: Phase space for averaged simulations for 10^3 noise realizations of a stochastic Lotka-Volterra model with multiplicative noise, represented by the green line in Figure 5.2 of Vadillo [29]. The simulation time is $T_{\text{sim}} = mT_{\text{lin}} \simeq 13.3$. This figure is produced with our own Python code [109], for the same parameters as in Ref. [29].

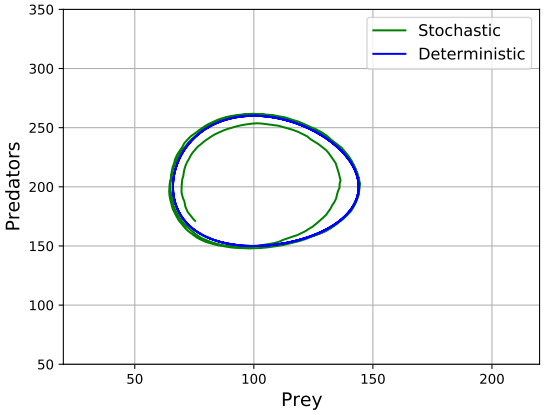

Figure 5.8: Phase space of simulations of a stochastic Lotka-Volterra model with multiplicative noise as in de la Hoz & Vadillo [28]. The blue line corresponds to the deterministic model, while the green line is the average of 10^3 noise realizations for $T_{\text{sim}} = mT_{\text{lin}} \simeq 13.3$. This figure is produced with our own Python code [109], for the same parameters as in Ref. [28].

These results, obtained with our code, can be compared to the original results in Figures 5.2-5.3 found by de la Hoz & Vadillo. In Figure 5.7, only the model represented by the green line in Figure 5.2 is simulated, as this has the most similarities with model (5.1) and it has explicit noise amplitudes given by $\Xi_u = \Xi_v = 0.001$. The results in both figures are almost completely equivalent. Figure 5.3 shows a trajectory for one noise realization in black, which is not reproducible, as every noise value is drawn randomly. In both Figures 5.3 and 5.8, the blue line corresponds to the deterministic solution, while the green line represents an average trajectory of stochastic simulations. First of all, the deterministic trajectory is the same in both figures. The average stochastic trajectory also shows the same general behavior in both cases. However, as the simulation time $T_{\text{sim}} \simeq 13.3$ is slightly larger than 12, used by de la Hoz & Vadillo, the stochastic trajectory in Figure 5.8 traverses the phase space slightly longer. The green trajectories in both figures show comparable general behavior, but they are not entirely similar. As the average in Figure 5.3 from Ref. [28] is only calculated for 100 noise realizations, this does not yield a reliable ensemble average. The average trajectory in Figure 5.8 is computed over 10^3 noise realizations, which gives a more reliable ensemble average. Over all, the simulations used here are able to reproduce the results found by these other studies, so the algorithm can be assumed to yield reliable results.

[42] For the model used in Ref. [29], these are the standard parameters also used in other simulations in this work.

Now, the stochastic Lotka-Volterra model (5.1) of interest with additive noise will be analyzed. Figures 5.5-5.6 showed a stochastic trajectory for one noise realization, compared to the deterministic trajectory. Averaging over 10^4 noise realizations results in the time evolution of the populations in Figure 5.9 and the phase space in Figure 5.10. For each simulation, the standard parameters and initial conditions are used, with noise amplitudes $\Xi_u = 0.2$ and $\Xi_v = 0.4$. The simulation time is again $T_{\text{sim}} = 5T_{\text{lin}}$. Both figures show that the average stochastic trajectory $(\langle u_n(t)\rangle, \langle v_n(t)\rangle)$, which consists of the average total populations after 10^4 noise realizations, remains close to and almost completely overlaps with the deterministic solution $(u_d(t), v_d(t))$. A naive explanation of this behavior can be given as follows. As the noise has a zero mean value and a Gaussian distribution, which is a symmetric distribution, the probability of having a negative noise value is equal to the probability of a positive value. This holds for both species at each point in time. Therefore, a stochastic trajectory for a single noise realization can propagate inside the curve enclosed by the deterministic periodic evolution or outside this curve, both with equal probability. This also explains why a single stochastic trajectory shows fluctuations both inside and outside the deterministic solution, as in Figure 5.6. So, after averaging over a large number of simulations, one could expect that the average stochastic evolution exactly follows the deterministic evolution of the system. This seems to be the case for a few cycles, up to $m = 3$, but after a larger amount of time, the average stochastic trajectory in Figure 5.10 shows inward spiraling motion. So, this explanation is not sufficient.

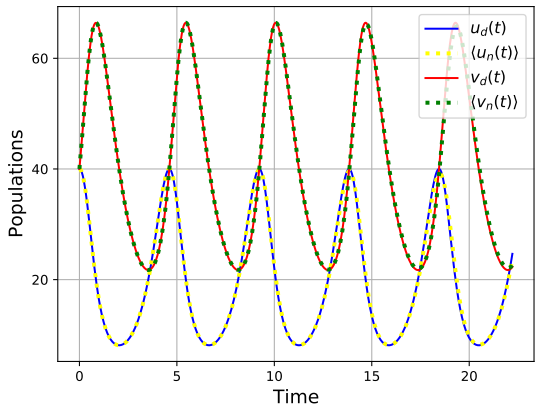

Figure 5.9: Periodic solution $(u_d(t), v_d(t))$ of the deterministic model represented by the solid lines, and an average of simulations $(\langle u_n(t)\rangle, \langle v_n(t)\rangle)$ for 10^4 noise realizations represented by the dotted lines. Simulations are performed with the standard parameters and noise amplitudes $\Xi_u = 0.2, \Xi_v = 0.4$, for $T_{\text{sim}} = 5T_{\text{lin}}$.

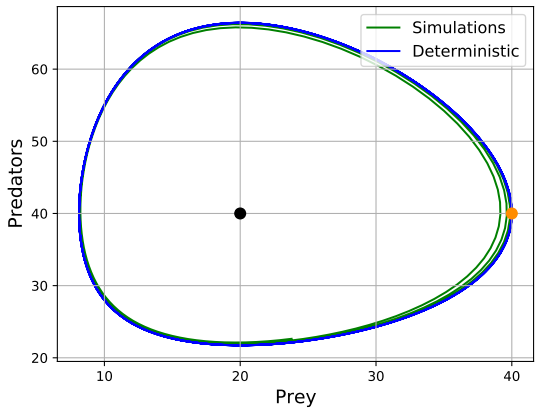

Figure 5.10: Corresponding phase space for deterministic solution (blue) and average of simulations (green) for 10^4 noise realizations of the stochastic Lotka-Volterra model. The orange dot represents the initial populations $(u_0, v_0) = (40, 40)$. The black dot is the fixed point of the model, which is $(20, 40)$ for these parameters.

To observe and analyze this inward spiraling motion better, the simulations are performed for the same parameters, but for a longer simulation time $T_{\text{sim}} = 10T_{\text{lin}}$. This yields Figure 5.11 for the time evolution and Figure 5.12 for the corresponding phase space. The evolution of the average stochastic populations seems to follow the deterministic results for a while, until the amplitude of the stochastic populations starts to decrease around $t = 5T_{\text{lin}}$. This also slightly decreases the period $T(E)$ of the motion, as this decreases for a smaller energy $E = M - M^*$. The phase space in Figure 5.12 confirms the smaller amplitude in the evolution of both species. Also, it seems here that the inward spiraling motion is directed towards the fixed point $(20, 40)$.

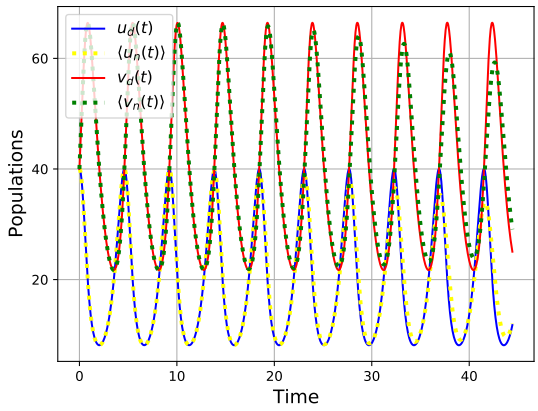

Figure 5.11: Periodic solution $(u_d(t), v_d(t))$ of the deterministic model (solid), and an average of simulations $(\langle u_n(t)\rangle, \langle v_n(t)\rangle)$ (dotted) for 10^4 noise realizations. The simulations are performed with the same parameters as in Figure 5.9, for $T_{\text{sim}} = 10T_{\text{lin}}$.

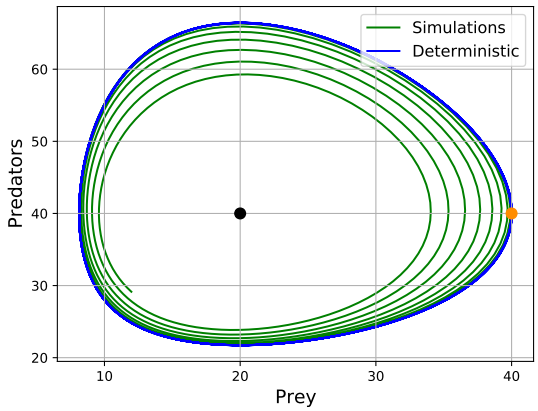

Figure 5.12: Corresponding phase space for deterministic solution (blue) and average of simulations (green) for 10^4 noise realizations of the stochastic Lotka-Volterra model (5.1). The simulations are performed with the same parameters as in Figure 5.10, for $T_{\text{sim}} = 10T_{\text{lin}}$.

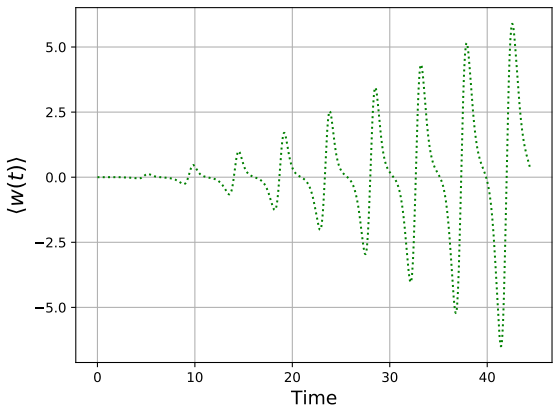

Figure 5.13: Average fluctuations $\langle w(t)\rangle = \langle u_n(t)\rangle - u_d(t)$ in the prey population of 10^4 noise realizations, for $T_{\text{sim}} = 10T_{\text{lin}}$.

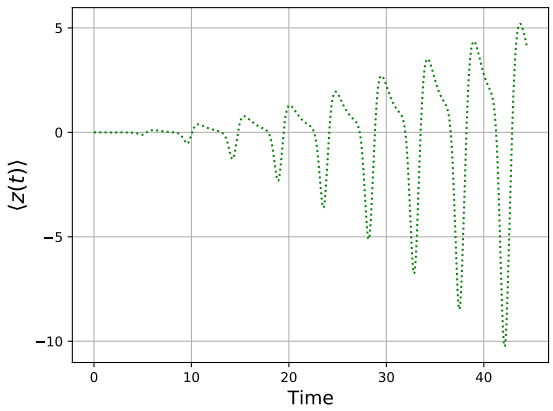

Figure 5.14: Average fluctuations $\langle z(t)\rangle = \langle v_n(t)\rangle - v_d(t)$ in the predator population of 10^4 noise realizations, for $T_{\text{sim}} = 10T_{\text{lin}}$.

It is interesting to study the average fluctuations in both species for this longer time behavior, shown for the prey as $\langle w(t)\rangle$ in Figure 5.13 and for the predator as $\langle z(t)\rangle$ in Figure 5.14. These fluctuations show the same periodicity as both the simulation[43] and deterministic trajectories, as the difference between two periodic trajectories is also periodic. Also, both figures show periodic behavior around 0, as inside the deterministic curve both populations are larger for half of the period, and smaller for the other half. Furthermore, it is interesting to see that fluctuations spend a relative large amount of time around zero, especially for the prey. This can be explained by the fact

[43] Although the period $T(E)$ of the average simulations is slightly smaller than the period of the deterministic trajectory, due to the inward spiraling motion.

that this happens when both populations have lower numbers. This results in a slower evolution of both species, hence the system, and thus the small fluctuations, spend a larger amount of time in this part of the phase space. The general behavior of the fluctuations can be described as an exponentially growing envelope. The amplitude of negative and positive fluctuations in the prey is approximately equal, while for the predators larger negative fluctuations occur. This is represented in the phase space by the larger deviation in the upper right part of Figure 5.12. This can be due to the fact that the noise is scaled through the fixed point, which does not yield exactly the same effect of the noise on each species.

A possible explanation of this inward spiraling motion could be that the noise gives rise to a bifurcation in the phase space of the system, which changes the character of the fixed point. Such a bifurcation is called a noise-induced transition. In the deterministic system, the fixed point is a center, which is neither attracting nor repelling. In the stochastic system, the fixed point appears to be a stable spiral, which would cause the average stochastic trajectory to spiral towards the fixed point. To determine the character of the fixed point for the stochastic Lotka-Volterra model, a linear stability analysis has to be performed. This yields exactly the same Jacobian[44] (4.8) evaluated in the fixed point (u^*, v^*) as for the deterministic model. This results from the additive nature of the noise, which does not depend on the populations and therefore does not contribute to the Jacobian. The fixed point is also a center for the stochastic system (5.1); hence this does not explain the inward spiraling motion. Note that this behavior is also completely different from the outward spiraling motion observed by Tian et al. [30], as their model also describes the spatial evolution of both species and it includes carrying capacities.

To find an explanation for this inward spiraling motion, it should first be investigated if it is directed towards the fixed point. An average of 10^3 noise realizations[45] for the same standard parameters and a simulation time $T_{\text{sim}} = 25T_{\text{lin}}$ yields the phase space in Figure 5.15. It shows that the average stochastic trajectory indeed spirals towards the fixed point, around which it keeps fluctuating, as the deterministic evolution vanishes at the fixed point. This figure also shows the last result of each simulation as an orange dot, which are distributed widely in phase space.

This spreading of the endpoints is caused by the individual stochastic trajectories that deviate from the deterministic trajectory due to the noise. As the noise is small compared to the deterministic contribution, each simulated trajectory still evolves around the periodic solution. The fluctuations cause each stochastic trajectory to either 'accelerate' or 'delay', by respectively moving faster towards or staying for a larger amount of time in a part of phase space than the deterministic trajectory. Because each noise value is drawn independently from a Gaussian distribution at each point in time, on average these effect should be the same for each simulation, so they should not spread out through phase space. However, the period $T(E)$ of a deterministic trajectory is shown to depend on the "energy" $E = M - M^*$ of the solution [106]. As M^* is the constant of motion in the fixed point (4.15), the energy scales with the distance of the trajectory from the fixed point. Hence, the period of a stochastic trajectory changes when it deviates from the deterministic one. As this period $T(E)$ is a nonlinear function of the energy E, this effect is not averaged out by the Gaussian distribution of the noise. So, this indeed yields an effective delay or acceleration for each simulated trajectory, which causes them to diffuse in phase space. This effect increases with the

[44] For the two species Lotka-Volterra system, the Jacobian evaluated at the fixed point is called the community matrix.

[45] The number of noise realizations is set to 10^3 to have clearly distinguishable endpoints. As the general features of the average results do not change for 10^3 compared to 10^4 simulations, this is justifiable.

simulation time T_{sim}. The effect on the period of the average stochastic trajectory is small, but this spreading is what causes the behavior of the average trajectory.

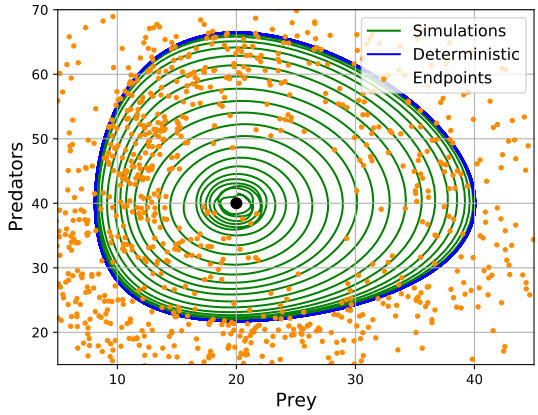

Figure 5.15: Phase space for deterministic solution (blue) and average of simulations (green) for 10^3 noise realizations. The simulations are performed with the same parameters as in Figure 5.10, for $T_{\text{sim}} = 25T_{\text{lin}}$. The orange dots represent the endpoints of each simulation.

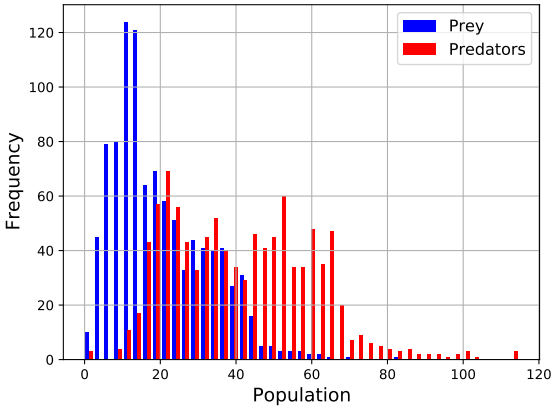

Figure 5.16: Corresponding histogram of the endpoints of the 10^3 simulations, for $T_{\text{sim}} = 25T_{\text{lin}}$. The blue bins represent the prey, while the red bins represent the predators. At $t = T_{\text{sim}}$, the average number of prey is 20.2 and the average number of predators is 41.5.

The question remains why this diffusive behavior of the simulations results in the inward spiraling motion towards the fixed point. As the spreading of the simulations increases with the simulation time, Figure 5.15 shows the endpoints at $t = T_{\text{sim}}$ of each simulation. The deterministic function $C(\boldsymbol{y}, t)$ contributes the most to the evolution, so the simulations diffuse around the deterministic trajectory. The spreading of these endpoints in phase space shows some interesting features. To analyze the distribution of the endpoints, the corresponding histogram is shown in Figure 5.16. The distribution of the prey is peaked around 12 and skewed, while the predator distribution seems to be more symmetric. This skewness can again be explained by the slower evolution of the system for smaller populations, which causes the system to spend more time in this area of the phase space. The reversed effect can also be observed. For larger populations, the nonlinear contributions increase and accelerate the evolution of the system. This affects every stochastic trajectory through larger fluctuations at larger populations, which are also observable in the average stochastic trajectory. This explains the larger negative fluctuations for the predators in Figure 5.14, as the predator population consists of larger numbers.

The difference in distributions indicates that the effect of the noise on the predator species is larger, due to the different amplitudes. But, most importantly, these distributions confirm that the endpoints are widely spread through phase space. That this effect increases in time can be observed by comparing the histogram for $T_{\text{sim}} = 25T_{\text{lin}}$ in Figure 5.16 with the result for $T_{\text{sim}} = 10T_{\text{lin}}$ in Figure 5.17, which is also obtained for 10^3 simulations. For a smaller simulation time, the distribution of the endpoints is even more skewed. Also, the distributions in Figure 5.17 have a small variance compared to Figure 5.16, indicating that the diffusion of the simulations is still small at this point in time.

By calculating the average population of the deterministic trajectory after a large simulation time ($T_{\text{sim}} = 25T_{\text{lin}}$), it can be shown that this average is exactly given by the fixed point $(20, 40)$.

Calculating the average of the endpoint distributions in Figure 5.16 yields an average endpoint of $(20.2, 41.5)$, which is very close to the fixed point. After a large amount of time, the (ensemble) average of the simulations follows the (time) average of the deterministic solution, as they are spread around this trajectory. So, in some sense, the simulation endpoints in Figure 5.15 mimic a deterministic solution. The average of the endpoint distributions in Figure 5.17 is given by $(12.2, 29.2)$, which is also caused by the small diffusion at time $T_{\text{sim}} = 10T_{\text{lin}}$. This average is far below the fixed point, as at this point in time the simulations are in the area of phase space with small populations.

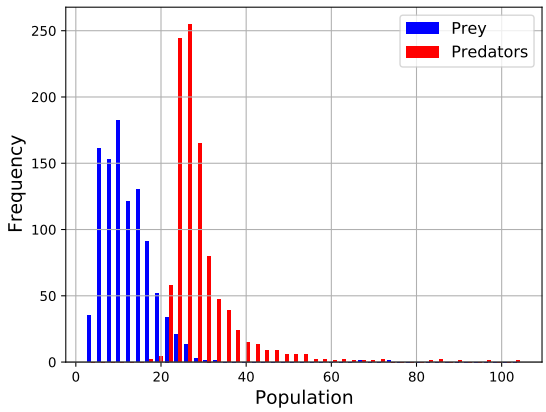

Figure 5.17: Histogram of the endpoints of 10^3 simulations, for $T_{\text{sim}} = 10T_{\text{lin}}$. The blue bins represent the prey, while the red bins represent the predators. At $t = T_{\text{sim}}$, the average number of prey is 12.2 and the average number of predators is 29.2.

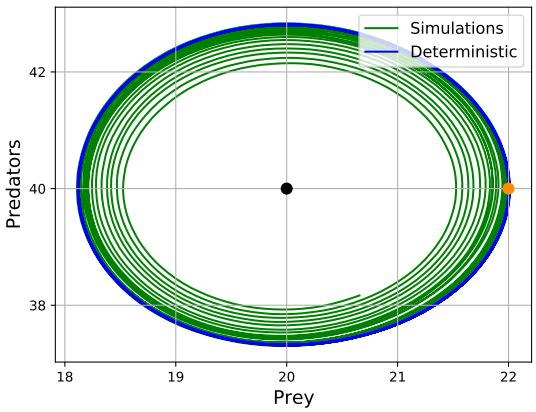

Figure 5.18: Phase space for deterministic solution (blue) and average of simulations (green) for 10^4 noise realizations. Simulations are performed with the same parameters as in Figure 5.10, except for the initial populations $(u_0, v_0) = (22, 40)$ and the simulation time $T_{\text{sim}} = 25T_{\text{lin}}$.

Hence, as the diffusion increases with the simulation time, the average stochastic trajectory propagates after a larger amount of time towards the fixed point, which is the average population of the deterministic trajectory. This explains the inward spiraling motion towards the fixed point. Although other studies, like de la Hoz & Vadillo [28], seem to observe this behavior[46], it has never been analyzed or explained before, for this particular type of stochastic Lotka-Volterra models. Therefore, this is one of the new findings in this work.

One of the reasons that the individual simulations can distribute through phase space, is that the deterministic solution for fixed initial populations (u_0, v_0) is not an attractor of this system, but a saddle point. Hence, although this trajectory contributes to the evolution through the deterministic function $C(\boldsymbol{y}, t)$, the general evolution with noise is not attracted towards this periodic curve. As also the fixed point $(20, 40)$ is still a center, there is no attractor in this system. Due to the large deterministic contribution to the evolution, the simulations remain close to this periodic trajectory, but without this the distribution of the simulations would become uniform without any structure. This is also important for the semiclassical approach in Section 5.3, as it makes use of a saddle-point expansion. A more detailed explanation is given in Appendix B.

[46] In their case, although the noise is multiplicative, the same inward spiraling motion is observed. It is however not analyzed in their work.

It could also be that a numerical inaccuracy partially causes the inward spiral of the average stochastic trajectory. This inaccuracy could be similar to the one for the deterministic solutions for different initial populations observed in Figure 4.6. Therefore, simulations are performed with the same standard parameters except for the initial populations, which are set to $(u_0, v_0) = (22, 40)$. Also, the simulation time is set to $T_{\text{sim}} = 25T_{\text{lin}}$. The resulting phase space is depicted in Figure 5.18. Indeed the inward spiraling motion is less for these initial populations compared to Figure 5.12, as the simulation time is more than twice as large in this case. However, the difference in behavior for both initial conditions is not as large as for the numerical inaccuracies in the deterministic solutions Figure 4.6. Also, in this case the fluctuations seem to grow exponentially in time, as is confirmed by Figures 5.13-5.14. This does not occur for the numerical inaccuracies in the deterministic case. Instead, this behavior for initial populations closer to the fixed point can be explained in a different way. For $(u_0, v_0) = (22, 40)$, the system evolves closer to the fixed point, where it can be linearized by Eq. (4.10). So, the nonlinear contributions are small in this case, and the period of the system is given by $T(E) \simeq T_{\text{lin}}$. This causes a smaller diffusion of the stochastic solutions, which reduces the inward spiraling motion. Hence, the nonlinear evolution also contributes to the strength of the inward motion.

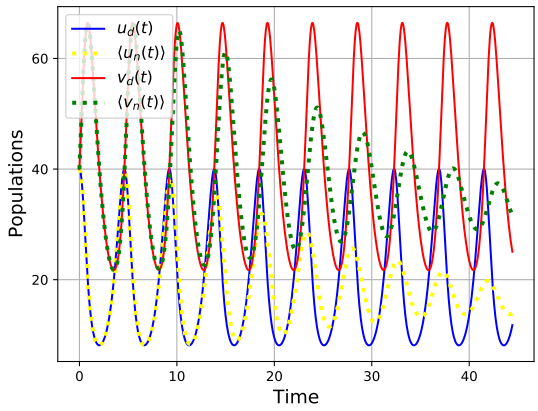

Figure 5.19: Periodic solution $(u_d(t), v_d(t))$ of the deterministic model represented by the solid lines, and an average of simulations $(\langle u_n(t)\rangle, \langle v_n(t)\rangle)$ for 10^4 noise realizations represented by the dotted lines. Simulations are performed with the standard parameters and noise amplitudes $\Xi_u = 2.0$, $\Xi_v = 4.0$, for $T_{\text{sim}} = 10T_{\text{lin}}$.

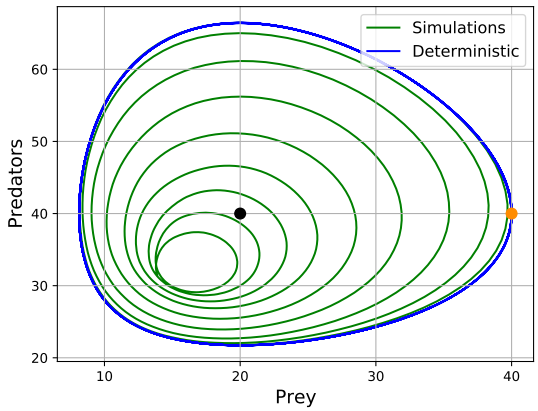

Figure 5.20: Corresponding phase space for deterministic solution (blue) and average of simulations (green) for 10^4 noise realizations of the stochastic Lotka-Volterra model (5.1). The simulations are performed with the standard parameters and noise amplitudes $\Xi_u = 2.0$, $\Xi_v = 4.0$, for $T_{\text{sim}} = 10T_{\text{lin}}$.

The noise amplitudes Ξ_u and Ξ_v have a large influence on the velocity of the inward spiraling motion. This is depicted in Figures 5.19-5.20, which show the average results for 10^4 noise realizations with noise amplitudes $\Xi_u = 2.0$ and $\Xi_v = 4.0$. The phase space in Figure 5.20 shows faster inward spiraling motion. However, in this case, this is not directed towards the fixed point. This is caused by the simulations that go extinct due to the larger noise amplitudes. Out of the 10^4 simulations, 1689 have gone extinct. In the implementation of extinction in the algorithm, this either contributes a completely extinct population or a constant prey and zero predators to the average. Hence, the average stochastic trajectory does not converge to the fixed point, but slightly more to the lower left. This can also be observed in the time evolution of the populations in Figure 5.19. At first, the periodic behavior of the average simulations of both species is symmetric around the fixed point

value. At later times, the inward motion reduces the amplitude of the average stochastic trajectory, but the extinct simulations also cause the trajectory to decay towards smaller populations.

Although the noise amplitudes scale as $\Xi_v = v * \Xi_u / u*$, the effect of the noise on both species turns out to be different. It would be difficult to determine noise amplitudes that yield equal effects, as both noises induce fluctuations in the other species indirectly through interactions. Therefore, slightly changing the noise scaling does not have a large influence on the general behavior. Taking extreme cases, like for example $\Xi_u = 0$ and $\Xi_v = 0.4$ or the other way around, show that the noise effect is delayed in one of the species, but still occurs at later times. This should be expected, as the system is nonlinear, so noise effects in one of the species should affect the other. Another interesting test to verify the results is by implementing negative noise amplitudes. As the noise has a Gaussian distribution, which is symmetric, this should not influence the results. This indeed does not yield any difference.

5.3 MSR approach for additive noise

The simulations discussed in the previous section already yield some insights on the effects of additive noise on the populations in the stochastic Lotka-Volterra model. Here, the same equations will be analyzed using the MSR formalism discussed in Section 3.3. This method allows for an analytical approach to the stochastic model via the calculation of (connected) correlation functions. The two-dimensional system of SDEs (5.1) will be studied in a similar way as is done for the Langevin equation in Sections 3.3.3 and 3.4. As $\eta_u(t)$ and $\eta_v(t)$ are external white noises that are added to the deterministic EoM, it is justified to apply the MSR formalism in the Itô interpretation, as it was derived in Section 3.3.1. Also, as the noise is additive, both interpretations should yield the same results, as was explained in Section 2.3.3. The results obtained via the MSR formalism are compared with the simulations.

In order to write down the correct MSR action, the initial number of prey $u(t_0) = u_0$ and predators $v(t_0) = v_0$ have to be included in Eq. (5.1) in the form of Dirac delta functions as

$$\begin{aligned} \dot{u}(t) &= r_u u(t) - \alpha u(t)v(t) + u_0\delta(t-t_0) + \sqrt{\Xi_u}\,\eta_u(t), \\ \dot{v}(t) &= -r_v v(t) + \beta u(t)v(t) + v_0\delta(t-t_0) + \sqrt{\Xi_v}\,\eta_v(t). \end{aligned} \tag{5.5}$$

In later calculations, the initial time is set to $t_0 = 0$. Now we define the two-dimensional population vectors $\boldsymbol{y}(t) = (u(t), v(t))^T$, $\boldsymbol{y}_0 = (u_0, v_0)^T$, the deterministic evolution vector $C(\boldsymbol{y}, t) = (r_u u - \alpha uv, -r_v v + \beta uv)^T$, the noise vector $\boldsymbol{\eta}(t) = (\eta_u(t), \eta_v(t))^T$ and the noise coupling matrix

$$D(\boldsymbol{y}, t) = \begin{pmatrix} \sqrt{\Xi_u} & 0 \\ 0 & \sqrt{\Xi_v} \end{pmatrix}. \tag{5.6}$$

Note that this matrix $D(\boldsymbol{y}, t)$ determines the character of the noise. This separation of the deterministic and stochastic part is exactly similar to the simulations. The stochastic Lotka-Volterra model in Eq. (5.5) can be written in terms of these quantities as a two-dimensional nonlinear Langevin equation

$$\dot{\boldsymbol{y}}(t) = C(\boldsymbol{y}, t) + \boldsymbol{y}_0\delta(t-t_0) + D(\boldsymbol{y}, t)\boldsymbol{\eta}(t), \tag{5.7}$$

similar to Eq. (3.38). The corresponding auxiliary vector for the MSR action is given by $\boldsymbol{\varphi}(t) = (q_u(t), q_v(t))^T$, which consists of the auxiliary fields $q_u(t)$ and $q_v(t)$, for the prey and predator

population respectively. The MSR action for the stochastic Lotka-Volterra model with additive noise can now be obtained directly from Eq. (3.45) as

$$\begin{aligned} S[\boldsymbol{y},\boldsymbol{\varphi}] &= \int \Big\{ \boldsymbol{\varphi}(t)\big[\dot{\boldsymbol{y}}(t) - C(\boldsymbol{y},t) - \boldsymbol{y}_0\delta(t-t_0)\big] - \frac{1}{2}D^2(\boldsymbol{y},t)\boldsymbol{\varphi}^2(t)\Big\}\,\mathrm{d}t, \\ &= \int \Big\{ q_u\big[\dot{u} - r_u u + \alpha uv - u_0\delta(t-t_0)\big] - \frac{\Xi_u}{2}q_u^2 \\ &\qquad + q_v\big[\dot{v} + r_v v - \beta uv - v_0\delta(t-t_0)\big] - \frac{\Xi_v}{2}q_v^2\Big\}\,\mathrm{d}t, \end{aligned} \tag{5.8}$$

where the time dependence of the fields is neglected for notational convenience.

5.3.1 Semiclassical approximation

The simulated trajectory shown in Figure. 5.6 is the solution of the SDEs (5.5) for a single noise realization. It fluctuates around the periodic solution of the corresponding deterministic system. Therefore, it is interesting to study the stochastic Lotka-Volterra model in terms of fluctuations around the deterministic solution, for fixed initial populations u_0 and v_0. This can be done by applying the semiclassical approach. So, the MSR action is written as an expansion around a saddle point $(\boldsymbol{y}_s,\boldsymbol{\varphi}_s) = (u_s, v_s, q_{u_s}, q_{v_s})$, with the perturbation parameters given by the noise amplitudes Ξ_u and Ξ_v. Disregarding the source fields[47], the saddle-point equations (3.82) for this Lotka-Volterra model are given by

$$\left.\frac{\delta S[\boldsymbol{y},\boldsymbol{\varphi}]}{\delta u(t)}\right|_{u=u_s} = -\dot{q}_{u_s} - r_u q_{u_s} + \alpha q_{u_s} v_s - \beta q_{v_s} v_s = 0, \tag{5.9}$$

$$\left.\frac{\delta S[\boldsymbol{y},\boldsymbol{\varphi}]}{\delta v(t)}\right|_{v=v_s} = -\dot{q}_{v_s} + r_v q_{v_s} - \beta q_{v_s} u_s + \alpha q_{u_s} u_s = 0, \tag{5.10}$$

$$\left.\frac{\delta S[\boldsymbol{y},\boldsymbol{\varphi}]}{\delta q_u(t)}\right|_{q_u=q_{u_s}} = \dot{u}_s - r_u u_s + \alpha u_s v_s - u_0\delta(t-t_0) - \Xi_u q_{u_s} = 0, \tag{5.11}$$

$$\left.\frac{\delta S[\boldsymbol{y},\boldsymbol{\varphi}]}{\delta q_v(t)}\right|_{q_v=q_{v_s}} = \dot{v}_s + r_v v_s - \beta u_s v_s - v_0\delta(t-t_0) - \Xi_v q_{v_s} = 0. \tag{5.12}$$

As the initial conditions of the auxiliary fields q_{u_0} and q_{v_0} are not fixed, these equations have multiple solutions. To determine an appropriate saddle-point configuration around which the expansion can be performed, these initial values are set to $q_{u_0} = 0 = q_{v_0}$. Using the first two saddle-point equations, this results in $\boldsymbol{\varphi}_s = (q_{u_s}, q_{v_s})^T = (0,0)^T$. This choice might seem arbitrary, but it can actually be justified. The equations for the real fields vanish for $\boldsymbol{\varphi}_s = 0$, but the ones for the auxiliary fields yield the deterministic Lotka-Volterra equations with initial populations (u_0, v_0). Hence, this choice for the auxiliary fields q_{u_s} and q_{v_s} exactly retrieves the deterministic evolution of the populations, which is the behavior that can be expected in the limit of zero noise. As also the simulations show trajectories and average results close to this deterministic trajectory, it is a good starting point to study fluctuations around this periodic solution due to the noise. Defining the deterministic solution of the system as $(u_d(t), v_d(t))$, the saddle point is given by $(u_s, v_s, q_{u_s}, q_{v_s}) = (u_d, v_d, 0, 0) = (\boldsymbol{y}_d, \boldsymbol{\varphi}_d)$. Note, however, that this is not the only possible saddle point, as nonzero initial conditions for the auxiliary fields would yield a different saddle point. As the saddle-point expansion is performed in order of the noise amplitudes Ξ_u and Ξ_v, it follows automatically that the saddle point itself

[47] This is possible, as there are no actual sources in this system. The source fields only appear as a tool to calculate correlation functions, and are put to zero afterwards.

should be of zeroth order in both these amplitudes. Therefore, as this retrieves the deterministic system, it is legitimate to set the saddle point to the corresponding deterministic evolution. Also, the contributions of q_{u_s} and q_{v_s} in the equations for the auxiliary fields are of first order in the noise amplitude, which is another argument for neglecting these fields in determining the saddle point. In the quantum mechanical interpretation of the semiclassical approach, these saddle points are the classical solutions of the system. Consequently, the zero noise limit for stochastic systems is equivalent to the classical limit for quantum systems. A more elaborate discussion on the saddle-point approximation and this particular choice for the stochastic Lotka-Volterra equations is given in Appendix B.

The arguments above also justify why regular perturbation theory is not a suitable first approach to this model, instead of the semiclassical approach. As explained in Section 3.4, this would yield an expansion in orders of the coupling constants of the nonlinear contributions, which are α and β for the Lotka-Volterra model. However, these nonlinear contributions to the equations describe the interaction of the species, which is exactly the behavior that results in the periodic solutions of the system. A perturbative expansion up to first or second order in these coefficients would therefore not include this nonlinear behavior. Hence, the semiclassical approach in the form of the saddle-point expansion around (u_d, v_d) is a more natural technique to describe the effect of noise on the deterministic evolution. Nevertheless, perturbation theory is still required later, as the Lotka-Volterra model contains quadratic contributions, which yield cubic terms in the MSR action.

The general saddle-point expansion of the action up to third order in the fluctuations $(\delta\boldsymbol{y}, \delta\boldsymbol{\varphi}) \equiv (\boldsymbol{y} - \boldsymbol{y}_d, \boldsymbol{\varphi} - \boldsymbol{\varphi}_d)$ can be written as

$$\begin{aligned} S[\boldsymbol{y}, \boldsymbol{\varphi}] =& S[\boldsymbol{y}_d, \boldsymbol{\varphi}_d] + \frac{1}{2} \int \left. \frac{\delta^2 S[\boldsymbol{y}, \boldsymbol{\varphi}]}{\delta(\boldsymbol{y}, \boldsymbol{\varphi})^2} \right|_{\substack{\boldsymbol{y}=\boldsymbol{y}_d \\ \boldsymbol{\varphi}=\boldsymbol{\varphi}_d}} \begin{pmatrix} \delta\boldsymbol{y} \\ \delta\boldsymbol{\varphi} \end{pmatrix}^2 \mathrm{d}t\, \mathrm{d}t' \\ &+ \frac{1}{3!} \int \left. \frac{\delta^3 S[\boldsymbol{y}, \boldsymbol{\varphi}]}{\delta(\boldsymbol{y}, \boldsymbol{\varphi})^3} \right|_{\substack{\boldsymbol{y}=\boldsymbol{y}_d \\ \boldsymbol{\varphi}=\boldsymbol{\varphi}_d}} \begin{pmatrix} \delta\boldsymbol{y} \\ \delta\boldsymbol{\varphi} \end{pmatrix}^3 \mathrm{d}t\, \mathrm{d}t'\, \mathrm{d}t''. \end{aligned} \tag{5.13}$$

The contribution $S[\boldsymbol{y}_d, \boldsymbol{\varphi}_d]$ of the action evaluated at the saddle point vanishes, because $\boldsymbol{\varphi}_d = 0$. This also yields $\delta\boldsymbol{\varphi} \equiv \boldsymbol{\varphi} - \boldsymbol{\varphi}_d = \boldsymbol{\varphi}$. For the prey and predator fields, it is convenient to write the fluctuations as $\delta\boldsymbol{y} = (\delta u, \delta v) = (u - u_d, v - v_d) \equiv (w, z) \equiv \boldsymbol{\psi}$. The first-order contribution is zero by definition of a saddle point. So, the first nonzero contribution to the saddle-point expansion of the MSR action for the Lotka-Volterra model is given by the second-order term, which contains the *Hessian*

$$\left. \frac{\delta^2 S[\boldsymbol{y}, \boldsymbol{\varphi}]}{\delta(\boldsymbol{y}, \boldsymbol{\varphi})^2} \right|_{\substack{\boldsymbol{y}_d \\ \boldsymbol{\varphi}_d}} = \begin{pmatrix} 0 & 0 & \left.\frac{\delta\dot{u}}{\delta u}\right|_{u_d} - r_u + \alpha v_d & -\beta v_d \\ 0 & 0 & \alpha u_d & \left.\frac{\delta\dot{v}}{\delta v}\right|_{v_d} + r_v - \beta u_d \\ \left.\frac{\delta\dot{u}}{\delta u}\right|_{u_d} - r_u + \alpha v_d & \alpha u_d & -\Xi_u & 0 \\ -\beta v_d & \left.\frac{\delta\dot{v}}{\delta v}\right|_{v_d} + r_v - \beta u_d & 0 & -\Xi_v \end{pmatrix} \delta(t - t').$$

To get rid of the functional derivatives, the following tricks are useful:

$$\frac{\delta\dot{x}(t)}{\delta x(t')} = \frac{\partial}{\partial t} \frac{\delta x(t)}{\delta x(t')} = \delta'(t - t'), \tag{5.14}$$

$$\int \delta'(t - t') f(t')\, \mathrm{d}t' = f'(t). \tag{5.15}$$

Applying these rules for functional differentiation to the second-order contribution results in derivatives $\dot{w}$ and $\dot{z}$ of the fluctuations. The third-order contribution follows from taking another functional derivative of the Hessian. This yields a $(4,4)$-tensor, of which each part gives similar contributions. Applying the Dirac delta functions, two of the time integrations are canceled, resulting in an action that is local in time[48]

$$S[\boldsymbol{\psi},\boldsymbol{\varphi}] = \int \Big\{ q_u[\dot{w} - r_u w + \alpha v_d w + \alpha u_d z] + q_v[\dot{z} + r_v z - \beta u_d z - \beta v_d w] \\ + \alpha w z q_u - \beta w z q_v - \frac{\Xi_u}{2} q_u^2 - \frac{\Xi_v}{2} q_v^2 \Big\} \,\mathrm{d}t, \tag{5.16}$$

where time dependence is omitted for notational convenience. This expression actually has a similar structure as the original action in Eq. (5.8). This is no coincidence. The saddle-point expansion up to third order in the fluctuations is equivalent to transforming the original action in terms of the perturbations $w = u - u_d$ and $z = v - v_d$, because there are no higher-order contributions. Hence, this expansion really is an exact expression for the MSR action in terms of the fluctuations. This holds in general for SDEs that have no cubic or higher-order contributions.

For the linear Langevin equation in Section 3.3.3, it was possible to calculate the generating functional exactly by performing the Gaussian integrals for the quadratic contributions. As the MSR action (5.16) for the Lotka-Volterra model contains contributions that are cubic in the fluctuations, the generating functional can not be computed exactly. Therefore, just as for the nonlinear Langevin equation in Section 3.4, perturbation theory is required. The action can be split in a quadratic free part S_0, that only contains the terms on the first line of Eq. (5.16), and an interacting part S_I, that contains the cubic and noise contributions on the second line of Eq. (5.16). In the corresponding Feynman diagrams, the contributions to S_0 and S_I are, respectively, given by propagators and vertices. Note that the noise contributions in S_I are also quadratic, and could be included in S_0. However, as the semiclassical approach is performed in the order of the noise amplitudes, it is more convenient to treat the noise contributions as vertices.

For the free part of the action S_0, it is useful to define a Green's function. As there are multiple quadratic contributions, such a Green's function is not unique and the different possibilities should be examined carefully. A first guess can be to define an inverse Green's function

$$G_B^{-1}(t,t') = \begin{pmatrix} \frac{\mathrm{d}}{\mathrm{d}t} - r_u & 0 \\ 0 & \frac{\mathrm{d}}{\mathrm{d}t} + r_v \end{pmatrix} \delta(t-t'), \tag{5.17}$$

which yields a free action

$$\begin{aligned} S_0^B[\boldsymbol{\psi},\boldsymbol{\varphi}] &= \int \left[\boldsymbol{\varphi}^T(t) G_B^{-1}(t,t') \boldsymbol{\psi}(t') \,\mathrm{d}t' + \boldsymbol{\varphi}^T(t) \begin{pmatrix} \alpha v_d(t) & \alpha u_d(t) \\ -\beta v_d(t) & -\beta u_d(t) \end{pmatrix} \boldsymbol{\psi}(t) \right] \mathrm{d}t, \\ &= \int \boldsymbol{\varphi}^T(t) Q_B(t,t') \boldsymbol{\psi}(t') \,\mathrm{d}t' \,\mathrm{d}t, \end{aligned} \tag{5.18}$$

where the matrix $Q_B(t,t')$ is given by

$$Q_B(t,t') = G_B^{-1}(t,t') + \begin{pmatrix} \alpha v_d(t) & \alpha u_d(t) \\ -\beta v_d(t) & -\beta u_d(t) \end{pmatrix} \delta(t-t'). \tag{5.19}$$

[48] This only holds in the case of white noise, when the autocorrelation function of the noise is $\delta(t-t')$. If this is not the case, the autocorrelation function and hence the action are nonlocal in time.

Using its definition and Eq. (5.17) for the inverse Green's function $G_B^{-1}(t,t')$, it can be seen that the *bare* Green's function $G^B(t,t')$ is also diagonal, with nonzero entries $G_u^B(t,t')$, $G_v^B(t,t')$ satisfying

$$\left(\frac{\mathrm{d}}{\mathrm{d}t} - r_u\right) G_u^B(t,t') = \delta(t-t'), \tag{5.20}$$

$$\left(\frac{\mathrm{d}}{\mathrm{d}t} + r_v\right) G_v^B(t,t') = \delta(t-t'). \tag{5.21}$$

This is a set of uncoupled differential equations that is easily solved by

$$G^B(t,t') = \begin{pmatrix} G_u^B(t,t') & 0 \\ 0 & G_v^B(t,t') \end{pmatrix} = \Theta(t-t') \begin{pmatrix} \mathrm{e}^{r_u(t-t')} & 0 \\ 0 & \mathrm{e}^{-r_v(t-t')} \end{pmatrix}. \tag{5.22}$$

Note that $G_{u,v}^B(t,t) = 0$ in the Itô interpretation. The expression for $G_v^B(t,t')$ can be recognized as the Green's function for the Langevin equation, obtained in (3.62). Here, these Green's functions describe the linearized solution of the Lotka-Volterra system around the fixed point for extinction $(u_e^*, v_e^*) = (0,0)$, as described in Section 4.2. Around this point, the populations are so small that the species almost do not interact, resulting in a decoupled system. This also justifies calling this the bare Green's function. So, the predator and prey populations show only the noninteracting part of their evolution, which is, respectively, exponential decay and growth.

However, this decoupled behavior would only occur in the case of small populations. The saddle-point expansion is performed around the deterministic solution (u_d, v_d), which is a periodic trajectory with nonzero populations. Even if the initial populations are chosen such that they get close to extinction, there are also other points in time where the populations are too large to neglect their interactions. Consequently, the assumption that around the deterministic saddle point the evolution of the system is given only by the bare contributions is in contradiction with the saddle-point expansion.

Luckily, the free action also includes other quadratic contributions in the second part of the matrix Q_B, which already contains some part of the interactions of both species. These can be called *mean-field* contributions, as for each term one of the species obeys its deterministic trajectory, which is the field configuration without noise perturbations. To better describe the interacting behavior of the species, a different choice could be to also include these mean-field contributions in the Green's function. As the second contribution to Q_B in Eq. (5.19) has nonzero off-diagonal entries, this would result in four coupled differential equations that should be solved to obtain the Green's function. This system is solvable, but yields intractable and uninsightful solutions. An intermediate possibility is to only include the contributions that still result in a diagonal inverse Green's function, given by

$$G_M^{-1}(t,t') = \begin{pmatrix} \frac{\mathrm{d}}{\mathrm{d}t} - r_u + \alpha v_d(t) & 0 \\ 0 & \frac{\mathrm{d}}{\mathrm{d}t} + r_v - \beta u_d(t) \end{pmatrix} \delta(t-t'), \tag{5.23}$$

for which the corresponding mean-field Green's function is

$$\begin{aligned} G^M(t,t') &= \begin{pmatrix} G_u^M(t,t') & 0 \\ 0 & G_v^M(t,t') \end{pmatrix}, \\ &= \Theta(t-t') \begin{pmatrix} \mathrm{e}^{r_u(t-t') - \alpha \int_{t'}^t v_d(t_1)\,\mathrm{d}t_1} & 0 \\ 0 & \mathrm{e}^{-r_v(t-t') + \beta \int_{t'}^t u_d(t_1)\,\mathrm{d}t_1} \end{pmatrix}. \end{aligned} \tag{5.24}$$

As for the bare case, also $G^M_{u,v}(t,t) = 0$ in the Itô interpretation. For the prey part G^M_u, the interaction with the predators is fixed by the deterministic trajectory v_d, while for the predator part G^M_v, the interaction is fixed by the prey trajectory u_d. Hence, this can be interpreted as a Green's function where the interactions are fixed by the mean-fields u_d and v_d. As this description is more realistic than the bare one, the rest of the calculations will be performed using the mean-field approach. The mean-field free action S^M_0 is equivalent to the bare case S^B_0 (5.18), only that the matrix Q_M is now written as

$$Q_M(t,t') = G^{-1}_M(t,t') + \begin{pmatrix} 0 & \alpha u_d(t) \\ -\beta v_d(t) & 0 \end{pmatrix} \delta(t-t'). \tag{5.25}$$

For the Feynman diagrams, the contributions to S_0 are drawn as propagators, while the contributions to S_I are given by vertices. As the choice of the Green's function does not affect this separation, the Feynman rules for the bare and mean-field case will be the same. This also yields the same diagrams for both cases, where only the propagators correspond to different expressions. Hence, this allows for a comparison of both methods with the simulations. Since the bare description is less realistic, it is interesting to verify if this also yields correlation functions that deviate more from the simulation results than for the mean-field approach. This comparison will be performed in Section 5.4.

The complete MSR action for the stochastic Lotka-Volterra model with additive noise is now given by

$$\begin{aligned} S[\boldsymbol{\psi},\boldsymbol{\varphi}] =& S_0[\boldsymbol{\psi},\boldsymbol{\varphi}] + S_I[\boldsymbol{\psi},\boldsymbol{\varphi}], \\ =& \int \Bigg[\boldsymbol{\varphi}^T(t) G^{-1}_M(t,t') \boldsymbol{\psi}(t') \,\mathrm{d}t' + \boldsymbol{\varphi}^T(t) \begin{pmatrix} 0 & \alpha u_d(t) \\ -\beta v_d(t) & 0 \end{pmatrix} \boldsymbol{\psi}(t) \\ & + \alpha w z q_u - \beta w z q_v - \frac{\Xi_u}{2} q_u^2 - \frac{\Xi_v}{2} q_v^2 \Bigg] \,\mathrm{d}t. \end{aligned} \tag{5.26}$$

With this expression, it is possible to calculate the generating functional $Z[\boldsymbol{J}_{\boldsymbol{y}}, \boldsymbol{J}_{\boldsymbol{\varphi}}]$ in a convenient way. Here, the source fields are defined by $\boldsymbol{J}_{\boldsymbol{y}} = (J_u, J_v)^T$ and $\boldsymbol{J}_{\boldsymbol{\varphi}} = (J_{q_u}, J_{q_v})^T$. The definition of the MSR generating functional in Eq. (3.46) now yields

$$\begin{aligned} Z[\boldsymbol{J}_{\boldsymbol{y}}, \boldsymbol{J}_{\boldsymbol{\varphi}}] &= \int \exp\left\{ -S[\boldsymbol{y},\boldsymbol{\varphi}] + \int \boldsymbol{J}^T_{\boldsymbol{y}}(t) \boldsymbol{y}(t) \,\mathrm{d}t + \int \boldsymbol{J}^T_{\boldsymbol{\varphi}}(t) \boldsymbol{\varphi}(t) \,\mathrm{d}t \right\} \mathcal{D}\boldsymbol{y}\, \mathcal{D}\boldsymbol{\varphi}, \\ &= \int \exp\left\{ -S[\boldsymbol{\psi},\boldsymbol{\varphi}] + \int \boldsymbol{J}^T_{\boldsymbol{y}}(t) [\boldsymbol{\psi}(t) + \boldsymbol{y}_d(t)] \,\mathrm{d}t + \int \boldsymbol{J}^T_{\boldsymbol{\varphi}}(t) \boldsymbol{\varphi}(t) \,\mathrm{d}t \right\} \mathcal{D}\boldsymbol{y}\, \mathcal{D}\boldsymbol{\varphi}, \\ &= Z_{\mathrm{cl}}[\boldsymbol{J}_{\boldsymbol{y}}]\, Z_{\psi}[\boldsymbol{J}_{\boldsymbol{y}}, \boldsymbol{J}_{\boldsymbol{\varphi}}]. \end{aligned} \tag{5.27}$$

By using that $\boldsymbol{y}(t) = \boldsymbol{\psi}(t) + \boldsymbol{y}_d(t)$ and $\delta\boldsymbol{\varphi}(t) = 0$, the generating functional is split in a deterministic part Z_{cl} and a contribution for the fluctuations Z_{ψ}. The classical[49] generating functional $Z_{\mathrm{cl}}[\boldsymbol{J}_{\boldsymbol{y}}]$, containing only the contribution from the deterministic saddle point, is given by

$$Z_{\mathrm{cl}}[\boldsymbol{J}_{\boldsymbol{y}}] = \exp\left\{ \int \boldsymbol{J}^T_{\boldsymbol{y}}(t) \boldsymbol{y}_d(t) \,\mathrm{d}t \right\}. \tag{5.28}$$

[49] Classical here means in the quantum-mechanical interpretation of the semiclassical approach. Here, the zeroth-order contribution to the generating functional is obtained from the deterministic solutions.

$Z_\psi[\boldsymbol{J_y}, \boldsymbol{J_\varphi}]$ contains the contributions of the fluctuations around the saddle point. As the saddle point $\boldsymbol{y}_d(t)$ is a fixed trajectory in phase space, it is possible to write $\mathcal{D}\boldsymbol{y} = \mathcal{D}(\boldsymbol{y}_d + \boldsymbol{\psi}) = \mathcal{D}\boldsymbol{\psi}$. Thus, the contribution of the deviations is

$$\begin{aligned} Z_\psi[\boldsymbol{J_y}, \boldsymbol{J_\varphi}] &= \int \exp\!\left\{-S[\boldsymbol{\psi}, \boldsymbol{\varphi}] + \int \boldsymbol{J}_{\boldsymbol{y}}^T(t)\boldsymbol{\psi}(t)\,\mathrm{d}t + \int \boldsymbol{J}_{\boldsymbol{\varphi}}^T(t)\boldsymbol{\varphi}(t)\,\mathrm{d}t\right\} \mathcal{D}\boldsymbol{\psi}\,\mathcal{D}\boldsymbol{\varphi}, \\ &= \exp\!\left\{-\int \left[\boldsymbol{\varphi}^T(t_1)\begin{pmatrix} 0 & \alpha u_d(t_1) \\ -\beta v_d(t_1) & 0 \end{pmatrix}\boldsymbol{\psi}(t_1) - \frac{\Xi_u}{2}q_u^2(t_1) - \frac{\Xi_v}{2}q_v^2(t_1)\right. \right. \\ &\quad \left. \left. + \alpha w(t_1)z(t_1)q_u(t_1) - \beta w(t_1)z(t_1)q_v(t_1)\right]\mathrm{d}t_1\right\} Z_0[\boldsymbol{J_y}, \boldsymbol{J_\varphi}]. \end{aligned} \tag{5.29}$$

This expression introduces the free generating functional $Z_0[\boldsymbol{J_y}, \boldsymbol{J_\varphi}]$, just as was done for the Langevin equation (3.59). This can be written in terms of the free action $S_0[\boldsymbol{\psi}, \boldsymbol{\varphi}]$, which only contains the contribution from the (inverse) Green's function, as

$$\begin{aligned} Z_0[\boldsymbol{J_y}, \boldsymbol{J_\varphi}] &= \int \exp\left\{-\int \boldsymbol{\varphi}^T(t)G_M^{-1}(t,t')\boldsymbol{\psi}(t')\,\mathrm{d}t\,\mathrm{d}t' + \int \boldsymbol{J}_{\boldsymbol{y}}^T(t)\boldsymbol{\psi}(t)\,\mathrm{d}t + \int \boldsymbol{J}_{\boldsymbol{\varphi}}^T(t)\boldsymbol{\varphi}(t)\,\mathrm{d}t\right\} \mathcal{D}\boldsymbol{\psi}\,\mathcal{D}\boldsymbol{\varphi}, \\ &= \exp\left\{\int \boldsymbol{J}_{\boldsymbol{y}}^T(t)G^M(t,t')\boldsymbol{J}_{\boldsymbol{\varphi}}(t')\,\mathrm{d}t\,\mathrm{d}t'\right\}. \end{aligned} \tag{5.30}$$

In the last line, the Green's function arises from completing the square and performing the Gaussian path integrals. Again, the nonlinear contributions in $Z_\psi[\boldsymbol{J_y}, \boldsymbol{J_\varphi}]$ can now be written as functional derivatives with respect to the source fields, acting on the free generating functional $Z_0[\boldsymbol{J_y}, \boldsymbol{J_\varphi}]$ as

$$\begin{aligned} Z_\psi[\boldsymbol{J_y}, \boldsymbol{J_\varphi}] = \exp\!\Bigg\{ &-\int \Bigg[\left(\frac{\delta}{\delta \boldsymbol{J_\varphi}}\right)\begin{pmatrix} 0 & \alpha u_d(t_1) \\ -\beta v_d(t_1) & 0 \end{pmatrix}\left(\frac{\delta}{\delta \boldsymbol{J_y}}\right) - \frac{\Xi_u}{2}\left(\frac{\delta}{\delta J_{q_u}}\right)^2 - \frac{\Xi_v}{2}\left(\frac{\delta}{\delta J_{q_v}}\right)^2 \\ &+ \frac{\delta^2}{\delta J_u \delta J_v}\left(\alpha\frac{\delta}{\delta J_{q_u}} - \beta\frac{\delta}{\delta J_{q_v}}\right)\Bigg]\mathrm{d}t_1\Bigg\} Z_0[\boldsymbol{J_y}, \boldsymbol{J_\varphi}]. \end{aligned} \tag{5.31}$$

The off-diagonal quadratic contributions from the matrix Q_M remain in Z_ψ as functional derivatives. These should be contained in the free part Z_0, as this corresponds to the free action S_0, and therefore to the propagators of this field theory. Applying these functional derivatives explicitly gives rise to the mean-field Green's matrix

$$\begin{aligned} B(t,t') &= \begin{pmatrix} G_u^M(t,t') & -\alpha\int_{t'}^t G_u^M(t,t_1)\,u_d(t_1)\,G_v^M(t_1,t')\,\mathrm{d}t_1 \\ \beta\int_{t'}^t G_v^M(t,t_1)\,v_d(t_1)\,G_u^M(t_1,t')\,\mathrm{d}t_1 & G_v^M(t,t') \end{pmatrix}, \\ &\equiv \begin{pmatrix} B_{uu}(t,t') & B_{uv}(t,t') \\ B_{vu}(t,t') & B_{vv}(t,t') \end{pmatrix}, \end{aligned} \tag{5.32}$$

such that the free generating functional Z_0 transforms to the mean-field generating functional

$$Z_0^M[\boldsymbol{J_y}, \boldsymbol{J_\varphi}] = \exp\left\{\int \boldsymbol{J}_{\boldsymbol{y}}^T(t)B(t,t')\boldsymbol{J}_{\boldsymbol{\varphi}}(t')\,\mathrm{d}t\,\mathrm{d}t'\right\}. \tag{5.33}$$

It is important to note that each entry $B_{ij}(t,t) = 0$ for all $i,j \in \{u,v\}$. This follows directly from the fact that $G_{u,v}^M(t,t) = 0$, as $\Theta(t-t) = 0$ in the Itô interpretation. The generating functional of the fluctuations becomes

$$\begin{aligned} Z_\psi[\boldsymbol{J_y}, \boldsymbol{J_\varphi}] = &\exp\left\{\int\left[\frac{\delta^2}{\delta J_u \delta J_v}\left(\beta\frac{\delta}{\delta J_{q_v}} - \alpha\frac{\delta}{\delta J_{q_u}}\right) + \frac{\Xi_u}{2}\left(\frac{\delta}{\delta J_{q_u}}\right)^2 + \frac{\Xi_v}{2}\left(\frac{\delta}{\delta J_{q_v}}\right)^2\right]\mathrm{d}t_2\right\} \\ &\exp\left\{\int \boldsymbol{J}_{\boldsymbol{y}}^T(t)B(t,t')\boldsymbol{J}_{\boldsymbol{\phi}}(t')\,\mathrm{d}t\,\mathrm{d}t'\right\}. \end{aligned} \tag{5.34}$$

5.3.2 Perturbative calculations

Now that an expression is obtained for both the classical and fluctuation part of the complete generating functional $Z[\boldsymbol{J_y}, \boldsymbol{J_\varphi}] = Z_{\mathrm{cl}}[\boldsymbol{J_y}]\, Z_\psi[\boldsymbol{J_y}, \boldsymbol{J_\varphi}]$ in terms of a Green's function, it is possible to calculate correlation functions that describe the average and variance in the populations. This will be done by applying perturbation theory to the contribution of the fluctuations Z_ψ. The classical part $Z_{\mathrm{cl}}[\boldsymbol{J_y}]$ only contains contributions from the deterministic Lotka-Volterra system. As this system is already solved by the saddle point $\boldsymbol{y}_d$, calculating correlation functions from Z_{cl} does not yield any new information on the stochastic system. Also, the main interest is to look at deviations from this deterministic evolution. This justifies calculating the average fluctuations $\langle w(t)\rangle$, $\langle z(t)\rangle$, and their covariances through the two-point functions $\langle w(t)w(t')\rangle$, $\langle z(t)z(t')\rangle$ and $\langle w(t)z(t')\rangle$. This requires only the part of the generating functional that contains these fluctuations, which is Z_ψ. The total average populations can easily be retrieved by also taking into account the deterministic evolution. Writing the exponents in Eq. (5.34) as a Taylor expansion yields

$$\begin{aligned} Z_\psi[\boldsymbol{J_y}, \boldsymbol{J_\varphi}] = \sum_{V=0}^{\infty} \frac{1}{V!} \left\{ \int \left[\frac{\delta^2}{\delta J_u \delta J_v} \left(\beta \frac{\delta}{\delta J_{q_v}} - \alpha \frac{\delta}{\delta J_{q_u}} \right) + \frac{\Xi_u}{2} \left(\frac{\delta}{\delta J_{q_u}} \right)^2 + \frac{\Xi_v}{2} \left(\frac{\delta}{\delta J_{q_v}} \right)^2 \right] \mathrm{d}t_2 \right\}^V \\ \sum_{P=0}^{\infty} \frac{1}{P!} \left\{ \int \left(J_u(t), J_v(t) \right) \begin{pmatrix} B_{uu}(t,t') & B_{uv}(t,t') \\ B_{vu}(t,t') & B_{vv}(t,t') \end{pmatrix} \begin{pmatrix} J_{q_u}(t') \\ J_{q_v}(t') \end{pmatrix} \mathrm{d}t\, \mathrm{d}t' \right\}^P . \end{aligned} \tag{5.35}$$

In the expansions, V represents the number of vertices and P the number of propagators. This expression shows that there are four different vertices and four different propagators in this field theory. As for the nonlinear Langevin equation, it is convenient to assign each a separate value. This can be implemented in Z_ψ by writing separate expansions for the four vertices and four propagators, instead of only one for both as in Eq. (5.35). For notational convenience, this will not be done explicitly. The total number of propagators is given by $P_{uu} + P_{uv} + P_{vu} + P_{vv}$, where each contribution corresponds to one of the entries of the matrix $B(t,t')$. The number of vertices is separated in cubic vertices $V_c = V_\alpha + V_\beta$, where the subscript corresponds to the coefficient of the cubic interaction, and noise vertices $N = N_u + N_v$ that correspond to the interaction with the prey and predator noise amplitudes as coefficients. Hence, the total number of vertices is given by $V_c + N$. The number of remaining external legs after applying the functional derivatives is then for each field given by the following consistency relations

$$\begin{aligned} E_u &= P_{uu} + P_{uv} - V_\alpha - V_\beta, \\ E_v &= P_{vu} + P_{vv} - V_\alpha - V_\beta, \\ E_{q_u} &= P_{uu} + P_{vu} - V_\alpha - 2N_u, \\ E_{q_v} &= P_{uv} + P_{vv} - V_\beta - 2N_v. \end{aligned} \tag{5.36}$$

As only one- and two-point correlation functions will be calculated for the populations in this model, the number of external legs for the prey and predator fields can be restricted to $1 \leq E_u + E_v \leq 2$. The auxiliary fields themselves do not describe a physically interesting quantity, but they do contribute to the response functions, as these are obtained from the two-point correlation functions that couple one real field to one auxiliary field. Looking at the structure of $Z_0^M[\boldsymbol{J_y}, \boldsymbol{J_\varphi}]$, it can be seen that this free part already contains the required coupling of source functions that yields nonzero contributions to the response functions, even for $V = 0$. Hence, it is justified to set $E_{q_u} = E_{q_v} = 0$ and calculate only these contributions to the response functions, which are zeroth order in the perturbation[50].

[50] This is reasonable because the auxiliary fields do not arise in the simulations. Hence, the analytical results can not be compared to any simulated response function. In addition, allowing nonzero values for E_{q_u} and E_{q_v} would give rise to many more Feynman diagrams, which would not contribute to the correlation functions.

As stated earlier, the saddle-point expansion can be performed in orders of the noise amplitudes, to analytically describe the effect of random noise in the system through the fluctuations. Therefore, the number of noise vertices N should be restricted to fix the order of the noise. For this work, the fluctuations are studied up to first order in the noise amplitudes, so $N = N_u + N_v \leq 1$. Subtracting the equations for E_u and E_v from $E_{q_u} + E_{q_v}$ yields

$$V_\alpha + V_\beta = 2(N_u + N_v) - (E_u + E_v) \leq 2 \cdot 1 - 1 \leq 1. \tag{5.37}$$

Hence, the consistency relations together with the conditions for the external legs and noise vertices also restrict the number of cubic vertices $V_c \leq 1$. Conditions for the number of propagators now follow directly from each consistency relation. Using these restrictions, all possible combinations of propagators, vertices, and external legs can be calculated. The diagrams are then given by rearrangements of these combinations. This also justifies why the expansion is done up to first order in the noise amplitudes. This is to keep the calculation of diagrams tractable, as the second-order correction already gives rise to 40 possible combinations of propagators, vertices, and external legs, for $\langle w(t) \rangle$ only. As the diagrams consist of all rearrangements of these combinations, the total number of diagrams will be even larger. Despite the fact that several of these diagrams vanish, because $B_{ij}(t,t) = 0$ due to Itô's convention, second-order corrections will not be considered in this work.

A short note can be made on the number of loops arising in these diagrams. As stated in Section 3.4.1, the number of loops in a connected diagram is given by $L = I - V + 1$, where I is the number of internal legs. This relation holds for any field theory. For the nonlinear Langevin equation, it was also shown that a connected diagram was of order Ξ^{E+I-V}. This is not valid for the stochastic Lotka-Volterra equations. Using the consistency relations, one finds that the total noise order is $N = E + 2I - 3V_c$. Hence, for this model, the noise order can not be expressed conveniently in terms of the number of loops L, as this depends on the kind of vertices in a diagram. Furthermore, due to the different kinds of vertices and propagators, there are several different possible loops. Therefore, the expansion will be performed in orders of the noise amplitudes instead of the number of loops.

To draw the Feynman diagrams corresponding to the contributions to the correlation functions, Feynman rules have to be defined for this stochastic field theory. For the external sources and propagators, these are given by

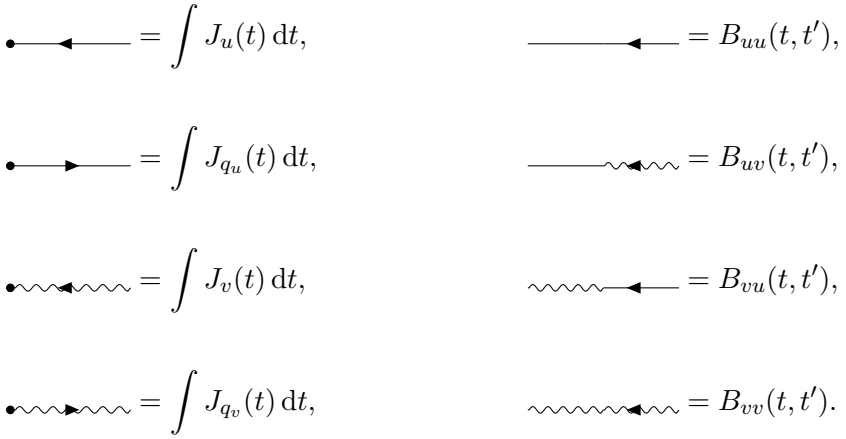

The prey fields are depicted by straight lines, while the wiggled lines represent the predator fields. An arrow pointing towards the source indicates a 'real' prey or predator field, while arrows pointing

away from the sources correspond to the auxiliary fields. Each propagator represents an entry of the mean-field Green's matrix $B(t, t')$. The diagonal entries contain only prey or only predator Green's functions, so they are depicted by a complete straight or wiggled line. In the off-diagonal entries in Eq. (5.32), the different Green's functions couple, so these are represented by mixed lines. Note that these contributions already include an integration over time t_1, which is the point in time when the Green's functions couple to one of the deterministic fields. This is not shown explicitly in the Feynman diagrams.

The Feynman rules for the four vertices of this field theory are given by

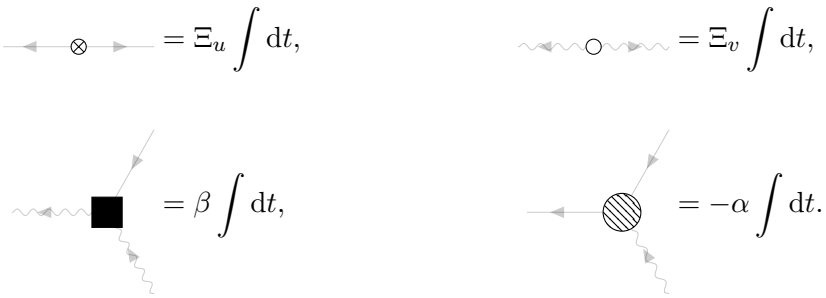

There are two noise vertices with a crossed and open dot for the noise amplitude of the prey and predators, respectively. The factor 1/2 in both these interactions in Eq. (5.35) cancels the symmetry factor for the vertices. For the cubic vertices, the interaction with coefficient β is depicted by the filled square, while the interaction with coefficient $-\alpha$ is represented by the dashed dot. The vertices also show the incoming and outgoing lines that connect to the propagators and external sources. It is important to note that the noise vertices can only have outgoing lines.

Using the conditions for the number of external legs, propagators, and vertices, it is possible to write down a complete expression for Z_ψ in terms of Feynman diagrams, up to first order in the noise amplitudes. The main goal is to derive correlation functions for the fluctuations from this generating functional. Therefore, only these correlation functions will be expressed as Feynman diagrams here. To determine all diagrams that have a nonvanishing contribution to these quantities, all rearrangements of the different combinations of external legs, propagators, and vertices that can contribute should be taken into account. Consider for example the average fluctuations in the prey species $\langle w(t) \rangle$. By definition of the generating functional, this is given by

$$\langle w(t) \rangle = \frac{\delta}{\delta J_u(t)} Z_\psi[\boldsymbol{J_y}, \boldsymbol{J_\varphi}] \bigg|_{\boldsymbol{J_y}=\boldsymbol{J_\varphi}=0}. \tag{5.38}$$

Hence, to obtain a nonzero contribution, the external legs should be set to $E_u = 1$ and $E_v = 0$. It can be shown that up to first order in the noise amplitudes, this gives rise to six possible combinations for the remaining propagators and vertices. All possible rearrangements then yield twelve different Feynman diagrams. Several of these diagrams include loops that connect the cubic vertex to itself. Take for example $P_{vv} = 1$, $P_{uv} = 2$, $V_\beta = 1$ and $N_v = 1$, for which one possible diagram is


. (5.39)

As the cubic vertices are local in time, the propagator in these loops is also local, i.e. it is given by $B_{ij}(t,t)$ for some $i,j \in \{u,v\}$. As mentioned earlier, $B_{ij}(t,t) = 0$ in the Itô interpretation. Hence, all diagrams with loops that connect the cubic vertex to itself vanish. There are nine of these diagrams for $\langle w(t)\rangle$, so this leaves only three nonzero contributions. Hence, the average fluctuations in the prey up to first order in the noise are

$\langle w(t)\rangle =$ 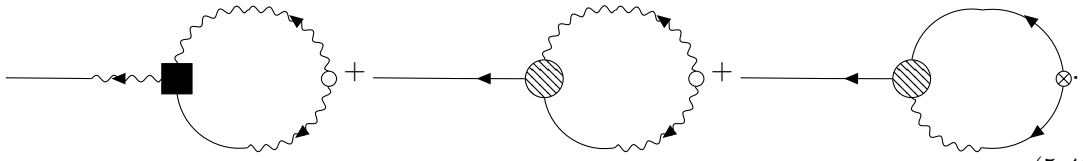 (5.40)

The average fluctuations in the predator species can be calculated in a similar way as $\langle z(t)\rangle = \delta Z_\psi / \delta J_v(t)$, by setting $E_v = 1$ and $E_u = 0$. This also yields three nonvanishing diagrams up to first order in the noise,

$\langle z(t)\rangle =$ 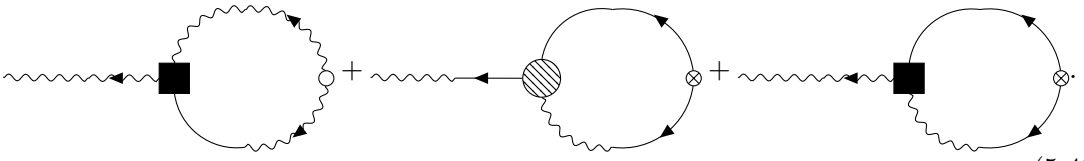 (5.41)

All contributing diagrams contain a loop that connects one of the noise vertices to one of the cubic vertices. This can be interpreted as the noise (amplitudes) coupling to the interactions in the system, which scale with the coefficients α and β. A similar coupling was also observed in the one-point function (3.78) for the nonlinear Langevin equation. These loops also contain an interaction with one of the deterministic fields, through the off-diagonal entries of $B(t,t')$. For the average prey fluctuations, two diagrams include an empty dot, which contains the noise amplitude Ξ_v of the predators. This is interesting, as there is only one diagram with a crossed dot, representing the noise Ξ_u in the prey itself. For the predator diagrams, this is reversed. Fluctuations due to random effects in one species affect the other species via the interaction in the system. Therefore, the noise effects in one species have an indirect effect on the other species.

The two-point correlation functions for the fluctuations can be calculated in a similar way, by fixing again the number of external legs E_u and E_v, which should satisfy $E_u + E_v = 2$. This gives no diagrams with cubic interactions, as Eq. (5.37) yields that $V_\alpha + V_\beta \leq 0$ for a noise order of $N = 1$. Hence, every diagram only contains one noise vertex and two external legs. All two-point correlation functions are then given by

$\langle w(t)w(t')\rangle =$ 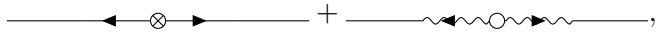 (5.42)

$\langle z(t)z(t')\rangle =$ 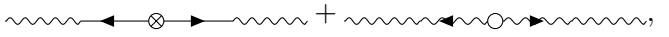 (5.43)

$\langle w(t)z(t')\rangle =$ 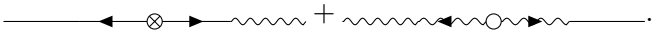 (5.44)

The different endpoints in the diagrams describe different points t, t' in time. Hence, when $t = t'$ for the comparison with the simulations, this corresponds to a loop in the Feynman diagrams. Each two-point function contains one contribution for each noise vertex. Just as for the one-point functions, this can be expected due to the indirect effect of noise in one species on the other species, through their interactions.

The obtained correlation functions, which only contain connected diagrams, describe the behavior of the fluctuations in the populations. To find expressions for the correlation functions of the total populations $u(t)$ and $v(t)$ in terms of Feynman diagrams, also disconnected diagrams should be included. Hence, this also contains contributions from the classical generating functional $Z_{\text{cl}}[\boldsymbol{J_y}]$, as the total generating functional is given by $Z[\boldsymbol{J_y}, \boldsymbol{J_\varphi}] = Z_{\text{cl}}[\boldsymbol{J_y}]\, Z_\psi[\boldsymbol{J_y}, \boldsymbol{J_\varphi}]$. Luckily, these disconnected contributions can simply be derived by looking at the one- and two-point functions for the total populations. The average total prey population is given by $\langle u(t)\rangle = u_d(t) + \langle w(t)\rangle$, so it can be obtained from $\langle w(t)\rangle$ by just adding the deterministic evolution. Its two-point function is given by $\langle u(t)u(t')\rangle = u_d^2(t) + u_d(t)\langle w(t')\rangle + u_d(t')\langle w(t)\rangle + \langle w(t)w(t')\rangle$, so this can also be calculated directly. The covariance $\langle u(t)u(t')\rangle_c$ is then obtained via Eq. (5.4). Similar relations hold for the total predator population $v(t)$ and its fluctuations $z(t)$.

As the correlation functions for the fluctuations are compared with the simulations, they need to be calculated explicitly. Using the Feynman rules, the diagrams in Eq. (5.40)-(5.44) can be converted back into integral expressions. For the average fluctuations in the prey, this yields

$$\begin{aligned}\langle w(t)\rangle =& \Xi_v\beta \int_0^t B_{uv}(t,t_2)B_{uv}(t_2,t_1)B_{vv}(t_2,t_1)\,\mathrm{d}t_2\,\mathrm{d}t_1 - \Xi_v\alpha\int_0^t B_{uu}(t,t_2)B_{vv}(t_2,t_1)B_{uv}(t_2,t_1)\,\mathrm{d}t_2\,\mathrm{d}t_1\\ &-\Xi_u\alpha\int_0^t B_{uu}(t,t_2)B_{uu}(t_2,t_1)B_{vu}(t_2,t_1)\,\mathrm{d}t_2\,\mathrm{d}t_1. \end{aligned} \tag{5.45}$$

Calculating these integrals is not an easy task. First of all, every integral contains at least one off-diagonal entry of the matrix $B(t,t')$. These elements already contain an integration in time, which also includes the deterministic population trajectories $u_d(t)$ and $v_d(t)$. These periodic solutions are also contained in each Green's function. As stated in Section 4.2, there is no analytical expression for these periodic solutions of the deterministic Lotka-Volterra model. So, they can only be computed numerically at discrete points in time, with a separation given by the simulation time step Δt. Therefore, it is not possible to perform these integrals symbolically. A solution to this problem could be to determine an interpolation of these numerical deterministic solutions, but this turned out to result in extremely large runtimes in both Mathematica and Python. A different possibility is to calculate the Fourier transforms of the deterministic solutions, $\hat{u}_d(\omega)$ and $\hat{v}_d(\omega)$. As ω is the frequency, one could expect that these Fourier transforms are peaked around the frequency $\omega_d = 2\pi/T$ of the deterministic evolution with period T. It turns out that taking into account only this frequency is not enough to get well-behaving Fourier transformed functions. This resulted in nonzero imaginary contributions to the correlation functions. Furthermore, this also gives large runtimes. As these methods do not work, it is better to use the discrete numerical solutions for $u_d(t)$ and $v_d(t)$. This requires all integrals to be calculated numerically as explicit Riemann sums, with a discrete time step Δt. This approach, which is also contained in our code in Ref. [109], solves the integrations. Another issue might be that the mean-field Green's functions can be exponentially increasing. As the integrations are done for $t \in [0, T_{\text{sim}}]$ to compare with the results of the simulations, this can lead to exponential behavior that grows quickly in time. This will be discussed elaborately in the following section.

The last interesting quantities to be considered are the response functions. These determine the response of the average $\langle \boldsymbol{y}(t)\rangle$ due to an external force $\boldsymbol{f}(t') = (f_u(t'), f_v(t'))$, for $t \geq t'$. Via Eq. (3.53), these can be calculated in terms of a connected two-point function consisting of one real field and one auxiliary field. For this two-dimensional system there are four different response functions, as there are two real fields $u(t), v(t)$ and two auxiliary fields $q_u(t), q_v(t)$. As mentioned earlier, the free part $Z_0^M[\boldsymbol{J_y}, \boldsymbol{J_\varphi}]$ of the generating functional already yields nonzero contributions

to the response functions. These contributions are exactly given by one of the entries of the matrix $B(t,t')$. As the response functions are not simulated, it suffices to only look at these contributions, which are zeroth order in the perturbation theory. So, for $t \geq t'$,

$$\begin{aligned} R_{uu}(t,t') &= \langle u(t) q_u(t') \rangle_c, \\ &= \frac{\delta^2}{\delta J_u(t) \delta J_{q_u}(t')} \log Z_0^M[\boldsymbol{J_y}, \boldsymbol{J_\varphi}] \Big|_{\boldsymbol{J_y}=\boldsymbol{J_\varphi}=0}, \\ &= B_{uu}(t,t'), \end{aligned} \tag{5.46}$$

$$R_{vv}(t,t') = \langle v(t) q_v(t') \rangle_c = B_{vv}(t,t'), \tag{5.47}$$

$$R_{uv}(t,t') = \langle u(t) q_v(t') \rangle_c = B_{uv}(t,t'), \tag{5.48}$$

$$R_{vu}(t,t') = \langle v(t) q_u(t') \rangle_c = B_{vu}(t,t'). \tag{5.49}$$

Note that the real fields $u(t)$ and $v(t)$ in the response function determine the coupling constant, α and β respectively. As the off-diagonal entries of $B(t,t')$ include integrations containing the deterministic fields $u_d(t)$ and $v_d(t)$, the response functions are also calculated numerically via Riemann sums. For $T_{\text{sim}} = 10T_{\text{lin}}$, the results are shown in Figure 5.21. The time t' at which the perturbation or external force is applied is set to $t' = t_0 = 0$. The response functions $R_{uu}(t,0)$ and $R_{vv}(t,0)$, describing responses of the populations to a perturbation in its own species, show periodic behavior. Hence, up to zeroth order in the noise and cubic interactions, these responses do not decay to zero, but remain in the system with a constant amplitude. Although the periodic behavior can be explained by the periodicity of the deterministic system, the constant amplitude is one of the unrealistic features of this zeroth order approach, as an interacting system usually reacts to such a perturbation, which affects the response function later in time. The coupled response functions $R_{uv}(t,0)$ and $R_{vu}(t,0)$, describing responses of the populations to a perturbation in the other species, also show periodic behavior. However, these responses grow in time, respectively in a positive and negative direction. So, a perturbation in one species amplifies the response in the other species.

Next to the physical interpretation of these response functions, it is also useful to observe the long time behavior of the elements of the mean-field Green's matrix $B(t,t')$ (5.32), as these will be used in the computation of the Feynman diagrams. The diagonal entries $B_{uu}(t,0)$ and $B_{vv}(t,0)$ are periodic due to the deterministic fields contained in the Green's functions $G_u^M(t,t')$ and $G_v^M(t,t')$. Hence, including these mean-fields indeed yields more realistic behavior, by diminishing the exponential growth and decay that was observed in the bare Green's functions. Also note that these contributions have an approximate phase difference of $\pi/4$, which is the phase difference of the linearized solution around the fixed point. The off-diagonal entries $B_{uv}(t,0)$ and $B_{vu}(t,0)$ are also periodic due to the coupling to the mean-fields $u_d(t)$ and $v_d(t)$. The respective negative and positive growth of their amplitudes arise from the integration in time in Eq. (5.32). Hence, as all correlation functions contain at least one off-diagonal element of $B(t,t')$, which is again integrated in time through the Feynman rules, this behavior can cause exponential growth or decay in the diagrams. This will be analyzed further in the following section.

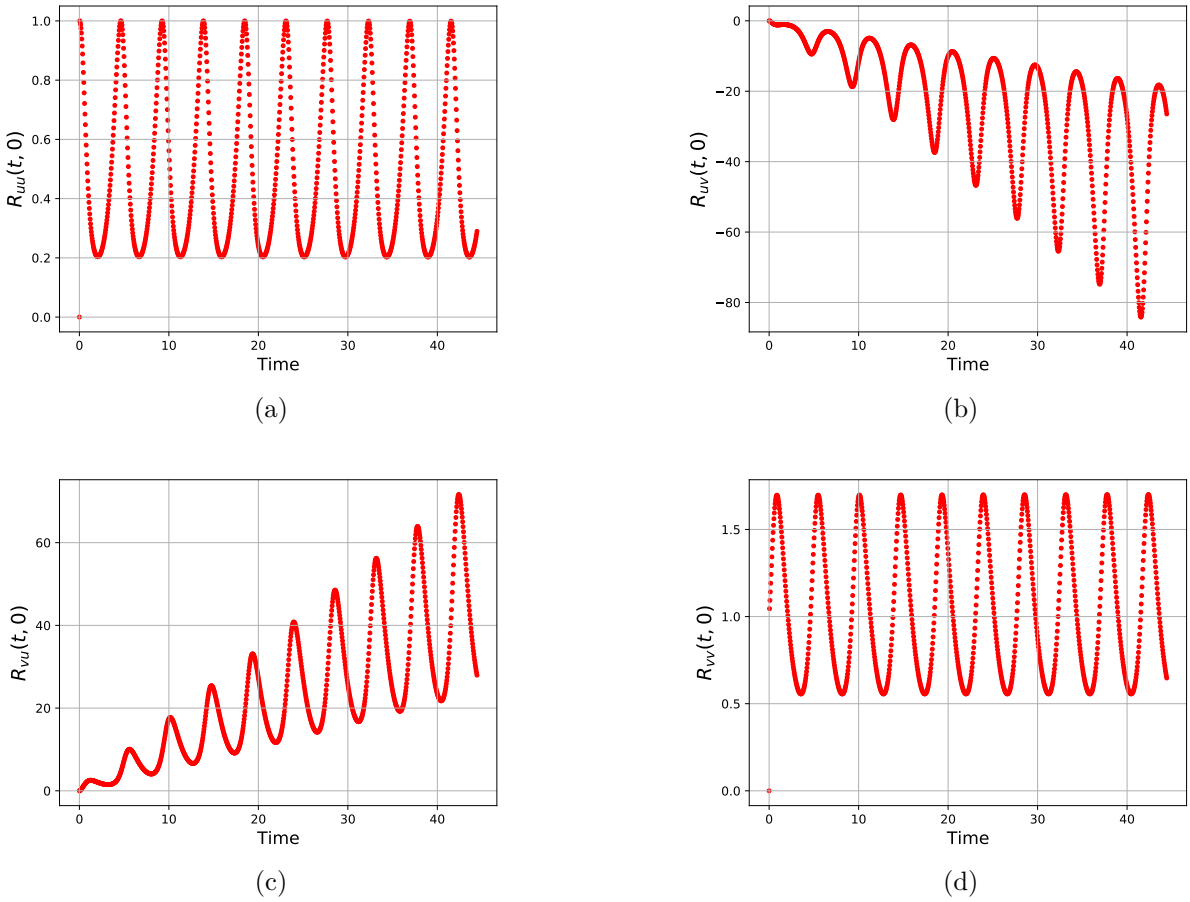

Figure 5.21: The four response functions (a) $R_{uu}(t,0)$, (b) $R_{uv}(t,0)$, (c) $R_{vu}(t,0)$ and (d) $R_{vv}(t,0)$ of the two species stochastic Lotka-Volterra system, for $t' = t_0 = 0$ and $T_{\text{sim}} = 10T_{\text{lin}}$.

5.4 Results & Comparison

The analytical expressions for the correlation functions in this system obtained with the MSR formalism in the last section are already insightful by themselves. However, to see whether the MSR formalism is really a useful tool to describe this stochastic system, these analytical results have to be compared with the averaged simulated results for the same correlation functions. All calculations are performed with the standard parameters $[r_u, r_v, \alpha, \beta] = [2, 1, 0.05, 0.05]$ and initial populations $(u_0, v_0) = (40, 40)$. The noise amplitudes are given by $\Xi_u = 0.2$ and $\Xi_v = 0.4$. All simulations are performed for 10^4 noise realizations, unless specified otherwise. The total number of time steps is $N = 100m$. The results are shown for different times $T_{\text{sim}} = T_{\text{lin}}, 2T_{\text{lin}}$ and $10T_{\text{lin}}$.

Figure 5.22 shows the results for a simulation time $T_{\text{sim}} = T_{\text{lin}}$. The dashed red lines represent the correlation functions obtained with the MSR formalism via the mean-field Green's functions $G^M(t,t')$. The dotted green lines show the average results from the simulations. The average fluctuations yield a well-defined measure of the deviation of both stochastic results with respect to the deterministic fields. However, to give an interpretation for this stochastic model with the chosen standard parameters, it is better to rescale the absolute fluctuations by the initial populations (u_0, v_0). This is to compare the size of the fluctuations with respect to the total populations. Hence, all correlation functions of fluctuations are relative with respect to the initial populations.

The relative average fluctuations for both species are depicted in Figures 5.22a-5.22b. As the simulation time corresponds to only one linear cycle, the averaged simulations only deviate slightly from the deterministic trajectory, resulting in small average fluctuations of about -0.1% in the prey and -0.5% in the predators. This indicates again that the noise effect is larger for the predator species, as its fluctuations are larger. The analytical result for these average fluctuations, given by the Feynman diagrams in Eq. (5.40)-(5.41), has the same order of magnitude. Hence, even though the time integrals in the Feynman diagrams show exponential behavior as in Figure 5.21, for $T_{\text{sim}} = T_{\text{lin}}$, their order of magnitude is still similar to the simulation results. The predator fluctuations $\langle z(t)\rangle$ obtained from the MSR formalism grow faster in the negative direction than the simulation results, but the general behavior is similar. Except for a sign change, the prey fluctuations $\langle w(t)\rangle$ are also comparable, which can be seen by inverting the analytical result in the time axis. So, for short time, the MSR formalism captures the correct general behavior of the fluctuations with only a sign difference in the prey species.

Figure 5.22c shows the total average populations. The deterministic populations are also shown for reference, represented by a solid blue line for the prey $u_d(t)$ and a solid red line for the predators $v_d(t)$. The dashed lines correspond to the analytical populations, which are obtained from $\langle u_a(t)\rangle = u_d(t) + \langle w(t)\rangle$ and $\langle v_a(t)\rangle = v_d(t) + \langle z(t)\rangle$. The averaged simulations are represented by dotted lines. As the average fluctuations in both species are smaller than 1%, these are not visible in the total populations. This also indicates that the inward spiraling motion of the average simulations is not yet observable.

The two-point correlation functions for the total populations at equal times $t = t'$ are shown in Figures 5.22d-5.22f. These are depicted instead of the two-point functions of the fluctuations, as these already show exponential growth that yields much larger fluctuations than found for the simulated case[51]. Hence, the fluctuation two-point functions appear to be zero compared to the analytical ones. The results of the analytical two-point functions for the fluctuations are shown in Appendix C.1. These are compared with separate results for the simulations. Here, the exponential behavior of the Feynman diagrams becomes visible. This is mainly due to the behavior of the coupled propagators, which arise in at least one Feynman diagram of each two-point correlation function (5.42)-(5.44). These represent the off-diagonal elements $B_{uv}(t,t)$ and $B_{vu}(t,t)$ of the mean-field Green's matrix. This behavior seems to be inherent to every time integration of $G^M_{u,v}(t,t')$.

Nevertheless, it is still interesting to study the total two-point functions. Clearly, the exponential growth in $\langle w(t)w(t)\rangle$ is already large enough that also the analytical result for $\langle u(t)u(t)\rangle$ grows exponentially. This indicates that the largest exponential behavior is caused by the prey Green's function $G^M_u(t,0)$, as this is the part of the propagator at each end time t in the diagrams for $\langle w(t)w(t)\rangle$. Hence, even though the mean-field approach diminishes some of the exponential growth in $G^M_u(t,0)$ compared to the bare Green's function $G^B_u(t,0)$ (5.22), it is still not a good enough description to obtain correct higher moments. Some of the periodicity of the system arising from the coupling to the deterministic fields is still contained in $\langle u(t)u(t)\rangle$. This periodicity is better visible in the other two-point correlation functions $\langle v(t)v(t)\rangle$ and $\langle u(t)v(t)\rangle$. These total two-point functions show better results compared to the simulations. First of all, they show comparable orders of magnitude, but also they follow the same periodic behavior. However, also here the exponential behavior becomes visible close to $t = T_{\text{sim}}$. Nevertheless, it can be concluded that the MSR formalism shows general behavior similar to the simulations for these two-point functions.

[51] This is also the case for the non-equal time correlation functions like $\langle w(t)w(t')\rangle$ for $t' = T_{\text{lin}}/2$; thus these are also not shown here.

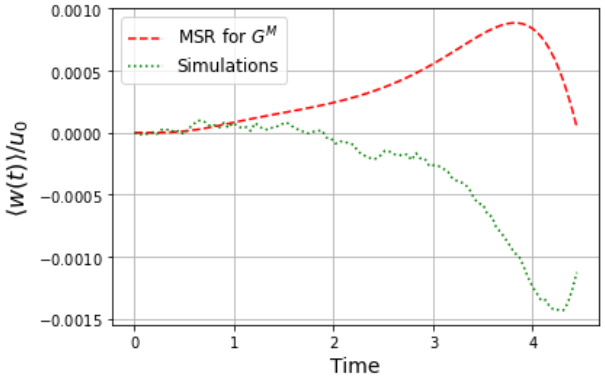

(a) Relative average fluctuations in prey $\langle w(t)\rangle$.

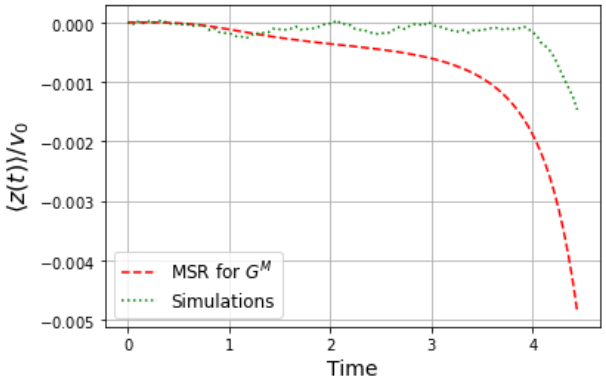

(b) Relative average fluctuations in predators $\langle z(t)\rangle$.

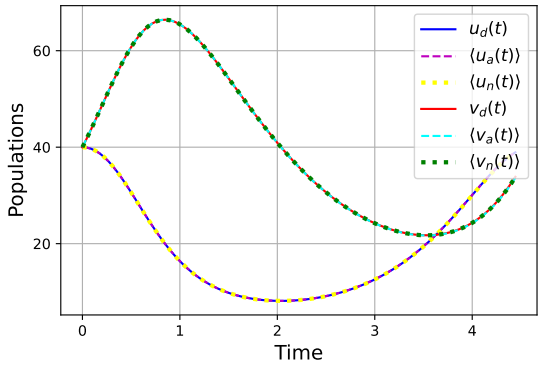

(c) Total average populations $u(t)$ and $v(t)$, for the deterministic d, analytical a and simulated n case.

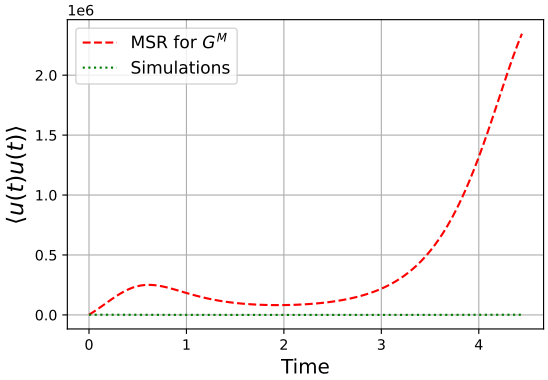

(d) Total two-point correlation function for the prey $\langle u(t)u(t)\rangle$.

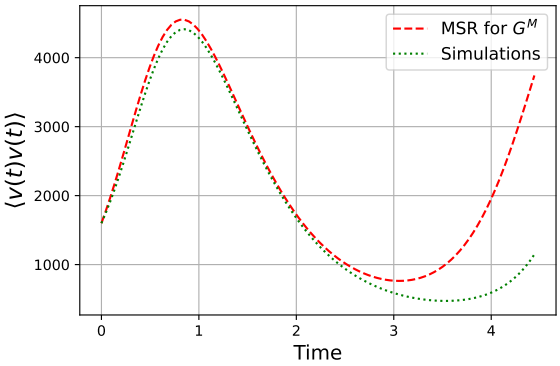

(e) Total two-point correlation function for the predators $\langle v(t)v(t)\rangle$.

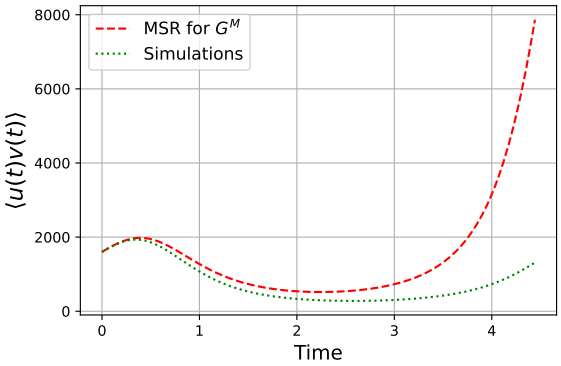

(f) Total coupled two-point correlation function $\langle u(t)v(t)\rangle$.

Figure 5.22: Results for $T_{\text{sim}} = T_{\text{lin}}$ and noise amplitudes $\Xi_u = 0.2$, $\Xi_v = 0.4$. The dashed red line represents quantities obtained with the MSR formalism using the mean-field Green's functions G^M. The dotted green line corresponds to the average of 10^4 simulations. Figure (c) shows the total populations, where the solid lines represent the deterministic results $u_d(t)$ and $v_d(t)$. The analytical results a (dashed) are obtained from $\langle w(t)\rangle$ and $\langle z(t)\rangle$, while the simulated results n (dotted) correspond to the average stochastic trajectories.

The MSR formalism turns out to show also comparable results for some correlation functions for $T_{\text{sim}} = T_{\text{lin}}$, while it breaks down for other quantities. Therefore, it is interesting to compare the same quantities for a larger time $T_{\text{sim}} = 2T_{\text{lin}}$. The results are shown in Figure 5.23. The relative average fluctuations now also start to show the exponential behavior that arises from the coupled propagators $B_{uv}(t,0)$ and $B_{vu}(t,0)$ and other time integrations in the corresponding Feynman diagrams. While the fluctuations in the simulations stay around 0.2% for both species, the analytical results for the prey grow up to 6%. The prey fluctuations also show the same sign difference as was observed for $T_{\text{sim}} = T_{\text{lin}}$. For the predators, $\langle z(t) \rangle$ remains negative and even becomes 30%. Hence, for larger time $T_{\text{sim}} = 2T_{\text{lin}}$ the exponential behavior also appears in the analytical average fluctuations, which causes a deviation from the simulated results.

This effect on the analytical fluctuations now also becomes visible in the total average populations in Figure 5.23c. The simulated results still follow the deterministic paths $(u_d(t), v_d(t))$, but the analytical total populations represented by the dashed lines start to deviate from these periodic solutions at larger times. It is also insightful to observe the same behavior in the phase space representation in Figure 5.23d. Both trajectories for the simulations and for the MSR formalism follow the deterministic periodic trajectory slightly longer than one linear period T_{lin}. Right after passing the initial populations (u_0, v_0), the analytical trajectory represented by the dashed red line starts to show inward spiraling motion due to the large negative fluctuations in the predator species. However, as these fluctuations keep increasing to larger negative numbers and the prey fluctuations start to become significant, the analytical trajectory evolves outside of the deterministic path. For this simulation time and noise amplitude, the simulations are not diffused enough to observe the inward spiraling motion, hence the average simulated trajectory remains close to the deterministic one. So, the analytical trajectory shows inward spiraling motion for some amount of time, although much earlier than the simulated case.

The MSR formalism with the mean-field Green's functions starts to break down for $T_{\text{sim}} = 2T_{\text{lin}}$. The results obtained with this mean-field approach can also be compared to an approach using the bare Green's functions G^B (5.22). As mentioned earlier, these represent the unrealistic exponential growth and decay of the respective prey and predator species in the case of no interactions. As the exponential behavior of these Green's functions is not suppressed at all, it is expected that this approach yields much worse results. Indeed, this yields an exponential behavior in the correlation functions that is growing even faster than for the mean-field approach. The MSR formalism with bare Green's functions already breaks down for $T_{\text{sim}} = T_{\text{lin}}$. To still give a quantitative comparison between both methods, the logarithm of the absolute average fluctuations is shown in Figures 5.24a-5.24b, for $T_{\text{sim}} = 2T_{\text{lin}}$. The results for the bare Green's functions are depicted by the solid blue lines. For very short times $t < T_{\text{sim}}/4$, both methods yield the same order of magnitude as the simulations, but the bare approach starts to grow exponentially almost immediately. These figures also show that for short times, the mean-field approach yields an accurate order of magnitude compared to the bare method. Also, the growth rate shows some stabilization for G^M, while for G^B it keeps growing linearly, which indicates faster exponential growth. The local minima in both analytical cases are a result from taking the absolute average fluctuations, as the logarithm is only defined on $\mathbb{R}_{>0}$. This transforms the sign change in the average fluctuations, which arises from the periodicity of the deterministic model, to a local minimum in the logarithm. In general, it can be concluded that although deviations are observed in both cases, the MSR formalism with a mean-field approach is far better comparable to the simulated results than the bare approach.

For completeness, also the results for the total two-point functions are shown in Figures 5.24c-5.24e. The behavior of the prey two-point function is still showing the same features as for $T_{\text{sim}} = T_{\text{lin}}$.

Despite the growth of the amplitude, it still has the same periodicity as the system itself. This can also be observed in the other two-point functions. Hence, even for larger times, the MSR formalism captures the correct periodicity of the system. The growing deviations for the analytical predator two-point function compared to the simulated result observed in Figure 5.22e are suppressed again at later times, so the general behavior of this total correlation function is still well-described by the MSR formalism. However, the deviations from the simulated case start to grow for the coupled two-point function $\langle u(t)v(t)\rangle$. This correlation function thus shows an intermediate behavior, with features from both other two-point functions.

The break down of this approach for larger times can partially be explained by the deviation of the evolution of the system from the deterministic trajectory. As the Green's functions use this solution as mean fields, this method starts to break down further away from the deterministic solution. This increases for long times and/or large noise amplitudes, but as the system is nonlinear, the deterministic evolution of the system is also affected by the deviation from the initial deterministic evolution.

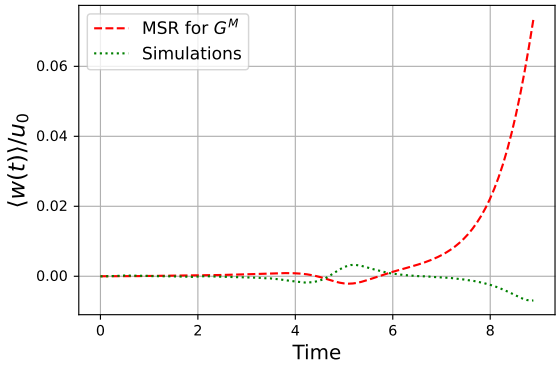

(a) Relative average fluctuations in prey $\langle w(t)\rangle$.

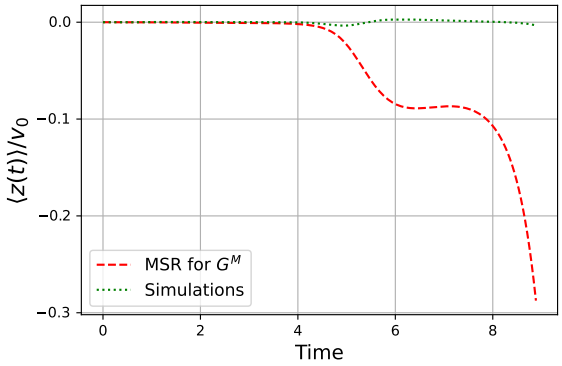

(b) Relative average fluctuations in predators $\langle z(t)\rangle$.

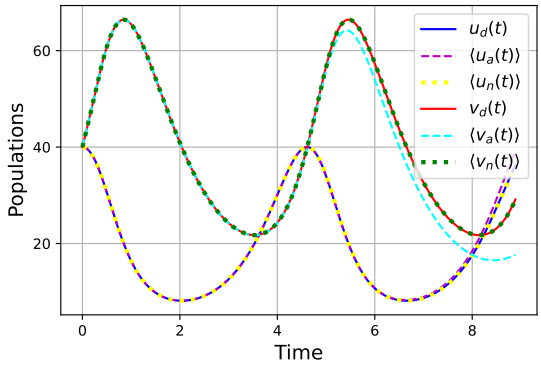

(c) Total average populations $u(t)$ and $v(t)$, for the deterministic d, analytical a and simulated n case.

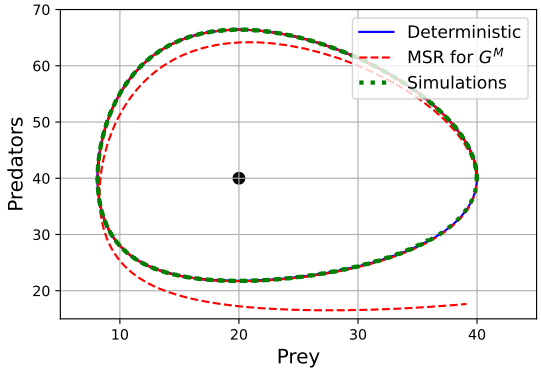

(d) Phase space containing the deterministic path, the MSR result and the average simulated trajectory.

Figure 5.23: Results for $T_{\text{sim}} = 2T_{\text{lin}}$ and noise amplitudes $\Xi_u = 0.2$, $\Xi_v = 0.4$. The dashed red line represents quantities obtained with the MSR formalism using the mean-field Green's functions G^M. The dotted green line corresponds to the average of 10^4 simulations. Figures (c) and (d) show the total populations, where the solid lines represent the deterministic results $u_d(t)$ and $v_d(t)$.

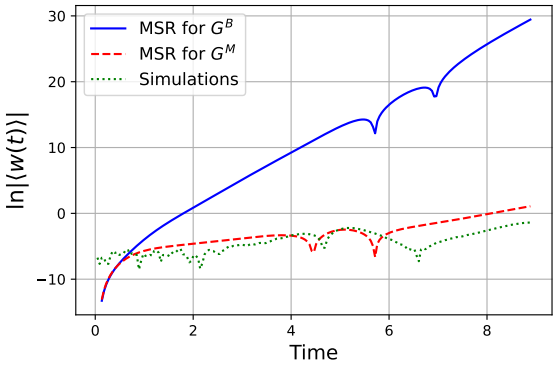

(a) Logarithm of the absolute average fluctuations in the prey.

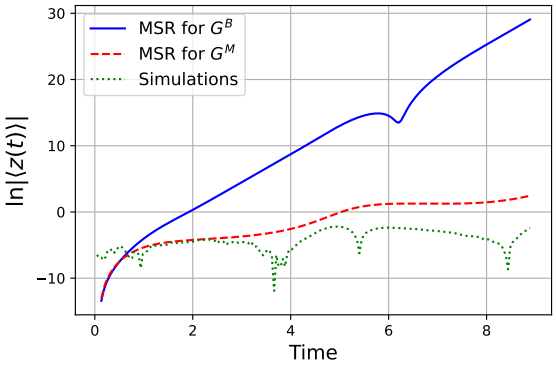

(b) Logarithm of the absolute average fluctuations in the predators.

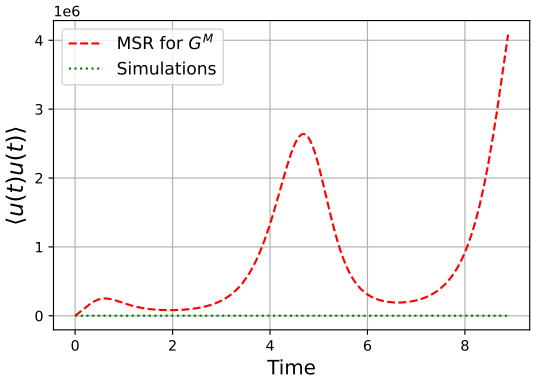

(c) Total two-point correlation function for the prey $\langle u(t)u(t)\rangle$.

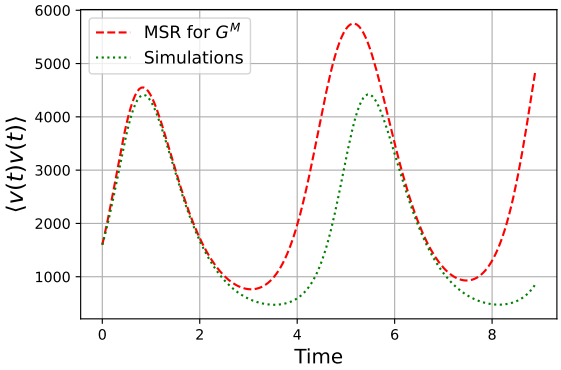

(d) Total two-point correlation function for the predators $\langle v(t)v(t)\rangle$.

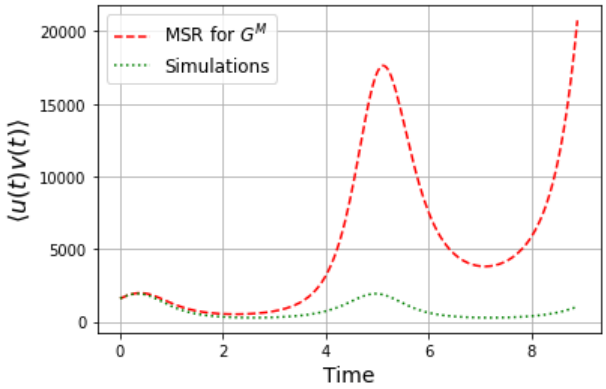

(e) Total coupled two-point correlation function $\langle u(t)v(t)\rangle$.

Figure 5.24: Results for $T_{\text{sim}} = 2T_{\text{lin}}$ and noise amplitudes $\Xi_u = 0.2$, $\Xi_v = 0.4$. The dashed red line represents quantities obtained with the MSR formalism using the dressed Green's functions G^M. The dotted green line corresponds to the two-point correlations of 10^4 simulations. Figures (a) and (b) show the logarithm of the average fluctuations. The solid blue line corresponds to the results obtained with the MSR formalism using the bare Green's functions G^B. Figures (c), (d) and (e) show the total two-point correlation functions.

The average fluctuations for the simulations calculated in Section 5.2.1 also grow, due to the inward spiraling motion. These fluctuations show periodic behavior, but also grow exponentially[52], as observed in Figures 5.13-5.14. However, this exponential growth reduces and eventually stops, as the average simulated trajectory will reach the fixed point and will fluctuate around it. The analytical correlation functions still need to be studied at larger times. As for $T_{\text{sim}} = 2T_{\text{lin}}$ the analytical trajectory already moves outside of the periodic deterministic trajectory, these quantities do not seem to take the inward spiraling motion into account for larger times, when $T_{\text{sim}} = 10T_{\text{lin}}$. This is confirmed by the average fluctuations in Figures 5.25a-5.25b. This shows that the fluctuations reach values that are even more than twice as large as the populations themselves, which can not be expected for a small noise amplitude. Next to the difference in growth rate, the periodic behavior in both analytical fluctuations is also not centered around zero as in Figures 5.13-5.14. For the prey, $\langle w(t) \rangle$ remains positive after $t > 3T_{\text{lin}}/2$, while for the predator species the fluctuations $\langle z(t) \rangle$ are always negative. However, the periodicity of the system remains accurate even for long times.

The large negative fluctuations even result in negative total predator populations. Next to the fact that this is biologically not possible, this also destroys the validity of the Lotka-Volterra model, which is only defined for positive populations $u(t)$ and $v(t)$. This negative predator population is therefore not shown in the phase space in Figure 5.25c. After evolving outside of the deterministic trajectory, the analytical trajectory spirals towards larger prey populations and smaller predator populations, which eventually become negative. This behavior in phase space is consistent with the behavior of the fluctuations. For $T_{\text{sim}} = 10T_{\text{lin}}$, the average simulated trajectory now also shows the inward spiraling motion, which was already observable in the analytical trajectory for $T_{\text{sim}} = 2T_{\text{lin}}$.

The only total two-point correlation function $\langle v(t)v(t) \rangle$ that was showing a similar order of magnitude as the simulations for small simulation times, is now also exponentially growing in the negative direction, which is in line with the result for $\langle z(t) \rangle$. Nevertheless this quantity still shows the correct periodicity of the system. As the behavior of the other two-point correlation functions is similar to the results for smaller times, these are not shown here.

The logarithm of the absolute average fluctuations for both Green's functions approaches for $T_{\text{sim}} = 10T_{\text{lin}}$ is shown in Figures 5.25e-5.25f. These show a continuation of the behavior that is observed in Figures 5.24a-5.24b. The average fluctuations for the bare approach keep growing exponentially, with a linearly increasing growth rate. Although the average fluctuations for the mean-field approach are growing much faster than for the simulations, their growth rates are comparable with respect to the bare approach. In addition, the growth rate stabilizes in both the mean-field and simulated case. For the simulations, this was expected as the simulated trajectory approaches the fixed point, so the growth rate stabilizes around zero. For the mean-field Green's functions, this result indicates that a renormalization of the Green's functions or propagators could be useful to obtain results that align better with the simulations. For the bare case, such a procedure could also work; however it might be necessary to calculate higher-order contributions to obtain better results. These figures also show similar local minima as for $T_{\text{sim}} = 2T_{\text{lin}}$, which arise from the absolute fluctuations required for the logarithms. These minima show that the periodicity is taken into account by both the bare and mean-field approach.

[52] Although their exponential growth is very slow compared to the analytical results.

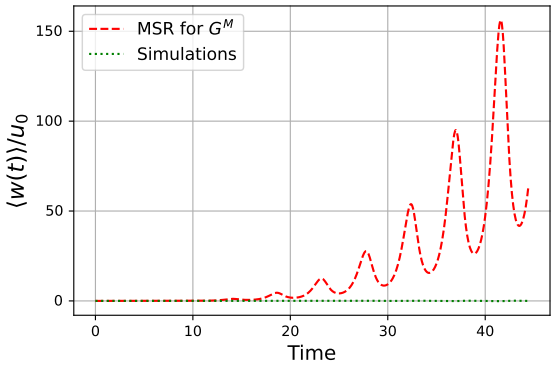

(a) Relative average fluctuations in prey $\langle w(t)\rangle$.

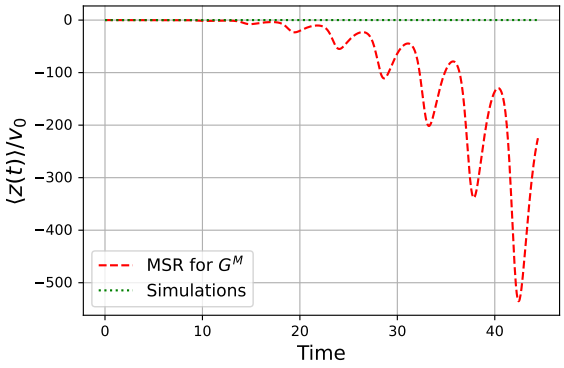

(b) Relative average fluctuations in predators $\langle z(t)\rangle$.

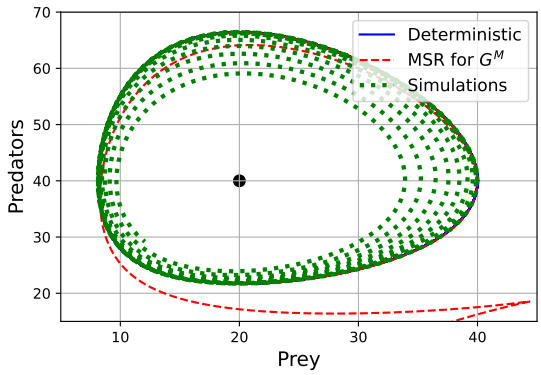

(c) Phase space containing the deterministic path, the MSR result and the average simulated trajectory.

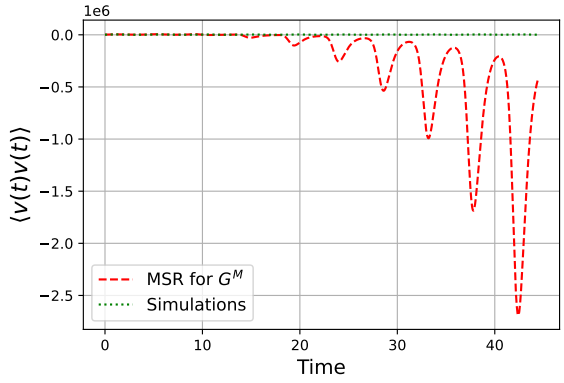

(d) Total two-point correlation function for the predators $\langle v(t)v(t)\rangle$.

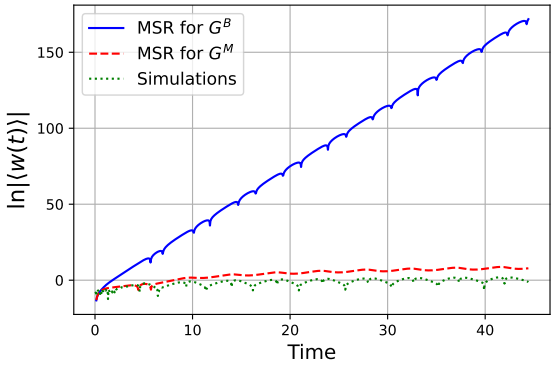

(e) Logarithm of the absolute average fluctuations in the prey.

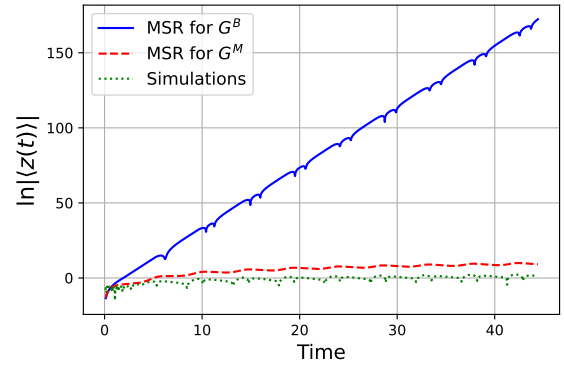

(f) Logarithm of the absolute average fluctuations in the predators.

Figure 5.25: Results for $T_{\text{sim}} = 10T_{\text{lin}}$ and noise amplitudes $\Xi_u = 0.2$, $\Xi_v = 0.4$. The dashed red line represents quantities obtained with the MSR formalism using the mean-field Green's functions G^M. The dotted green line corresponds to the average of 10^4 simulations. Figure (d) shows the phase space, where the solid blue line represent the deterministic results $u_d(t)$ and $v_d(t)$. Figures (e) and (f) show the logarithm of the average fluctuations. The solid blue line corresponds to the results obtained with the MSR formalism using the bare Green's functions G^B.

The eventual changes in the system for a noise average $\langle \eta(t) \rangle \neq 0$ were also studied. In this case, the noise still has a white spectrum and a Gaussian distribution, but the average of this distribution is given by $\mu \neq 0$. This corresponds to a constant noise perturbation on average, which basically adds an extra deterministic effect to the system. A more elaborate discussion and the results for a nonzero noise average are given in Appendix C.2. This appendix also contains some results for a stochastic Lotka-Volterra model with multiplicative noise. As this noise scales with the prey $u(t)$ and predator $v(t)$ fields, this yields noise contributions to the MSR action that are cubic instead of quadratic, as for additive noise. Hence, the Feynman rules for the vertices corresponding to these cubic noise interactions contain three fields instead of two. This quickly increases the number of nonvanishing diagrams, even up to first order in the noise amplitudes. Changing the character of the noise from additive to multiplicative in the simulations is however easily done, as it only requires a different noise coupling matrix $D(\boldsymbol{y}, t)$ (5.3). Therefore, only simulation results for multiplicative noise are shown in Appendix C.3. Despite that a comparison with analytical results obtained with the MSR formalism is not possible, this already gives a short view on the stochastic Lotka-Volterra model with a different kind of noise.

5.4.1 Improvements & Outlook

A possible cause of the deviating results obtained with the MSR formalism for larger simulation time is the breakdown of the perturbative approximation. To truncate the series expansion of the generating functional at first order in the noise amplitudes Ξ_u and Ξ_v, the coupling constants of the interacting contributions should be small compared to the coefficients of the free part Z_0. For the standard parameters and noise amplitudes this condition seems to be satisfied, but it is useful to check this by reproducing the results for $T_{\text{sim}} = 2T_{\text{lin}}$ with 10^3 noise realizations and noise amplitudes $\Xi_u = 0.05$ and $\Xi_v = 0.1$. The results for the relative average fluctuations are shown in Figure 5.26. The order of magnitude in the relative fluctuations is smaller compared to Figures 5.23a-5.23b for the noise amplitudes $\Xi_u = 0.2$ and $\Xi_v = 0.4$. However, this is an obvious effect of implementing a smaller noise amplitude, as it reduces fluctuations. The same effect is consequently also observed in the simulated averages. Hence, the general behavior of the analytical average fluctuations compared to the average fluctuations of the simulations does not change significantly with respect to the larger noise amplitudes. It can therefore be concluded that the choice of $\Xi_u = 0.2$ and $\Xi_v = 0.4$ is small enough to truncate the perturbative expansion up to first order in the noise amplitudes. So, this does not explain the exponential behavior of the analytical results with respect to the average simulations. The only difference is observed in Figure 5.26a, where the simulation average shows a small minimum around $t = 5$ instead of the maximum depicted in Figure 5.23a. The behavior of the average of the simulations changes slightly due to the finite number of simulations. As for short times the fluctuations are also small, this can suddenly change a local minimum to a local maximum. A larger amount of simulations should be taken into account to reduce this finiteness effect.

An explanation of the deviating results lies in the saddle-point expansion of the MSR action around the deterministic solution. As explained in Appendix B, only one solution of the saddle-point equations (5.9) of this system is taken into account. This saddle point corresponds to the deterministic trajectory $(u_d(t), v_d(t))$, which is not a stable solution of the deterministic Lotka-Volterra model. Hence, this is not necessarily a minimum of the action and therefore not the (only) dominating contribution to the generating functional in the weak noise limit. The choice to take only this saddle point into account was based on the deterministic trajectory and the fluctuations around it for small noise amplitudes. The assumption that only this saddle point dominates the generating

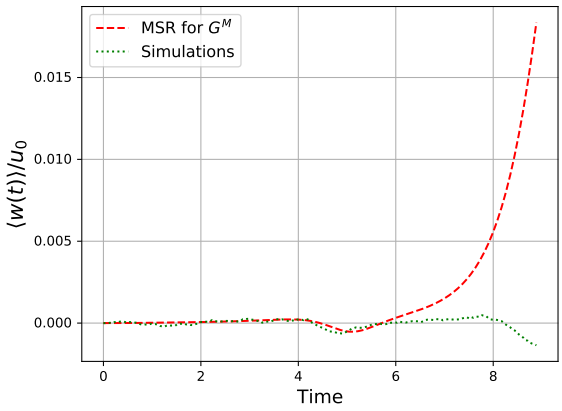

(a) Relative average fluctuations in prey $\langle w(t)\rangle$.

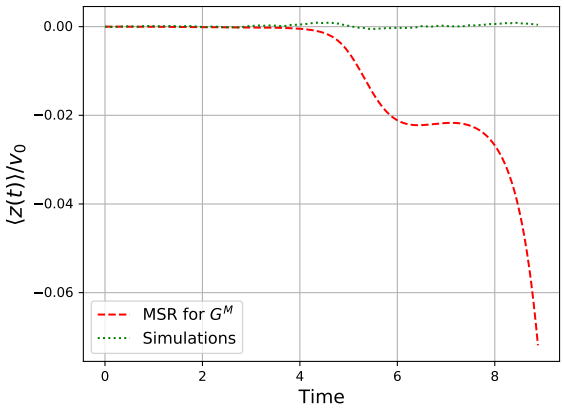

(b) Relative average fluctuations in predators $\langle z(t)\rangle$.

Figure 5.26: Simulations and analytical calculations are performed with the standard parameters for $T_{\text{sim}} = 2T_{\text{lin}}$ with 10^3 noise realizations and noise amplitudes $\Xi_u = 0.05$ and $\Xi_v = 0.1$.

functional is therefore only valid for short times $t \leq T_{\text{lin}}$. So, the stability character of the deterministic solution affects both the analytical calculations through the saddle-point expansion and the simulations, which resulted in the inward spiraling motion as explained in Section 5.2.1. To get a better description of the stochastic effects in this system, other saddle points should be taken into account in the expansion. This is however outside the scope of this work, as it requires a detailed analysis of all possible solutions of the saddle-point equations (5.9) and their stabilities.

The logarithmic results in Figures 5.24-5.25 show that the mean-field Green's functions G^M yields much better results than the bare ones G^B. However, this is only relative as the results for the mean-field approach still deviate from the simulation results for larger times. The general framework of (quantum) field theory includes more rigorous methods to deal with the exponential behavior observed in the analytical results. In QFT, divergences appear in Feynman diagrams due to singularities in momentum space. For some systems, these can be renormalized by introducing a *cutoff* Λ, which limits the energy or momentum in these calculations [88]. However, the Feynman diagrams for this stochastic Lotka-Volterra model are not diverging due to singularities, but show exponential growth due to the integrations in time of the exponential Green's functions. A constant cutoff Λ would not work for this behavior, as the renormalization should be time dependent. In such a case, the Green's functions could be renormalized by a *self-energy* Σ. In QFT, this corresponds to the energy that a particle obtains through self-interactions [87]. Instead of using mean-field theory by adding extra terms to the Green's function, the self-energy does this in a rigorous way by including loop corrections to the two-point correlation functions. These are all one-particle irreducible diagrams. The self-energy Σ can be obtained from the Green's functions via the Dyson equation [87]. Implementing Σ in the Green's functions renormalizes the evolution in time. Effectively, this changes the model parameters r_u and r_v, such that the evolution occurs at a slower rate. Also, it renormalizes the evolution time t. This reduces the exponential behavior of the Green's functions, and consequently also the behavior of the Feynman diagrams.

There are also interesting extensions of this stochastic Lotka-Volterra model and the corresponding application of the MSR formalism. First of all, as mentioned above, multiplicative instead of additive noise can be studied. This yields different Feynman diagrams due to the cubic noise vertices. As

there are more studies on stochastic Lotka-Volterra equations with multiplicative noise than there are for additive noise, it would be interesting to compare results obtained with the MSR formalism with this research. Some simulation results for multiplicative noise are contained in Appendix C.3.

The Gaussian white noises $\eta_u(t)$ and $\eta_v(t)$ in this stochastic Lotka-Volterra model are uncorrelated in time and also independent. Real-life random effects are usually not instantaneous and can also be correlated with other (random) events. A way to incorporate this is by introducing colored noise, with an autocorrelation function different from the Dirac delta function. The MSR action for colored noise is given by Eq. (3.49). Another way to take non-local effects in time into account is by introducing a *fractional* time derivative $\mathrm{d}^a/\mathrm{d}t^a$ for some $a \in (0, 1]$ [111, 112]. Transforming the time derivatives in the Lotka-Volterra model to fractional derivatives effectively adds a memory to the system. This memory could also reduce the exponential behavior of the propagators, without having to renormalize them. Recent studies of fractional Lotka-Volterra models are performed by Zibaei & Namjoo [113] and Amirian et al. [114]. A stochastic fractional Lotka-Volterra model has however never been investigated before.

Other effects can also be studied by extending the predator-prey model itself. One of the shortcomings of this model is the lack of a maximum population size of the prey species in the absence of predators. The finite resources in the system should give rise to a carrying capacity, which yields a finite stable prey population. This changes the stability character of the fixed point from a center to a stable spiral, as shown in Figure 4.5. The deterministic solutions of the system now spiral towards the fixed point, similar to the average stochastic trajectory of the stochastic Lotka-Volterra model with additive noise but without a carrying capacity. A stochastic Lotka-Volterra system with carrying capacity is, for example, studied by Zhang et al. [104]. As the fixed point is stable, the problem of the saddle point character of the deterministic solution is solved. This would change the behavior of the simulations and it could also solve the difficulties that arise from the deterministic solution used in the saddle-point expansion. Including spatial diffusion of the species in their environment would also give a more realistic ecological model. This also allows for a comparison with the work of Täuber [25].

Next to extensions of the two species predator-prey model, also other Lotka-Volterra models can be studied with the MSR approach. By taking both interaction coefficients α, $\beta < 0$, the interaction between the species becomes competitive. This yields a phase diagram as shown in Figure 4.3. The fixed point is now an unstable saddle point, but the system also has two stable fixed points at which one of the species is extinct. Stochastic competitive Lotka-Volterra models are studied by Jiang et al. [115]. Instead of two species, one could also add an extra prey or predator species, as is done in Zhang et al. [104]. This completely alters the phase space of the system, but it would still be suitable to analyze the noise effects through the MSR formalism by including two extra fields. Generalizing the model to N species would make it possible to compare the results with Sidhom & Galla [24].

6 Conclusion

Stochastic systems appear everywhere, either due to unknown microscopic effects that are modeled by noise contributions, or due to an inherent uncertainty in the system. In this work, we started with a general introduction to stochastic systems and methods to describe them. These methods were briefly applied to physical and general complex systems. Especially interesting was the physical approach of Langevin to describe Brownian motion. This was extended to a functional description by Wiener and Chandrasekhar, which yielded similar results. This field theoretical approach to stochastic systems formed the basis for the MSR formalism, which can be used to describe the dynamics of the observables as a stochastic field theory. This formalism allows for an analytical description of noise effects in general stochastic systems. To validate this method, correlation functions for a linear Langevin equation were calculated using the MSR approach. They were found to be in agreement with the results found by Langevin. The formalism was also applied to a nonlinear Langevin equation, which required perturbative methods and a semiclassical approximation.

A nonlinear Langevin equation already yields interesting results, but this can be extended to multidimensional coupled models. A prototypical example is given by the two species Lotka-Volterra model describing the evolution of interacting predator and prey populations. First, the deterministic case was studied elaborately. As this system does not have an explicit analytical solution, its phase space was investigated through a dynamical system analysis and its periodic solutions were determined numerically. Stochastic extensions of this model include a noise contribution to describe external environmental effects. Earlier research studied such a system using simulations or a mathematical approach. Generalizations of the Lotka-Volterra model are studied by Sidhom & Galla and Täuber using field-theoretical methods like the MSR formalism.

In this thesis, a stochastic two species Lotka-Volterra model with additive noise was first studied through simulations. For a single noise realization, the stochastic trajectory fluctuates around the deterministic periodic trajectory. Averaging over 10^4 noise realizations yielded an ensemble average of the trajectory of this stochastic model in phase space. A new result found in this work is that the average stochastic trajectory shows inward spiraling motion towards the fixed point. This is a result from the diffusion of the individual simulations in phase space, which is caused by the noise and the saddle point character of the deterministic solution. As this changes the periodicity of each simulated trajectory, the simulations spread around the fixed point, causing an average inward spiraling motion towards this point.

One of the main contributions of this work is the application of the MSR formalism to a stochastic two species Lotka-Volterra model with additive noise. General noise effects in this simple model have never before been studied using this functional method. Correlation functions for the fluctuations and total populations were calculated via a mean-field approach, and compared with simulated results. For short times $t \simeq T_{\text{lin}}$, the general behavior of the one-point correlation functions is similar, with only a deviating sign for the prey species. Around $t \simeq 2T_{\text{lin}}$, the analytical calculations start to deviate exponentially from the simulations. This causes the inward spiraling motion in phase space, similar to the observations for the simulations, to evolve outside the deterministic trajectory, even up to negative populations. Comparison with the bare Green's function approach reveals that the mean-field theory shows better behavior, but it is only comparable with the simulations for short times.

To improve the results obtained with the MSR formalism, the saddle point expansion of the action should be analyzed carefully, as the deterministic solution is not necessarily the (only) dominant

contribution to the generating functional in the small noise limit. The time evolution of the Green's functions can be renormalized by including a self-energy, which reduces the exponential growth. This behavior can also be diminished by accounting for non-local effects in time through a fractional time derivative. Simulated results for multiplicative noise show a similar inward spiraling motion, but applying the MSR formalism to this kind of noise can lead to new insights. Other extensions of this model by including a carrying capacity, multiple species, or different interactions can also be studied using a similar approach. As the MSR formalism can be applied to stochastic systems in general, this work paves the way to a large amount of potential research topics, after improvements have been implemented.

A Jacobian for the MSR formalism

An important note has to be made on the Jacobian $\mathcal{J}$, arising from the change of variables $y(t) \to \dot{y}(t)$ in Eq. (3.47). This substitution was also implicitly performed in the discetized procedure in Eqs. (3.41) and (3.43), which therefore also requires a Jacobian. Using the properties of the Dirac delta functional, one obtains

$$\delta[y - y_\eta] = \frac{\delta[\dot{y} - \mathcal{L}_\eta(y)]}{\partial y/\partial \eta} = \delta[\dot{y} - \mathcal{L}_\eta(y)]\mathcal{J}, \tag{A.1}$$

where $\mathcal{L}_\eta(y)$ is the differential operator corresponding to the general Langevin equation. It turns out that this Jacobian $\mathcal{J} = \partial\eta/\partial y$ depends on the chosen prescription. To see this, it is insightful to look at the discretization (3.40) for both the Itô and Stratonovich prescription. It can be shown [116] that a general discretized Langevin equation is given by

$$\begin{aligned} y_{j+1} - y_j =& [\epsilon\, C(y_j, t_j) + (1-\epsilon)C(y_{j+1}, t_{j+1})]\Delta t \\ &+ [\epsilon\, D(y_j, t_j) + (1-\epsilon)D(y_{j+1}, t_{j+1})]w_j\sqrt{\Delta t} + y_0\delta_{0,j}. \end{aligned} \tag{A.2}$$

The parameter ϵ defines the prescription. If $\epsilon = 1/2$, the Stratonovich interpretation is used, since the contributions of $C(y_{j+1}, t_{j+1})$ and $D(y_{j+1}, t_{j+1})$ are nonzero. The Itô prescription is assumed when $\epsilon = 1$, for which Eq. (A.2) reduces to Eq. (3.40). It is convenient to define discretized white noise values as $\eta_j = w_j/\sqrt{\Delta t}$, which is also in line with the definition of white noise as time derivative of a Wiener process. Furthermore, it is useful to write

$$B_{j,j+1} = \frac{(y_{j+1} - y_j - y_0\delta_{0,j})/\Delta t - [\epsilon\, C(y_j, t_j) + (1-\epsilon)C(y_{j+1}, t_{j+1})]}{\epsilon\, D(y_j, t_j) + (1-\epsilon)D(y_{j+1}, t_{j+1})}, \tag{A.3}$$

such that Eq. (A.2) reduces to

$$B_{j,j+1} - \eta_j = 0. \tag{A.4}$$

Now, the discretized Jacobian can be written as

$$\mathcal{J} = \frac{\partial(\eta_0, ..., \eta_{N-1})}{\partial(y_1, ..., y_N)} = \det A, \quad \text{with } A_{j,k} = \frac{\partial \eta_j}{\partial y_{k+1}} = \frac{\partial B_{j,j+1}}{\partial y_{k+1}}. \tag{A.5}$$

From the definition of $B_{j,j+1}$, it can be seen that the only nonzero entries of A have indices $k = j-1, j$. Since the matrix A has this form, only the diagonal entries $A_{j,j}$ contribute to its determinant, which can be calculated via the regular quotient rule for derivatives as

$$\begin{aligned} A_{j,j} &= \frac{\partial B_{j,j+1}}{\partial y_{j+1}}, \\ &= \frac{\frac{1}{\Delta t} - (1-\epsilon)C'(y_{j+1}, t_{j+1})}{\epsilon\, D(y_j, t_j) + (1-\epsilon)D(y_{j+1}, t_{j+1})} \\ &- (1-\epsilon)D'(y_{j+1}, t_{j+1}) \left\{ \frac{\frac{1}{\Delta t}(y_{j+1} - y_j - y_0\delta_{0,j}) - [\epsilon\, C(y_j, t_j) + (1-\epsilon)C(y_{j+1}, t_{j+1})]}{[\epsilon\, D(y_j, t_j) + (1-\epsilon)D(y_{j+1}, t_{j+1})]^2} \right\}, \end{aligned} \tag{A.6}$$

where C', D' denote derivatives with respect to y_{j+1}. For $\epsilon = 1$ in the Itô prescription, this simplifies to

$$\mathcal{J}\big|_{\epsilon=1} = \det A = \prod_j A_{j,j} = \prod_j \frac{1}{\Delta t\, D(y_j, t_j)}. \tag{A.7}$$

Hence, for additive noise with $D(y,t) = D(t)$, the Jacobian does not depend on y. For multiplicative noise, when the interpretation actually matters, $\mathcal{J} \propto (\det D(y,t))^{-1}$ in the continuum limit $\Delta t \to 0$. This is an important result, since it can give rise to extra (nonlinear) contributions to the effective action $S_{\text{eff}} = S[y,q] + \text{Tr}[\log D]$, which results from using the identity $\det D = \mathrm{e}^{\text{Tr}[\log D]}$.

B Saddle point approximation for the stochastic Lotka-Volterra model

The saddle point approximation for the MSR formalism was explained in Section 3.4.1. This approximation is a truncated expansion of the MSR action around its saddle points $(\boldsymbol{y}_s(t), \boldsymbol{q}_s(t))$, which can be obtained from the saddle-point equations

$$\left.\frac{\delta S[y,q]}{\delta y(t)}\right|_{y=y_s} = J_y(t), \quad \left.\frac{\delta S[y,q]}{\delta q(t)}\right|_{q=q_s} = J_q(t). \tag{B.1}$$

In the weak noise limit $\Xi \to 0$, these saddle points are the dominant contributions to the generating functional, so these contributions also determine the behavior of the correlation functions. This method for approximating the action is a standard field-theoretical technique [15]. In general, the saddle-point equations can have multiple solutions, corresponding to different saddle points for the action. Depending on their stability character, a few or all should be taken into account in the saddle-point expansion, through a summation over all contribution saddle points. In the case of stable saddle points, which correspond to minima of the action, it is possible to only include these in the expansion.

For the stochastic Lotka-Volterra model with additive noise, the saddle point used for the expansion is $(u_s, v_s, q_{u_s}, q_{v_s}) = (u_d, v_d, 0, 0) = (\boldsymbol{y}_d, \boldsymbol{\varphi}_d)$, which corresponds to the deterministic solution of the Lotka-Volterra system without noise. As the interactions in the predator-prey system are quadratic, the saddle-point expansion (5.16) up to third order in the fluctuations (w, z) yields an exact expression for the MSR action. Nevertheless, there are multiple solutions of the saddle-point equations (5.9), as the deterministic one is only found for vanishing auxiliary fields $\boldsymbol{\varphi}_s = (q_{u_s}, q_{v_s})^T = (0,0)^T$. In this case, the choice of taking only this saddle point into account can be justified by the fact that this governs the deterministic[53] evolution of the system. In the weak noise limit, the fluctuations around this trajectory are small, hence this can be considered as a dominant contribution.

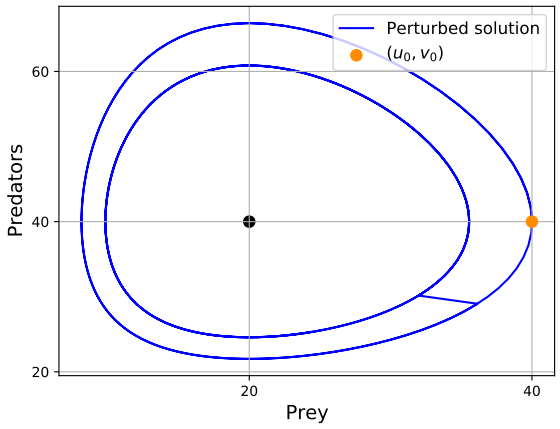

Figure B.1: The phase space of the deterministic Lotka-Volterra model with a periodic solution starting at initial populations $(u_0, v_0) = (40, 40)$, for a simulation time $T_{\text{sim}} = 5T_{\text{lin}}$. At $t = 2T_{\text{lin}}$, 5 predators die instantly. The system jumps to a different periodic solution.

The phase space analysis in Section 4.2 of the deterministic two species Lotka-Volterra model showed that the fixed points $(0,0)$ and $(r_v/\beta, r_u/\alpha)$ are both not stable fixed points. The extinction point is a saddle point, while the coexistence point is a center, around which the periodic trajectories evolve. As the center is neither stable nor unstable, there is no attractor in this system. Also the periodic solutions are neither stable nor unstable. This can be observed by applying a large instantaneous perturbation to a numerical solution of the system at a time $t > 0$, and letting it evolve undisturbed for the remaining amount of the simulation time. The result is shown in Figure B.1. At $t = 2T_{\text{lin}}$,

[53] Classical in the quantum mechanical interpretation of the semiclassical approach.

five predators die instantly. This causes the system to jump from one periodic solution to the other. For the rest of the simulation time, the system remains in this periodic trajectory. So, perturbing the system in a direction other than the direction of the evolution of the periodic trajectory causes the system to change from one deterministic trajectory to another. Therefore, every periodic solution of the deterministic system can be interpreted as a saddle point solution of the system.

In Section 5.2.1 it is shown that including additive noise does not result in a bifurcation, i.e. it does not change the stability character of the phase diagram. As all periodic solutions are saddle points, noise perturbations can cause the system to change to a different solution. As the deterministic evolution $C(\boldsymbol{y}, t)$ corresponds to the solution for the initial populations (u_0, v_0), this change is small for small noise amplitudes. However, it does partially explain how the individual simulations can distribute through phase space, which causes the inward spiraling motion of the average trajectory.

This can also cause a problem for the saddle-point expansion, as the deterministic solution of the system is not stable. The corresponding saddle point $(u_d, v_d, 0, 0)$ is not necessarily a minimum of the action, so there can be other dominating contributions to the generating functional in the weak noise limit. The argument that only this saddle point dominates the generating functional is therefore only applicable for short times $t \leq T_{\text{lin}}$, when the stochastic trajectory is still close to the deterministic one. To verify this, other saddle points should be included in the expansion. These should have nonzero initial conditions q_{u_0} and q_{v_0} for the auxiliary fields. Taking constant auxiliary fields would also yield constant populations u_0 and v_0 to solve Eq. (5.9), so this is not a feasible solution for this system. The choice of vanishing auxiliary fields was based on the argument that this yields the solution of the deterministic system. Such an argument is not applicable to saddle points with time dependent auxiliary fields, so the question remains how to find other contributing saddle points. This can be determined based on their stability. This requires however a detailed analysis of the solution space of the saddle-point equations (5.9), which is outside the scope of this work.

C Other results for stochastic Lotka-Volterra models

C.1 Two-point correlation functions of fluctuations

In Section 5.4, the two-point functions of the total populations are shown, instead of the two-point functions of the fluctuations. The reason for this choice is that these quantities for the fluctuations already show exponential growth in the analytical case, which yields much larger fluctuations than found for the simulated case. This also holds for the correlation functions at different times. Hence, the fluctuation two-point functions of the simulations appear to vanish compared to the analytical ones. The exponential behavior is mainly due to the behavior of the coupled propagators, which arise in at least one Feynman diagram of each two-point correlation function (5.42)-(5.44). For completeness, the two-point correlation functions of the fluctuations are shown here.

The relative two-point correlation functions at equal times $t = t'$ are depicted in Figure C.1. The analytical results for the predators and the coupling between prey and predators show exponential behavior in the amplitude of the oscillations, similar to the two-point function for the total predator population in Figure 5.25d. As this scales with the populations squared, the values at earlier times appear to be zero compared to the results at later times. Interestingly, the two-point function for the prey in Figure C.1a shows different behavior. The amplitude of the fluctuations increases relatively slow, before decreasing again later until it becomes negative. An investigation of the Feynman diagrams at larger times should clarify what is causing this behavior.

Compared to the analytical results, the two-point correlations calculated from the simulations for 10^4 noise realizations are negligible. Therefore, these are shown in separate figures next to the combined results. They also show an increasing amplitude of the oscillatory behavior, but much slower than for the analytical case. The periodicity for the analytical and simulated results is similar, as was also observed in earlier results. Hence, also for the two-point correlations, the MSR formalism captures the correct period of the system. However, for larger times there appears a sign difference for the predator correlations, while for the prey the sign is correct. This is exactly the opposite of the sign difference for the one-point functions. Furthermore, all simulated results show local extrema next to the main peak of each cycle. A possible explanation for this is the changing periodicity of each simulation that causes the inward spiraling motion of the ensemble average. This also changes the periodicity of the average and gives rise to multiple contributing frequencies next to the main frequency $2\pi/T_{\text{lin}}$ of the deterministic solution. In the correlation functions, this effect can appear as local extrema in the correlation functions.

Figure C.2 shows the two-point correlation functions at different times for $t \geq t'$, where $t' = T_{\text{lin}}/2$ is fixed. In the simulations, this time point corresponds to $N = 50$, as the number of time points per linear cycle is taken to be 100. Again, the exponential behavior of the integrations causes the simulated results to be negligible compared to the analytical results. So, also here the simulated results for 10^4 noise realizations are shown separately next to the combined results. In the analytical results, the amplitude remains approximately the same, except for the predator two-point function, which decreases and even becomes negative. This behavior seems comparable with the prey two-point function at equal times in Figure C.1a, so a better analysis of the mean-field approach at larger times is required to explain this. For the simulated results, the amplitude of the oscillations is fluctuating, but not increasing. Although this amplitude is much smaller for all two-point functions, this general behavior is similar. The periodicity of the simulations differs slightly from the period of the analytical results, however this deviation disappears at later times. This could be due to setting $t' = T_{\text{lin}}/2$, which in some sense changes the initial conditions for both approaches.

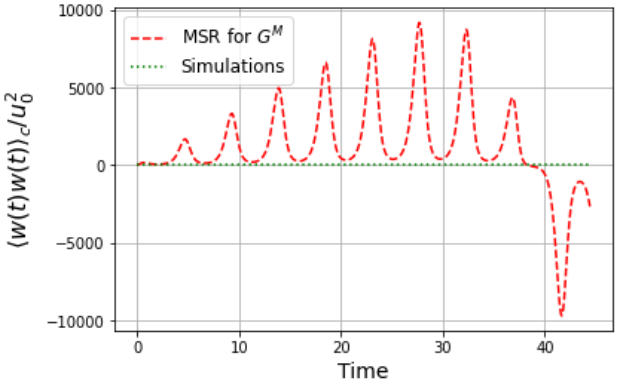

(a) Relative two-point correlation function of the fluctuations in prey $\langle w(t)w(t)\rangle/u_0^2$.

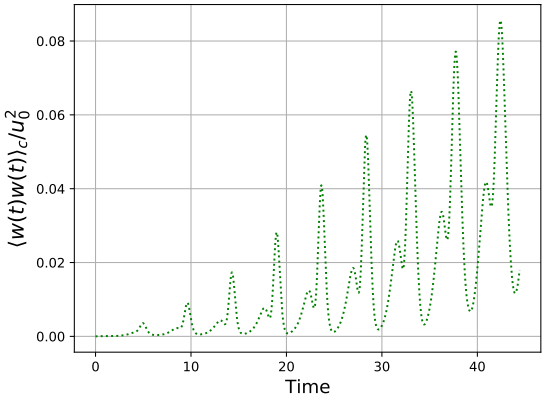

(b) Simulated results for the relative two-point correlation function of the fluctuations in prey.

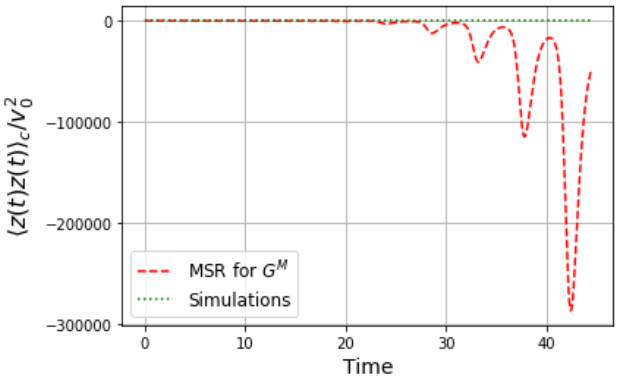

(c) Relative two-point correlation function of the fluctuations in predators $\langle z(t)z(t)\rangle/v_0^2$.

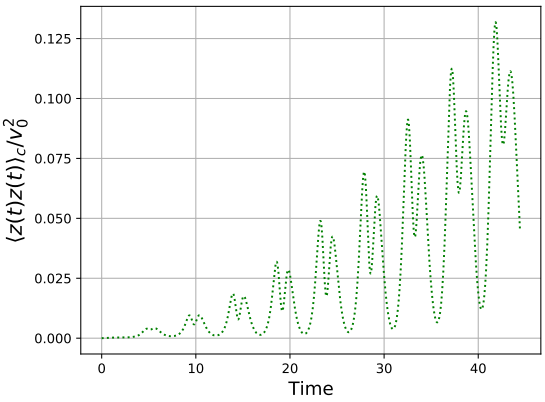

(d) Simulated results for relative two-point correlation function of the fluctuations in predators.

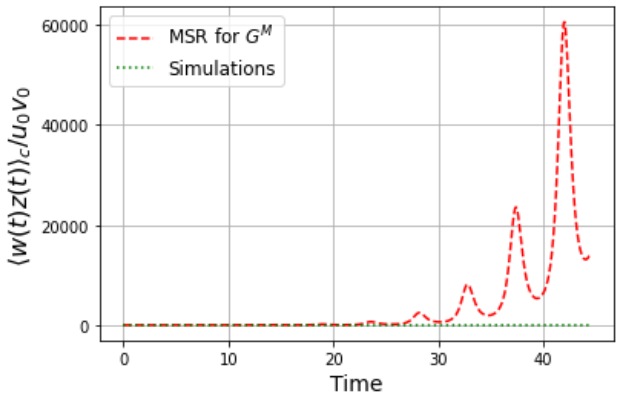

(e) Relative two-point correlation function of the coupled fluctuations $\langle w(t)z(t)\rangle/u_0v_0$.

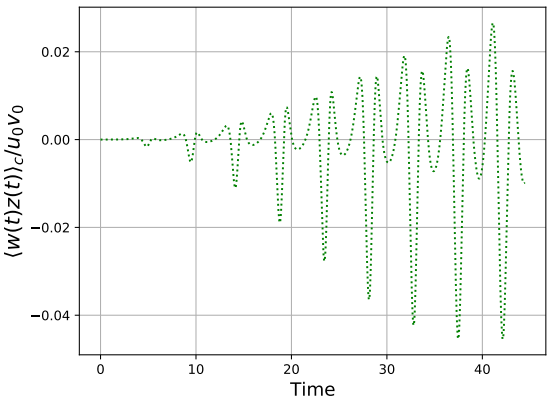

(f) Simulated results for relative two-point correlation function of the coupled fluctuations.

Figure C.1: Relative two-point correlation functions of the fluctuations at equal times. Simulations are performed with the standard parameters for $T_{\text{sim}} = 10T_{\text{lin}}$. The dashed red line represents quantities obtained with the MSR formalism using the mean-field Green's functions G^M. The dotted green line corresponds to the average of 10^4 simulations.

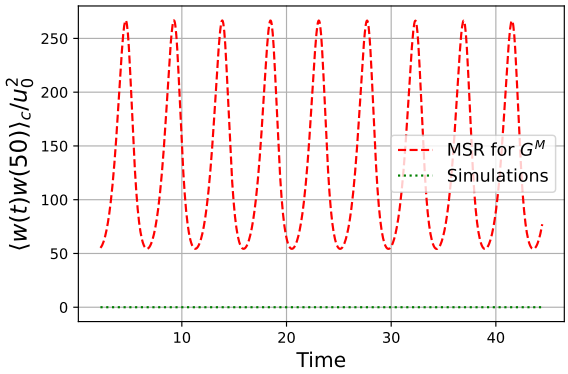

(a) Relative two-point correlation function of the fluctuations in prey $\langle w(t)w(50)\rangle/u_0^2$.

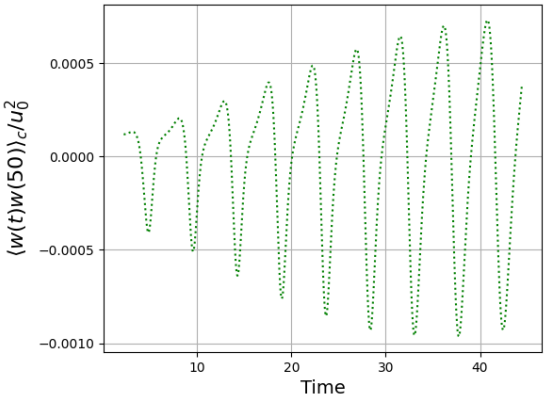

(b) Simulated results for the relative two-point correlation function of the fluctuations in prey.

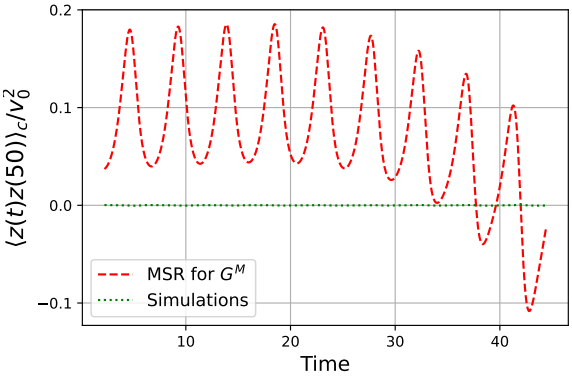

(c) Relative two-point correlation function of the fluctuations in predators $\langle z(t)z(50)\rangle/v_0^2$.

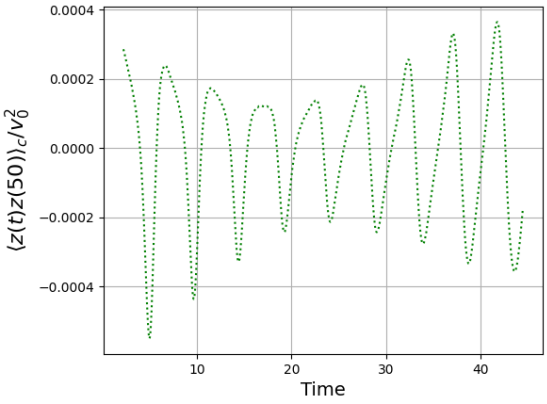

(d) Simulated results for relative two-point correlation function of the fluctuations in predators.

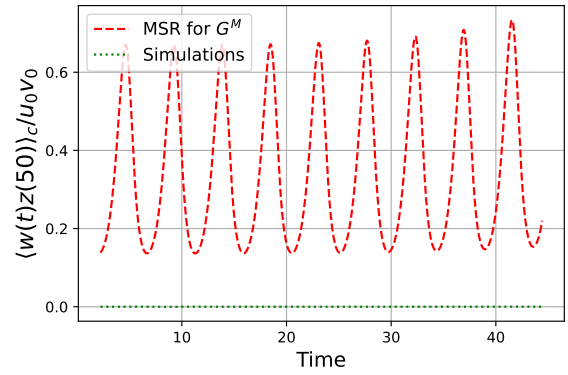

(e) Relative two-point correlation function of the coupled fluctuations $\langle w(t)z(50)\rangle/u_0v_0$.

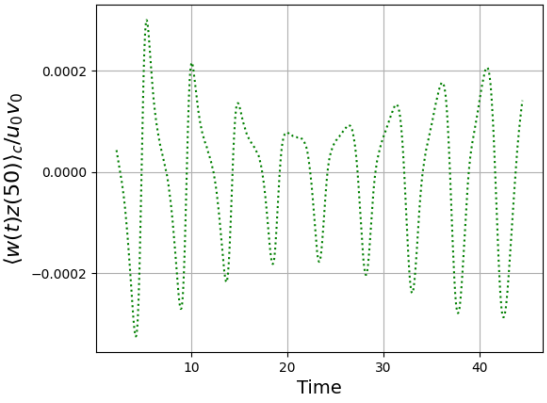

(f) Simulated results for relative two-point correlation function of the coupled fluctuations.

Figure C.2: Relative two-point correlation functions of the fluctuations at different times t and $t' = T_{\text{lin}}/2$, which is at time point $N = 50$ in the simulations. Simulations are performed with the standard parameters for $T_{\text{sim}} = 10T_{\text{lin}}$. The dashed red line represents quantities obtained with the MSR formalism using the mean-field Green's functions G^M. The dotted green line corresponds to the average of 10^4 simulations.

C.2 Nonzero noise average

In the stochastic Lotka-Volterra model with additive noise (5.1), the independent stochastic processes $\eta_u(t)$ and $\eta_v(t)$ are taken to be Gaussian white noise. This is the simplest kind of noise that can appear in an SDE. It is possible to study other stochastic effects by assuming a different distribution than a normal distribution, or to use correlated noise with an autocorrelation function that is no Dirac delta function. A more straightforward extension is to implement a noise average $\langle \eta_{u,v}(t) \rangle \neq 0$. Hence, the noises still have a white spectrum and a Gaussian distribution, but the average of this distribution is given by $\mu \neq 0$. This corresponds to a constant average noise perturbation, which basically adds an extra deterministic effect to the system. For a nonlinear Langevin equation like the stochastic Lotka-Volterra model with additive noise one should be careful, as $\langle C(y,t) \rangle \neq C(\langle y \rangle, t)$. However, it is possible to rescale the noise fields $\eta_{u,v}(t) \to \eta_{u,v}(t) - \mu$. This yields again Gaussian white noises with a vanishing average, but it also includes a constant deterministic contribution $\sqrt{\Xi_{u,v}}\mu$ in both equations as

$$\dot{u}(t) = r_u u(t) - \alpha u(t)v(t) + \sqrt{\Xi_u}\,\mu + \sqrt{\Xi_u}\,\eta_u(t), \tag{C.1}$$

$$\dot{v}(t) = -r_v v(t) + \beta u(t)v(t) + \sqrt{\Xi_v}\,\mu + \sqrt{\Xi_v}\,\eta_v(t). \tag{C.2}$$

This changes the location of the coexistence point ny approximately 1%, depending on the sign of μ. More importantly, this breaks the periodicity of the deterministic solutions, as this system does not have a constant of motion. This contribution gives rise to a constant shift in the evolution, which causes the deterministic solution to spiral inward for $\mu > 0$ and spiral outward for $\mu < 0$. This is represented by the dashed red lines in Figure C.3. For the simulations represented by the solid green lines, this effect is amplified. The noise distribution is not symmetric around zero, so at every time step in each individual simulation, the noise has a higher probability to be either positive or negative. So, this effect remains also in the average stochastic trajectory. This results in either faster inward spiraling motion as in Figure C.3a, or in outward spiraling motion as in Figure C.3a.

One might think that for $\mu < 0$, a balance can be found between the inward spiraling motion of the average stochastic trajectory due to the diffusion of the simulations and the outward motion due to the noise average, such that the effects annihilate and the periodic deterministic evolution is followed. It turns out that this is not possible, as the inward motion increases with time, while the outward motion is a constant effect already arising in the deterministic part of the equation. Hence, for every $\mu < 0$, there is a time t after which the inward motion becomes stronger than the outward motion.

The analytical consideration of a nonzero noise average μ through the MSR formalism is similar to the rescaling of the noise fields. In the derivation of the MSR formalism, the average μ can be included directly via the PDF of the noise, as used in Eq. (3.47). For the resulting MSR action, this gives rise to the same extra constant contributions as in Eq. (C.1). Hence, it is also possible to transform $\eta_{u,v}(t) \to \eta_{u,v}(t) - \mu$ directly in the MSR formalism. This constant effect also changes the solutions of the saddle-point equations (5.9), as it would be equivalent to including constant source fields $\boldsymbol{J_y}(t)$. For vanishing auxiliary fields, this yields the saddle point that corresponds to the inward or outward spiraling solution that is represented by the dashed red line in Figure C.3. A next step for this research could be to see if this changes the comparison between the simulated and analytical results.

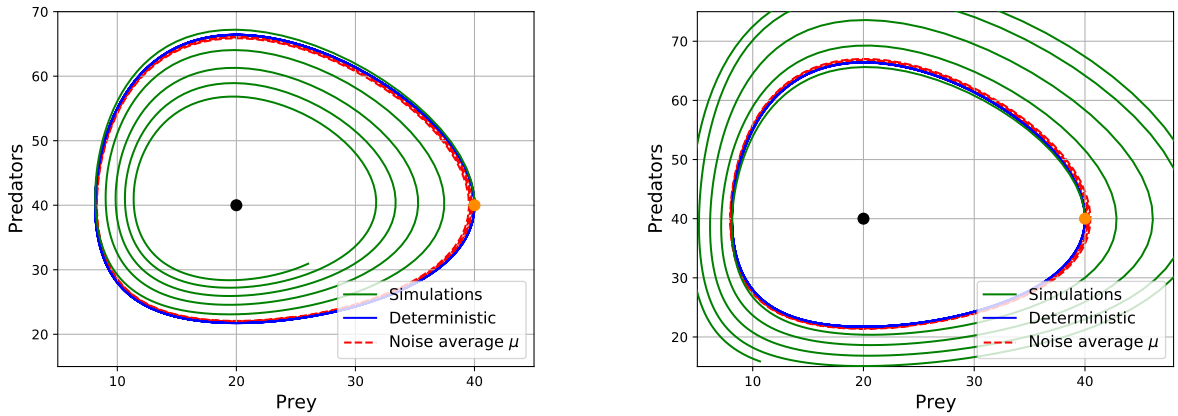

(a) Phase space for a noise average $\mu = 0.05$.

(b) Phase space for a noise average $\mu = -0.05$.

Figure C.3: Phase spaces for a stochastic Lotka-Volterra model with additive Gaussian white noise with $\langle \eta_{u,v}(t) \rangle = \mu \neq 0$, for $T_{\text{sim}} = 5T_{\text{lin}}$ and noise amplitudes $\Xi_u = 0.2$ and $\Xi_v = 0.4$. The solid blue line represents the deterministic solution for $\mu = 0$ and the dashed red line corresponds to the deterministic solution for $\mu \neq 0$. The solid green line corresponds to the average of 10^4 simulations with $\mu \neq 0$.

C.3 Multiplicative noise

One example of a stochastic Lotka-Volterra model with multiplicative noise is given by the following system

$$\dot{u}(t) = r_u u(t) - \alpha u(t)v(t) + \sqrt{\Xi_u\, u(t)}\, \eta_u(t), \tag{C.3}$$

$$\dot{v}(t) = -r_v v(t) + \beta u(t)v(t) + \sqrt{\Xi_v\, v(t)}\, \eta_v(t). \tag{C.4}$$

As the noises scale with the (square roots of the) prey $u(t)$ and predator $v(t)$ populations, this kind of noise results in much larger random perturbations compared to additive noise for constant noise amplitudes Ξ_u and Ξ_v. This kind of noise can model effects that scale directly with the size of the populations, like diseases or seasonal effects that result in fluctuating growth rates r_u and r_v. This yields noise contributions to the MSR action that are cubic, instead of the quadratic form for additive noise. Hence, the Feynman rules for the vertices corresponding to these cubic noise interactions contain three fields. This increases the number of nonvanishing diagrams, even up to first order in the noise amplitudes. Also, the Jacobian $\mathcal{J}$ given by Eq (A.7) should be included. Therefore, only results for the simulations are shown here. This requires only a change in the noise coupling matrix $D(\boldsymbol{y}, t)$ (5.3).

The average results for 10^4 noise realizations for a simulation time $T_{\text{sim}} = 10T_{\text{lin}}$ and the standard parameter with noise amplitudes $\Xi_u = 0.2$ and $\Xi_v = 0.4$ are depicted in Figure C.4. The time evolution of the total populations and the corresponding phase clearly show a similar inward spiraling motion as for the model with additive noise. Comparing these results with the ones for additive noise in Figures 5.11-5.12, the inward spiraling motion for multiplicative noise occurs at a much higher velocity. In this case, the average stochastic trajectory already deviates visibly from the deterministic trajectory at $t = T_{\text{lin}}$, while for additive noise this starts to become visible at $t = 5T_{\text{lin}}$. This effect is caused by the larger noise perturbations, as their total amplitudes are increased by a factor $\sqrt{40} \simeq 6$ at the start of each simulation. Even for small populations around 10 prey or

predators, the multiplicative noise is still three times as large as the corresponding additive noise. As the inward spiral motion is shown to scale with noise amplitudes in Figure 5.20, this behavior is in line with the earlier results and therefore not surprising. This is also observed in Figure 5.2, produced by Vadillo in Ref. [29], and in our own reproduction in Figure 5.7. These simulations are performed for larger initial populations, different multiplicative noise and less simulation time ($T_{\text{sim}} \simeq 3T_{\text{lin}}$). Nevertheless, these figures already show a similar inward spiraling motion, with a higher velocity than for additive noise.

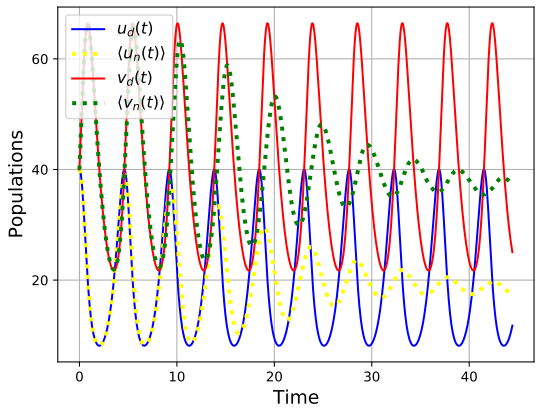

(a) Total populations $(u_d(t), v_d(t))$ of the deterministic model (solid), and an average of simulations $(\langle u_n(t)\rangle, \langle v_n(t)\rangle)$ (dotted).

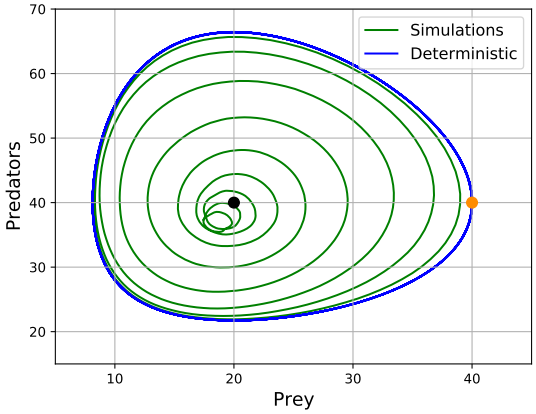

(b) Corresponding phase space for deterministic solution (blue) and average of simulations (green) for multiplicative noise.

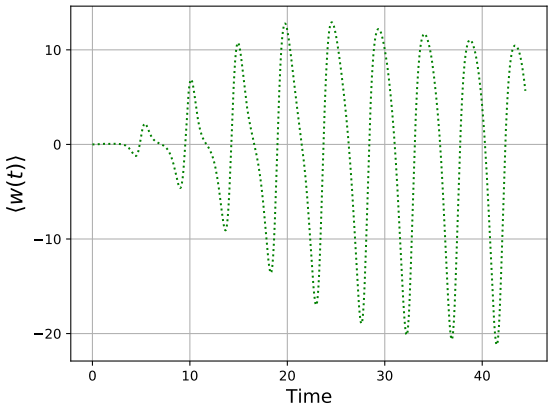

(c) Average fluctuations $\langle w(t)\rangle = \langle u_n(t)\rangle - u_d(t)$ in the prey population.

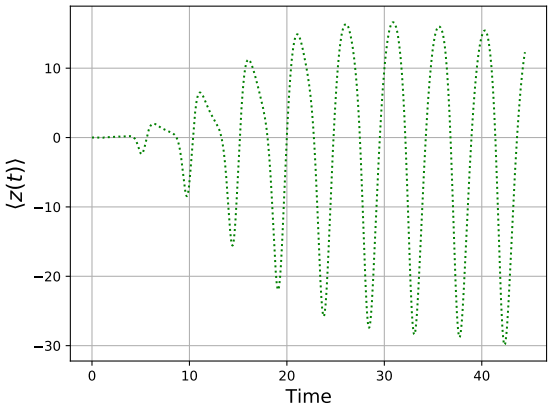

(d) Average fluctuations $\langle z(t)\rangle = \langle v_n(t)\rangle - v_d(t)$ in the predator population.

Figure C.4: Results for a stochastic Lotka-Volterra model with multiplicative noise (C.3), for $T_{\text{sim}} = 10T_{\text{lin}}$ and noise amplitudes $\Xi_u = 0.2$ and $\Xi_v = 0.4$. The solid and dotted green lines correspond to the average of 10^4 simulations.

As the noise amplitudes are much larger than in the standard additive case, it is more likely that a simulation reaches extinction of one of the two species. As explained in Section 5.2, the implementation of the extinction results in an inward spiraling motion of the average stochastic trajectory to the lower left of the coexistence point. This is due to the vanishing contribution to the average of the extinct simulations, which are 634 out of the 10^4 simulations. This behavior can also

be observed in the phase space in Figure C.4b. For the total populations in Figure C.4a, this results in a damping of the oscillation towards stable populations slightly below their fixed point values. In both these figures, the stochastic trajectory keeps fluctuating around (the lower left of) the fixed point due to the relatively large noise amplitudes. This can also be seen in the average fluctuations in both populations in Figures C.4c-C.4d. Up to $t = 5T_{\text{lin}}$, these fluctuations show the same general behavior as for additive noise in Figures 5.13-5.14. Only the amplitudes grow much faster due to the accelerated inward spiraling motion. When the average stochastic trajectory gets close to the fixed point, the amplitudes of the fluctuations saturate, as the deviation of the coexistence point with respect to the deterministic solution is fixed for every point in time.

In general, it can be concluded that multiplicative noise does not give any qualitative different behavior than additive noise. The only observable quantitative change is the different velocity of the inward spiraling motion. It would be interesting to see if this is also the case for the analytical results obtained with the MSR formalism.

References

[1] J. R. Taylor, *Classical Mechanics*. University Science Books, 2005.

[2] S. Blundell and K. Blundell, *Concepts in Thermal Physics*. OUP Oxford, 2nd ed., 2010.

[3] N. G. van Kampen, *Stochastic processes in physics and chemistry*. North Holland, 3rd ed., 2007.

[4] B. Øksendal, *Stochastic Differential Equations: An Introduction with Applications*. Springer Berlin Heidelberg, 5th ed., 2010.

[5] S. Salinas, *Introduction to Statistical Physics*. Graduate Texts in Contemporary Physics, Springer New York, 2001.

[6] D. Lemons and A. Gythiel, "Paul Langevin's 1908 paper "On the Theory of Brownian Motion"," *American Journal of Physics*, vol. 65, pp. 1079–1081, 1997.

[7] N. Wiener, "The Average of an Analytic Functional and the Brownian Movement," *Proceedings of the National Academy of Sciences*, vol. 7, no. 10, pp. 294–298, 1921.

[8] R. P. Feynman, "Space-time approach to non-relativistic quantum mechanics," *Reviews of Modern Physics*, vol. 20, pp. 367–387, 1948.

[9] N. D. H. Dass, "Dirac and the path integral." arXiv:2003.12683 [physics.hist-ph], 2020.

[10] S. Chandrasekhar, "Stochastic problems in physics and astronomy," *Reviews of Modern Physics*, vol. 15, pp. 1–89, 1943.

[11] P. C. Martin, E. D. Siggia, and H. A. Rose, "Statistical dynamics of classical systems," *Physical Review A*, vol. 8, pp. 423–437, 1973.

[12] H. Janssen, "On a Lagrangian for classical field dynamics and renormalization group calculations of dynamical critical properties," *Zeitschrift für Physik B Condensed Matter*, vol. 23, pp. 377–380, 1976.

[13] C. Dominicis, "Techniques de Renormalization de la Theorie des Champs et Dynamique des Phenomenes Critiques," *Le Journal De Physique Colloques*, vol. 37, pp. 247–253, 1976.

[14] J. A. Hertz, Y. Roudi, and P. Sollich, "Path integral methods for the dynamics of stochastic and disordered systems," *Journal of Physics A: Mathematical and Theoretical*, vol. 50, no. 3, 2016.

[15] A. Altland and B. D. Simons, *Condensed Matter Field Theory*. Cambridge University Press, 2nd ed., 2010.

[16] P. Bressloff, "Stochastic neural field theory and the system-size expansion," *SIAM Journal of Applied Mathematics*, vol. 70, pp. 1488–1521, 2009.

[17] M. A. Buice, J. D. Cowan, and C. C. Chow, "Systematic fluctuation expansion for neural network activity equations," *Neural Computation*, vol. 22, no. 2, p. 377–426, 2009.

[18] M. Buice and C. Chow, "Beyond mean field theory: Statistical field theory for neural networks," *Journal of Statistical Mechanics Theory and Experiment*, vol. 2013, p. P03003, 2013.

[19] C. Chow and M. Buice, "Path integral methods for stochastic differential equations," *Journal of mathematical neuroscience*, vol. 5, 2015.

[20] A. Lotka, *Elements of Physical Biology*. Williams and Wilkins, London, 1925.

[21] V. Volterra, "Variazioni e fluttuazioni del numero d'individui in specie animali conviventis," *Memoire della R. Accademia Nazionale dei Lincei*, vol. 2, pp. 31–113, 1926.

[22] M. Mobilia, I. T. Georgiev, and U. C. Täuber, "Phase Transitions and Spatio-Temporal Fluctuations in Stochastic Lattice Lotka–Volterra Models," *Journal of Statistical Physics*, vol. 128, no. 1-2, p. 447–483, 2006.

[23] A. Altieri, F. Roy, C. Cammarota, and G. Biroli, "Properties of equilibria and glassy phases of the random Lotka-Volterra model with demographic noise," *Physical Review Letters*, vol. 126, no. 25, 2021.

[24] L. Sidhom and T. Galla, "Ecological communities from random generalized Lotka-Volterra dynamics with nonlinear feedback," *Physical Review E*, vol. 101, no. 3, p. 032101, 2020.

[25] U. C. Täuber, "Population oscillations in spatial stochastic Lotka–Volterra models: a field-theoretic perturbational analysis," *Journal of Physics A: Mathematical and Theoretical*, vol. 45, no. 40, p. 405002, 2012.

[26] A. J. Lotka, "Contribution to the theory of periodic reactions," *Journal of Physical Chemistry*, vol. 14, no. 3, p. 271–274, 1910.

[27] N. Goel and S. Maitra, "On the Volterra and Other Nonlinear Models of Interacting Populations," *Reviews of Modern Physics*, vol. 43, pp. 231–276, 1971.

[28] F. Hoz and F. Vadillo, "A mean extinction-time estimate for a stochastic Lotka–Volterra predator–prey model," *Applied Mathematics and Computation*, vol. 219, p. 170–179, 2012.

[29] F. Vadillo, "Comparing stochastic Lotka–Volterra predator-prey models," *Applied Mathematics and Computation*, vol. 360, pp. 181–189, 2019.

[30] C. Tian, L. Lin, and L. Zhang, "Additive noise driven phase transitions in a predator-prey system," *Applied Mathematical Modelling*, vol. 46, pp. 423–432, 2017.

[31] M. Liu and M. Fan, "Permanence of Stochastic Lotka–Volterra Systems," *Journal of Nonlinear Science*, vol. 27, pp. 425–452, 2017.

[32] L. Arnold, W. Horsthemke, and J. Stucki, "The Influence of External Real and White Noise on the Lotka-Volterra Model," *Biometrical Journal*, vol. 21, pp. 451–471, 1979.

[33] R. May and P. Allen, "Stability and complexity in model ecosystems," *Systems, Man and Cybernetics, IEEE Transactions on*, vol. 44, pp. 887 – 887, 1977.

[34] BIPM, *Le Système international d'unités / The International System of Units ('The SI Brochure')*, `http://www.bipm.org/en/si/si_brochure/`. Bureau international des poids et mesures, 9th ed., 2019.

[35] R. C. Tolman, *The Principles of Statistical Mechanics*. Oxford: The Clarendon Press., 1938.

[36] B. Altaner, *Foundations of Stochastic Thermodynamics*. PhD thesis, University of Luxembourg, 2014.

[37] S. Sobolev, *Partial Differential Equations of Mathematical Physics*. Pergamon Press, 1964.

[38] H. Nyquist, "Thermal Agitation of Electric Charge in Conductors," *Physical Review*, vol. 32, no. 1, pp. 110–113, 1928.

[39] P. Szendro, G. Vincze, and A. Szasz, "Pink-noise behaviour of biosystems," *European biophysics journal*, vol. 30, pp. 227–31, 2001.

[40] A. Einstein, "Über die von der molekularkinetischen Theorie der Wärme geforderte Bewegung von in ruhenden Flüssigkeiten suspendierten Teilchen," *Annalen der Physik*, vol. 322, no. 8, pp. 549–560, 1905.

[41] J. D. Scargle, "Studies in Astronomical Time Series Analysis. V. Bayesian Blocks, a New Method to Analyze Structure in Photon Counting Data," *The Astrophysical Journal*, vol. 504, pp. 405–418, 1998.

[42] P. Ehrenfest and T. Ehrenfest, *The Conceptual Foundations of the Statistical Approach in Mechanics*. Dover Phoenix editions, Dover Publications, 2002.

[43] G. E. Uhlenbeck and L. S. Ornstein, "On the Theory of the Brownian Motion," *Phyical Review*, vol. 36, pp. 823–841, 1930.

[44] A. Mardinoglu, "Inclusion of interactions in mathematical modelling of implant assisted magnetic drug targeting," *Applied Mathematical Modelling*, vol. 36, no. 1, pp. 1–34, 2009.

[45] S. Chikazumi and C. Graham, *Physics of Ferromagnetism 2e*. International Series of Monographs on Physics, OUP Oxford, 2009.

[46] J. Orear, E. Fermi, A. Rosenfeld, and R. Schluter, *Nuclear Physics: A Course Given by Enrico Fermi at the University of Chicago*. Midway reprint, University of Chicago Press, 1950.

[47] C. Van Vliet, *Equilibrium and Non-equilibrium Statistical Mechanics*. World Scientific, 2008.

[48] A. Einstein, "Strahlungs-Emission und -Absorption nach der Quantentheorie," *Verhandlungen der Deutschen Physikalischen Gesellschaft*, vol. 18, no. 13/14, pp. 318–323, 1916.

[49] H. Kramers, "Brownian motion in a field of force and the diffusion model of chemical reactions," *Physica*, vol. 7, no. 4, pp. 284 – 304, 1940.

[50] J. Moyal, *Stochastic Processes and Statistical Physics*. Journal of the Royal Statistical Society, Series B, Wiley, 1949.

[51] R. Brown, "27: A brief account of microscopical observations made on the particles contained in the pollen of plants," *The Philosophical Magazine*, vol. 4, no. 21, pp. 161–173, 1828.

[52] R. Capone, I. D'Acunto, U. D. Iacono, and F. D. Regno, "Brownian motion: an interdisciplinary teaching proposal." `https://www.researchgate.net/publication/311734269_Brownian_motion_an_interdisciplinary_teaching_proposal`, 2016.

[53] M. M. Smoluchowski, "Sur le chemin moyen parcouru par les molécules d'un gaz et sur son rapport avec la théorie de la diffusion," *Bulletin International de l'Académie des Sciences de Cracovie*, vol. 202, 1906.

[54] H. B. Callen and T. A. Welton, "Irreversibility and Generalized Noise," *Physical Review*, vol. 83, no. 1, pp. 34–40, 1951.

[55] N. G. van Kampen, "Langevin-like equation with colored noise," *Journal of Statistical Physics*, vol. 54, no. 5-6, pp. 1289–1308, 1989.

[56] W. Coffey, Y. Kalmykov, and J. Waldron, *The Langevin Equation: With Applications In Physics, Chemistry And Electrical Engineering*. Contemporary Chemical Physics, World Scientific, 1996.

[57] R. L. Stratonovich, "A new representation for stochastic integrals and equations," *SIAM Journal on Control*, vol. 4, no. 2, pp. 362–371, 1966.

[58] K. Itô, "Stochastic integral," *Proceedings of the Imperial Academy*, vol. 20, no. 8, pp. 519–524, 1944.

[59] E. Wong and M. Zakai, "On the convergence of ordinary integrals to stochastic integrals," *Annals of Mathematical Statistics*, vol. 36, no. 5, pp. 1560–1564, 1965.

[60] L. Nadel and D. Stein, *1990 Lectures In Complex Systems*. CRC Press, 2018.

[61] S. H. Strogatz, *Nonlinear Dynamics and Chaos: With Applications to Physics, Biology, Chemistry and Engineering*. Westview Press, 2000.

[62] G. Giacomin, C. Poquet, and A. Shapira, "Small noise and long time phase diffusion in stochastic limit cycle oscillators," *Journal of Differential Equations*, vol. 264, 2015.

[63] A. Friedman and C.-Y. Kao, *Mathematical Modeling of Biological Processes*. Springer International Publishing, 2014.

[64] P. Zgliczynski, "Geometric proof of the Grobman-Hartman Theorem." arXiv:1405.6733 [math.DS], 2014.

[65] W. Horsthemke and R. Lefever, *Noise-Induced Transitions: Theory and Applications in Physics, Chemistry, and Biology*. Springer Series in Synergetics, Springer Berlin Heidelberg, 2006.

[66] "Dynamicalsystems.jl." `https://juliadynamics.github.io/DynamicalSystems.jl/latest/chaos/lyapunovs/`. Accessed: 19-11-2020.

[67] G. Vasziová, J. Tóthová, L. Glod, and V. Lisy, "Thermal Fluctuations in Electric Circuits and the Brownian Motion," *Journal of Electrical Engineering*, vol. 61, no. 4, pp. 252–256, 2010.

[68] J. Clarke and A. Braginski, *The SQUID Handbook: Fundamentals and Technology of SQUIDs and SQUID Systems*. Wiley, 2006.

[69] B. Josephson, "The discovery of tunnelling supercurrents," *Reviews of Modern Physics*, vol. 46, pp. 251–254, 1974.

[70] J. Hizanidis, N. Lazarides, and G. Tsironis, "Flux bias-controlled chaos and extreme multistability in SQUID oscillators," *Chaos: An Interdisciplinary Journal of Nonlinear Science*, vol. 28, no. 6, p. 063117, 2018.

[71] C. Morais Smith, *Dissipation in Quantum Systems*. ITP, Utrecht University, 2010.

[72] G. B. Apolinário, *Large Fluctuations in Stochastic Models of Turbulence*. PhD thesis, Universidade Federal do Rio de Janeiro, 2020.

[73] R. Benzi, G. Parisi, A. Sutera, and A. Vulpiani, "Stochastic resonance in climatic change," *Tellus*, vol. 34, no. 1, pp. 10–15, 1982.

[74] R. Benzi, A. Sutera, and A. Vulpiani, "The mechanism of stochastic resonance," *Journal of Physics A*, vol. 14, pp. L453–L457, 1981.

[75] K. Wiesenfeld and F. Moss, "Stochastic resonance and the benefits of noise: From ice ages to crayfish and SQUIDs," *Nature*, vol. 373, pp. 33–36, 1995.

[76] L. Bachelier, "Théorie de la spéculation," *Annales Scientifiques de L'Ecole Normale Supérieure*, vol. 17, pp. 21–88, 1900.

[77] R. Friedrich, J. Peinke, and C. Renner, "How to Quantify Deterministic and Random Influences on the Statistics of the Foreign Exchange Market," *Physical Review Letters*, vol. 84, pp. 5224–5227, 2000.

[78] T. E. Harris, *The theory of branching processes*. Die Grundlehren der Mathematischen Wissenschaften, Bd. 119, Springer-Verlag, 1963.

[79] P. Verhulst, *Recherches mathématiques sur la loi d'accroissement de la population*. M. Hayez, 1845.

[80] J. Zinn-Justin, *Quantum Field Theory and Critical Phenomena*. International series of monographs on physics, Clarendon Press, 2002.

[81] M. Chaichian and A. Demichev, *Path Integrals in Physics: Volume I Stochastic Processes and Quantum Mechanics*. Institute of physics series in mathematical and computational physics, Taylor & Francis, 2001.

[82] R. Durrett, *Brownian Motion and Martingales in Analysis*. Wadsworth & Brooks/Cole Mathematics Series, Wadsworth Advanced Books & Software, 1984.

[83] G. Papadopoulos and J. Devreese, *Path Integrals: And Their Applications in Quantum, Statistical and Solid State Physics*. Nato Science Series B:, Springer US, 2013.

[84] C. Dewitt-Morette and A. Folacci, *Functional Integration: Basics and Applications*. Nato Science Series B: 261, Springer US, 1997.

[85] R. MacKenzie, "Path integral methods and applications." arXiv:quant-ph/0004090, 2000.

[86] P. C. Hohenberg and B. I. Halperin, "Theory of dynamic critical phenomena," *Reviews of Modern Physics*, vol. 49, pp. 435–479, 1977.

[87] H. T. C. Stoof, D. B. M. Dickerscheid, and K. Gubbels, *Ultracold Quantum Fields*. Springer, Utrecht, 2009.

[88] M. Srednicki, *Quantum Field Theory*. Cambridge University Press, 2007.

[89] M. Ornigotti and A. Aiello, "The Faddeev-Popov Method Demystified." arXiv:1407.7256 [hep-th], 2014.

[90] R. Bausch, H. K. Janssen, and H. Wagner, "Renormalized field theory of critical dynamics," *Zeitschrift fur Physik B Condensed Matter*, vol. 24, no. 1, pp. 113–127, 1976.

[91] M. A. Buice and C. C. Chow, "Correlations, fluctuations, and stability of a finite-size network of coupled oscillators," *Physical Review E*, vol. 76, no. 3, p. 031118, 2007.

[92] T. Galla, "Dynamically evolved community size and stability of random Lotka-Volterra ecosystems," *EPL (Europhysics Letters)*, vol. 123, no. 4, p. 48004, 2018.

[93] A. Auerbach, *Interacting Electrons and Quantum Magnetism*. Graduate texts in contemporary physics, Springer-Verlag, 1994.

[94] R. Spigler and M. Vianello, "A survey on the Liouville-Green (WKB) approximation for linear difference equation of the second order," *Advances in Difference Equations*, 1998.

[95] D. Amit and V. Martin-Mayor, *Field theory, the renormalization group, and critical phenomena: Graphs to computers*. World Scientific Publishing Company, 2005.

[96] C. S. Holling, "The Components of Predation as Revealed by a Study of Small-Mammal Predation of the European Pine Sawfly," *The Canadian Entomologist*, vol. 91, no. 5, 1959.

[97] M. L. Rosenzweig and R. H. MacArthur., "Graphical representation and stability conditions of predator-prey interactions," *The American Naturalist*, vol. 97, no. 895, p. 209–223, 1963.

[98] C. Jost, G. Devulder, J. A. Vucetich, R. O. Peterson, and R. Arditi, "The wolves of Isle Royale display scale-invariant satiation and ratio-dependent predation on moose," *Journal of Animal Ecology*, vol. 74, no. 5, pp. 809–816, 2005.

[99] M. E. Gilpin, "Do hares eat lynx?," *The American Naturalist*, vol. 107, no. 957, pp. 727–730, 1973.

[100] R. Goodwin, "A growth cycle," *Essays in Economic Dynamics*, pp. 165–170, 1967.

[101] T. Idema, "The behaviour and attractiveness of the lotka-volterra equations," Master's thesis, Universiteit Leiden, 2005.

[102] I. Bomze, "Lotka-Volterra equation and replicator dynamics: A two-dimensional classification," *Biological Cybernetics*, vol. 48, pp. 201–211, 1983.

[103] R. de Boer, "Biological modeling of populations," Utrecht University, 2021.

[104] Zhang, Qiumei and Jiang, Daqing, "The coexistence of a stochastic Lotka–Volterra model with two predators competing for one prey," *Applied Mathematics and Computation*, vol. 269, pp. 288–300, 2015.

[105] M. Kot, *Elements of Mathematical Ecology*. Elements of Mathematical Ecology, Cambridge University Press, 2001.

[106] S. D. Shih, "The period of a Lotka-Volterra System," *Taiwanese Journal of Mathematics*, vol. 1, no. 4, 1997.

[107] E. Hairer, C. Lubich, and G. Wanner, *Geometric numerical integration*, vol. 31 of *Springer Series in Computational Mathematics*. Springer-Verlag, Berlin, 2nd ed., 2006.

[108] M. J. Aburn, "Numerical integrator of Ito or Stratonovich SDEs." `https://pypi.org/project/sdeint/`, 2021.

[109] M. Droste and R. Arouca de Albuquerque, "Python code for simulations and calculations for stochastic Lotka-Volterra model with additive noise." `https://github.com/maartendroste/Stochastic-Lotka-Volterra`, 2021.

[110] L. Berthier, G. Biroli, P. Charbonneau, E. I. Corwin, S. Franz, and F. Zamponi, "Gardner physics in amorphous solids and beyond," *The Journal of Chemical Physics*, vol. 151, no. 1, p. 010901, 2019.

[111] M. Lazarević, M. Rapaić, and T. Šekara, *Introduction to Fractional Calculus with Brief Historical Background*, pp. 3–16. WSEAS Press, 2014.

[112] R. C. Verstraten, R. F. Ozela, and C. Morais Smith, "Time glass: A fractional calculus approach," *Physical Review B*, vol. 103, p. L180301, May 2021.

[113] S. Zibaei and M. Namjoo, "Solving fractional-order competitive Lotka-Volterra model by NSFD schemes," *TWMS Journal of Applied and Engineering Mathematics*, vol. 6, pp. 264–277, 2016.

[114] M. M. Amirian, I. Towers, Z. Jovanoski, and A. J. Irwin, "Memory and mutualism in species sustainability: A time-fractional Lotka-Volterra model with harvesting," *Heliyon*, vol. 6, no. 9, 2020.

[115] D. Jiang, C. Ji, X. Li, and D. O Regan, "Analysis of autonomous lotka–volterra competition systems with random perturbation," *Journal of Mathematical Analysis and Applications*, vol. 390, no. 2, pp. 582–595, 2012.

[116] H. Nakazato, K. Okano, L. Schülke, and Y. Yamanaka, "Symmetries in stochastic quantization and Ito-Stratonovich related interpretation," *Nuclear Physics B*, vol. 346, no. 2-3, pp. 611–631, 1990.